University of Twente – Biomedical Photonic Imaging Group

Discovering the lactating breast with Diffuse Optical Spectroscopic Imaging

Master thesis Biomedical Engineering – track: Imaging and In Vitro Diagnostics

Miriam van der Hoek
March 2020 - May 2021

PREFACE

The report that lays in front of you is the product of my master thesis BME. I already encountered the subject, the lactating breast, in my bachelor thesis and I found it fascinating how quick the breast can change, and it can produce all the nutrients the baby needs in the early days of live. This is the reason I contacted Nienke Bosschaart for my master thesis again. Moreover, the atmosphere of the group is very pleasant. Unfortunately, one week after I started the first lockdown of the Netherlands started due to the COVID-pandemic, this means my research had to change from a practical research to a theoretical research.

I would like to thank Nienke Bosschaart for her guidance and positivity, which helped me through all the changes and helped me when I get stuck. Thereby, I would like to thank Srirang Manohar and Wiendelt Steenbergen for judging and reading my report. Also, I would like to thank Hanna de Wolf for all the lovely meetings we had and Margherita for guiding me through the process of writing academical English. Thereby, I would like to thank my family and friends. Especially, my niche, Rosalie, and my sister, Josien, with whom I formed an online study club. My boyfriend for having lots and lots of patients with me. And last but not least, my roommates for keeping me company in this roaring times.

ABSTRACT

Introduction: Human breast milk is the best nutrient for newborns [1][2], but a lot of mothers experience breastfeeding problems and quit breastfeeding. Only approximately 40% of all mothers exclusively breastfeeds in the first 6 months after birth [3]. The most given reasons for quitting exclusive breastfeeding in the Netherlands is the perception of insufficient milk supply (for 33% of mothers) [4]. The perception of insufficient milk supply occurs when the mother suspects or knows that her infant has drunk an inadequate volume of breast milk [5]. Obtaining an objective measurement helps mothers gain and maintain confidence in their breastfeeding [6]. This research is focused on investigating the composition of the (lactating) breast and to determine milk transfer with Diffuse Optical Spectroscopic Imaging (DOSI). DOSI is used to determine two optical properties of breast tissue: the absorption coefficient, μ_a, and the reduced scattering coefficient, μ_s'. These optical properties relate to several functional properties of the investigated breast tissue: water concentration, lipid concentration, deoxyhemoglobin concentration, oxyhemoglobin concentration, the scattering prefactor, a, and the scattering power, b. The research question is: ***"To what extent can we predict milk transfer during a breastfeed from a DOSI measurement on the lactating breast?"***

Theory: The theory is divided in two chapters: The theory behind DOSI (the diffusion equation) and the anatomy and the physiology of the (lactating) breast. Literature values for the optical and functional properties of the (lactating) breast and the layers of the (lactating) breast are described. Important highlights are differences between the lactating and the non-lactating breast: the blood flow in the breast doubles during pregnancy [7][8] and the lactating breast contains on average 30% more glandular tissue than the non-lactating breast [9][10], the ratio glandular tissue to adipose tissue is approximately 2:1 for the lactating breast [11].

Model: A model is developed to predict the DOSI outcomes for the non-lactating and lactating breast and to predict the extracted milk volume during a breastfeeding session. The model is based on the optical and functional properties of the tissue layers of the breast. This is combined with the average sensitivity of DOSI as a function of tissue depth. The model outcomes of the functional properties are compared to the literature values of the functional properties of the breast, which are in good agreement.

Experiments: Previously acquired data from a pilot study in November 2019 with DOSI on the lactating breast were analyzed in order to compare the model to experimental data. Four lactating women and five non-lactating women participated in this study. For the lactating group, DOSI data were acquired from the breast before (pre), during (peri) and after (post) milk extraction with a breast pump. The extracted milk weight was recorded as a function of time with a digital scale. The same DOSI measurements were performed on the non-lactating group in the absence of milk extraction to assess method reproducibility. The total hemoglobin (THb) concentrations were approximately twice as high for the lactating breast. The range of the medians for water concentration is higher and for lipid concentration is lower for the lactating breast than for the non-lactating breast, (water: $22-80\%$, lipid:$1-69\%$) and (water: $13-65\ \%$, lipid: $27-79\%$), respectively. This indicates that the lactating breast contains more glandular tissue than adipose tissue. With the available data, no correlation was found between the pre- and post-expression functional and optical properties. Nevertheless, the functional properties of the peri-data exhibited some similarities to the milk flow rate, especially for THb and oxygen saturation (stO_2) a drop is observed during a milk ejection reflex.

Validation of the model: To validate the model, the model is compared to the results of the experiments. The average breast model is compared to the range of the experiments in the optical and functional properties. In general, the average breast model, lactating and non-lactating, were in agreement with the experiments. There are two exceptions, the THb concentration (and therefore μ_a in the below 900 nm) of the non-lactating breast and the scattering prefactor a (hence, μ_s' as well) of the lactating breast. The average non-lactating breast model was maximum $\mu_a \approx 0.001\ mm^{-1}$ and $THb \approx 1\ \mu M$ higher than the median of the experiments. The average lactating breast model was maximum $\mu_s' \approx 0.06\ mm^{-1}$ and $a \approx 0.08\ mm^{-1}$ than the median of the experiments. The variations of the breast were used to fit the μ_a per participant of the experiments using the

"Newton-Raphson" method, resulting in optical and functional properties per subject for pre and post milk extraction. It is possible to fit the μ_a spectra with the corresponding functional properties (the chromophore concentrations) to the experiments using the model and the variations of the breast, the maximum error of $\mu_a \approx 4 * 10^{-3}\, mm^{-1}$.

Prediction of the model: There are two methods used to predict the milk transfer of the subject of the pilot study with the model: The "water concentration" method and the "Newton-Raphson" method. The "water concentration" method only uses the median difference of the water concentration between before and after expression of the experiments. The "water concentration" method was neither accurate nor precise: The non-lactating breast should be around 0, but values differ between -117 ml to 143 ml and the lactating breast should be in range of 0 to 200 ml, but differ between -35 ml to 740 ml. The "Newton-Raphson" method predicted the milk transfer accurately, but was imprecise: of the four lactating subjects, the smallest range was still 115-200 ml for a subject that had 153.3 g milk supply.

Conclusion and outlook: The absorption coefficient and corresponding functional properties of the model were in line with the experiments. This supports the underlying theory about the lactating breast and the non-lactating breast. To answer the research question: the prediction of milk transfer was accurate, but imprecise. To improve this prediction and to confirm other results in this report, more experiments are needed, and the model should be improved, especially for μ_s'.

SAMENVATTING (NL)

Probleemstelling: Borstvoeding is de beste voeding voor een neonaat [1][2]. Er zijn veel moeders met borstvoedingsproblemen die stoppen met borstvoeding in de eerste zes maanden [3]. De belangrijkste reden die moeders aangeven voor het stoppen van exclusieve borstvoeding in Nederland is het geven van weinig melk (33% van de moeders die stoppen geven dit als reden) [4]. Het meten van de borstvoeding helpt moeders vertrouwen krijgen of houden in hun borstvoeding [6]. Dit onderzoek focus zich op onderzoek doen naar de samenstelling van de (lacterende) borst en het vaststellen van de hoeveelheid afgegeven melkvolume. Het onderzoek wordt gedaan met "Diffuse Optical Spectroscopic Imaging" (DOSI, vertaling: diffuse optische spectroscopische beeldvorming). DOSI wordt gebruikt voor het verkrijgen van de optische eigenschappen: de absorptiecoëfficiënt, μ_a , en de gereduceerde verstrooiingcoëfficiënt, μ_s' en functionele eigenschappen: waterconcentratie, lipidenconcentratie, deoxyhemoglobineconcentratie, oxyhemoglobineconcentratie, verstrooiingfactor, a, en de verstrooiingsmacht, b. De onderzoeksvraag luidt: ***"In hoeverre kunnen we de melkverplaatsing tijdens een borstvoeding voorspellen met DOSI-metingen op de lacterende borst?"***

Theorie: De theorie is opgedeeld in twee hoofdstukken: Hoe DOSI gebaseerd is op de diffusievergelijking en de anatomie en fysiologie van de borst. Daarnaast is er literatuuronderzoek gedaan naar de optische en functionele eigenschappen van de (lacterende) borst en de lagen van de (lacterende) borst. Belangrijk zijn de verschillend tussen de niet-lacterende borst en de lacterende borst: De doorbloeding verdubbeld tijdens een zwangerschap [7][8] en de lacterende borst bevat gemiddeld 30% meer klierweefsel dan de niet-lacterende borst [9][10], de ratio klierweefsel tot vetweefsel is bijna 2:1 voor de lacterende borst [11].

Model: In dit hoofdstuk wordt er een model gemaakt, voor het voorspellen van de DOSI-uitkomsten voor de niet-lacterende en lacterende borst en het afgegeven melkvolume tijdens een borstvoeding. Het model is gebaseerd op de optische en functionele eigenschappen van de lagen van de borst. Dit wordt gecombineerd met de gemiddelde sensitiviteit van DOSI voor de verschillende lagen van de borst. Aan het einde gecontroleerd of het door het model voorspelde functionele eigenschappen overeenkomen met de functionele eigenschappen van de borst uit de literatuur.

Experimenten: In 2019 is er een proefonderzoek gestart met DOSI naar de lacterende borst. Hierbij namen vier lacterende proefpersonen en vijf niet-lacterende proefpersonen deel. Bij de lacterende proefpersonen is er voor (pre), tijdens (peri) en na (post) een borstvoeding gemeten. Tijdens een borstvoeding werd er met en weegschaal het veranderende melkvolume gemeten. Dezelfde metingen werden uitgevoerd op niet-lacterende personen in de afwezigheid van melkextractie om de reproduceerbaarheid van de methode te bepalen. De doorbloeding van de lacterende borst is ongeveer twee keer zo hoog als voor de niet-lacterende borst. Ook is het bereik van de mediaan van de lipidenconcentraties lager en waterconcentraties hoger voor de lacterende borst, (water: $22-80\%$, lipiden: $1-69\%$) en (water: $13-65\ \%$, lipiden: $27-79\%$), respectievelijk. Dit is een indicatie dat er meer klierweefsel dan vetweefsel in de lacterende borst zit dan de niet lacterende borst. Voorlopig is er nog geen verband te zien tussen voor en na een borstvoeding van de optische en functionele eigenschappen. Tijdens een borstvoeding, is er een verlaging te zien van totaal hemoglobine (THb) en zuurstofsaturatie (stO_2) tijdens een toeschietreflex.

Validatie van het model: Het model is vergeleken met de resultaten van het experiment om het model te valideren. Het gemiddelde borst model is vergeleken met het bereik van de optische en functionele eigenschappen van de experimenten. Over het algemeen lag de gemiddelde borst, zowel lacterend als niet lacterend, in het bereik van de experimenten op 2 uitzonderingen na. Van de niet lacterende borst is de concentratie THb niet in bereik (zie ook het μ_a onder de 900 nm) en van de lacterende borst is de verstrooiingsfactor a niet in bereik (zie ook μ_s'). Het gemiddelde niet-lacterende borst model was maximaal $\mu_a \approx 0.001\ mm^{-1}$ en $THb \approx 1\ \mu M$ hoger dan de mediaan van de experimenten. Het gemiddelde lacterende borst model was maximaal $\mu_s' \approx 0.06\ mm^{-1}$ en $a \approx 0.08\ mm^{-1}$ hoger dan de mediaan van de experimenten. Er

wordt gebruik gemaakt van de variaties van de borst om het model te passen aan de μ_a per proefpersoon van de experimenten via de “Newton-Raphson” methode van voor en na een borstvoeding. Hier blijkt de fit van μ_a en de bijbehorende functionele eigenschappen (de chromofoorconcentraties) van het model en de experimenten overeen te komen, de maximale fout was $\mu_a \approx 4 * 10^{-3}\, mm^{-1}$.

Voorspelling van het model: Er worden twee methodes gebruikt om de hoeveelheid afgegeven melk te voorspellen: de “waterconcentratie” methode en de “Newton-Raphson” methode. Waarbij de “waterconcentratie” methode de melkafgifte probeerde te voorspellen met alleen de waterconcentratie van de experimenten. De “waterconcentratie” methode was niet accuraat of precies: Voor de niet-lacterende borst zou geen melkextractie moeten worden voorspeld (0 ml), echter waren er waardes voor melkverplaatsing tijdens een borstvoeding van -117 ml tot 143 ml voorspeld. Ook bij de lacterende borst zouden waarden in het bereik van 0 tot 200 ml moeten liggen, maar er werden van -35 ml tot 740 ml voorspeld. Voor de “Newton-Raphson” methode was de voorspelling wel accuraat, maar niet precies: bij de vier proefpersonen was het kleinste bereik nog steeds 85 ml.

Conclusie en toekomstperspectief: Het absorptiegedeelte van het model komt overeen met de experimenten, dit is een indicatie dat de achterliggende theorie over de lacterende borst en niet-lacterende borst klopt. Om de onderzoeksvraag te beantwoorden: De voorspelling van melkafgifte is accuraat, maar niet precies. Om de voorspelling preciezer te maken en de beweringen te bevestigen zijn er meer experimenten nodig en kan het model worden verbeterd.

TABLE OF CONTENT

1. INTRODUCTION

Breastfeeding is important for several reasons. Breast milk contains the nutrients a baby needs in the first months of life, and has several advantages over breast-milk substitutes, such as helping the baby build an immune system [1][2]. Further, women who breastfeed have a lower risk of developing breast cancer [12]. An important WHO target for 2030 is that 70% of mothers exclusively breastfeeds for the first 6 months of life [3]. However, worldwide, approximately 40% of all mothers exclusively breastfeeds in the first 6 month after birth [3]. In the Netherlands, circa 80% of mothers is exclusively breastfeeding directly after birth, but at 6 months only 40% is still exclusively breastfeeding. The most given reasons for quitting exclusive breastfeeding in the Netherlands are pain (for 10% of mothers) and the perception of insufficient milk supply (for 33% of mothers) [4]. The perception of insufficient milk supply occurs when the mother suspects or knows that her infant has drunk an inadequate volume of breast milk [5]. There is a method to discern the milk supply by weighing the infant before and after a breastfeed [5][13][6]. Obtaining an objective measurement helps mothers gain and maintain confidence in their breastfeeding [6]. However, although test weighing is an accurate method to measure to assess milk intake, it is imprecise: The range between the weighted change of the newborn infants and the actual weighted change of the milk can differ from -12.4 to 15 ml [13]. These examples illustrate the need for a better understanding of lactation. However, despite its importance, breastfeeding has not been researched as much as other foods, such as tomatoes and cow milk [14].

This research is focused on an optical modality to investigate the composition of the lactating breast and its milk transfer. This will lead to more knowledge about the healthy lactating breast, and this could support mothers who experience breastfeeding problems.

The modality used to investigate the influence of lactation on the breast is Diffuse Optical Spectroscopic Imaging (DOSI). This technique can image approximately 1-2 cm deep into the tissue of the breast. From the measured tissue, optical properties (the reduced scattering coefficient μ_s' and the absorption coefficient μ_a) are obtained for a spectrum of wavelength (650 to 1000 nm). In turn, form the optical properties, functional properties can be determined. The functional properties in this research are the chromophores water, lipid, deoxyhemoglobin, and oxyhemoglobin, and the scattering properties are scattering prefactor (a) and scattering power (b). Both the optical and functional properties can contribute to a better understanding of the lactating breast. Since, functional properties relate to anatomical or physiological features. A high concentration of water could, for example, indicate the presents of glandular tissue or skin. Moreover, the measurement is safe, painless, and completely non-invasive.

This study is following upon a promising case study by Bosschaart and O'Sullivan et al. [15]. In the case study, one mother is measured with a DOSI device for a period of 8 months, starting from the moment she stopped breastfeeding. The goal was to get an understanding of the involution process. DOSI is a well-established technique in biomedical optics, but it is a novel technique in the field of breastfeeding. They found a significant increase in lipid content, and a decrease in water and total hemoglobin (THb) content over the eight- month period. This supports the theory that fibroglandular tissue was replaced by adipose tissue during involution. Besides this, no other study was found presenting optical properties of the lactating breast specifically, which encourages us to further investigate this area of study.

In this study, the research with DOSI on the (lactating) breast is continued. The emphasis of this research lays on how the DOSI outcomes will compare to the milk transfer in the lactating breast. In this research, the milk transfer is defined as the milk that is transferred from the breast to the outside surroundings during a breastfeeding session. A model is created to be able to explain the findings of the DOSI measurement. This model should be able to explain changes regarding milk transfer especially. The model should eventually consist of optical and functional properties that can be compared with the DOSI measurements for the lactating and non-lactating breast. The model should consider the possibilities of the DOSI outcome with respect to biological and physiological variabilities in the lactating and non-lactating breast. The model is digitally made in the program

MATLAB R2018a. It is based on the anatomy of the female breast. Diffusion theory is used to estimate the sensitivity of DOSI for the layers of the breast. In the future, this model could be used to optimize the DOSI measurement to measure milk transfer or even the amount of milk available or produced (milk supply). This can be parameters such as the source detector distance. Moreover, this model could be used to build an optical phantom or can be compared to other optical techniques used on the lactating breast, such as photoacoustic imaging. A possibility could be to use the knowledge of an optical phantom of a non-lactating breast [16] with the model of the lactating breast combined to build a phantom for the lactating breast.

Thereby, some DOSI experiments are carried out on the lactating and non-lactating breast. The way that milk transfer influences the measurements is an important physiological aspect of the measurements. Therefore, milk flow rate and milk volume are measured as well for the lactating participants. During a breastfeed, the milk flow rate and volume are determined by weighing the ejected milk in a bottle on a scale. These experiments allow us to obtain the optical and functional properties of the lactating breast, which are poorly described in the literature. Furthermore, the model that is made can be validated. These could give important insights in the lactation process.

The leading research question of this report is:

"TO WHAT EXTENT CAN WE PREDICT MILK TRANSFER DURING A BREASTFEED FROM A DOSI MEASUREMENT ON THE LACTATING BREAST?"

From this, the following sub-questions can be defined:

Chapter Model

1. How can a model be developed that predicts the outcomes of a DOSI experiment on lactating and non-lactating breasts, while accounting for biological variability between subjects and for physiological processes?

Chapter Experiments

2. What are the optical and functional properties of the lactating and non-lactating breast obtained by DOSI experiments?
3. How do the measurement outcomes for the areola area compare to the outcomes for the rest of the breast (the non-areola area)?
4. How do the measurement outcomes for the lactating breast compare to the measurement outcomes for the non-lactating breast?
5. How do the states of breastfeeding (i.e. before, during and after expression) influence the DOSI measurement outcomes?

Chapter Validation & prediction

Validation

6. How do the model outcomes compare to optical and functional properties obtained by the DOSI experiments?

Prediction

7. To what extent is it possible to predict milk transfer from DOSI experiments?
8. To what extent is the prediction influenced by biological variation between and within the breast?
9. What is the accuracy and precision with which the model can predict the ejected milk volume during a breastfeed, when comparing DOSI experiments to the weighted milk volume?

Optional: Evaluation prediction.

10. How can the DOSI system be further optimized to measure milk supply in the lactating breast?

This thesis is composed of seven chapters, where the first chapter is this introduction. The second and the third chapter consist of a literature research. More specifically, the second chapter is concerned with the underlying theory and the specific application of these DOSI experiments. The third chapter covers the anatomy and the physiology of the (lactating) breast, including the optical and functional properties of the breast. The fourth chapter follows, elaborating on the development of the model and the model itself, while in the fifth chapter, the experiments are described. The sixth chapter compares the model with the experiments. The chapter elaborates on the extent to which (a) the model agrees with the experiments and (b) milk transfer can be predicted by DOSI. Lastly, a discussion and a conclusion chapter are included, to discuss the results and give a perspective on the future of this research.

2. THEORY: DOSI

In this study, an optical technique is used to examine the female breast with an emphasis on lactation and milk transfer. The technique is diffuse optical spectroscopic imaging (DOSI). DOSI can be used to quantify the optical properties of tissue: The reduced scattering coefficient μ_s' and the absorption coefficient μ_a. In turn, the presence of chromophores (deoxyhemoglobin (Hb), oxyhemoglobin (HbO_2), water, and lipid) in the measured tissue volume can be determined from the absorption coefficient μ_a. The scattering prefactor a and the scattering power b are obtained from the reduced scattering coefficient μ_s'. The chromophores, the scattering prefactor and the scattering power together are referred to as the functional properties. The functional properties oxyhemoglobin and deoxyhemoglobin can be rewritten as total hemoglobin (THb) and the oxygen saturation of the blood (stO_2), where:

$$THb\ [\mu M] = deoxyhemoglobin\ [\mu M]\ + oxyhemoglobin\ [\mu M] \tag{2.1}$$

$$stO_2[\%] = 100 * \frac{oxyhemoglobin\ [\mu M]}{THb\ \ [\mu M]} \tag{2.2}$$

DOSI is based on diffusion theory. In this chapter, diffusion theory is explained first, followed by a description of the applied technique.

DIFFUSION THEORY

The different events that can occur when light is propagating through tissue are shown, see figure 2.1.

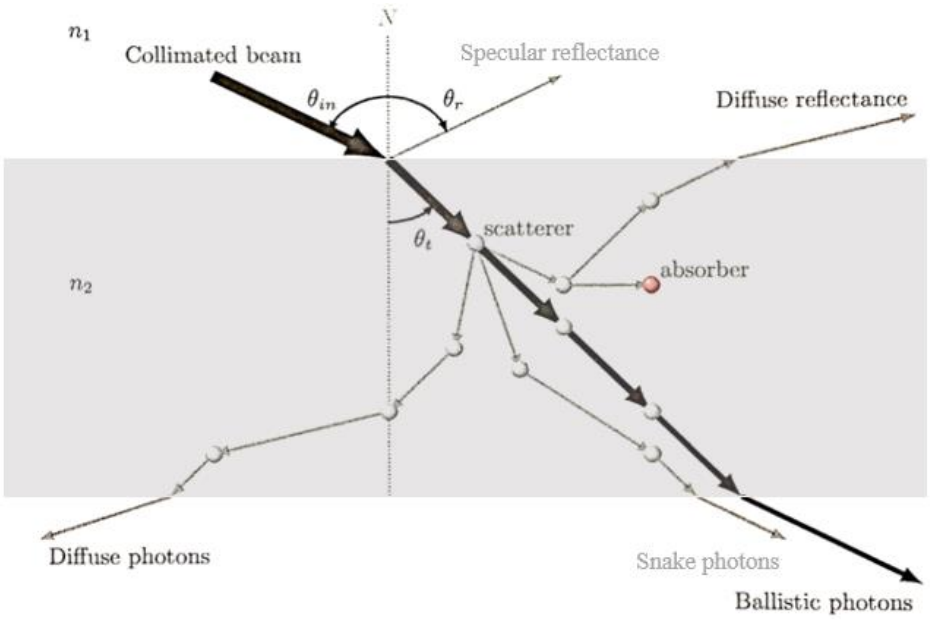

FIGURE 2.1: [17] **LIGHT EVENTS DESCRIBED BY THE RADIATIVE TRANSFER EQUATIONS.**

The propagation of light can be described by the radiative transfer equation (RTE). The RTE describes what the behavior of light is when you expose a medium to a light source and detect light originated from this medium. The events described by the RTE are:

The events causing a loss of light are absorption, scattering and if the source is divergent or convergent. This causes a loss of light, because light propagates not necessarily in the direction of the medium. The events causing a gain of light are the source, scattering and an external source (fluorescent, medium itself).

The RTE does not account for the 'wave'-character of light. For example, the diffraction and interference behavior are excluded from this equation. The diffusion equation (DE) is a simplification of the RTE. The DE can be derived from the RTE with the assumption of spherical harmonics. This is the assumption that every scattering event is perfectly isotropic. However, biological tissue scatters highly anisotropically, thus the DE seems not suitable for approaching biological tissue. Therefore, within a light pathway of a few millimeters, the Monto Carlo simulation is often used to simulate the optical behavior of the tissue. However, when there are enough scattering events in the biological tissue, where the distance must be larger than a few millimeters, the scattering is approachable as isotropic scattering. In this case, the DE is sufficient. In this technique, light travels several centimeters, which makes the DE suitable to describe the behavior of light. The diffusion equation can be written as:

$$\frac{\partial u}{\partial t} = D\nabla^2 u - c\mu_a u + S\,, \tag{2.3}$$

Where u is optical density in [J m^{-3}], D is the diffusion constant in [m^2 s^{-1}], S the source of the medium in [W m^{-3}], c the speed of light in [m s^{-1}], and t is the time in [s]. How the DE is mathematically derived from the RTE, as well as the meaning of the symbols, is described in the appendix – Mathematics DOSI. [18][17]

Absorption coefficient

The absorption coefficient is a measurement of how much the incoming light is absorbed per mm tissue. The principle of absorptivity is described by the Lambert-Beer Law. It is important to note that μ_a is proportional to chromophore concentration. [18]

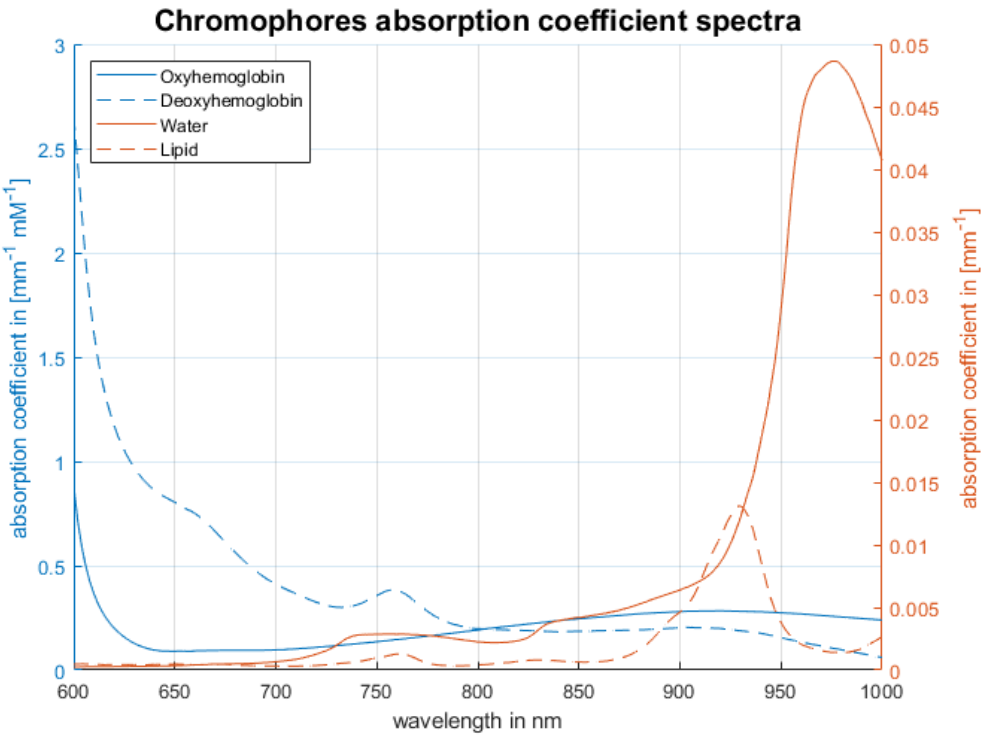

FIGURE 2.2: CHROMOPHORE ABSORPTION COEFFICIENT SPECTRA. THESE ARE THE CHROMOPHORES USED TO FIT THE ABSORPTION SPECTRA OF THE MEASUREMENTS TO DETERMINE THE COMPOSITION OF THE MEASURED VOLUME OF THE LACTATING BREAST. IN THIS REPORT THE CHROMOPHORES WILL BE USED TO BUILD A MODEL.

The four different chromophore absorption spectra are provided by Chris Campbell via email correspondence (C. Campbell, personal communication, April 24, 2020), see figure 2.2. The spectra for water and lipid represent the μ_a , when light has propagated through pure water and lipid (the concentration is then 100%). For deoxyhemoglobin and oxyhemoglobin, this is slightly different. The spectra are shown for a concentration of 1 millimole (de)oxyhemoglobin per liter (also written as 1 mM). This chromophore sheet is used to fit the chromophores to the obtained absorption coefficient by DOSI. This will approximate the ratio present of these chromophores in the measured volume. For the model, this can be done the other way around. The chromophore sheet is used to build a possible absorption coefficient spectrum for the lactating and non-lactating breast. This is further explained in the Chapter 4. The model.

Reduced scattering coefficient.

Scattering is an event where the direction of light is changed. The scattering coefficient μ_s is a property of a material and it indicates how much of the incoming light is scattered per mm of a material. The reduced scattering coefficient is defined as $\mu_s' = \mu_s(1-g)$, where g is the anisotropy coefficient. The anisotropy coefficient gives information on the dominant direction where light is scattered towards, $g \equiv < \cos\theta >$ is the weight average of the cosines of all scattering angles θ [18]. When $g = -1$, backward scattering is dominant and, when $g = 1$, forward scattering events are dominant instead. For biological tissue, g ranges between 0.8 – 0.98, indicating that biological tissues are strongly forward-scattering media [17].

The reduced scattering coefficient, μ_s' in [mm^{-1}], is obtained by the DOSI method using the formula:

$$\mu_s' = a\left(\frac{\lambda}{\lambda_0}\right)^{-b}, \tag{2.4}$$

where a is a scattering prefactor in [mm^{-1}], b is the scattering power in arbitrary units, λ the wavelength in [nm] and in this study λ_0 is 500 nm. This is an empirical approach often used to approximate the reduced scattering coefficient [19] [15] [20] [21] [22] [23]. Hereby is sometimes distinguished between scattering according to the Rayleigh theorem. The Rayleigh theorem is applicable on particles that are significantly smaller than the wavelength. Then, the scattering coefficient is proportional to λ^{-4}. With Rayleigh scattering, $g = 0$, meaning that light will scatter isotropically in every direction. When particles are no longer significantly smaller than the wavelength of light, Rayleigh theory is no longer suitable, and particles will scatter more anisotropically. [18]

How diffusion theory is applied in DOSI

For diffuse optical imaging (DOI), a light source is placed on the tissue and multiple millimeters further a detector is placed. With the DE, it is possible to calculate an energy density area, where the light detected by the detector has propagated through the tissue. This area is shaped like a banana and therefore also referred to as the photon propagation banana or light propagation, figure 2.3.

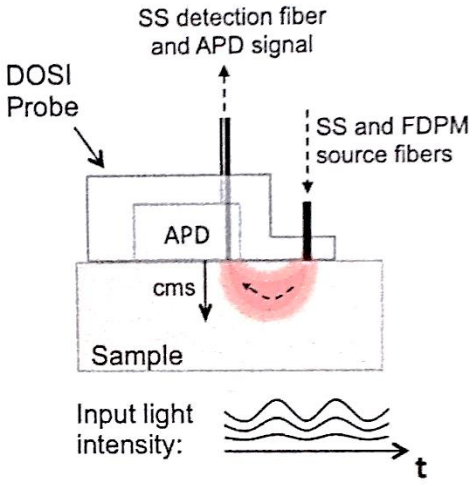

FIGURE 2.3: [17] **A SCHEMATIC DISPLAY OF THE PROPAGATION OF LIGHT THROUGH TISSUE.**

The handheld DOSI device for in this study uses 2 DOI methods, see figure 2.4:

- The steady state (SS) mode
- The frequency domain photon migration (FDPM) mode

How mathematically the DE is solved for these methods is shown in the appendix – Mathematics DOSI.

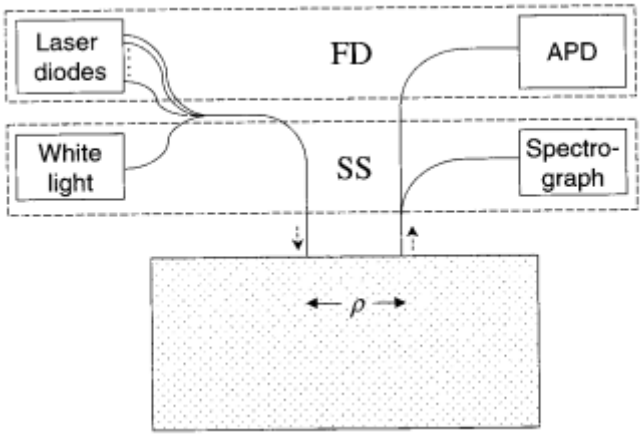

FIGURE 2.4: [23] **A SCHEMATIC OF THE HANDHELD DOSI DEVICE. THE ILLUMINATION OF THE STEADY STATE MODE IS A WHITE HALOGEN LAMP AND USES A SPECTROGRAPH AS DETECTOR. THE FREQUENCY DOMAIN PHOTON MIGRATION USES AS INPUT THE LASER DIODES AND DETECT LIGHT WITH APD, AVALANCHE PHOTODIODES.**

STEADY STATE (SS) MODE

The steady state method uses continuous illumination on the tissue and measures a spectrum between wavelengths 650 to 1000 nm with white light, see figure 2.5 (left). This means it is possible to gather information on a whole spectrum of wavelengths. However, it is not possible to immediately determine the optical properties of the tissue such as the scattering and the absorption coefficient. A way to determine these properties is frequency domain photon migration (FDPM). The spectra obtained by SS will be fit to the optical properties obtain by using FDPM. [17][24][23][20]

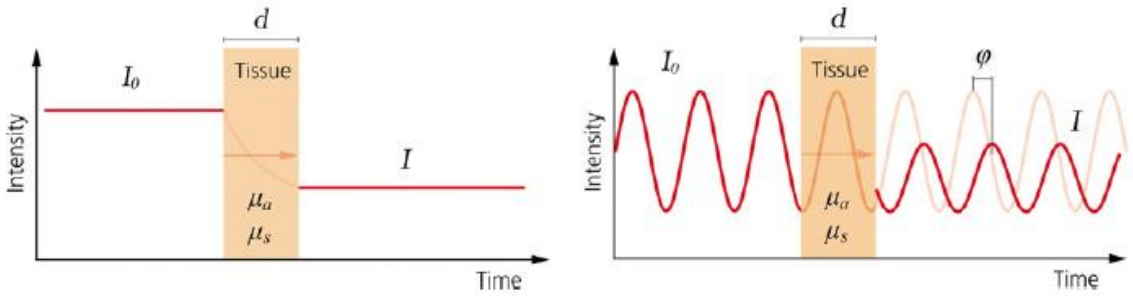

FIGURE 2.5: [25] **LEFT: CONTINUOUS ILLUMINATION. RIGHT: AMPLITUDE MODULATED ILLUMINATION.**

FREQUENCY DOMAIN PHOTON MIGRATION (FDPM) MODE

In this mode a whole spectrum of light is not used. Instead, only 4 photodiodes with one wavelength are illuminating the tissue: 660 nm, 690 nm, 850 nm and 970 nm. The tissue is not continuously illuminated but is illuminated in an amplitude modulation (50-500MHz) manner, see figure 2.5 (right). Hereby, the intensity amplitude of the incoming light is changed in a sinusoidal way, which is not the frequency of the light itself. To illustrate, this can be compared to turning a light dimmer on and off at different speeds. When the light is detected, the amplitude and the phase of every modulation have changed due to interaction with the tissue. In FDPM mode, the reduced scattering coefficient and absorption coefficient can be derived for the used wavelength. [17][24][23][20]

COMBINING FDPM AND SS MODE

FDPM can be done for all four wavelengths. This will result in the μ_s' and the μ_a for four wavelengths. By using the SS mode, information on the whole spectrum is gained. However, it is not possible to separate for which part of the attenuation the reduced scattering coefficient is responsible, and for which part absorption coefficient is responsible. With the use of the equation 2.4 and the μ_s' obtained for the four wavelengths by the FDPM mode, a spectrum μ_s' can be fit. Since μ_s' is now known, it is possible to fit the μ_a for the whole spectrum using the SS mode measurements and the already known μ_a for the four wavelengths. This results into the known values of μ_s' and of μ_a for the whole spectrum. It is possible to fit known absorption coefficient spectra of figure 2.2 (water, lipid, deoxyhemoglobin, and oxyhemoglobin) to the obtained spectrum of μ_a, which results in a concentration value for each chromophore. It is important to emphasize that not all absorption coefficient spectra of the chromophores that could be present in the breast are included. For example, the spectrum of collagen is not included. There is only chosen for four spectra due to complexity and overfitting of the spectra. In particular, these four chromophores are chosen because they are probably the most dominant absorbers in the breast. Moreover, it is not possible to locate where the chromophores are in the tissue, as their bulk concentrations are derived for the entire tissue volume that is probed by DOSI. [17][24][23]

3. Theory: The Breast

Anatomy and physiology of the female breast

Overall anatomy of the female breast

The breast consists of different types of tissue, see figure 3.1. The mean volume of a left breast and right breast is 561 ml and 567 ml, respectively [26]. Sizes of the breast variate approximately between 100 ml – 2000 ml [27][28][29]. Thereby, it is noticeable that cup sizes are not uniform for a volume of the breast and can differ per brand. The average breast is less than 4 cm deep in a supine position [30]. The total thickness of the left and right lactating breast is 24.5 ± 4.0 mm and 25.1 ± 5.1 mm [11]. The breast is located anterior to the m. pectoralis major, the big breast muscle [31]. Between the fascia of the breast and the m. pectoralis major there is a space called the submammary space. Proximal to the fibroglandular tissue and anterior to the pectoralis major, there is some retromammary fat [11]. Subcutaneous fat and the skin cover the anterior of the breast. In the breast, just below the skin, there are cooper ligaments [32]. This is a supporting connective tissue, connecting the underlying breast tissue with the skin. The radius area around the nipple where the skin is darker is called the areola. In the areola are the Montgomery's glands. These glands secrete an oil substance that protects the surrounding skin during breastfeeding and secretes a scent of the mom to attract the baby to drink. [31]

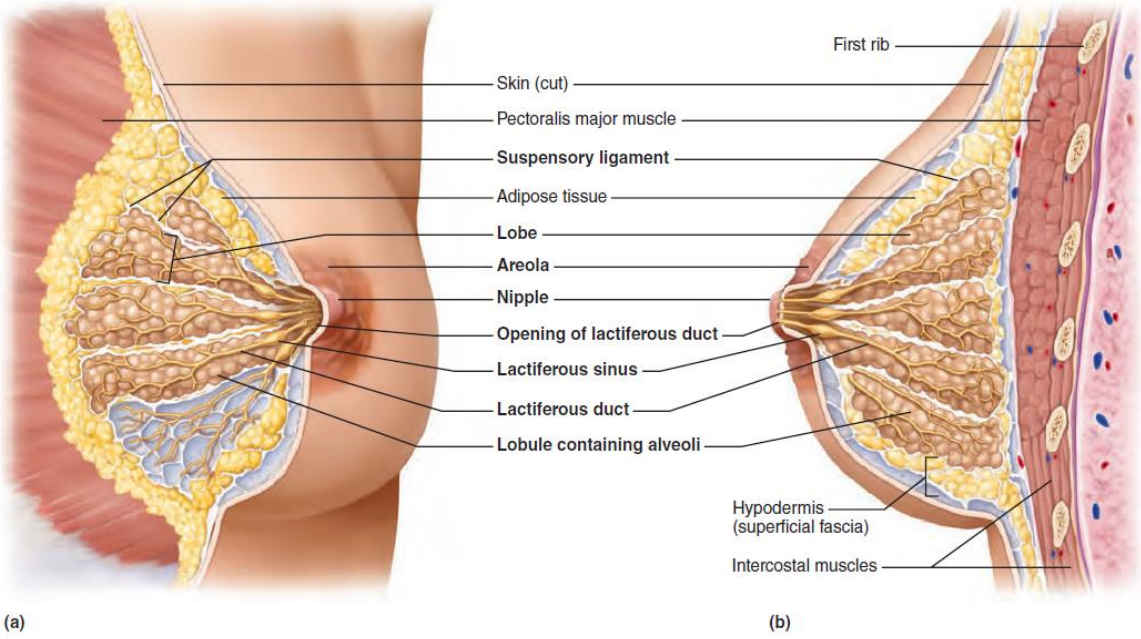

FIGURE 3.1: [31] **ANATOMY OF A FEMALE BREAST A) FRONTAL VIEW OF THE BREAST B) SIDE VIEW OF THE BREAST. IN THIS FIGURE THE LACTIFEROUS SINUS IS SHOWN, HOWEVER THE EXISTENCE OF THESE SINUSES IS DOUBTED.**

Anatomy of mammary glands

The glandular tissue is divided into lobes. Between the lobes there is connective tissue and fat. This fat is called intraglandular fat. In the lobes are the lobules, which contain the mammary glands. The glands are exocrine glands [32]. The milk-secreting cells are located on the inside layer of the alveoli [33]. Alveoli are balloons-shaped sacs where the milk is produced. On the outside of the alveoli there is muscle-like tissue of myoepithelial cells [33]. The milk is transported out of the alveoli to the nipple via milk ducts. Smaller ducts merge into bigger milk ducts that emerge in the nipple. The literature is not consistent about what the number of milk ducts ending in the nipple is. According to a research by Ramsay et al. in 2015 the mean amount of ducts is nine [11]. Just before the end of the ducts, the ducts widen, the so-called lactiferous sinuses. These are sinus-shape storage places for milk. However, the existence of these sinuses is doubted [11]. Figure 3.2 Illustrate the anatomy of the glands.

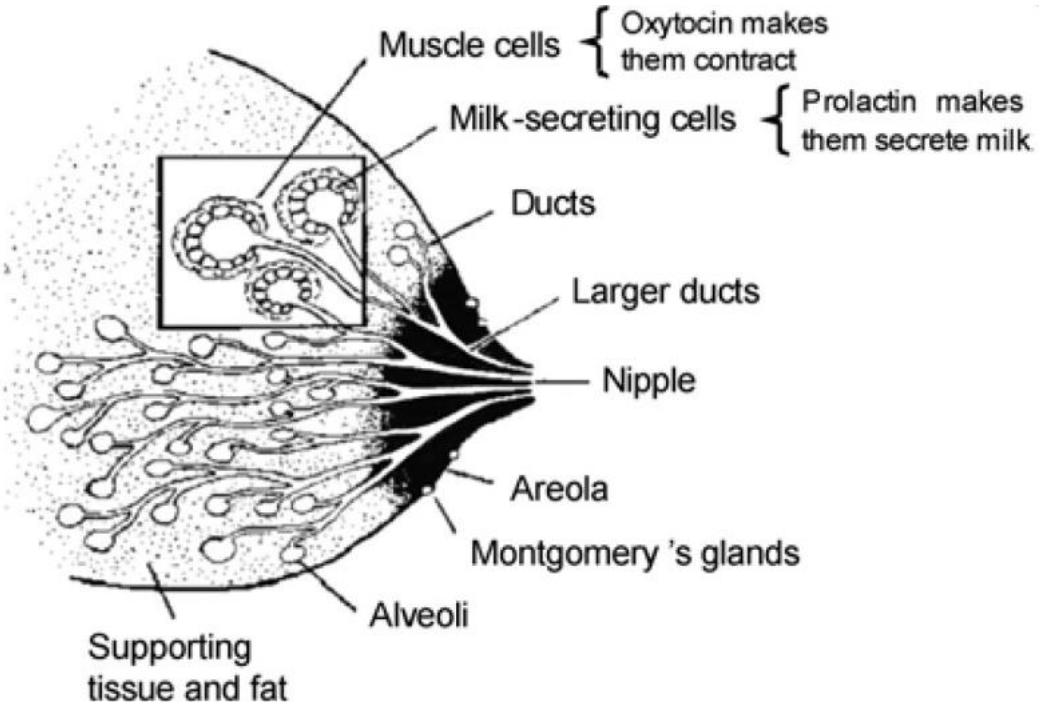

FIGURE 3.2: [33] **THE LACTATING BREAST WITH THE ALVEOLI.**

There has been a very insightful research on the anatomy of the lactating breast with ultrasound conducted by Ramsay et al. [11]. In the article, the characteristics of milk ducts are described, see table 3.1. A notable detail found in the study is that milk ducts are easily compressible.

TABLE 3.1: [11] **THE CHARACTERISTICS OF THE MILK DUCTS.**

Ramsay et al. [11]	**Left breast**	**Right breast**
Measurements on the outside of the breast		
Mean areola radius (n=14) [mm]	27.8 ± 5.5	25.6 ± 5.5
Nipple diameter (n=14) [mm]	15.7 ± 1.8	15.8 ± 2.4
Milk duct structure		
Mean number of main ducts (>0.5 mm diameter) at the base of the nipple	9.6 ± 2.9	9.2 ± 2.6
Mean depth of the main milk ducts w.r.t. the skin at the nipple base [mm]	4.50 ± 1.98	4.74 ± 1.59
The mean diameter of the main ducts [mm]	1.9 ± 0.6	2.1 ± 0.7
Mean depth of the first branch w.r.t. the skin [mm]	8.21 ± 3.96	7.20 ± 2.43
The mean diameter the first branch [mm]	1.35 ± 0.58	1.25 ± 0.68
Mean distance between first branch to the nipple base [mm]	8.20 ± 6.27	7.00 ± 3.98

VASCULATURE AND LYMPH NODES

In figures 3.3 and 3.4, the vasculature and lymph nodes are presented.

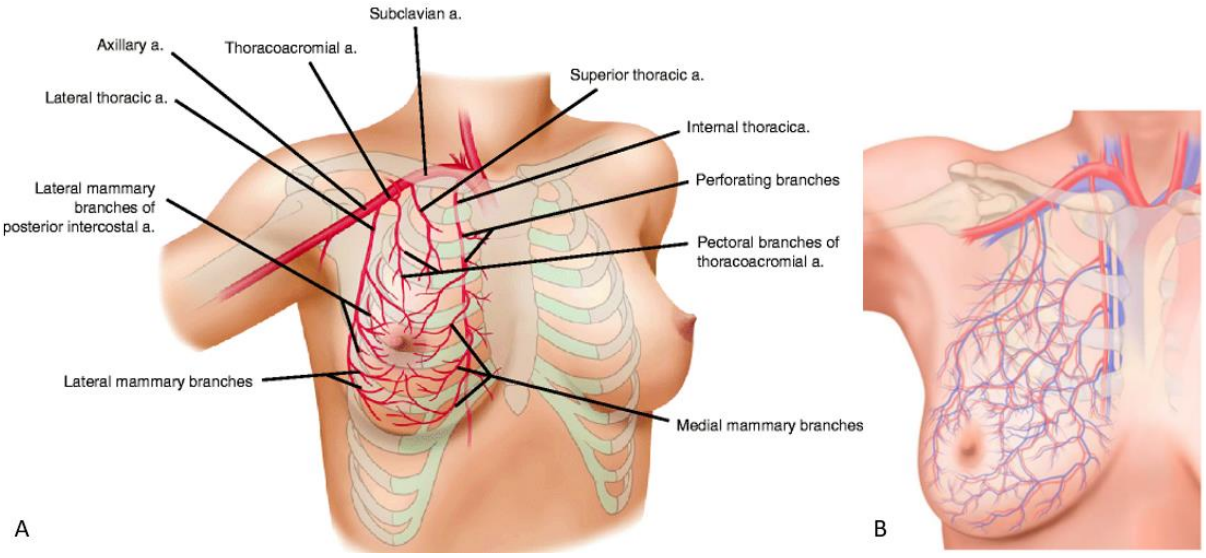

FIGURE 3.3 A: [34] **ARTERIES OF THE BREAST. B:** [32] **THE VEINS ARE PARALLEL TO THE ARTERIES IN DEEP BREAST TISSUE.**

To make blood supply more insightful, the blood supply will be split into blood supply from the medial side and from the lateral side. The arteries responsible for the medial side of the breast originate from the internal thoracic artery (also known as the internal mammary artery) [8][32], which is responsible for approximately 60% of the blood supply to the breast [8]. The main arterial supply (approximately 30% [8]) on the lateral side of the breast comes from the lateral thoracic artery [32]. Also, the thoracoacromial artery supplies blood to the upper lateral side of the breast. The intercostal arteries are approximately responsible for 5% to 10% of mammary blood supply [8].

The veins are situated close to the corresponding arteries. The small venules in the breast eventually will merge into the axillary vein or into the internal thoracic veins [35]. Superficially, the veins and venules are not accompanying the arterial supply. The superficial veins normally drain to the center of the breast and could be connected to the contralateral breast. The central drainage is generally that the veins will emerge on a periareolar circular network of veins called the circulus venosus of Haller. [32]

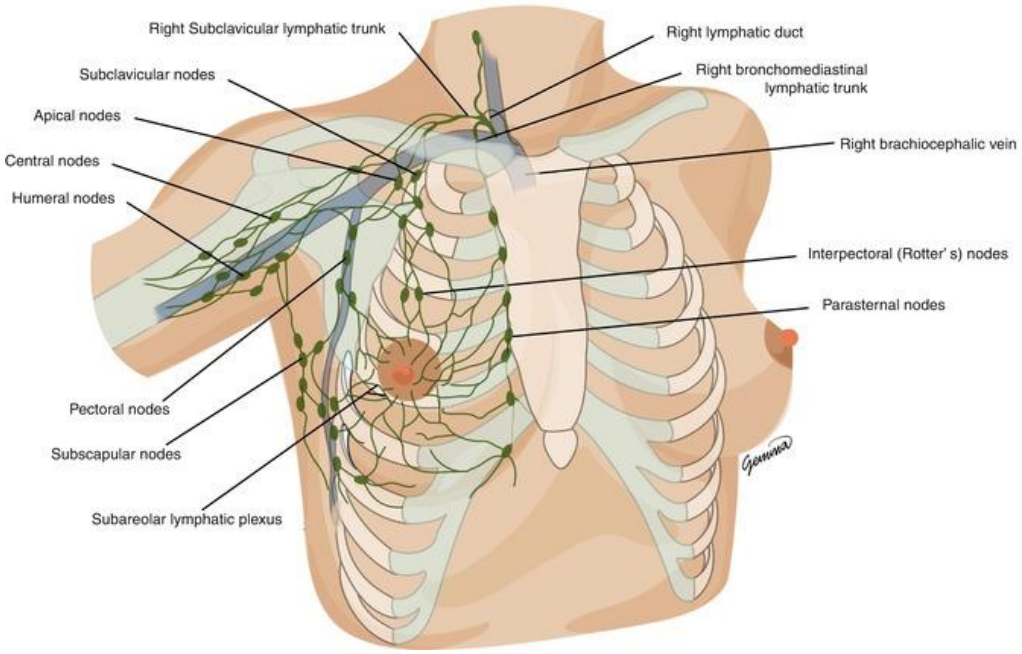

FIGURE 3.4: [36] **VEINS AND LYMPH NODES.**

The lymphatic drainage of the breast is received by three big groups of lymph nodes. The most important group of nodes are the axillary nodes. This group is located near the armpit (axilla) and divided in several other groups of lymph nodes: the pectoral, posterior, central, lateral, and apical nodes. The other lymphatic drainage nodes groups are the parasternal nodes and the posterior intercostal nodes. The skin, nipple and areola of the breast also have lymphatic drainages. The lymph from the nipple and areola drains into the subareolar lymphatic plexus. [35][32]

The change of the composition of the breast

The female breast changes over a lifetime. There are several important phases where the breast changes: during puberty, during pregnancy, during lactation, after lactation (involution) and in menopause [32]. In this research, the focus is on a healthy lactating breast that is compared to a healthy non-lactating breast. To clarify, in this case the women in the non-lactating breast subgroup, have gone through puberty, are premenopausal and not pregnant.

One of the most important differences between a lactating and a non-lactating breast is the volume of the breast. The breast volume increases during pregnancy and lactation with a mean of 211 ml to 1 month after giving birth [37]. However, it is important to note that the total breast volume can fluctuate during the menstrual cycle [38][39] (with a mean of 76 ml [26]). Another aspect of menstruation is that in the last two weeks of the menstrual cycle (luteal phase), there is an average increase of THb concentrations [39]. Thereby, for the non-lactating breast, there is also difference between pre-menopausal and post-menopausal women. Pre-menopausal women usually have a higher concentrations of hemoglobin [39].

In a lactating breast, the ratio of glandular tissue to adipose tissue is almost 2:1 [11]. This is twice as high as the same ratio for non-lactating women (1:1) [11].

Mammary blood flow also doubles during pregnancy [7][8]. Mammary blood flow (MBF), in specific the internal mammary artery and the lateral thoracic artery, is not related to milk production [8].

Physiology of breastfeeding

The suckling of the baby stimulates the anterior part of the pituitary gland to secrete prolactin in the blood. Prolactin is a hormone that is especially produced overnight in the pituitary gland. The released prolactin in the blood will have effect on the mammary glands. The mammary glands will produce milk. Prolactin is important for milk production. There are also processes inhibiting milk production. For example, In the whey of the breast milk is a polypeptide, the feedback inhibitor of lactation (FIL), which signals the epithelial cells to stop producing milk [40]. [33][41]

The suckling of the baby also stimulates another process. The posterior part of the pituitary gland will secrete oxytocin. This hormone is associated with calmness and relaxation (reduce stress). This hormone is also known as the ‘cuddling-hormone’, since it is also secreted by touches that are experienced as pleasant. This hormone will initiate the let-down reflex (milk ejection reflex, MER). The myoepithelial cells will contract, causing the milk to flow into the milk ducts. The baby will therefore be able to suck up the milk more easily, and therefore this will cause a forward feedback loop until the baby is satisfied and stops drinking. [33]

A summary of relevant milk supply characteristics is given in table 3.2. These studies given an estimate of the storage capacity. With the term ‘storage capacity’ is meant the amount of milk available to the infant when the breast is full [42][43]. Therefore, the creamatocrit (volume percentage of fat in milk) of samples is used to estimate the degree of fullness of the breast over a day. By using a regression line between the degree of fullness of the breast and the measured amount of milk intake at one breastfeeding session, the storage capacity was calculated.

TABLE 3.2: MILK TRANSFER PROPERTIES.

	Left breast	Right breast	both breasts	One of the breast
Mean normal milk production 24h				
Prime et al. [44] **– Ultrasound vs Showmilk pump experiment (n=13)**	350 ± 96 g	347 ± 79 g	697 ± 148 g	
Prime et al. [44] – Double pumping experiment (n=28)	408 ± 129 g	373 ± 132 g	781 ± 188 g	
Ramsay et al. [11] **– milk ducts ultrasound experiment (n=22)**	387 ± 101 g	407 ± 121 g		Range: 23 ml to 121 ml
Geddes et al. [8] **– temperature experiment (n=55)**	381 ml	397 ml		
Mean storage capacity				
Prime et al. [44] **– Ultrasound vs Showmilk pump experiment (n=13)**	160 ± 56 g	171 ± 37 g		
Prime et al. [44] **– Double pumping experiment (n=28)**	177 ± 63 g	151 ± 53 g		
Ramsay et al. [11] **– milk ducts ultrasound experiment (n=22)**	169 ± 51 g	175 ± 54 g		Range: 56 ml to 355ml
Mean milk intake in one breastfeeding session				
Prime et al. [44] **– Ultrasound vs Showmilk pump experiment (n=13)**	79 ± 34 ml	76 ± 21 ml		
Prime et al. [44] **– Double pumping experiment (n=28)**	64 ± 19 ml	60 ± 22 ml		
Kent et al. [6] **– weighing infant for perspective (n=184 total, of which 82 were exclusively breast feeding)**				75 ml (range: 30 ml to 135 ml)
Mean peak flow rate				
Prime et al. [44] **– Ultrasound vs Showmilk pump experiment (n=13)**	0.34 ± 0.13 g/s	0.33 ± 0.15 g/s		

The let-down reflex can be felt by 79% of the mothers [44]. During the milk ejection reflex (MER), the hemodynamics of the breast change. In the breast the overall blood volume seems to decline during the MER [45]. However, the perfusion in the skin is increasing during the MER [46][47]. The duration of this is approximately 23.7 seconds [46]. This could be due to the fact that the oxytocin hormone functions as a vasodilator. Another explanation is that the milk in the milk ducts deliver pressure to the blood to the skin. It is important to note that both breasts hemodynamics seem to react on a MER and this could be explained by the system regulation by hormones such as oxytocin [45][48][46].

FUNCTIONAL PROPERTIES OF THE BREAST

There is literature available of DOSI and other optical techniques performed on the whole breast. An overview of the functional properties is provided in table 3.3 based on Appendix – DOSI on the breast. This will mostly be used to verify the model. This table can help to gain an insight into realistic values for the functional properties while making the model. A more elaborate explanation is given in the method section of the model.

TABLE 3.3: CHECK IF THE VALUES OF THE MODEL ARE REALISTIC BY REVIEWING WHETHER THEY ARE IN THE RANGE OF THIS TABLE. THE AVERAGE VALUES ARE GIVEN FROM APPENDIX – DOSI ON THE BREAST. NOTE, FOR THE TOTAL HEMOGLOBIN CONCENTRATION, THE NON-LACTATING BREAST AND THE LACTATING BREAST ARE NAMED SEPARATELY.

Functional property	Range
THb in [µM]	Non-lactating breast:13-35 Lactating breast: 48-70
stO_2 [%]	52-87
Water [%]	21-85
Lipid [%]	10-76
scattering prefactor a [mm^{-1}]	1-2
Scattering power b	0.35-1.6

One of the articles where table 3.3 is based on found an interesting positive correlation between the scattering power and water, and water and THb [49]. This might be useful when analyzing the experiments.

OPTICAL AND FUNCTIONAL PROPERTIES OF THE LAYERS OF THE NON-LACTATING & LACTATING BREAST

This paragraph provides the anatomical properties of the breast in order to make a model of the layers of the non-lactating and lactating breast. The model should be based on the depth and the volume that DOSI can measure in the breast, combined with required theoretical characteristics of the anatomy of the lactating breast, such as the thickness of the subcutaneous fat layer below the areola. By estimating what type of tissue DOSI can measure, new absorption and reduced scattering coefficient spectra can be made. These spectra will form the model. The absorption coefficient spectra will be made using the four chromophores: water, lipid, oxyhemoglobin, and deoxyhemoglobin. The reduced scattering coefficient spectra will be based on scattering properties per layer. It is worth mentioning that not every substance of the breast is important to take in consideration to make this model of optical properties. Therefore, the taxonomy used in this model is explained in figure 3.5.

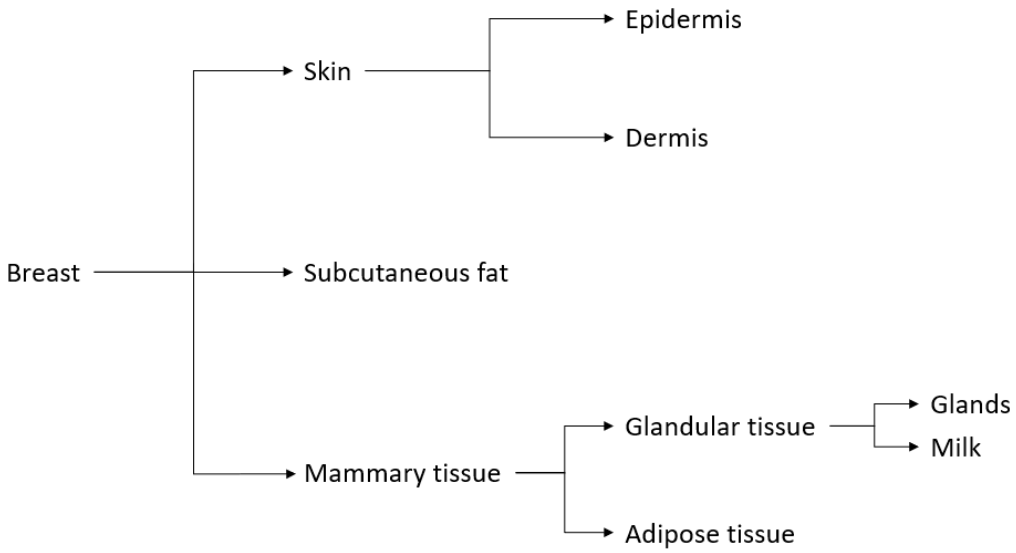

FIGURE 3.5: THE TAXONOMY OF THE BREAST THAT IS USED FOR MODELING.

BLOOD

Although blood is not a layer of the breast, DOSI outcomes heavily depend on hemodynamics and other blood properties, with two functional properties of DOSI in particular: oxyhemoglobin, and deoxyhemoglobin. Thereby,

the concentration of water should also have a dependency to the concentration of blood in the measured tissue. The hematocrit is the ratio of the red blood cells (erythrocytes) volume to the whole blood volume. The average hematocrit is 45% [50][31]. This is equivalent to 150 g/L [51][50]. For women, the hemoglobin values should be in a range between 7.5-10.0 mmol/L [52]. It is important to note that this is per heme and not for the whole molecule of hemoglobin. To consider the concentration of whole molecules of hemoglobin in figure 2.2 and this probably a concentration per heme, the concentration mmol/L should be divided by 4. Plasma and erythrocytes consist of 90% [31][50] and 66% [50] out of water, respectively. Bosschaart et al. [50] published (multiple) reduced scattering coefficient of blood, where from deduced is that of blood $a \approx 2\ mm^{-1}$, $b \approx 0.63$ and $\lambda_0 \approx 600\ nm$.

SKIN

Approximately 65% of the skin consists of water [53]. The mean skin thickness of a breast is 1.45 ± 0.30 mm [54] [30], ranging from 0.9 to 2.3 mm [55]. Another research suggested that the skin thickness ranges 0.6 to 2.7 mm [54]. The thickness of the skin is not specified for lactating women in the aforementioned report. The skin is slightly thicker than 2 mm and darker at the areola area [10]. The darkness of the areola can be due to an increase of pigmentation [32]. The study by Bosschaart et al. [15] indicated that the areola area has a higher total concentration of hemoglobin (THb) than the non-areola area [15]. Further, an empirical study of the lactating breast by Gardner et al. [56] measured a higher temperature and darker skin in the areola area in comparison to the rest of the breast. They suggest that this can be explained by a higher blood flow. They found that the temperature of the nipple itself is often lower compared to the areola.

There are multiple studies on the hemoglobin content of the skin. Based on anatomy, it is important to know what the vasculature of the skin is [54]. Some studies divide the skin into layers and make literature-based estimations dependent on the blood concentration in this layer [57][58], see table 3.4. The overall volume fraction of the blood content of the dermis is in the range of 2-12% [57]. The StO_2 of the skin is approximately 60% [57].

TABLE 3.4: THE BLOOD CONCENTRATION IN THE SKIN PER LAYER, WHERE C_{BLOOD} IS AN ESTIMATE OF THE VOLUME FRACTION OF THE BLOOD CONTENT OF THIS LAYER.

Meglinski and Matcher [57] **- Layers**	**thickness [µm]**	**C_{blood}**
Stratum corneum	20	0
Living epidermis	80	0
Papillary dermis	150	0.04
Upper blood net dermis	80	0.3
Reticular dermis	1500	0.04
Deep blood net dermis	100	0.1
Subcutaneous fat	6000	0.05

Melanin is present in the epidermis, causing the skin to have a darker color. With DOSI experiments done on the skin, melanin can be an important chromophore [25][59]. However, since in this experiment the source-detector distance is bigger, there will be measured more deeply into the tissue. Therefore, there is expected that the measurement will be less sensitive for the more superficial layer where melanin is present. Moreover, an extra chromophore will make the fitting to the chromophores to the absorption coefficient complex and maybe less reliable.

There are several papers reporting on the scattering properties of the skin. These papers are summarized in table 3.5.

TABLE 3.5: THE SCATTERING PROPERTIES OF THE SKIN. IN THESE ARTICLES, EXCEPT FOR JONASSON ET AL., THE VALUES OF A AND B WHERE NOT DIRECTLY GIVEN. INSTEAD, THE EQUATION IS FITTED TO THE REPORTED VALUES OF μ_s' IN THE ARTICLES TO OBTAIN a AND b. IN JONASSON ET AL., THE EQUATION $a\left((1-\rho)\left(\frac{\lambda}{\lambda_0}\right)^{-b}+\rho\left(\frac{\lambda}{\lambda_0}\right)^{-4}\right)$ IS USED TO OBTAIN THE SCATTERING PROPERTIES. HEREBY $\rho = 0.277 \pm 0.144$.

Article	Measured on	amount of subjects n	$a\ mm^{-1}$	b	$\lambda_0\ nm$
Tseng et al. [59]	Skin (in vivo)	15	2.2 (1.8-2.5)	1.83	650
Jonasson et al. [60]	Skin (in vivo)	1734	1.93 ± 0.39	0.940 ± 0.487	600
Shimojo et al. [58]	Epidermis (samples)	15	5.55 ± 1.25	1.28	632
Shimojo et al. [58]	Dermis (samples)	15	3.06	1.59	632
Mignon et al. [61] **(review)**	Epidermis of different papers	28	3.3	1.25	600
Mignon et al. [61] **(review)**	Dermis of different papers	10	3	1	600

SUBCUTANEOUS FAT

Beneath the skin is subcutaneous fat (often referred to as subcutaneous adipose tissue, SAT). This layer is sometimes seen as a section of the skin. However, in this report, the subcutaneous fat layer is an individual layer and not interpreted as a part of the skin. The range of the thickness of subcutaneous fat layer is approximately between 2 and 16 mm [62] [63] [49] [64]. Thereby, one of the articles notes that the amount of subcutaneous adipose tissue can range from only a couple of kilograms to more than 50% of the body weight [63]. There is a positive correlation between body mass index (BMI) and SAT [65]. SAT consists mostly of fat (85%), but still contains water (15%) [66].

The blood concentration reported by Meglinski and Matcher [57] in the subcutaneous fat layer is explained in the previous section. Another research reported a value of 19.9 ± 15.8 µM THb of which 13.4 ± 11.7 µM oxyhemoglobin and 6.88 ± 6.31 µM deoxyhemoglobin in the abdomen [67]. The stO_2 of this layer is 80% [68].

Ramsay et al. [11] mentioned that the subcutaneous fat layer increases gradually if the radius with respect to the nipple increases. For the overall breast, the measurements show that 24 ± 9% on the left and 22 ± 10 % on the right breast is subcutaneous fat. Ramsay et al. specify values for the area in a 30 mm radius with respect to the nipple. For this region, 17 ± 5.3% of the left and 18 ± 7.6 % of the right breast is subcutaneous fat.

Besides, there are several papers reporting on the scattering properties of the subcutaneous fat. These papers are summarized in table 3.6.

TABLE 3.6: SCATTERING PROPERTIES OF SUBCUTANEOUS FAT. IN THESE ARTICLES THE VALUES OF a AND b WHERE NOT DIRECTLY GIVEN. INSTEAD, THE EQUATION 2.4 IS FITTED TO THE REPORTED VALUES OF μ_s' IN THE ARTICLES TO OBTAIN a AND b.

Article	amount of subjects n	$a\ mm^{-1}$	b	$\lambda_0\ nm$
Shimojo et al. [58]	15	1.72 ± 0.30	0.84	632
Mignon et al. [61] **(review)**	10	1.3	0.51	600

MAMMARY TISSUE

For the differences in functional properties between glandular tissue and adipose tissue, two studies have been found, namely Nachabé et al. [51] and Brooksky et al. [19]. Peters et al. [69] also reported optical properties of this tissue. The values are summarised in tables 3.7 and 3.8. Nachabé et al. [51] is a study carried out in 2011 which applied DOSI on tissue samples. For glandular tissue, they gathered 189 samples from 23 subjects and, while for adipose tissue they gathered 327 samples from 43 subjects. The values noted in table 3.7 and 3.8 are interpreted from figure 4 of this article. Brooksby et al. [19] is a study from 2005 and contains an in-vivo case

study that adopted a combination of two modalities: near infrared (NIR) tomography together with magnetic resonance imaging (MRI). In 1990, Peters et al. [69] carried out a study on 7 samples of adipose tissue and 8 samples of glandular tissue.

TABLE 3.7: THE FUNCTIONAL PROPERTIES OBTAINED FOR GLANDULAR TISSUE. HEREBY, SOME REMARKS ARE MADE. NACHABÉ ET AL. USES A SLIGHTLY DIFFERENT FORMULA FOR THE SCATTERING PROPERTIES: $\mu_s'(\lambda) = a\left(\rho\left(\frac{\lambda}{\lambda_0}\right)^{-b} + (1-\rho)\left(\frac{\lambda}{\lambda_0}\right)^{-4}\right)$, THE VALUE FOR $\rho = 0.85$. THEREBY, PETERS ET AL. DOES NOT MENTION VALUES FOR THE FUNCTIONAL SCATTERING PROPERTIES BUT A μ_s'. FROM THIS μ_s', THE EQUATION 2.4 IS USED TO OBTAIN a AND b.

Article	blood volume fraction %	StO_2 %	Lipid %	Water %	$a\ mm^{-1}$	b	$\lambda_0\ nm$
Nachabé et al. [51]	0.2±0.2	55±20	5±10	50±10	0.7 (0.5-0.8)	0.4 (0.2-0.8)	800
Brooksky et al. [19]	1.25	65±5	-	55	0.9 (0.8-1.0)	0 (-0.1-0.1)	?
Peters et al. [69]	-	-	-	-	2.44±0.58	1.77	540

TABLE 3.8: THE GLANDULAR PROPERTIES FOUND FOR ADIPOSE TISSUE. ONCE AGAIN, SOME REMARKS ARE MADE. NACHABÉ ET AL. USES A SLIGHTLY DIFFERENT FORMULA FOR THE SCATTERING PROPERTIES: $\mu_s'(\lambda) = a\left(\rho\left(\frac{\lambda}{\lambda_0}\right)^{-b} + (1-\rho)\left(\frac{\lambda}{\lambda_0}\right)^{-4}\right)$, THE VALUE FOR $\rho = 0.7$. THEREBY, PETERS ET AL. DOES NOT MENTION VALUES FOR THE FUNCTIONAL SCATTERING PROPERTIES BUT A μ_s'. FROM THIS μ_s', THE EQUATION 2.4 IS USED TO OBTAIN a AND b.

article	blood volume fraction %	StO_2 %	Lipid %	Water %	$a\ mm^{-1}$	b	$\lambda_0\ nm$
Nachabé et al. [51]	0.4±0.7	45±50	80±20	8±4	0.4 (0.35-0.55)	0.4 (0.3-0.7)	800
Brooksky et al. [19]	0.75	80±3	-	15	1 (0.7-1.2)	0.75 (0.5-1.1)	-
Peters et al. [69]	-	-	-	-	1.03±0.19	0.52	540

Specifically, the water-containing property of glandular tissue is often used for imaging modalities such as MRI [70] and mammography [30]. The water content makes it possible to differentiate glandular tissue from the surrounding tissue. Furthermore, collagen can be present in fibrous tissues such as mammary glands. In an absorption spectrum, collagen causes a peak at a wavelength of 900 nm.

In a lactating breast, the ratio of glandular tissue to adipose tissue is almost 2:1 [11], twice as high as for non-lactating breast. To quantify, the mean ratio of glandular tissue volume to total breast volume found using mammography is approximately 30% of the normal breast [9][10]. Ramsay et al. [11] found this ratio to be $62 \pm 11\%$ and $64 \pm 13\%$ for the left and right lactating breast respectively. The ratio intraglandular fat to glandular tissue of the lactating breast is 1:10 [11]. In mammography, often it is assumed that 50% of the breast is glandular tissue and 50% is adipose tissue of the non-lactating breast. However, a mean of 19.3% glandular tissue is also found [71]. In this study, where the youngest participant was 35 years old, they also suggest that the amount of glandular tissue declined with age [71]. Important is that Ramsay et al. used ultrasound and tried not to compress the breast, while during mammography the breast is compressed, which can cause differences in volume percentages.

HUMAN BREAST MILK

The composition of milk changes much over time even during a breastfeeding session [72]. The density of human milk is approximately 1.03 g/ml [73]. Therefore, the density of human milk is probably variable as well. From the chromophores of the chromophores sheet in figure 2.2, human breast milk contains the chromophores fat and water. 87% of human breast milk is water and 3.8% is fat [2][74][72]. The range of fat in human milk is large: fore

milk has an average of 1% fat [75][76], but can be as low as 0.4% [76], and hind milk has an average of 5% fat [75][76], but also values of 10% [76] are reported.

There are other known components of milk that could influence optical properties. Casein can cause scattering at the beginning of the detected spectrum (between 650 and 900 nm) [77][78]. In addition, the presence of casein in breast milk changes during the lactation period [2]. At the beginning of lactation, the whey/casein ratio ranges between 70/30 and 80/20. However, in a later phase of lactation, this decreases to 50/50. Another chromophore in human breast milk is riboflavin (Vitamin-B2) [76]. This can cause a slight increase between 600 and 800 nm in the absorption spectrum [78]. Furthermore, milk contains beta-carotene, which is an important chromophore for milk in the visible spectrum. Beta-carotene is also present in glandular tissue [51], hence this is not necessarily an indication for the presence of milk in glandular tissue.

The scattering properties of milk are fairly complex. The size, distribution and amount of fat globules and casein micelles heavily influence the scattering properties of milk and are very variable, not only between mothers, but also for fore milk, bulk milk and hind milk [76][79]. Casein is for 29% responsible for the reduced scattering coefficient of milk [79]. The scattering properties found are summarized in table 3.9. One study of human breast milk is included from Veenstra et al. [76]. In this study is denoted that the reduced scattering coefficient can variate with a factor 6 for bulk milk. Both Stokers et al. [78] and Aernouts et al. [77] carried out experiments on dairy cow milk.

TABLE 3.9: SCATTERING PROPERTIES OF MILK, WHICH ARE ESTIMATED FROM THE REDUCED SCATTERING SPECTRA IN LITERATURE.

Article	**Measured on**	**amount of subjects n**	$a\ mm^{-1}$	b	$\lambda_0\ nm$
Veenstra et al. [76]	Human bulk milk	14	1	1.17	450
Veenstra et al. [76]	Human fore milk	14	0.5	0.64	450
Veenstra et al. [76]	Human hind milk	14	1.7	0.36	450
Stocker et al. [78]	Dairy cow milk	3	1.1	0.72	400
Aernouts et al. [77]	Dairy cow milk	60	3 (1.5-5.0)	0.99	600

4. THE MODEL

The purpose of this chapter is to answer the following research question: *"How can a model be developed that predicts the outcomes of DOSI on lactating & non-lactating breasts, while accounting for biological variability between subjects and for physiological processes?"* The question can be divided in several parts to see what the requirements for the model are.

The model should "predict the outcomes of DOSI". The DOSI experiments will provide optical properties and functional properties of the measured tissue. The measured tissue is of the lactating and non-lactating breast. Thereby, there should be a distinction between the areola area and the non-areola area. Since the focus of the research is relating DOSI to milk transfer, the model should include the difference before (pre), during (peri) and after (post) a breastfeed. As already explained in the introduction, the choice is made to develop a digital model in MATLAB R2018a. Thereby, this model will rely on diffusion theory and the anatomical and physiological properties of the breast, such as the thickness of the subcutaneous fat layer below the areola. The purpose of this model will be the prediction of the outcomes of DOSI as well as potentially its ability to predict milk transfer and possibly even milk supply. Further, this model could have other applications such as predicting outcomes of other optical techniques on the lactating breast or designing a phantom of the lactating breast.

First, a model will be made of the average lactating and non-lactating breast. Then, the range of all the variabilities will be considered: the anatomical variability between subjects, and the changes caused by the physiological processes. In chapter 6. Validation and Prediction, the model will be compared to the outcomes of the experiments.

METHOD

AVERAGE BREAST

In figure 4.1, a flowchart shows how the model was developed. It is necessary to consider all the steps for the lactating breast (pre and post expression) and for the non-lactating breast, as well as to distinguish the areola area from the non-areola area. This model is based on the anatomy of the breast. The gathered information of the anatomy can be found in the chapter 3. Theory: The Breast. Below, all the steps are more extensively discussed. Subsequently, all the steps are executed, and examples are given.

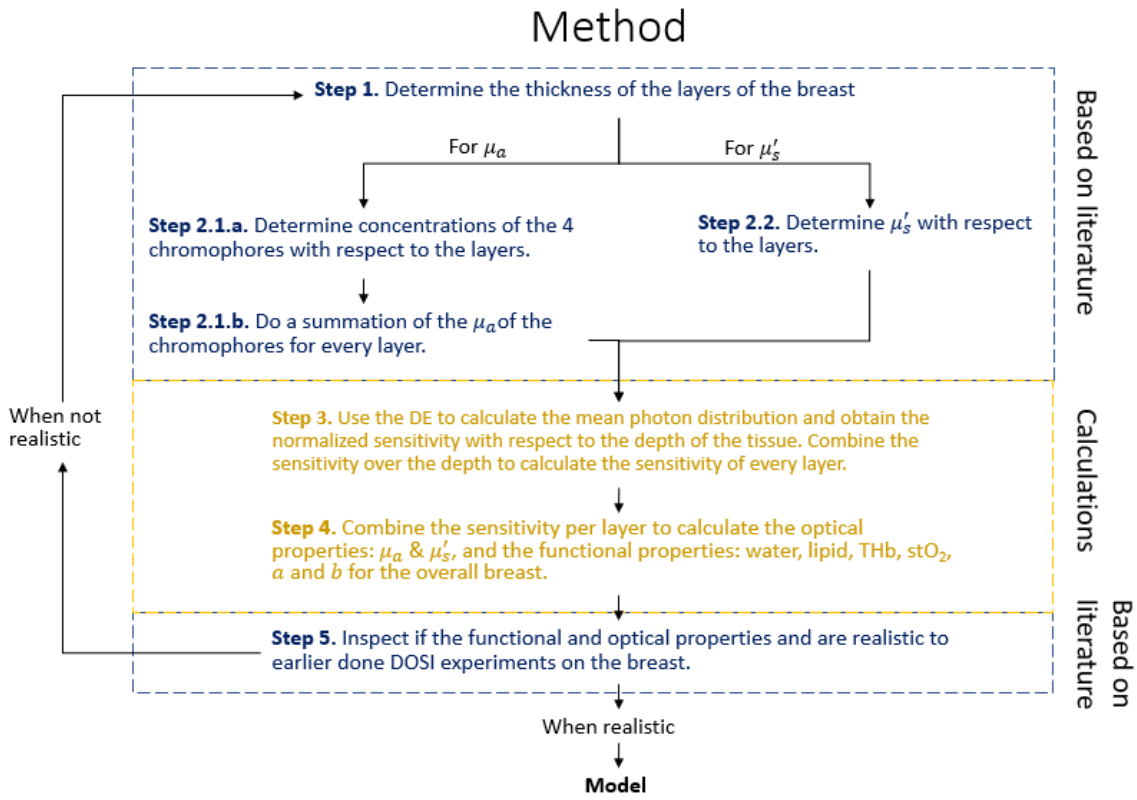

FIGURE 4.1: FLOWCHART OF THE METHOD OF HOW THIS MODEL IS DEVELOPED.

STEP 1 DETERMINE THE THICKNESS OF THE LAYERS OF THE BREAST.

Based on the anatomy of the breast, the measured light propagates from superficial to deep layers first through the skin, then through subcutaneous fat and then through glandular tissue (lobules) with intraglandular fat. The layer thicknesses are different for the areola area and the non-areola area. Not only is the thickness of the layers included in this step, but also other configurations of the breast, such as the amount of milk storage and the ratio glandular tissue to adipose tissue. For the lactating breast, it is important to know how much of the glandular tissue can hold milk. This should be determined for a full breast (before a breastfeed) and after a breastfeed. The layers of the breast are shown in figure 4.2.

Some assumptions are made:

- The skin and subcutaneous fat layer are assumed the same depth for the lactating and the non-lactating breast.
- Another assumption is that retroglandular fat is not measured with DOSI, since this lays too deep into the tissue to be measured by DOSI, see figure 4.2.
- The mammary tissue consists of lobules with glandular tissue and in between the lobules is intraglandular fat (adipose tissue). Since DOSI is not capable to detect the locations of these lobules, a homogenous mixture of glandular and adipose tissue in the mammary tissue layer is assumed.
- Breastfeeding deforms the breast. How this deformation works precisely is beyond the scope of this study. For example, the deformation of the pump is a non-linear process [80][81]. Therefore, there is assumed that the volume of the ejected milk is going out of the breast during a breastfeed (although probably some milk is produced as well during a breastfeeding session). Hereby, the empty space that is left post breastfeeding due to milk ejection is filled by glandular and adipose tissue.

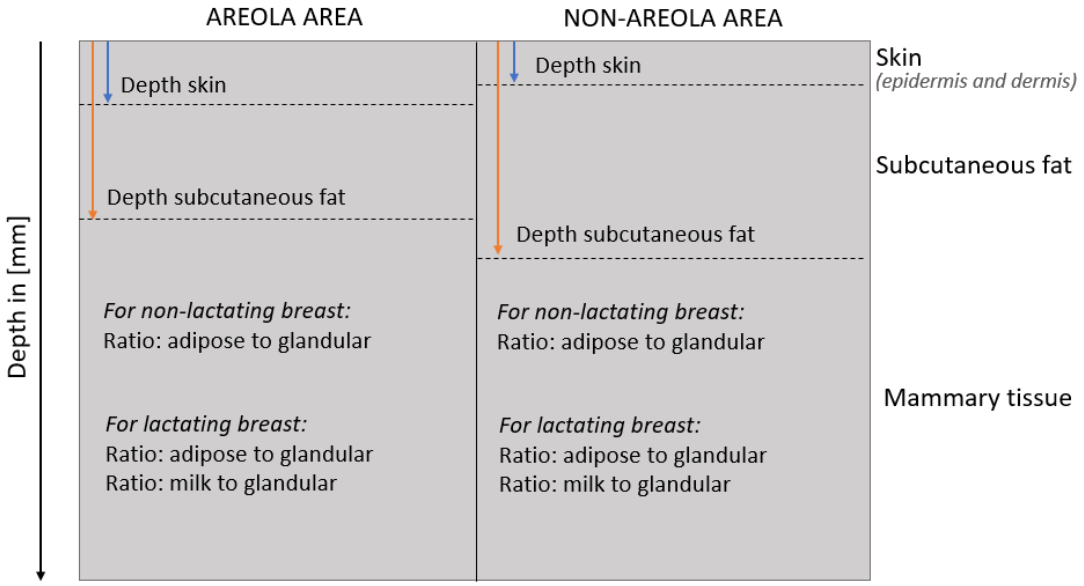

FIGURE 4.2: MODEL OF THE AVERAGE BREAST: DEPTHS AND RATIOS.

In the paragraph in chapter 3: Optical properties of the layers of the non-lactating & lactating breast the information found in the literature is reported. Some of these values can be directly used as input values. Other input values are derived from literature values. The model parameters and the input values for an average breast are shown in table 4.1.

TABLE 4.1: THE MODEL PARAMETERS FOR AN AVERAGE BREAST: DEPTH AND RATIOS

Model parameters		**Input values**
Skin depth	Areola	2.0 mm
	Non-areola [10][55]	1.45 mm
Subcutaneous fat depth	Areola	5.4 mm
	Non-areola	6.7 mm
Ratio adipose tissue to glandular tissue	Lactating [11]	1:10
	Non-lactating	1:2
Ratio milk to glandular tissue (lactating breast)	Storage (170 ml [44][11])	35.7 %
	Breastfeeding session (70 ml [44][6])	14.7 %

Below is explained what the range in table 4.1 is based on.

Depth skin: The values of the skin thickness are directly copied from the literature. The skin on the areola should be thicker than normal skin.

Depth subcutaneous fat: To calculate an approximate thickness of subcutaneous fat, the thickness of the total breast is needed. The average layer thicknesses are measured for the overall breast and the areola area. The total thickness of the left and right lactating breast is 24.5 ± 4.0 mm and 25.1 ± 5.1 mm, respectively [11]. Since the average breast is less than 4 cm deep in supine position [30] and ultrasound suppressed the breast a bit, the total breast depth is estimated at 3 cm in the areola area, while the non-areola area should be less and is estimated at 2 cm, which fits well with the values found by Ramsay et al. Ramsay et al. [11] does specify values for the area in a 30 mm radius with respect to the nipple. This is assumed to be the areola. For this region 17% of the left and 18% of the right breast is subcutaneous fat. 18% of 3 cm depth of the tissue is 5.4 mm [11]. Further, it is mentioned that the subcutaneous fat layer increases gradually if the radius increases with respect to the nipple. Thus, the layer subcutaneous fat should be thinner at the areola area than at the non-areola area. For the non-areola area is therefore the standard deviation added up to the mean, 24 ± 9% of the left and 22 ± 10 % of the right breast. This will give an approximation of the subcutaneous fat thickness of $\frac{(24+9)+(22+10)}{2} = 33\%$.

33% of 2 cm of the non-areola area is 6.7 mm [11]. The values are in range with 2-16 mm [62] [63] [49] [64] and are therefore assumed to be the same for the average non-lactating breast.

Ratio adipose tissue vs glandular tissue: The ratio intraglandular fat to glandular tissue of the lactating breast is based on literature. This is different for the non-lactating breast, since the ratio adipose tissue to glandular tissue is twice as high [11], the ratio is approximated as 1:5. For the non-lactating breast also the ratio 4:5 is reported [71]. At step 5, it was concluded that water values were too high and lipid values were too low for a ratio of 1:5, therefore the ratio was set to 1:2. The ratio adipose tissue to glandular tissue is assumed to be the same for the areola area and the non-areola area in both lactating and non-lactating women for the average breast model.

Ratio milk vs glandular tissue: This variable is only applicable to the lactating breast and assumed to be the same for the areola area and for the non-areola area. 755 ml is the assumed average volume of the lactating breast. Since, the average growth of the breast together with the average volume of the breast gives $\frac{561+567}{2} + 211 = 755\ ml$ [26] [37]. 63% of the lactating breast is glandular tissue [11], which means that 476 ml is glandular tissue. According to table 3.2, approximately 70 ml is the mean milk intake in one breastfeeding session [44][6] and the average milk storage of a breast is approximately 170 ml [44][11]. Then, the percentage of milk stored in the glandular tissue area is $\frac{170}{476} \approx 35.7\%$ and the percentage of milk that is extracted from the breast during a breastfeed is $\frac{70}{476} \approx 14.7\%$.

STEP 2.1.A. THE CONCENTRATIONS OF THE 4 CHROMOPHORES WITH RESPECT TO THE LAYERS.

In this step, the most suitable values of these concentrations are chosen as the input variable of the model of the average breast. It is necessary to find out the concentrations of lipid and water in percentage of the tissue volume. Furthermore, the blood concentrations, the concentration of THb in the blood, and stO_2 of the blood should be determined. It is also possible in some cases to directly find concentrations for deoxyhemoglobin and oxyhemoglobin in the tissue volume, but this is less common. Again, the values of these concentrations are based on the literature chapter 3: Optical properties of the layers of the non-lactating & lactating breast.

For every chromophore, a schematic figure of the layers of the breast is given. The values of the input variables of these concentrations for the model of the average breast are reported in a corresponding table. Thereby, a short explanation is given of how these values are determined.

TOTAL HEMOGLOBIN CONCENTRATIONS (THB)

The concentration THb present in the skin is calculated using the blood volume fraction mentioned in Meglinski and Matcher [57]: The epidermis consist 0% of blood and the (thickest part) of the dermis consist 4% of blood. For the mammary tissue, the blood volume fraction is deduced from Brooksky et al. [19]: 0.75% in adipose tissue and 1.25% in glandular tissue. For the subcutaneous fat layer, this was slightly more difficult, since literature values often resulted in a too high hemoglobin value in total, see step 5. Therefore, this blood volume percentage is set to 0.5% in subcutaneous fat. This is multiplied with the average concentration of hemoglobin (2.19 mM) in the blood [52], the total hemoglobin concentration is calculated, see table 4.2 and figure 4.3. For the lactating breast, the assumption is made that blood supply is twice as high as in the non-lactating breast [7][8].

TABLE 4.2: THE MODEL PARAMETERS FOR AN AVERAGE BREAST: TOTAL HEMOGLOBIN CONCENTRATIONS.

THb	Lactating breast [µM]	Non-lactating breast [µM]
Epidermis	0	0
Dermis	175.0	87.5
Subcutaneous fat	21.9	10.9
Mammary tissue	50.5	21.4
Adipose tissue	32.8	16.4
Glandular tissue	52.5	26.3

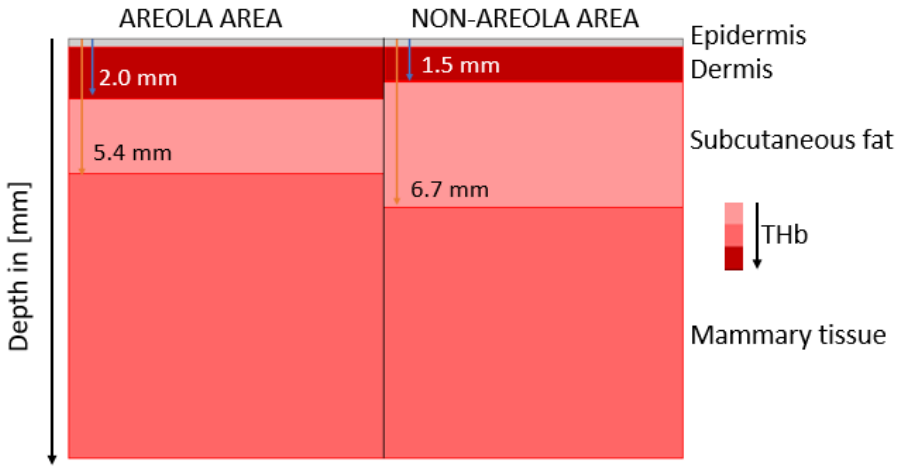

FIGURE 4.3: THE MODEL OF THE AVERAGE BREAST: TOTAL HEMOGLOBIN CONCENTRATION. THIS FIGURE IS SHOWN TO ILLUSTRATE THE DIFFERENCE OF CONCENTRATIONS BETWEEN THE DIFFERENT LAYERS. THE VALUES OF THB ARE REPORTED IN TABLE 4.2.

An important detail is that the skin is not a homogeneous layer at all with respect to blood. Blood vessels are ordered in networks on a certain depth. These networks are called plexus. However, the diffusion equation limited our model to $l_{tr} \approx 1\ mm$ and the layers should not be smaller than that. Therefore, we assume a homogeneous layer of blood in the dermis. Although the epidermis is thinner than 1 mm, the detector is sensitive for THb close to it. Therefore, the epidermis is still implemented in this model. For another model, for example using Monte Carlo, more layers can be used to better simulate the skin (see Appendix – Layers total hemoglobin).

OXYGEN SATURATION (StO_2)

The percentage stO_2 is the percentage of oxyhemoglobin in THb, see equation 2.2. The saturation of the blood is variable, since it depends on how much oxygen is used in the body. First, stO_2 of the skin was used at 60% [57]. However, this was too low, see step 5. An explanation for this is that this article uses samples. This situation can be compared to mammary tissue, where Nachabé et al. [51] uses samples and Brooksky et al. [19] measured in vivo. Note that for Nachabé et al. [51] the stO_2 is also lower than for Brooksky et al. [19]. Therefore, an educated guess is made and the skin is approximately 80% saturated and the values of Brooksky et al. [19] are used for adipose tissue and glandular tissue. Subcutaneous fat is set to 80 [68]. In figure 4.4 and table 4.3, the stO_2 of the average breast is shown.

TABLE 4.3: THE MODEL PARAMETERS FOR AN AVERAGE BREAST: OXYGEN SATURATION.

stO_2	Lactating breast %	Non-lactating breast %
Skin	80.0	80.0
Subcutaneous fat	80.0	80.0
Mammary tissue	66.5	72.5
Adipose tissue	80.0	80.0
Glandular tissue	65.0	65.0

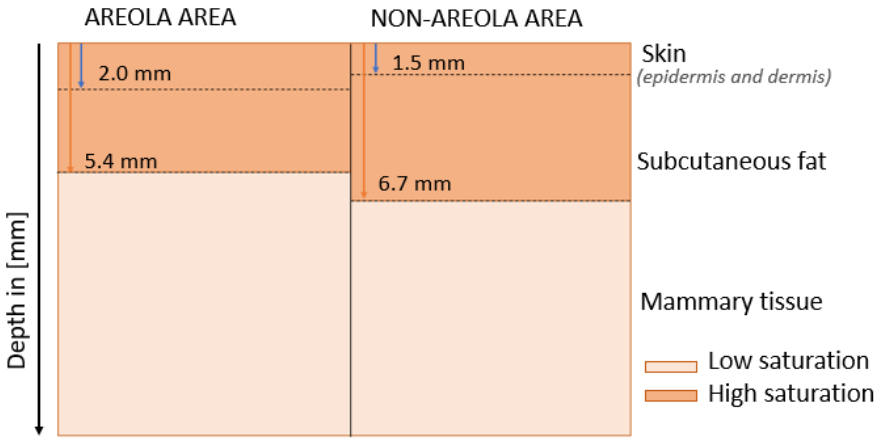

FIGURE 4.4: THE MODEL OF THE AVERAGE BREAST: OXYGEN SATURATION. THIS FIGURE IS SHOWN TO ILLUSTRATE THE DIFFERENCE OF STO_2 BETWEEN THE DIFFERENT LAYERS. THE VALUES OF STO_2 ARE REPORTED IN TABLE 4.3.

WATER AND LIPID CONCENTRATIONS

The chromophore sheet in figure 2.2 contains the two chromophores water and lipid. Most of the values of this layers are directly obtained via literature of the literature, see table 4.4.

TABLE 4.4: CONCENTRATION WATER AND LIPID USED IN THE MODEL. *THIS VALUE IS AN EDUCATED GUESS. THE GUESS IS BASED ON WHEN SEARCHING FOR THE CONCENTRATION OF LIPID IN THE SKIN, THEY MOSTLY REFER TO THE SUBCUTANEOUS FAT LAYER.

Model parameters	Input values
Concentration water in the skin	65% [53]
Concentration lipid in the skin	0% *
Concentration water in subcutaneous fat	15% [66]
Concentration lipid in subcutaneous fat	85%[66]
Concentration water in glandular tissue	50% [51]
Concentration lipid in glandular tissue	5% [51]
Concentration water in adipose tissue	8% [51]
Concentration lipid in adipose tissue	80% [51]
Concentration water in milk	87% [2]
Concentration lipid in milk	3.8% [2]

Note that the lactating breast has twice as much blood supply [7][8]. This also influences the water content of the blood. With the standard hematocrit, it is possible to calculate how much water is in the blood.

$$water_{\ blood}[\%] = \frac{THb_{experiment}[mM]}{THb_{blood}[mM]}\Big((1-hct)\ water_{plasma} + hct\ water_{RBC}\Big)100 \qquad (4.1)$$

In this equation the values for hct (hematocrit), the percentage water in plasma, the percentage water in the RBC (red blood cells) and hemoglobin concentrations are considered average [50]. The ratio $\frac{THb_{experiment}[mM]}{THb_{blood}[mM]}$ reflects how much of the measured volume consist of blood. Substituting the average values in the equation will give:

$$water_{\ blood}[\%] = \frac{THb_{experiment}[mM]}{2.19}\ (0.55 * 0.9 + 0.45 * 0.66) * 100$$

This is in the order of 1 or 2% added to the water volume, which is small in comparison to the water content of the most layers of the breast. Furthermore, the lactating breast contains milk. 87% of milk is water and 3.8% of

milk is fat [2]. This means that post breastfeeding, the glandular tissue should contain 5.5% less water and 1.2% more fat. This results in table 4.5 and table 4.6 and in figure 4.5.

TABLE 4.5: THE MODEL PARAMETERS FOR AN AVERAGE BREAST: LIPID CONCENTRATION.

lipid	Lactating breast %	Non-lactating breast %
Skin	0.0	0.0
Subcutaneous fat	85.0	85.0
Mammary tissue	Pre: 13.7 post: 14.9	42.5

TABLE 4.6: THE MODEL PARAMETERS FOR AN AVERAGE BREAST: WATER CONCENTRATION.

water	Lactating breast %	Non-lactating breast %
Skin	69.9	65.0
Subcutaneous fat	15.6	15.0
Mammary tissue	Pre: 74.7 post: 69.2	29.0

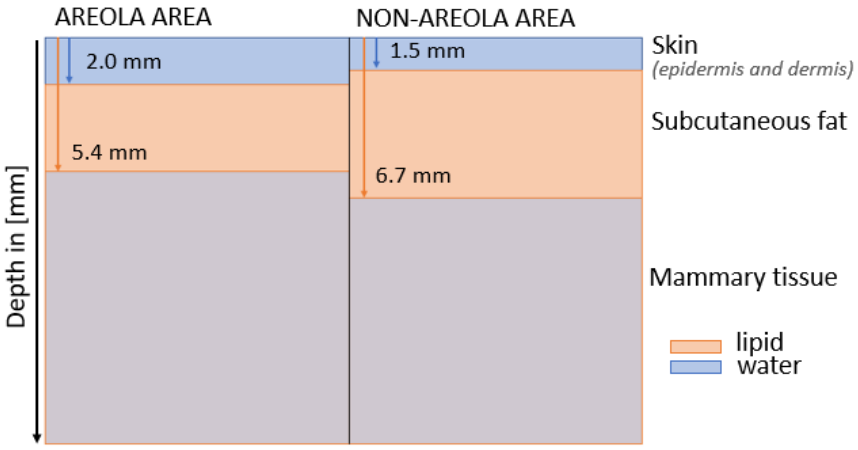

FIGURE 4.5: THE MODEL OF THE AVERAGE BREAST: WATER AND LIPID CONCENTRATION. THIS FIGURE IS SHOWN TO ILLUSTRATE THE DIFFERENCE OF CONCENTRATIONS BETWEEN THE DIFFERENT LAYERS. THE VALUES OF LIPID CONCENTRATION ARE REPORTED IN TABLE 4.5 AND THE WATER CONCENTRATION IN TABLE 4.6.

STEP 2.1.B A SUMMATION OF THE μ_a OF THE CHROMOPHORES OF EVERY LAYER.

The concentration of every chromophore is determined per layer for the non-lactating and the lactating breast. Now, it is possible to add the absorption coefficient spectra (see figure 2.2) in the right concentration to calculate the absorption coefficient spectra per layer:

$$\mu_{a,l} = \sum_{i=1}^{4} C_i * \mu_{a,i} \ , \tag{4.2}$$

where $\mu_{a,i}$ is the absorption coefficient spectra for a chromophore "i", C_i is the concentration of a chromophore "i", and $\mu_{a,l}$ is the average model of the breast in the layer "l". This will result in figure 4.6.

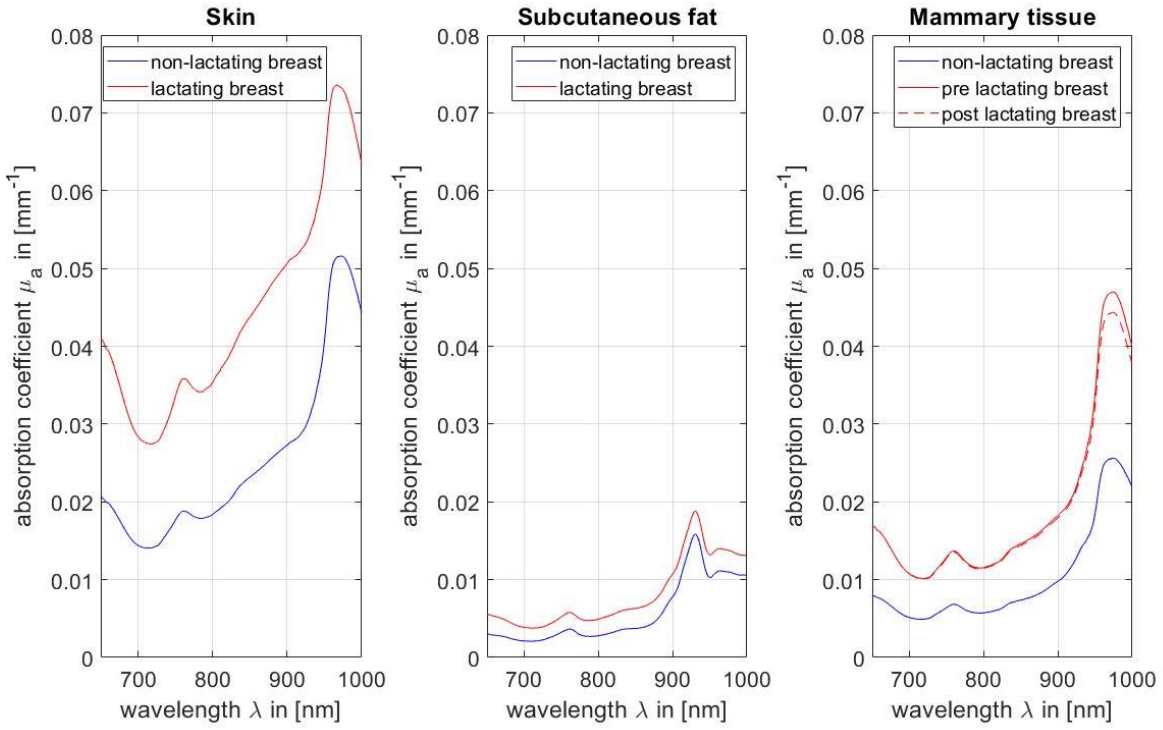

FIGURE 4.6: ABSORPTION COEFFICIENT μ_a FOR EVERY LAYER OF THE AVERAGE BREAST.

STEP 2.2. μ_s' WITH RESPECT TO THE LAYERS.

For every layer of the breast, it is necessary to find a suitable μ_s'. This can also be based on parameters for formulae to calculate μ_s'. Again, the values could be found in chapter 3: Optical properties of the layers of the non-lactating & lactating breast and the most suitable one should be chosen as input. Multiple reduced scattering spectra are available for the different layers of the skin. The choice of the spectrum per layer for the model is based on:

- Preferably 'in vitro'
- Preferably a high 'n' number of subjects
- For the skin: preferably multiple skin types (high variability)
- Preferably the measured layer is originating from the breast.

Eventually, the reduced scattering spectrum of Jonasson et al. [60] for skin, Mignon et al. [61] for subcutaneous fat, Nachabé et al. [51] for mammary tissue and Veenstra et al. [76] for (bulk) milk are chosen. Note, not much is known about the lactating breast (only 1 paper with 1 case study [15] available over the optical properties of the lactating breast). All spectra are plotted using equation 2.4. For some spectra such as the milk spectra, since they are not measured in the NIR, the spectra are extrapolated.

Some reduced scattering coefficient spectra are a combination of different literature spectra according to equation 4.3:

$$\mu_{s,l}' = \sum_{g=1}^{z} \mu_{s,g}' * r_g \ , \tag{4.3}$$

where, $\mu_{s,g}'$ is the reduced scattering coefficient per tissue type g and r_g is the ratio for this tissue type g to the total amount of tissue in this layer. Since the lactating breast contains more blood, an extra reduced scattering

coefficient spectrum [76][82] is added to mimic this. Mammary tissue consists of glandular tissue, adipose tissue, blood and, in case of the lactating breast, milk.

This results in figure 4.7, where the reduced scattering coefficient spectra per layer are shown.

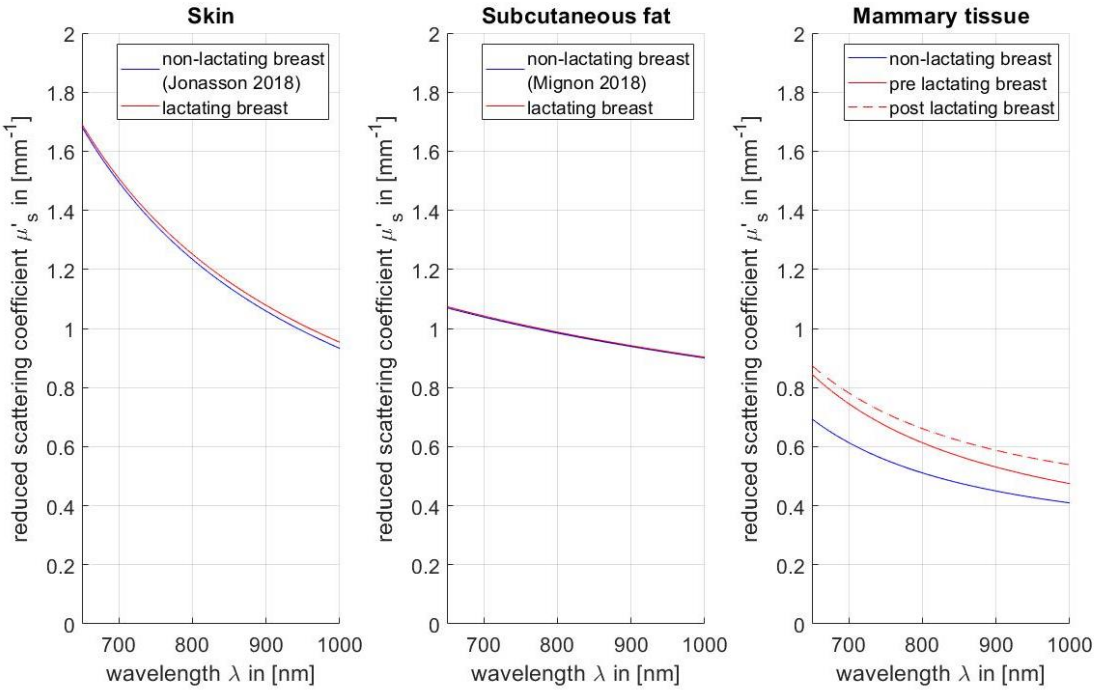

FIGURE 4.7: REDUCED SCATTERING COEFFICIENT μ_s' FOR EVERY LAYER OF THE AVERAGE BREAST MODEL.

STEP 3 THE CALCULATION OF SENSITIVITY OF EVERY LAYER.

The light propagation is calculated in 2D according to the diffusion equation, using the script on the BMPI's P-drive of the author with the directory masteropdracht_Lactation_and_DOSI\Matlab\model \DepthSensitivity_OLA. An email of Ola Abdalsalam (O. Abdalsalam, personal communication, May 12 & November 12, 2020) provided this script to calculate normalized amplitude sensitivity of the 2D distribution of the propagation of light. The script used the DE to calculate the light propagation. This script is used for other DOSI analyses and research.

To model light propagation distribution with the DE, four input values are needed: a μ_s', a μ_a, a modulation frequency and a source-detector distance. The source-detector distance will be set at a constant value of 28 mm. To simulate steady state illumination, the modulation frequency is zero. With these input values set, the light propagation only depends on μ_a and μ_s'. The higher μ_a and μ_s', the more light will be attenuated and the less deep the light will propagate in the tissue (the smaller the light propagation distribution). It is good to keep in mind that the DE cannot be used within the length of the mean free path l_{tr} and it should be scattering dominant tissue. Thus, the input values of μ_a & μ_s' should satisfy $10\ \mu_a \leq\ \mu_s'$.

To simplify the calculation of reflection, the source was set to l_{tr} depth. This is possible because from l_{tr} of the source in depth it is possible to assume that the light is diffused completely and, since μ_a should be small, not much light is lost to reach "l_{tr} depth". However, there should be accounted for this assumption because l_{tr} is the smallest step size you can measure at the source, since then can be assumed that the scattering behavior is isotropic. Therefore, it is not possible to measure it in more detail or to measure more layers around the source.

The choice is made to use two light distributions for the model, see figure 8, since the attenuation of the lactating breast is higher than for the non-lactating breast. For more information about the light distribution, see Appendix

– A small research to the behavior of the light propagation distribution & script. For the average breast, two light distributions are used with a value of $\mu_s' = 1\ mm^{-1}$ and $\mu_a = 0.02\ mm^{-1}$ for the lactating breast and a light distribution with the value of $\mu_s' = 0.9\ mm^{-1}$ and $\mu_a = 0.01\ mm^{-1}$ for the non-lactating breast. The 2D light distribution is calculated for 0 to 20 mm depth (z-direction) in 200 steps and -10 to 40 mm width (x-direction) in 600 steps.

These light distributions are also checked with the outcome of the model. First, the values of μ_a and μ_s' were chosen too low, resulting in a not realistic DOSI outcome, because the resulting μ_a and μ_s' spectra were higher in general than the input values of μ_a and μ_s', see step 5. Therefore, new values were chosen, resulting in figure 4.8.

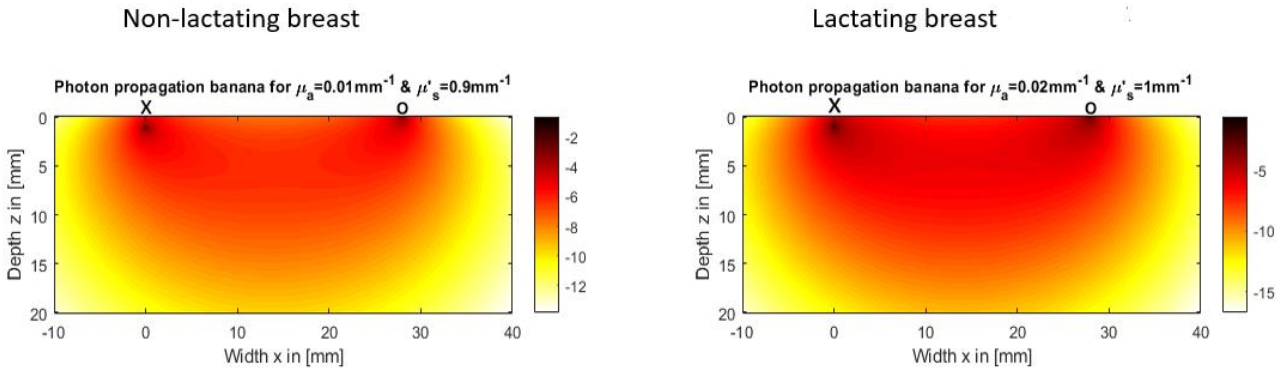

FIGURE 4.8: THIS GRAPH IS THE LOG OF THE NORMALIZED SENSITIVITY OF THE LIGHT PROPAGATION DISTRIBUTIONS FOR THE SHOWN VALUES OF μ_a & μ_s',. THE X MARKER IS THE SOURCE, AND THE O MARKER IS THE DETECTOR.

Then, for every sample size in the (depth) z-direction a summation of the values of the sensitivity in the (surface of the breast) x-direction will be taken. Lastly, the sensitivity over depth is normalized, see the equations 4.5.

$$sensitivity\ over\ depth\ SD(z) = \sum_{i=1}^{x} sensitivity\ \ (i, \text{for all values of } z)\,, \tag{4.4}$$

$$normalized\ sensitivity\ over\ depth\ NSD(z) = 100 * \frac{SD(z)}{\sum_{i=1}^{z} SD(i)}\ , \tag{4.5}$$

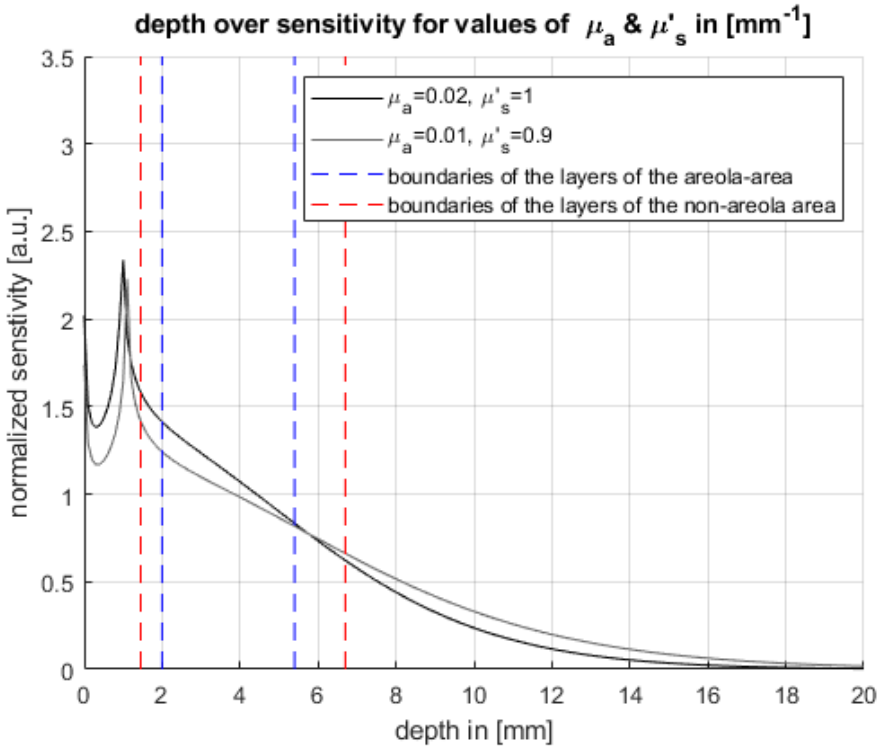

FIGURE 4.9: THE SENSITIVITY OVER DEPTH FOR CORRESPONDING μ_a & μ_s',. THE BOUNDARIES OF THE LAYERS OF THE AVERAGE BREAST ARE SHOWN. THE RIGHT BOUNDARY IS FROM THE SKIN TO THE SUBCUTANEOUS FAT LAYER. THE LEFT BOUNDARY IS THE BOUNDARY FROM SUBCUTANEOUS FAT TO THE MAMMARY TISSUE.

In figure 4.9, the sensitivity plot is shown. The corresponding sensitivity per layer can be found in table 4.7. Note, that $l_{tr} = 1\ mm$ for $\mu_s' = 1\ mm^{-1}$, which is close to the boundary of the skin. On this depth the source is simulated.

TABLE 4.7: SENSITIVITY OF THE LIGHT PROPAGATION DISTRIBUTION FOR THE LACTATING (AVERAGE) AND NON-LACTATING (AVERAGE) BREAST.

	layer	Sensitivity areola (%)	Sensitivity non-areola (%)
$\boldsymbol{\mu_a = 0.02\ mm}$, $\boldsymbol{\mu_s' = 1\ mm}$ **(lactating breast)**	Skin	32.6	25.2
	Subcutaneous fat	38.2	55.2
	Mammary tissue	29.2	19.7
$\boldsymbol{\mu_a = 0.01\ mm}$, $\boldsymbol{\mu_s' = 0.9\ mm}$ **(non- lactating breast)**	Skin	28.2	21.6
	Subcutaneous fat	34.8	51.0
	Mammary tissue	37.1	27.4

STEP 4. COMBINING THE SENSITIVITY PER LAYER TO CALCULATE THE OPTICAL AND FUNCTIONAL PROPERTIES.
In this step, the sensitivity per layer is combined to calculate the optical properties, μ_a & μ_s', and the functional properties, water, lipid, THb & stO_2, for the overall breast. These equations are used to calculate the eventual μ_a & μ_s':

$$\mu_a = \sum_{l=1}^{z} \mu_{a,l} * NSD(z = l)\ , \tag{4.6}$$

$$\mu_s' = \sum_{l=1}^{z} \mu_{s,l}' * NSD(z = l)\ , \tag{4.7}$$

where z is the number of layers in the sample, $\mu_{a,l}$ is the average absorption coefficient of layer "l", $\mu'_{s,l}$ is the average reduced scattering coefficient per layer "l", $NSD(z = l)$ is the approximated sensitivity of the detector for this layer, and μ_a & μ'_s are the average optical properties that will be part of the model. The functional properties can be determined by adding the chromophores the same way as how the μ_a is calculated: add the concentrations of every layer and multiply with the normalized sensitivity over depth. Scattering prefactor a and scattering power b can be determined by fitting the equation 2.4 to the found μ'_s. This will give the eventual model shown in the results in figure 4.10.

STEP 5. COMPARING THE OPTICAL AND FUNCTIONAL PROPERTIES TO LITERATURE VALUES.

The values of functional properties and the optical coefficient in step 5 are gathered in the paragraph chapter 3: Functional properties of the breast. If the model is in line with the literature, the model is approved. However, when this is not the case, there are multiple input variables that could be realistic but vary from each other, such as another thickness layer or another concentration of water in the skin. The suitable input values of the photon distribution should also be considered. Thereby, the μ_a and μ'_s used to calculate the photon distribution should be in line with the outcome spectra. Otherwise, it is necessary to change the input of the photon distribution to more realistic values.

The outcomes of this step can be found in the results section, the range of the given values can be found in table 3.3, the values of the functional properties should be in between these values. There is one value out of range in the results: THb of the post lactating breast of the areola area is 1.4 µM higher than the range. This can be logical, since the highest THb concentration is 70 µM on the boundary of the areola area [48], therefore it can be a bit higher for the areola itself. The model is therefore approved.

This step caused several changes in the model. For example, first there was only one light distribution, and this was set to $\mu'_s = 1\ mm^{-1}$ and $\mu_a = 0.02\ mm^{-1}$. However, when looking at the results, μ_a=0.02 for the non-lactating breast, the value is too high. Therefore, we choose to use two light distributions, one for the lactating breast and one for the non-lactating breast.

VARIATIONS OF THE BREAST MODEL.

It is possible to tweak the standard model in different ways. In this report, two distinctions are made between two variations: variations due to the anatomical diversity of the breast, and variations due to the physiology of the breast. The first variations will not change over time but do differ among subjects and the second type of variation will fluctuate over time and could vary during a breastfeeding measurement.

ANATOMICAL VARIABILITY

Thus far, the model is made for an average breast. However, to explore the limits of the model, it is important to take biological variation in consideration, since there can be several differences among subjects. These variables are static: they do change among subjects, but not over time (timespan breastfeeding session). Therefore, the change of this variable will not change the PRE, PERI and POST measurements but only among subjects.

In this paragraph, we account for the following variabilities:

- Thickness of the skin layer
- Thickness of the subcutaneous fat layer
- Ratio adipose tissue to glandular fat
- The hemoglobin value in blood

For the lactating breast, some extra variables are considered:

- The storage capacity for milk
- The volume of the lactating breast

TABLE 4.8: BIOLOGICAL VARIATION: THE RANGE OF PARAMETERS.

Parameter	Standard input value	Range
thickness skin of the areola	2.0 mm	1.15-3.25 mm
thickness skin of non-areola	1.45 mm	0.6-2.7 mm [54]
thickness subcutaneous fat of the areola	3.4 mm	2-16 mm [62]
thickness subcutaneous fat of non-areola	5.25 mm	2-16 mm
Ratio adipose tissue to glandular tissue of the non-lacting breast.	0.5	0-1
Ratio adipose tissue to glandular tissue of the lactating breast.	0.1	0-1
THb in blood (hematocrit)	2.19 mM	1.85-2.25 mM
Storage capacity of milk in the glands	170 ml	56 – 355 ml [11]
Volume of the lactating breast	755 ml	100 ml – 2000 ml [27][28][29]

Below is explained what the range in table 4.8 is based on.

The **thickness of the skin** of the non-areola area is directly based on the literature [54]. The thickness of the skin of the areola area is based on the difference between the areola area and the non-areola area of the standard input. Here we find that the areola is +0.55 thicker than the average skin. This is also implemented in the range, since no values were found for the areola separately.

For the **thickness of subcutaneous fat**, the highest reported range of the papers is used: 2-16 mm [62]. Note that none of the papers measured the subcutaneous fat on the breast.

The **ratio adipose tissue to glandular tissue** varies between 0 and 1 [71]. At the exact value of 0, the mammary tissue consists exclusively of glandular tissue, while at the value of 1, the mammary tissue is composed by only of adipose tissue.

THb value in blood ranges between 7.5-10.0 μM [52]. This value is divided by four since an extinction coefficient spectrum is used for whole hemoglobin molecules.

Storage milk is directly based on the literature [11].

Volume of the lactating breast is also directly based on the literature [27][28][29]. A sidenote: The literature did not mention this measurement on the lactating breast.

For every biological variation, the standard model of the average breast is held the same, except for one minimum of maximum. Therefore, the minimum storage capacity is set to 70 ml and the maximal volume of the lactating breast is set to 270 ml. The minimum and maximum DOSI outcomes are plotted, and the functional properties are compared to the outcomes of the average model.

PHYSIOLOGICAL VARIABILITY

During a breastfeeding session, some events can happen that change the outcome of the DOSI measurements. The two events that can happen are that the blood dynamics change per layer and that milk is extracted from the breast.

TABLE 4.9: PHYSIOLOGICAL VARIABILITY: THE RANGE OF PARAMETERS.

Parameter	Standard input value	Extremities (range)
THb in blood (Concentration in tissue)		
C_{blood} skin	4%	2-12%
C_{blood} subcutaneous fat	0.5%	0.5-1%
C_{blood} adipose tissue	0.75%	0.5-1%
C_{blood} glandular tissue	1.25%	0.83-1.67%
stO_2 correction	0	-0.2 – 0.2
Fat in milk	3.8%	0.4-10% [76]
Milk ejected during breastfeed	70 ml	10-200 ml

Blood concentration is the concentration of blood in the measured tissue and is directly based on the literature [57][19].

stO_2 correction: StO_2 can variate during a breastfeed due to physiological processes. Moreover, it depends on the anatomical structure slightly as well because it depends on to what extent of the measured volume is arterial blood or venous blood. The standard value of stO_2 depends on what tissue is present in the measured DOSI volume. The stO_2 correction value can be tweaked between -0.2 to 0.2, this is the fraction of the stO_2 can change. The highest value of stO_2 is 80% in the current model, therefore the stO_2 can never be higher than 100%. The lowest value of stO_2 is 65%, causing the value can never be lower than 45%.

Fat in milk range is directly based on the literature [76]. The same source is used to obtain the average reduced scattering coefficient for foremilk and hindmilk to mimic low fat and high fat percentages in the scattering properties. Although this is a static parameter, it is important to keep in mind that this can also be useful for the measurements during a breastfeeding session, since the lipid concentration of the milk changes in a breastfeed (foremilk has a low concentration of lipid and hindmilk a high concentration of lipid).

Milk is extracted: After a MER, milk is ejected out of the breast. The volume of milk that is extracted is based on table 3.2 where the lowest extracted milk volume is 10 ml and the highest ejected milk volume is 200 ml. Note, at the beginning of this chapter the assumption is made that glandular tissue and adipose tissue replace the empty space left behind by the milk volume ejected by the breast. When this substitution does not occur, the biggest differences are found between the PRE and POST measurements. This is also shown in the results.

Again, for every physiological variation, the standard model of the average breast is maintained the same, except for one minimum of maximum. Therefore, since the storage is set at 170 ml for the average breast, the maximum volume ejected is also set to 170 ml in order to avoid changing more parameters.

Other processes during a breastfeed are breathing ($\approx 0.26\,Hz$), heart beating ($\approx 1\,Hz$), and pumping ($\approx 0.1\,Hz$). Breathing and pumping processes cause deformation and displacement of the breast tissue. Again, since these processes are difficult to describe and predict, they are not considered in the model. Thereby, the sample frequency of the DOSI device for measurements during a breastfeed is $\approx 0.08\,Hz$ (with Nyquist frequency $\approx 0.04\,Hz$). This is slower than the mentioned processes, which makes it even more difficult to validate these processes. Note, even the MER itself has an approximate duration of 23.7 seconds [46], which is maybe even too slow to observe.

RESULTS

First, the model of the average breast will be shown. Secondly, the variations of the breast will be discussed. The script used to make the model can be found on the BMPI's p-drive of the author with the directory masteropdracht_Lactation and DOSI\Matlab\model\modeltweak5.

In figure 4.10 the optical properties of the average breast are shown. The corresponding functional properties of this model are reported in table 4.10.

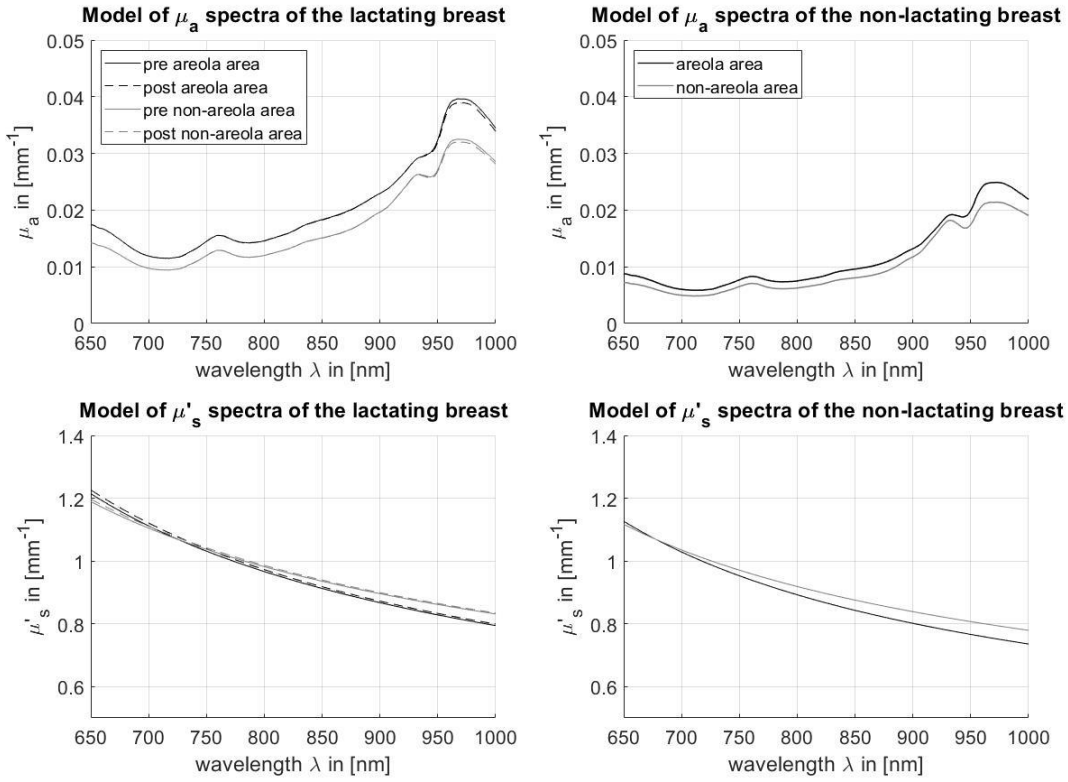

FIGURE 4.10: THE OPTICAL PROPERTIES, μ_a AND μ_s', OF THE LACTATING AND NON-LACTATING BREAST.

TABLE 4.10: FUNCTIONAL PROPERTIES OF THE MODEL OF THE AVERAGE BREAST. NOTE THAT NON-AR IS NON-AREOLA AREA, AR IS AREOLA AREA, NON-LAC IS THE NON-LACTATING BREAST, LAC PRE IS THE LACTATING BREAST BEFORE BREASTFEEDING AND LAC POST IS THE LACTATING BREAST AFTER BREASTFEEDING.

	HbO_2 [µM]	Hb [µM]	THb [µM]	StO_2 %	Lipid %	Water %	$a\ mm^{-1}$	b
non-ar non-lac	21.7	6.1	27.8	78.0	55.0	29.5	1.39	0.84
non-ar lac pre	44.3	12.2	56.6	78.3	49.3	35.8	1.48	0.83
non-ar lac post	45.3	12.8	58.1	78.0	49.5	34.8	1.49	0.84
ar non-lac	26.4	7.5	33.9	77.8	45.3	34.2	1.46	0.99
ar lac pre	53.9	15.2	69.1	78.0	36.0	43.6	1.57	0.99
ar lac post	55.4	16.0	71.4	77.6	38.4	42.1	1.59	0.99

Since this research is interested in milk transfer, the differences between pre- and post-expression are displayed in table 4.11. Moreover, because the pre-values could influence the amount of change in the functional properties, the percentagewise difference are shown in table 4.12.

TABLE 4.11: DIFFERENCES BETWEEN PRE- AND POST-BREASTFEEDING OF THE LACTATING BREAST OF THE FUNCTIONAL PROPERTIES. NOTE THAT HBO IS OXYHEMOGLOBIN AND HB IS DEOXYHEMOGLOBIN.

	ΔHbO_2 [µM]	ΔHb [µM]	ΔTHb [µM]	ΔStO_2 %	ΔLipid %	ΔWater %	$\Delta a\ mm^{-1}$	Δb
non-areola area	1.0	0.5	1.5	-0.3	0.2	-1.0	0.01	0.01
Areola area	1.5	0.8	2.3	-0.4	0.3	-1.5	0.02	0.01

TABLE 4.12: THE DIFFERENCES BETWEEN PRE- AND POST-BREASTFEEDING OF THE LACTATING BREAST OF THE FUNCTIONAL PROPERTIES PERCENTAGEWISE. NOTE THAT HBO_2 IS OXYHEMOGLOBIN AND HB IS DEOXYHEMOGLOBIN.

	ΔHbO_2 %	ΔHb %	ΔTHb %	ΔStO_2 %	ΔLipid %	ΔWater %	Δa %	Δb %
non-areola area	2.3	4.2	2.7	-0.4	0.5	-2.8	0.9	0.8
Areola area	2.8	5.0	3.3	-0.5	0.9	-3.5	1.2	0.9

The differences of the parameters in comparison to the average breast model can be found in the appendix. To give a sense of how the outcome of DOSI changes due to biological variability among subjects and physiological processes, table 4.13 is provided, summarizing the findings that can be found in the Appendix – Variations of the breast. Table 4.13 gives the order of magnitude per parameter in order of the power of ten.

TABLE 4.13: ORDER OF MAGNITUDE CHANGE PER PARAMETER IN COMPARISON TO THE AVERAGE BREAST. A MINUS SIGN REFLECTS THAT THE VALUE OF THE FUNCTIONAL PROPERTIES DECREASES WHEN THE VARIABLE INCREASES. A PLUS-MINUS SIGN IS USED IN CASE THE VALUE OCCASIONALLY DECREASES AND INCREASES. THE OPTICAL PROPERTIES ARE DIVIDED IN CLASSES. CLASS I: SPECTRUM CHANGE IS VISIBLE. CLASS II: SPECTRUM CHANGE IS NOT VISIBLE. CLASS III: THE SPECTRA OF SOME MODELS' CHANGE IS VISIBLE. NOTE THAT FOR PARAMETERS THAT INFLUENCE ONLY THE LACTATING BREAST, THE NON-LACTATING BREAST MODELS ARE NOT CONSIDERED.

	μ_a	μ_s'	HbO_2 [µM]	Hb [µM]	Lipid %	Water %	a mm^{-1}	b
biological								
thickness of the skin	I	I	10	1	-1	1	0.1	0.1
thickness of the subcutaneous fat	I	I	-1	-1	10	-10	+/- 0.01	-0.1
ratio adipose tissue to glandular tissue	I	I	-0.1	-1	10	-1	-0.1	-0.01
THb in blood (hematocrit)	I	II	1	1	0	0	0	0
storage capacity of milk	I	I	-1	-1	0.1	1	-0.01	-0.01
volume of the lactating breast	I	I	1	1	+/- 0.1	-1	0.1	0.01
physiological								
concentration in blood	I	I	10	1	0	1	0.01	-0.01
stO_2 correction	III	III	10	10	0	0	0	0
fat in milk	II	I	0	0	0.1	-0.1	0.01	+/- 0.01
milk extraction during a breastfeed	III	III	1	1	0.1	-1	0.01	0.01

To give an example how this translated to the μ_a and μ_s' spectra, figure 4.11 and figure 4.12 are shown. Here, figure 4.11 shows the difference in the thinnest skin reported and the thickest skin reported. In figure 4.12 the difference between 10 ml milk transfer and 170 ml milk transfer is shown, causing the plots for minimum milk transfer to overlap mostly everywhere the plots for maximum milk transfer. The only time where the plots do not overlap are the plots for post-expression of the lactating breast.

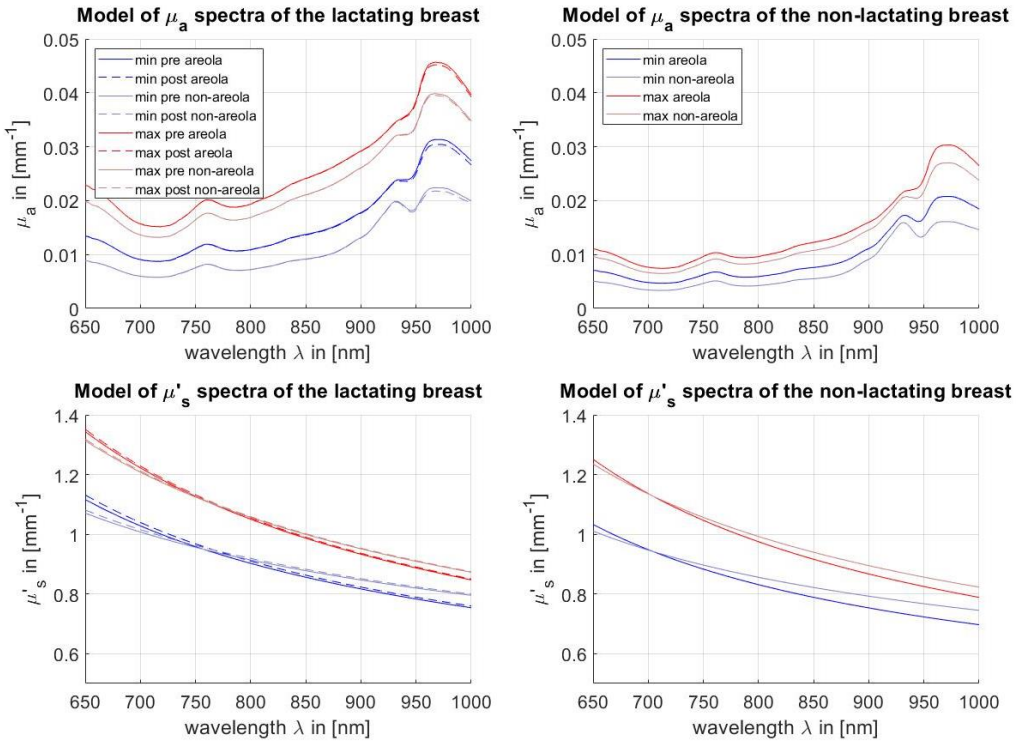

FIGURE 4.12: THE OPTICAL PROPERTIES, μ_a AND μ_s', OF THE LACTATING AND NON-LACTATING BREAST FOR THE RANGE IN THICKNESS OF THE SKIN. THE BLUE LINES ARE THE MINIMUM RANGE, THE THINNEST SKIN AND THE RED LINES ARE THE MAXIMUM RANGE, THE THICKEST SKIN.

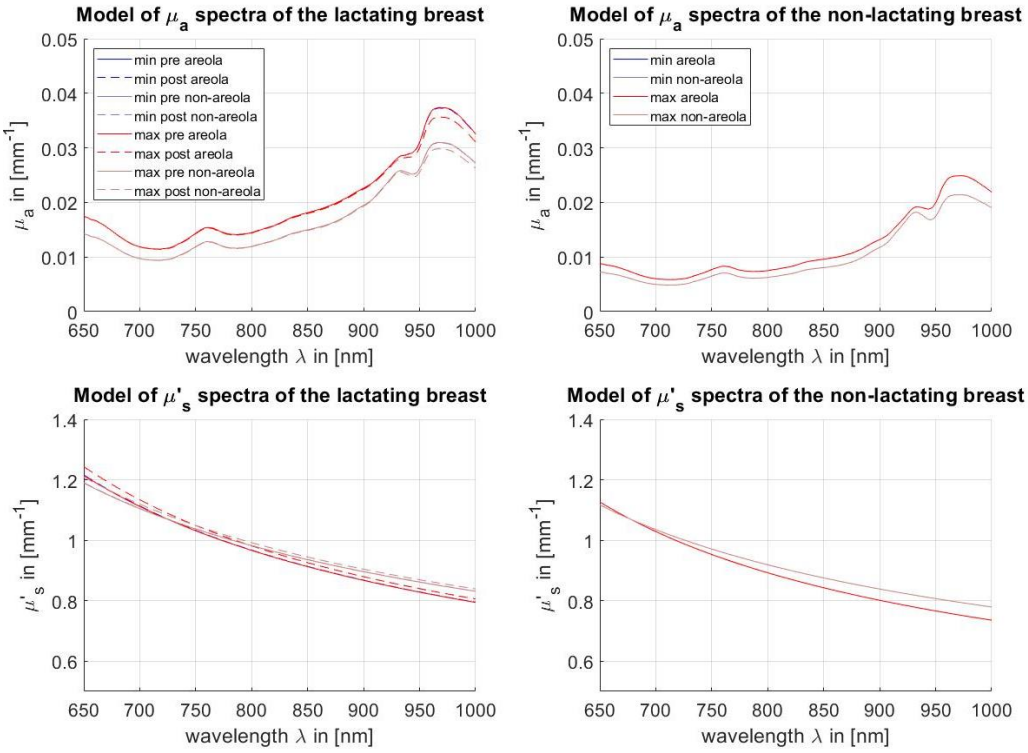

FIGURE 4.13: THE OPTICAL PROPERTIES, μ_a AND μ_s', OF THE LACTATING AND NON-LACTATING BREAST FOR THE RANGE IN MILK TRANSFER. THE BLUE LINES ARE THE MINIMUM RANGE, THE 10 ML AND THE RED LINES ARE THE MAXIMUM RANGE, THE 70 ML.

DISCUSSION

AVERAGE MODEL

This model is a rough estimation of an average lactating and non-lactating breast. Differentiation has been identified between the lactating and non-lactating breast, the areola area and the non-areola area and before (pre) and after (post) breastfeeding.

First, in figure 4.10, the optical properties of the average breast are shown. The absorption coefficient of the non-lactating breast is approximately twice as low as for the lactating breast. For the non-areola area, the absorption coefficient is approximately 20% lower than for the areola area as well. This is likely due to the fact that the deoxy- and oxyhemoglobin concentration are lower in the non-areola area and the non-lactating breast, see also table 4.10. The absorption coefficient for the POST lactating breast is slightly lower ($\mu_a \approx 0.001$) than the PRE lactating breast at 980 nm. This is due to water, which is also reflected in table 4.10.

The scattering coefficient of the lactating breast is higher than that of the non-lactating breast, reflected in functional property a. A cause for this could be the use of a smaller light distribution for the lactating breast, resulting in a more sensitive light propagation distribution for the skin spectrum.

The changes due to milk transfer can be seen in tables 4.11 and 4.12, which display the differences between pre breastfeeding and post breastfeeding. It is important to notice that the THb values and the scattering properties increase due to tissue shifting into the measurement volume. The oxygen saturation decreases for the same reason; since, mammary tissue is less saturated than the skin and the subcutaneous fat. Interestingly, lipid concentrations increase as well because of this. Although fat from the milk might no longer be that present in the measuring volume, a decline can also be expected, but the intraglandular fat also shifted slightly in the measuring volume, causing an increase. The absence of milk in the breast can be more directly measured by the decrease of water. For the non-areola area 1% and for areola area 1.5% of the water disappeared from the measuring tissue due to 70 ml milk ejection.

VARIATIONS OF THE BREAST

Thickness of the skin considerably affects the outcome of the DOSI measurements in comparison to other parameters, see table 4.13 and Appendix – Variations of the breast. The concentration of THb in the measured volume increases when the thickness of the skin increases. This effect is almost twice as high for the lactating breast. With thicker skin the measured concentration of lipid and water declines, probably since DOSI will be less sensitive to subcutaneous fat and more sensitive to the skin. Thereby, the μ_s' increases because the μ_s' is shifted towards the μ_s' of the skin.

The next parameter is the **thickness of subcutaneous fat**. This parameter affects the outcome of DOSI in comparison to the other parameters as well, see table 4.13 and Appendix - Variations of the breast. This behaves similarly to the thickness of the skin, since, when this layer is thinner, DOSI is more sensitive to the layer underneath (in this case the mammary tissue layer). Therefore, when the subcutaneous fat layer gets thicker, less blood and water will be measured but more fat. Also, the scattering properties are more similar to that of the subcutaneous fat layer than to that of the mammary tissue. For a higher thickness of the layer of subcutaneous fat, the μ_s' is overall higher than the average breast model.

If the **ratio adipose tissue to glandular tissue** increases, it will result in a higher concentration of lipid and stO_2, and less THb and water. Thereby, the scattering prefactor a and power b decline.

As expected, the **hemoglobin value** of the blood (biological variation) and the **blood concentration** have the same type of effect on the DOSI measurements. When hemoglobin levels or blood concentration increase, there is more THb in the measured volume, for, with the increase of blood concentration, there is also an increase of water. Only for an increase in blood concentration the scattering properties a and b change in the model. The effects of separate hemoglobin concentrations in the blood are not accounted for in the scattering properties of

the model. However, the changes seem to have a relatively small effect on μ_s' compare to other variations of the breast.

The **stO_2 correction** only has effect on the shape of the μ_a, especially for the wavelengths between 650 and 800 nm. It does not have an effect on μ_s'.

ONLY FOR THE LACTATING BREAST

The concentration **fat in milk** barely affects the outcome of the μ_a, but it does affect the μ_s'. Especially, a higher scattering prefactor a seems to be higher for higher concentrations of fat in milk. This is a property that does not change over time, but this effect could be seen in the PERI data, since the non-fat milk (foremilk) will be extracted from the breast first, then the bulk milk (in between fatty) and lastly the fatty milk (hindmilk). This could therefore also help with the physiological aspect of this research.

Then, for **storage capacity** and the **breast volume,** the effect on the DOSI outcome is reversed. This is logical, since, if the breast volume increases, less is measured of the overall breast and with the same storage capacity less milk is measured. If the storage capacity increases, more milk will be measured.

MILK TRANSFER

One of the physiological variabilities is **milk extraction**. If milk is extracted, only the model of the POST lactating breast will be affected. This was modeled by using 10 mL as the minimal amount of milk extraction, and 170 ml as a maximum. With an (linear) increase of milk ejection volume there is an (linear) increase of the differences mentioned in the discussion of the average breast model.

When nothing will replace the space of the ejected milk volume, the differences between pre- and post-breastfeeding increase. Thereby, the overall reduced scattering coefficient μ_s' will be lower, instead of higher, for post milk extraction than for pre milk extraction.

Variables that do not influence milk transfer measurability:

- the total hemoglobin value of the blood,
- storage capacity,
- blood concentration.

All the other variabilities affect the measurability of milk transfer. An increase indifference between PRE and POST data is:

- decrease of thickness of the skin.
- decrease of thickness of subcutaneous fat.
- Decrease of the ratio adipose tissue to glandular tissue.
- Increase of fat in milk.
- Decrease of volume of the lactating breast.
- (natural) increase of milk extraction.

Interestingly, thus far the graph of post breastfeeding has been higher than pre breastfeeding for μ_s'. However, for fatty milk (μ_s' spectrum of average hindmilk is used), this seems to be the other way around.

Luckily, the blood concentration does not have an impact on the changes between PRE and POST data due to milk supply. Since the other (biological) variations that do have an influence are stationary, they should not change greatly during a breastfeeding session. However, the changes caused by milk supply are relatively small and may therefore be hard to distinguish. Hopefully, it is possible to measure milk transfer and this model can potentially predict a volume of extracted milk using DOSI measurements.

It is expected that it is not possible to predict milk supply for every separate sample for the PERI measurement, because some processes are not accounted for, such as breathing or displacement of the measurement volume due to pumping, which makes it hard to interpret a single outcome of DOSI-measurements during breastfeeding. Thereby, with a point measurement, it is hard to predict what is measured, whether a gland, a duct, or fat, which will result in different DOSI-outcomes. However, the mean of the PERI measurements should be somewhere in between the PRE and POST data. This will not be the case for the blood-related properties, since ejected milk affect blood dynamics.

SHORTCOMINGS & LIMITATIONS

This model is based on the literature. When something was not precisely known, an educated guess was made, which could potentially be not as close to reality. In addition, the literature is not always in consensus.

The model is based on the DE. This comes with different limitations. Firstly, the breast is assumed to be homogenous in different layers, which is not true. Furthermore, the layers should not be smaller than l_{tr}, however the blood in the skin is not homogeneously divided. Moreover, only two light distributions are used here to describe the tissue. However, there should be more, considering that the adjustments shift the values of μ_a and μ_s'. Several of the assumption made because the model is based on the DE can be verified by making a model using Monte Carlo simulations.

The model of the μ_s' is maybe not really reliable, especially for the lactating breast. This is due to μ_s' varying already considerably in the literature, see chapter 3 – optical and functional properties of the layers of the non-lactating & lactating breast. Thereby, μ_s' is a complex variable, since it is probably highly dependent on the light distribution through the tissue, which is simplified in this model. Thereby, the model is based on literature, and not much is known about the optical properties: Only one paper, the involution case study of Bosschaart et al. [15], is used as a reference for the model's μ_s' of the lactating breast.

Not all the processes that deform the breast were considered. While this could deform the measurement volume as well and therefore could have an impacted for the predicted milk transfer. For the PERI measurements in particular, this could have an impact since the breast pump also deforms the breast.

For the variations of the breast, note that not all distributions are normal distribution. The range of this variable just gives an intuition how this variable could change and how the optical and functional properties change because of it. Note that it is not possible with DOSI to make a distinction between all these variables: this only gives an idea of how different anatomies of the breast could change the optical and functional properties found by DOSI, as well as how different anatomies change the measurability of milk transfer.

CONCLUSION

This model will give an insight into the differences and similarities of the breast optical properties measured by DOSI, into the differences in anatomical composition between the lactating and non-lactating breast, as well as into the differences between the areola area and the non-areola area. Nevertheless, in order to fully answer the research question, the model will be validated to see if it is an accurate description of DOSI in reality.

5. THE EXPERIMENTS

In this study, DOSI experiments are carried out. The purpose of these experiments is to obtain optical and function properties of the lactating breast and how these compare to the non-lactating breast. This is one of the first experiments to research the optical properties of the lactating breast, which makes this exciting on it is own. Thereby, the model will be combined with the experiments in the next chapter to validate the (theory behind) the model and to predict milk transfer.

Similar milk transfer experiments were carried out by Prime et al. with ultrasound [44]. Prime et al. [44] measured the dilation of the milk duct during a let-down reflex with ultrasound and the flow rate of milk. They found that milk can accumulate in the breast shield of the breast pump, which influenced the measured flow rate. Thereby, the distance between the pump and the shield can cause a dispersion of the signal compared to what occurs in the breast. They found that there was no significant difference between either the pump pressure, or between the left and right breast with the percentage of extracted milk. However, there was a difference between the milk supply of the left and right breast of the individual mothers, namely circa 23%. With the double pumping experiment, overall, both breasts responded simultaneously (95,5%). The fastest flow rate was at the first or at the second let-down reflex. Dilation of the milk ducts measured with ultrasound occurred when a let-down reflex occurred.

METHOD

BEFORE THE EXPERIMENT

This research is a collaboration of two research groups with project leaders Dr. Thomas O'Sullivan from the University of Notre Dame (USA) and Dr. ir. Nienke Bosschaart, from the University of Twente (The Netherlands). This research is executed in the Netherlands at the University of Twente with the help of two (female) PHD-students Hanna de Wolf and Sjoukje Schoustra. The author herself, Miriam van der Hoek, was present during one of the experiments, but did not execute them. The study was approved by the Committee on Research Involving Human Subjects (CMO Arnhem-Nijmegen, The Netherlands), and all participants gave written consent prior to the study. For the unsigned informed consent form, see the BMPI's p-drive of the author with the directory masteropdracht_Lactation and DOSI\Protocols\Borstvoeding in beeld - Proefpersooninformatie v1.1 (NL).

The subject load of the experiments is non-invasive and pain-free. The measurements are not expected to influence the lactation process. Subjects can use their own breast pump. During the experiments, the participants are instructed to move as little as possible. There will be drawn on the breast with surgical ink to mark the DOSI measurement grid.

The participants of this study can be divided in two groups, group i) consisting of four healthy lactating mothers (lactation period is minimally two weeks) with an age between 31 and 35 years old and a control group ii) consisting of five healthy, premenopausal non-lactating women with an age between 29 and 38 years old. All the subjects participating in this experiment are Caucasian. Furthermore, all lactating subjects had a milk ejection sensation. In table 5.1, more participant information can be found. The subject L3 did not show at the experiment and is therefore excluded from the dataset. There are some exclusion criteria for the participants in this research. To elaborate, pregnant women were excluded. Furthermore, women with lactation problems at the time of the experiment for the lactating group and women with known breast diseases or < 9 months postpartum for the non-lactating group are excluded as well.

TABLE 5.1 PARTICIPANT INFORMATION. FOR A MORE EXTENDED VERSION OF THIS TABLE, SEE BMPI'S P-DRIVE OF THE AUTHOR WITH THE DIRECTORY MASTEROPDRACHT_LACTATION AND DOSI\MEASUREMENTS\DATA SUMMARY FILES\INTAKE AND MEASUREMENT FORM DATA.

Subject	BMI	Cup size (NL)	Gravidity	Parity	Start last menstruation (d)	Menstrual cycle length (d)	Infant age (weeks)
L1	19.3	75-D	2	2	NA	NA	9
L2	25.4	75-F	2	1	NA	NA	20
L4	22.2	?-B/C	2	1	NA	NA	9
L5	20.1	70-C	2	2	20	26	25
N1	21.7	75-B	3	2	NA	NA	-
N2	21.4	75-C	2	2	6	30	-
N3	19.8	70-C	0	0	1	27	-
N4	23.4	80-B	3	3	22	32	-
N5	28.7	?-B	3	3	8	27	-

The experiments took place in November 2019. There were plans for more experiments in May 2020, but, due to the COVID-19 pandemic, they were no longer executable in the timeframe of this master assignment.

MATERIALS

The instrumentation consists mostly of the DOSI scanner and other materials. Below is a list of the DOSI scanners specification/properties, see table 5.2. The source-detector distance was set to 28 mm. Except for subject L5, there the source-distance was set to 22 mm. This results in an approximate depth sensitivity of 10 to 15 mm, also see figures 4.8 and 4.9.

TABLE 5.2: SCANNER SPECIFICATIONS OF THE DOSI DEVICE

	specifications	**details**
DOI device	Miniature diffuse optical spectroscopic imager (mDOSI)	Manufactured at University of Notre Dame, Notre Dame, IN, USA and Beckman Laser Institute, University of California, Irvine, CA, USA - Project lead: Dr. Thomas O'Sullivan, PhD
Steady state mode - Source	Halogen lamp	Near infrared: 650 to 1000 nm
Steady state mode - Detector	spectrometer	
Frequency domain photon migration mode - Source	laser diode	660, 690, 780 to 830 nm
Frequency domain photon migration mode - Detector	avalanche photodiodes	Temperature-controlled, 1-mm diameter active area

a) The mDOSI device with laptop

b) Handheld DOSI scanner probe

c) Fiber-coupled DOI probe

FIGURE 5.1: DOSI PROBES AND SETUP [83]**. A) IS THE DOSI SYSTEM WITH LAPTOP AND INSTRUMENTATION. B) IS THE PROBE USED FOR THE GRID MEASUREMENTS AND C) IS THE PROBE USED FOR THE SPOT MEASUREMENTS.**

Furthermore, the DOSI device is controlled by the corresponding laptop and programs. For calibration purposes, phantoms are used:

- black rubber for the dark test.
- breast tissue phantoms from Institut National d'Optique, Quebec, Canada; and UC Irvine Beckman Laser Institute, California.
- a Reflection standard: SRS-99-020, Labsphere Inc.

A transparent sheet is needed to notate the placement of the grid point and surgical ink to notate on the breast the placement of the DOSI device. The ink can be removed with an alcohol wipe once the measurements are done.

During this experiment, not only the optical and functional properties are measured, but also the extracted milk volume of the lactating breast during expression is measured. Moreover, the milk flow rate can be deduced by taking the derivative over time of the milk volume measured. To measure milk volume, a scale (OHAUS Ranger ™ 3000 R31P1502) is used. This scale can be connected to a computer and store weights over time with the print function. The scale's sample time is approximately 0.13 seconds, has a readability of 0.05 g and a repeatability of 0.1 g. The lactating subject should bring their own pump and breast shield. Also, a sterile tube is used to connect the breast shield to a milk bottle. See figure 5.2 for an overview of the setup.

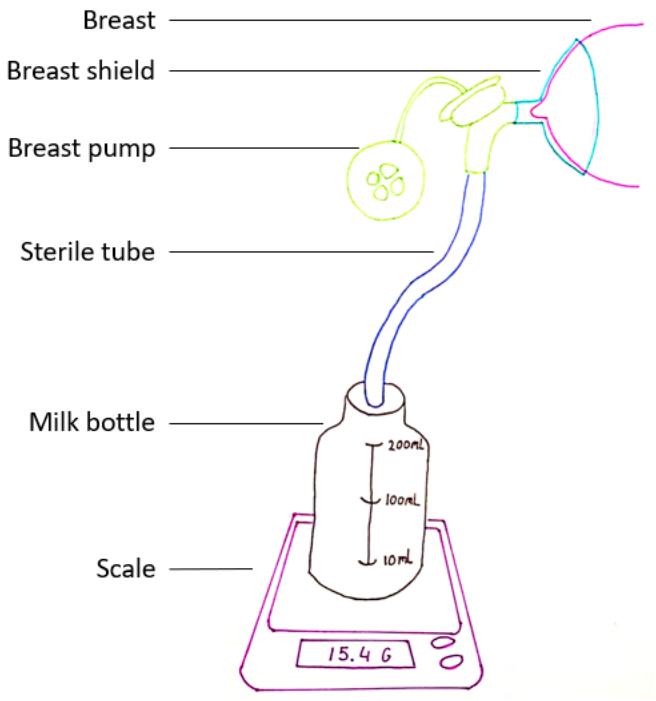

FIGURE 5.2: A SCHEMATIC OVERVIEW OF THE SET UP TO MEASURE CUMULATIVE MILK WEIGHING.

RESEARCH METHOD

The research method is split in grid measurements pre and post (before and after) a breastfeeding session and a spot measurement peri (during) a breastfeeding. For the non-lactating group, the peri measurement consists in sitting still for 10 minutes. The measurement with the DOSI device uses a standard scanning protocol, see the manual on the BMPI's p-drive of the author with the directory masteropdracht_Lactation and DOSI\Protocols\IRBForm_17-11-4250 (3) +manual. Below, a short summary is given of the measurement procedure. The subject is measured in a supine or reclined position and is instructed to move as little as possible during the experiments.

First, a calibration of the (miniature) DOSI device is performed, according to the manual on the BMPI's p-drive of the author with the directory masteropdracht_Lactation and DOSI\Protocols\IRBForm_17-11-4250 (3) +manual.

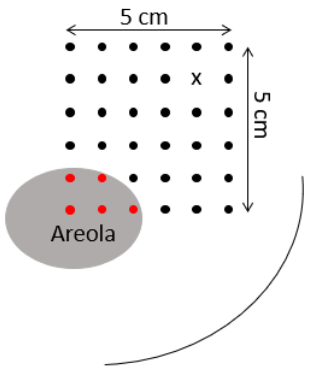

FIGURE 5.3: THE PLACEMENT OF THE GRID ON THE BREAST. 'X' IS DENOTED WHEN THERE ARE IRREGULARITIES ON THE SKIN, SUCH AS FRECKLES.

The upper outer quadrant (medical terms: cranial lateral quadrant) of the breast is measured with respect to the nipple. Thus, depending on measuring the left or right breast the upper right or left quadrant is measured. On

the sheet, the grid is notated, see figure 5.3 and, on the breast, the grid is notated with surgical ink. The grid is a quadrant of 5cmx5cm, with 10 mm spacing, giving 36 measuring points in total. Denote irregularities of the skin such as moles or freckles with a 'x'. Furthermore, mark the areola and the nipple. For the lactating group 1: The mass of the empty bottle will be measured on the scale pre-expression.

GRID MEASUREMENT

Each point of the grid is measured from top to bottom (every point of the grid takes approximately 3 seconds.) Important is to consider the following for the post-expression grid measurement: The position the handheld DOSI scanner should be held in the same way as the pre-expression grid measurement. Thereby, the sheet should be used to measure on the same location. For group 1: The extracted milk volume and bottle will be measured. At the pre-expression grid measurement, the weight of the empty bottle will be measured. The weight of the empty bottle will be subtracted later to obtain the milk volume.

SPOT MEASUREMENT

The peri-expression measurement is at a single location. For the PERI measurement the fiber-coupled DOI probe is used.

Group 1: The subject will be asked to connect her breast pump and breast shield to the breast. The bottle will be placed on a scale that reads out the mass of the milk over time. The breast shield and the bottle are connected to each other with a sterile tube. It is important to be aware that breast milk can accumulate in the breast shield when the subjects recline too much.

The peri probe will be placed horizontally above the breast shield; for the non-lactating group 2 this is approximately 5 cm above the areola. Group 2 is measured for 10 minutes.

The peri-expression spot measurement of the lactating group 1 can be split in several phases:

- 2-minute pre-expression phase.
- Starting expression phase (high frequent vacuum change for stimulating MER)
- Start of milk expression. When present, the MER is denoted.
- End of milk expression.
- 2-minute post-expression phase.

During the measurement, the timestamp of all these different phases or other events, such as the different pump phases or sudden movement, are marked.

ANALYSIS METHOD

This is partly explained in Chapter 2. Theory: DOSI. A short recap is provided here: based on the FDPM, the μ_a and μ_s' can be found for the wavelengths used for FDPM. The SS measurements can then be fitted for μ_a and d μ_s' to relate to these points. Assuming that μ_s' is exponential (see equation 2.4), it is possible to retrieve a and b from this. The μ_a absorption spectra can be fitted to the extinction coefficient of other spectra for water, lipid, oxyhemoglobin, and deoxyhemoglobin. The THb and stO_2 can be determined with oxyhemoglobin and deoxyhemoglobin, according to equations 2.1 and 2.2.

The fit of the optical properties (μ_a and μ_s') and the fit of the functional properties on the optical properties are carried out by the O'Sullivan Research Group (Biomedical Photonics Laboratory, Department of Electrical Engineering, College of Engineering, University of Notre Dame, USA). The analyses of the spectra of the optical properties, μ_a and μ_s', are done in MATLAB 2018a. The analysis of the functional properties is done in the program language R version 4.0.3 in RStudio. The data is presented mostly with the median and interquartile range (IQR), since the data was not always normally distributed, see Q-Q plots on the BMPI's p-drive of the author with the directory masteropdracht_Lactation and DOSI\R\figuresR\qqplotPREPOST and masteropdracht_Lactation and DOSI\R\figuresR\qqplotperi.

Optical properties

To answer the research questions, the data is shown for the median and the interquartile range of the measuring points categorized by the areola and non-areola area and the lactating and non-lactating breast, see figure 5.4 and 5.5 in the results. Also, the grid experiments pre- and post-expression are compared.

Functional properties

The median and interquartile range are calculated of the functional properties (water, lipid, stO_2, THb, oxyhemoglobin, deoxyhemoglobin, a and b) for the areola and non-areola area of the lactating and non-lactating breast for the PRE and POST measurement. The PERI measurement took place on the non-areola area and from this data the median and interquartile range is calculated and implemented as well. The whole spot measurements are shown in figure 5.6 for the lactating and the non-lactating breast per functional property. The goal of this figure is to compare the non-lactating and the lactating breast and not necessarily to examine the occurring events. For in-depth analysis of the grid and PERI per subject, see appendix - Qualitative analysis per subject.

The raw data of the milk volume measurements are shown in figure 5.7. The milk flow rate is derived by taking the derivative of the milk volume over time. The milk flow rate is also implemented in this figure.

In this report, there is a focus on milk transfer. Therefore, the milk mass is compared to the measurement of the functional properties. It was decided to plot a linear regression line for each optical property. This is done for both the grid and for the spot measurement. For both measurements, the absolute difference between PRE and POST measurements and the relative difference between PRE and POST measurements are plotted. The following equations are used to calculate these differences:

$$absolute\ difference = POST - PRE \tag{5.1}$$

$$relative\ difference = 100 * \frac{POST - PRE}{PRE} \tag{5.2}$$

The change for the grid measurements is calculated per grid point by subtracting the values pre- and post-expression. Then, the median and interquartile range are calculated per category (areola vs non-areola and lactating vs non-lactating). For peri-expression, the same analysis is done. As pre-expression data, the median of the two minutes before pumping is used and for the post-expression data, the median of the two minutes after pumping ended is used.

Results

First, the optical properties of the experiments are shown, followed by the results of the functional properties. The qualitative analysis per lactating subject can be found in the Appendix – Qualitative analysis per subject. The scripts developed for carrying out the analysis and the visualization can be found on the BMPI's p-drive of the author with the directory masteropdracht_Lactation and DOSI\R\main5.

An additional result is the mean sample time, see table 5.3.

TABLE 5.3: SAMPLE TIME OF THE DIFFERENT DOSI MEASUREMENTS.

subject	PRE sample time	POST sample time	PERI sample time
L1	26.5	20.7	13.0
L2	13.7	12.7	10.8
L4	19.1	14.9	6.6
L5	14.4	13.8	5.0
n1	13.9	15.5	8.1
n2	14.3	13.3	4.2
n3	13.5	13.3	9.7
n4	13.2	12.9	5.3
n5	12.3	11.7	4.0

OPTICAL PROPERTIES

In figure 5.4, the absorption coefficient spectra are shown and in figure 5.5, the reduced scattering coefficient spectra are shown. In both figures, the left side contains information about the areola area, and the right side about the non-areola area. Thereby, the top plots of these figures are the lactating subjects, and the bottom plots are the non-lactating subjects.

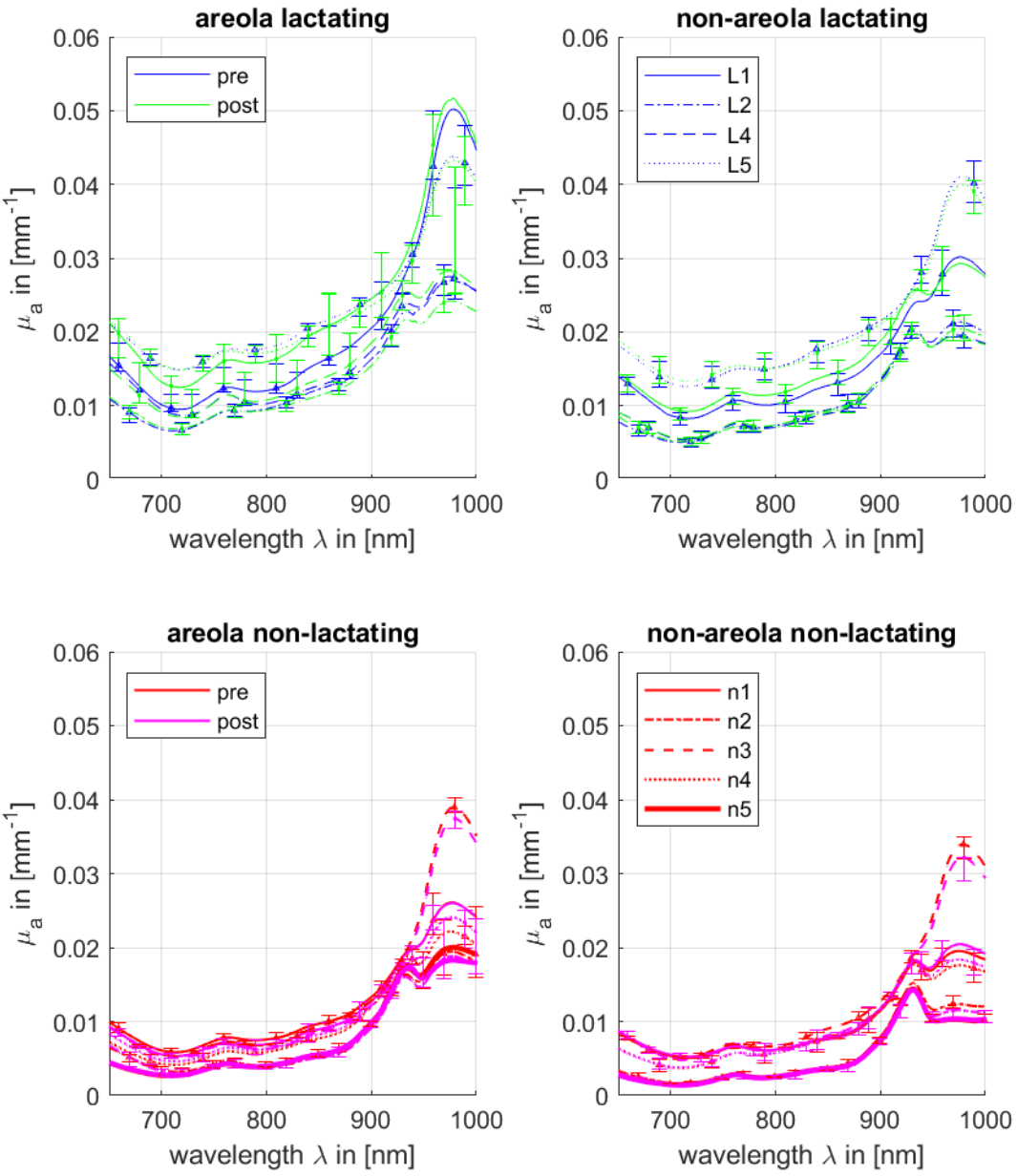

FIGURE 5.4: THE MEDIAN ABSORPTION COEFFICIENT OVER WAVELENGTH PER SUBJECT OF THE GRID MEASUREMENTS. THE ERROR BARS REFLECT THE INTERQUARTILE RANGE AT THE CORRESPONDING WAVELENGTH. THE UPPER TWO GRAPHS CORRESPOND TO THE RESULTS OF THE LACTATING SUBJECTS, THE BOTTOM TWO GRAPHS REFLECT THE NON-LACTATING SUBJECTS. THE LEFT FIGURES CORRESPOND TO THE AREOLA AREA, AND THE RIGHT FIGURES TO THE NON-AREOLA AREA. THE COLORS INDICATE THE DIFFERENCES BETWEEN PRE- AND POST-DATA. THE DIFFERENT LINE STYLES INDICATE THE DIFFERENT PARTICIPANTS, WHICH ARE THE SAME FOR THE NON-LACTATING FIGURES AND THE LACTATING FIGURES.

The following observations are done for the absorption coefficient spectra, see figure 5.4. The median of the μ_a spectrum 650 nm to 850 nm is twice as high for lactating (range $\mu_a \approx 0.005 - 0.021\ mm^{-1}$) than for non-lactating breasts (range $\mu_a \approx 0.001 - 0.010\ mm^{-1}$). Especially the peak of μ_a around the 970 nm (water) is greater for the lactating breast (range $\mu_a \approx 0.019 - 0.051\ mm^{-1}$) in comparison to the non-lactating breast (range $\mu_a \approx 0.010 - 0.039\ mm^{-1}$). In general, the IQR for the lactating breast is greater than the non-lactating breast. This shows in the maximum IQR present: 0.017 for the lactating breast and 0.011 for the non-lactating breast. The areola area absorbed slightly more than the non-areola area, for the lactating breast (range $\mu_a \approx 0.007 - 0.051\ mm^{-1}$ compared to $\mu_a \approx 0.005 - 0.041\ mm^{-1}$) and for the non-lactating breast (range $\mu_a \approx 0.003 - 0.039\ mm^{-1}$ compared to $\mu_a \approx 0.001 - 0.034\ mm^{-1}$), respectively. The difference is the clearest at, again, the water peak of 970 nm. The maximum differences between post and pre-expression in the μ_a spectrum

are obtained. The maximum difference for the non-lactating breast is $\mu_a = 0.002\ mm^{-1}$ (subject n4) and the maximum difference for the lactating breast is $\mu_a = 0.005\ mm^{-1}$ (subject L1). Overall, it is noticed that the peak at 930 nm (lipid) is not always observable.

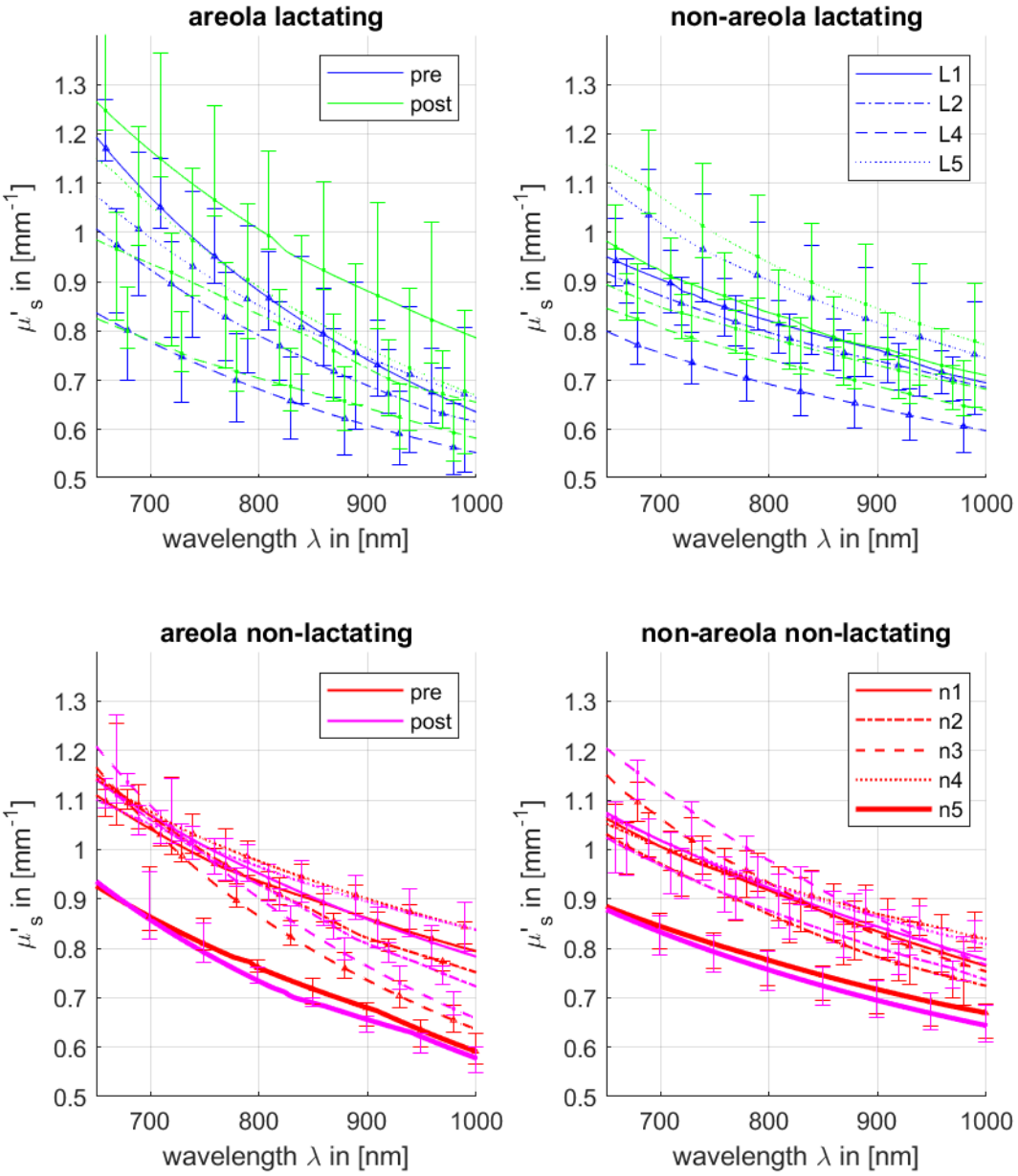

FIGURE 5.5: THE MEDIAN REDUCED SCATTERING COEFFICIENT OVER WAVELENGTH PER SUBJECT OF THE GRID MEASUREMENTS. THE ERROR BARS REFLECT THE INTERQUARTILE RANGE AT THE CORRESPONDING WAVELENGTH. THE UPPER TWO GRAPHS CORRESPOND TO THE RESULTS OF THE LACTATING SUBJECTS, THE BOTTOM TWO GRAPHS REFLECT THE NON-LACTATING SUBJECTS. THE LEFT FIGURES CORRESPOND TO THE AREOLA AREA, AND THE RIGHT FIGURES TO THE NON-AREOLA AREA. THE COLORS INDICATE THE DIFFERENCES BETWEEN PRE- AND POST-DATA. THE DIFFERENT LINE STYLES INDICATE THE DIFFERENT PARTICIPANTS, WHICH ARE THE SAME FOR THE NON-LACTATING FIGURES AND THE LACTATING FIGURES.

In figure 5.5, the reduced scattering coefficient spectra are shown. The μ_s' spectra for non-lactating breast (range $\mu_s' \approx 0.58 - 1.20\ mm^{-1}$) and for the lactating breast (range $\mu_s' \approx 0.55 - 1.27\ mm^{-1}$) are similar. Although, in general the IQR of the lactating subjects (maximum IQR $= 0.35\ mm^{-1}$) is greater than the IQR of the non-lactating subjects (maximum IQR $= 0.23\ mm^{-1}$). The last remarkable observation: The post-expression μ_s' spectrum is greater than the pre-expression μ_s' spectrum for every lactating subject, except for subject L2 in the

non-areola area. The maximum differences of the medians between pre- and post-expression μ_s' spectra for the non-lactating breast are $0.06\ mm^{-1}$ (subject n3) and for the lactating breast $0.15\ mm^{-1}$ (subject L1).

FUCTIONAL PROPERTIES

The functional properties are determined from the optical properties. Here the results of the functional properties are shown. First the median comparison between pre-, peri- and post-expression are shown in figure 5.6. Followed by figure 5.7, that included the milk volume and flow rate from the scale measurement. Then the peri-expression over time is shown, in figure 5.8. Finally, the relation between the functional properties to milk supply is shown, in figures 5.9 and 5.10. The previously mentioned qualitative analysis per lactating subject can be found in the Appendix – Qualitative analysis per subject.

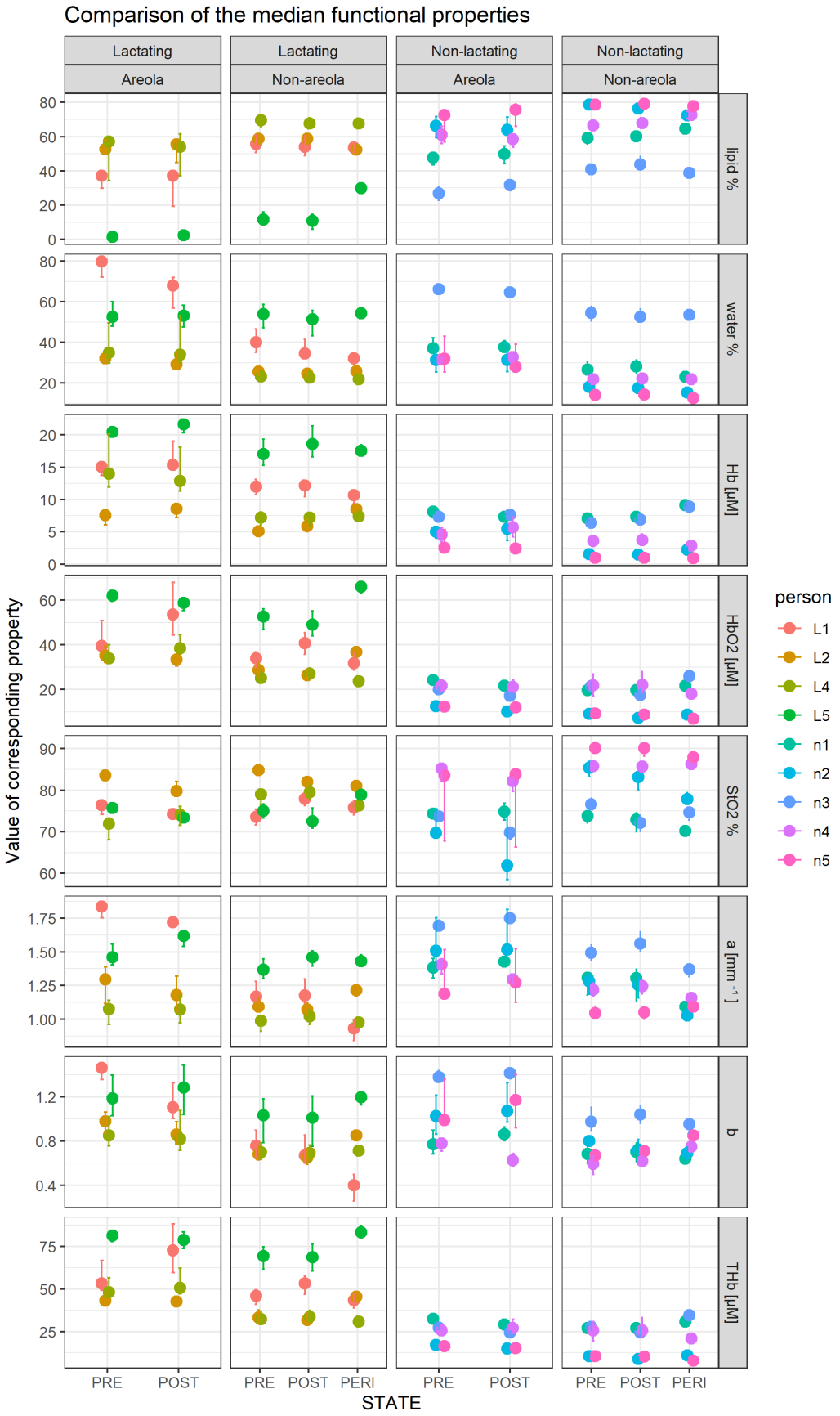

FIGURE 5.6: THE COMPARISON OF THE FUNCTIONAL PROPERTIES. IN THIS CASE, THE MEDIAN IS USED TO CALCULATE THE PROPERTIES. THE ERROR BARS SHOW THE INTERQUARTILE RANGE. THE COLORS IN THIS FIGURE INDICATE THE DIFFERENT SUBJECTS. THE LACTATING SUBJECTS AND THE NON-LACTATING SUBJECTS ARE SHOWN LEFT AND RIGHT, RESPECTIVELY.

In figure 5.6, the blood values, THb, HbO_2 and Hb, of the lactating breast are greater than of the non-lactating breast. To quantify, the THb medians of the subjects ranges from 31 to 83 µM and from 8 to 34 µM, for the lactating and non-lactating breast, respectively. Especially for L5, the blood values are high (median range of THb for L5: $69 - 83$ µM). The range of the medians for water concentration is higher and for lipid concentration is lower for the lactating breast than for the non-lactating breast, (water: $22 - 80\%$, lipid:$1 - 69\%$) and (water: $13 - 65$ %, lipid: $27 - 79\%$), respectively.

In general, the THb concentration, the water concentration, a and b are slightly higher for the areola area than the non-areola area per subject. The areola area is approximately a factor 1.3 higher than the non-areola area for the THb concentrations, a factor 1.5 for the water concentrations, a factor 1.1 for a and a factor 1.3 for b. The lipid concentration is approximately a factor 0.8 lower for the areola than for the non-areola area. There is not a clear overall difference between pre-expression and post-expression data. The peri-expression data seems in general in line with non-areola aera grid data. Lastly, subject n3 has a higher water concentration (median range: $51 - 65\%$) and lower fat concentration (median range: $27 - 43\%$) compared to other non-lactating subjects (median range of water: $13 - 38$ %, and of lipid: $48 - 79\%$).

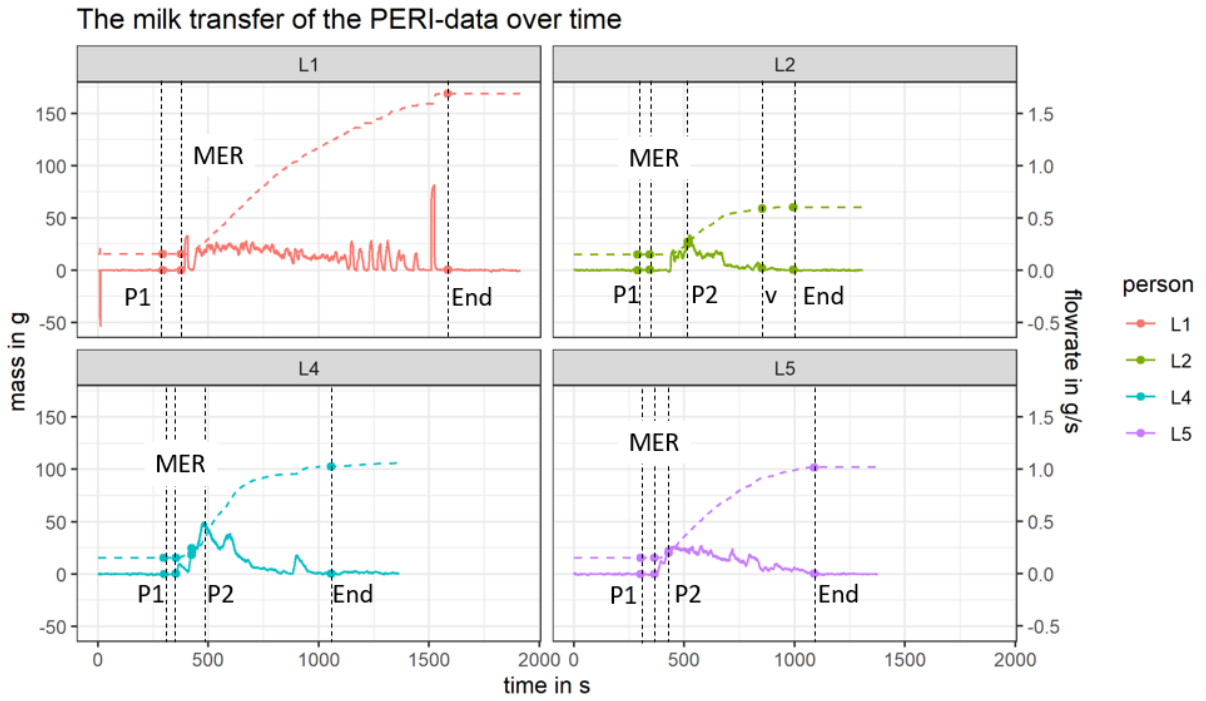

FIGURE 5.7: THE DASHED LINE IS THE MILK VOLUME, AND THE SOLID LINE IS THE MILK FLOW RATE OVER TIME. THE DOTS INDICATE EVENTS: P1 = PUMP IS TURNED ON IN THE STIMULATING STATE, P2 = PUMP IS SWITCH TO THE EXTRACTION STATE, V= THE PUMP IS SET TO A HIGHER PRESSURE, MER = THE FIRST MILK EJECTION REFLEX WHEN INDICATED BY THE SUBJECT AND END = END OF EXPRESSION. THE COLORS INDICATE SUBJECTS.

In figure 5.7, the milk transfer is shown. An important side note: Sometimes the milk of subject L1 accumulated in breast shield, therefore sometimes milk flows down into the bottle all at once.

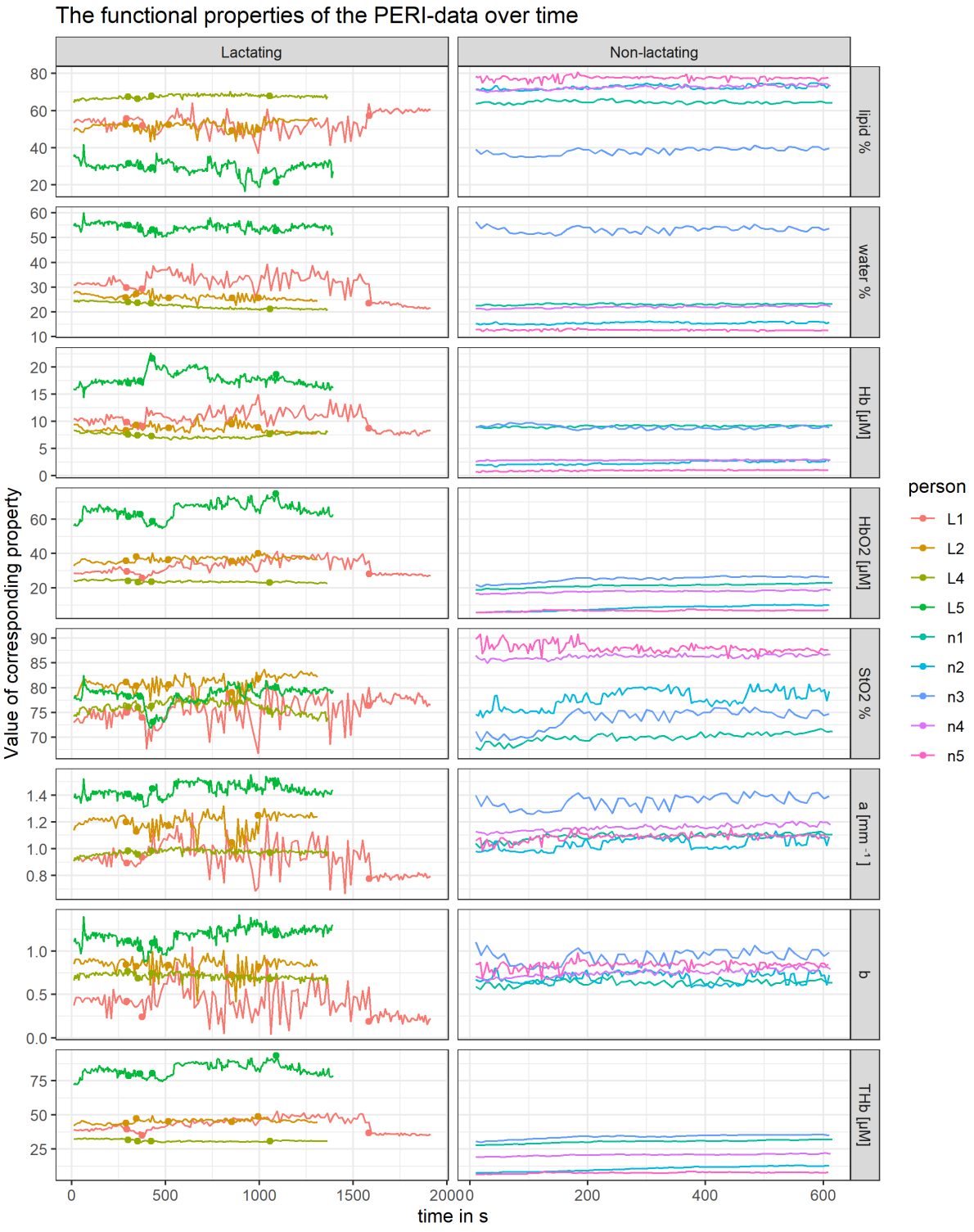

FIGURE 5.8: IN THIS FIGURE THE FUNCTIONAL PROPERTIES OVER TIME FROM THE SPOT MEASUREMENT ARE SHOWN. THE DOTS INDICATE THE SAME EVENTS AS LABELLED IN FIGURE 5.7. THE COLORS INDICATE SUBJECTS.

In figure 5.8, the spot measurements are shown. In general, the values of the functional properties fluctuate more for the lactating subjects when pumping compare to non-lactating subjects, see table 5.4, except for subject L4.

TABLE 5.4 THE SIZE OF THE RANGE BETWEEN THE MINIMUM VALUE AND THE MAXIMUM VALUE OF THE FUNCTIONAL PROPERTY OF THE PERI EXPERIMENTS.

	HbO_2 [µM]	Hb [µM]	THb [µM]	StO_2 %	Lipid %	Water %	$a\ mm^{-1}$	b
L1	15.4	7.6	18.0	14.6	26.9	18.4	0.60	1.01
L2	8.4	3.6	7.6	9.0	13.7	7.1	0.39	0.59
L4	2.7	1.8	3.1	5.1	6.0	4.1	0.11	0.18
L5	20.2	8.2	21.3	10.6	25.2	10.0	0.24	0.54
N1	4.3	0.8	4.5	4.3	3.5	1.3	0.13	0.16
N2	4.8	1.2	5.6	6.8	4.4	1.5	0.17	0.22
N3	6.3	1.5	5.7	6.9	6.6	5.7	0.17	0.32
N4	2.9	0.4	3.1	2.0	5.0	1.9	0.11	0.19
N5	2.0	0.6	2.5	5.0	7.1	1.6	0.17	0.31

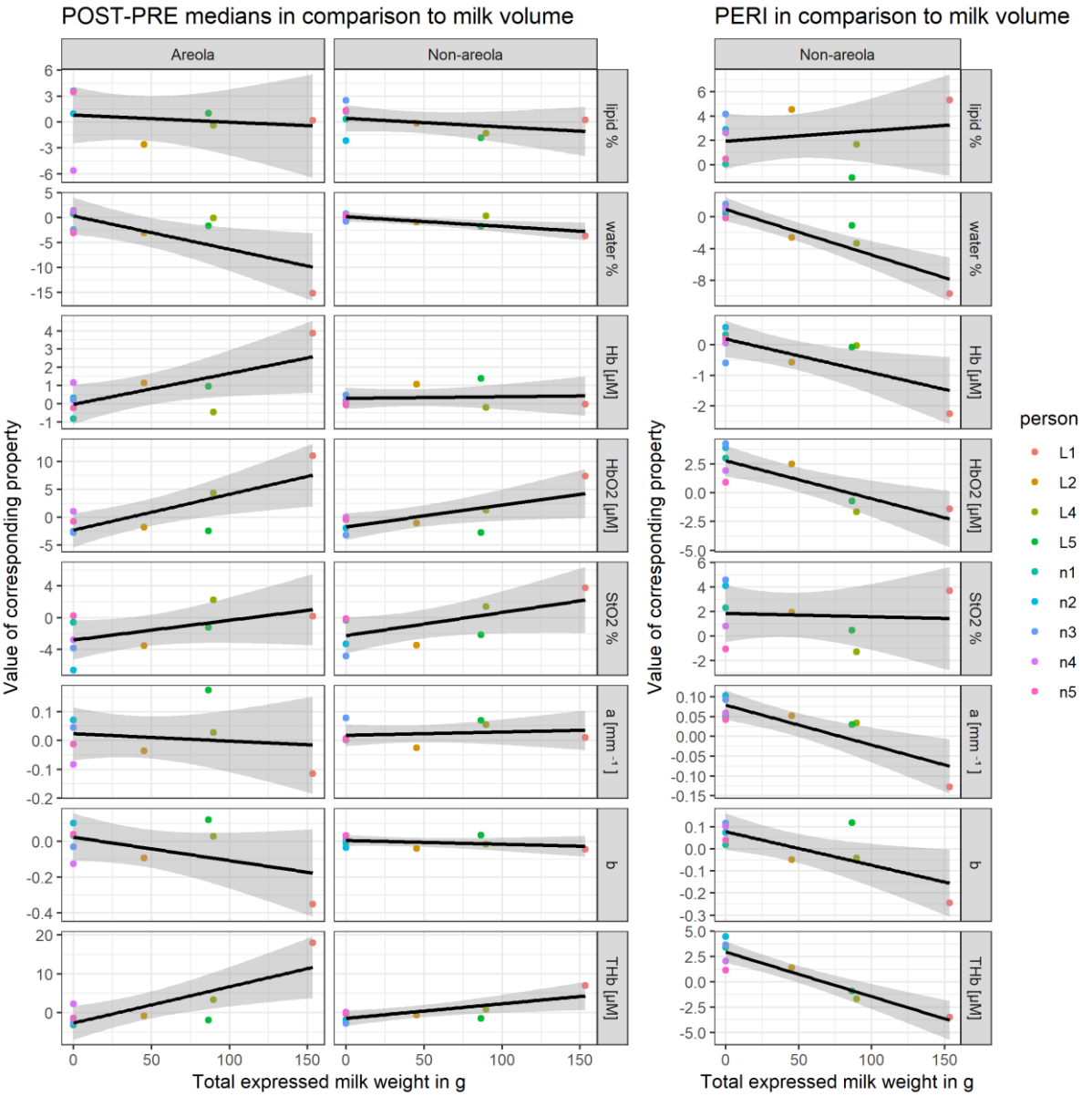

FIGURE 5.9: THE DOTS ARE THE MEDIAN OF THE DIFFERENCE BETWEEN BEFORE AND AFTER EXPRESSION PER SUBJECT. THE LINE IS A LINEAR FIT THROUGH THESE POINTS. THE GREY AREA INDICATES THE STANDARD ERROR OF THE FIT.

TABLE 5.5: IN THIS TABLE THE LINEAR FITS OF FIGURE 5.9 ARE SHOWN. ALSO, THE R^2 VALUE IS GIVEN, THIS CAN GIVE A FIRST INDICATION HOW STRONG THE CORRELATION IS BETWEEN THE CORRESPONDING FUNCTIONAL PROPERTY AND MILK SUPPLY.

Functional property	Grid measurement				Spot measurement	
	areola		Non-areola		Non-areola	
	Linear model	R^2	Linear model	R^2	Linear model	R^2
Lipid %	$y = 0.81 - 0.0082x$	0.02	$y = 0.43 - 0.0099x$	0.13	$y = 1.9 + 0.0086x$	0.05
Water %	$y = 0.33 - 0.067x$	0.54	$y = 0.15 - 0.019x$	0.59	$y = 0.96 - 0.058x$	0.84
Hb [µM]	$y = -0.015 + 0.017x$	0.47	$y = 0.30 + 8.8 * 10^{-4}x$	0.01	$y = 0.20 - 0.011x$	0.55
HbO_2 [µM]	$y = -2.3 + 0.064x$	0.61	$y = 1.7 + 0.039x$	0.48	$y = 2.8 - 0.033x$	0.69
stO_2 %	$y = -2.8 + 0.025x$	0.27	$y = -2.2 + 0.029x$	0.38	$y = 1.8 - 0.0027x$	0.01
a [mm^{-1}]	$y = 0.00 - 2.6 * 10^{-4}x$	0.03	$y = 0.02 - 1.1 * 10^{-4}x$	0.03	$y = 0.079 - 0.0010x$	0.72
b	$y = 0.02 - 0.0013x$	0.26	$y = 0.00 - 2.1 * 10^{-4}x$	0.14	$y = 0.078 - 0.0015x$	0.55
THb [µM]	$y = -2.6 + 0.093x$	0.63	$y = -1.5 + 0.038\,x$	0.57	$y = 3.0 - 0.044x$	0.86

In figure 5.9 with corresponding table 5.5, a linear regression is plotted for the differences in functional properties to milk supply. There is a slightly higher (above 0.50) R^2 for water, HbO_2, and THb. Thereby, note that HbO_2 and THb are depending on each other. Furthermore, THb for the pre- and post-expression measurement increase for an increase in milk volume, which differ from the peri-expression measurement, who indicate and decrease with an increase of milk volume. For the peri-expression data the R^2 scattering functional properties, a and b, is higher than for the pre- and post-expression data.

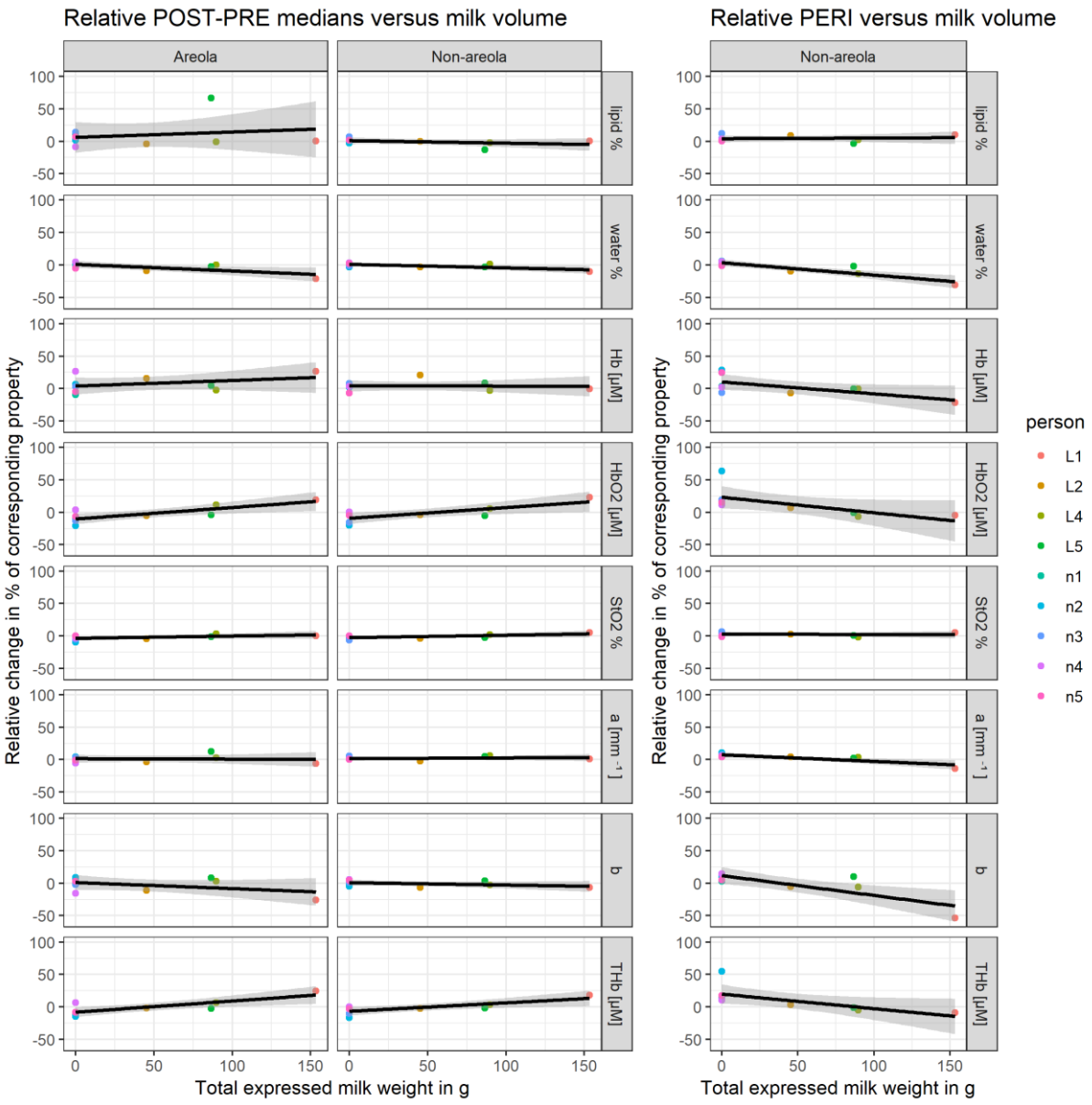

FIGURE 5.10: THE DOTS ARE THE RELATIVE DIFFERENCE BETWEEN BEFORE AND AFTER EXPRESSION PER SUBJECT. THE LINE IS A LINEAR FIT THROUGH THESE POINTS. THE GREY AREA INDICATES THE STANDARD ERROR OF THE FIT.

TABLE 5.6: IN THIS TABLE THE LINEAR FITS OF FIGURE 10 ARE SHOWN. ALSO, THE R^2 VALUE IS GIVEN, THIS CAN GIVE A FIRST INDICATION HOW STRONG THE CORRELATION IS BETWEEN THE CORRESPONDING FUNCTIONAL PROPERTY AND MILK SUPPLY.

Functional property	Grid measurement				Spot measurement	
	areola		Non-areola		Non-areola	
	Linear model	R^2	Linear model	R^2	Linear model	R^2
Lipid %	$y = 5.9 - 0.082x$	0.42	$y = 0.79 + 0.038x$	0.16	$y = 3.8 + 0.010x$	0.01
Water %	$y = 0.73 - 0.10x$	0.53	$y = 0.79 - 0.055x$	0.51	$y = 3.3 - 0.19x$	0.82
Hb [µM]	$y = 3.8 + 0.086x$	0.14	$y = 4.0 - 0.0035x$	0.00	$y = 10 - 0.18x$	0.45
HbO_2 [µM]	$y = -10 + 0.18x$	0.64	$y = -9.4 + 0.17x$	0.58	$y = 23 - 0.24x$	0.41
stO_2 %	$y = -3.8 + 0.035x$	0.27	$y = -2.8 + 0.038x$	0.38	$y = 2.6 - 0.0046x$	0.00
***a* [mm^{-1}]**	$y = 1.3 + 0.0075x$	0.01	$y = 1.3 + 0.012x$	0.06	$y = 7.3 - 0.10x$	0.71
b	$y = 1.1 - 0.094x$	0.20	$y = 0.78 - 0.037x$	0.19	$y = 12 - 0.31x$	0.66
THb [µM]	$y = -8.1 + 0.17x$	0.66	$y = -6.8 + 0.13x$	0.59	$y = 20 - 0.22x$	0.45

In figure 5.10 with corresponding table 5.6, the linear regression of the relative differences of the functional properties over milk volume are plotted. Again, there is a slightly higher (above 0.50) R^2 for water, HbO_2, and THb for the grid measurements. As well as that for the peri-expression data the R^2 scattering functional properties, water, a and b, is slightly higher (above 0.50) than the other functional properties and these values are higher than for the pre- and post-expression data as well.

DISCUSSION

The answer on the research question: *"What are the optical and functional properties of the lactating and non-lactating breast obtained by DOSI experiments"* is reported in the results section. The other three research questions, how the outcome of the measurements compare between the areola and non-areola, the lactating and the non-lactating breast, and the states of breastfeeding (i.e. before, during, and after expression), will be answered below.

OPTICAL PROPERTIES

First the absorption coefficient is discussed, followed by the analysis of the reduced scattering coefficient of the grid measurements.

ABSORPTION COEFFICIENT

The differences between the areola area and the non-areola area are probably due to blood supply [56] and due to the thicker skin in this area [32]. Furthermore, this could also be an indication that there is more glandular tissue present underneath the areola than the non-areola [11]. Whether the increase of absorption coefficient is due to a thicker skin, due to an increase in blood supply, or due to glandular tissue cannot be said. The overall absorption is approximately twice as high for the lactating breast than for the non-lactating breast. Probably mostly due to more blood supply causing a higher μ_a on the left side of the spectrum and more water at the longer wavelengths, see the figure 2.2. However, for the non-lactating breast, there is also a difference between pre- and post- at the water peak 970 nm and it is necessary to see if these changes are significant. There is more intra and inter variation for the lactating breast than for the non-lactating breast. This shows in the maximum IQR present: 0.017 for the lactating breast and 0.011 for the non-lactating breast and the range of the median of the lactating breast (range $\mu_a \approx 0.005 - 0.051\ mm^{-1}$) and non-lactating breast (range $\mu_a \approx 0.001 - 0.039\ mm^{-1}$). Both the inter as the intra subject variation could indicate the difference between glandular tissue and adipose tissue. Since the tissue is divided in lobules and is not actually homogenous. This can cause a difference within the subject measurements since there can be measured on a lobule or on a gland. The change intrasubject can indicate that there is a bigger variety of the ratio adipose tissue to glandular tissue for the lactating breast than for the non-lactating breast. Moreover, the variety can also be caused by the differences in blood supply for the lactating breast in comparison by the non-lactating breast.

REDUCED SCATTERING COEFFICIENT.

Again, thus far, there is more intra and inter variation for the lactating breast (maximum IQR $= 0.35\ mm^{-1}$ and range of median $\mu_s' \approx 0.55 - 1.27\ mm^{-1}$) than for the non-lactating breast (maximum IQR $= 0.23\ mm^{-1}$ and range of median $\mu_s' \approx 0.58 - 1.20\ mm^{-1}$). However, the range of the μ_s' spectra are similar for the lactating and non-lactating breast. In general, the post-expression data is higher than the pre-expression data, except for subject L2. Maybe this is because glandular tissue's μ_s' is higher than that of milk, indicating that the empty space left by the extracted milk is filled with the surrounding tissue (mostly glandular tissue).

FUNCTIONAL PROPERTIES

First, the average of the functional properties, in figure 5.4, categorized between the areola and the non-areola, the lactating and the non-lactating breast, and pre-, peri, and post-expression. It is important to remark that the deoxyhemoglobin and oxyhemoglobin (and therefore the THb) concentrations are larger for lactating subjects than for non-lactating subjects (a range of $THb = 31 - 83\ \mu M$ for the lactating breast and a range of $THb = 8 - 34\ \mu M$ for the non-lactating breast). This supports the literature findings [8][7]. The range of the medians

for water concentration is higher and for lipid concentration is lower for the lactating breast than for the non-lactating breast, (water: $22-80\%$, lipid:$1-69\%$) and (water: $13-65\ \%$, lipid: $27-79\%$), respectively. This could indicate that the lactating breast contains more glandular tissue than the non-lactating breast, which is in agreement with literature [11]. There was not a clear difference between the lactating and non-lactating groups for the other chromophores. Furthermore, the average peri-expression values are similar to the other non-areola values, which can be expected since the peri-expression values were done on the non-areola area. A significant difference between the average pre- and post- values is not observed. In addition, in general, the value of THb (approximately a factor 1.3), water (approximately a factor 1.5), a (approximately a factor 1.1) and b (approximately a factor 1.3) are slightly higher and the lipid concentration (approximately a factor 0.8) is lower for the areola than for the non-areola area. Especially that the water concentration is higher and the lipid concentration is lower could be an indication that there is more glandular tissue present underneath the areola than the non-areola [11]. That a and b are higher, could indicate that the photon distribution is more sensitive for skin, because the skin is thicker for the areola than for the non-areola. Since, in general, skin has a higher a and b than subcutaneous fat, see table 3.5 and table 3.6. Another interesting detail is that subject n3 had a higher water concentration and a lower lipid concentration than the other non-lactating subjects, see figure 5.4. This can be because she was on the only subject with a parity of 0 (meaning she has never given birth before) as only subject. Furthermore, in this figure is also shown that the lipid concentrations of L5 are low in comparison to the other subjects. This could indicate that there is not measured through the whole subcutaneous fat layer since the source detector distance of this subject is smaller and there is a lot of absorption, causing the photon propagation distribution to be smaller. Another possibility is that this subject has almost no subcutaneous fat.

Figure 5.5 shows the milk volume measurements. The total expressed milk weight was 153.3 g for L1, 45.3 g for L2, 89.7 g for L4 and 86.5 g, which correspond nicely with the approximately mean of 70 ml in literature, see table 3.2. The peaks in the milk flow rate are seen as an indication of MERs [44][48][45]. At the measurement of subject L1 the milk accumulated in the breast shield. This could be the cause of the high spikes in the milk flow rate peaks. For the other subjects, the highest peak was at the first or second MER, which is similar to literature. The highest peaks where 0.55 g/s for L2, 0.47 g/s for L4 and 0.37 g/s for L5, which is similar to literature as well [44], see also table 3.2.

Thirdly, the PERI data examined over time in figure 5.8. In the Appendix – Qualitative analysis per subject, a more elaborated version can be found per subject, where the PERI data is compared to the milk flow rate and milk volume. Of the lactating subjects, L5 shows the most similarities with the milk flow rate profile and was the only subject with shorter source-detector distances. In addition to this analysis, the relative low sample time of L5, see table 5.3, could explain why the PERI data had the most similarities. Observed is that pumping events, turning the pump on and off or on a different setting, are related to chromophore changes for most subjects. The MER is associated with a temporal dip in THb for most subjects. This is similar to what is found in two Japanese studies using NIRS [45] [48]. Another observation of the peri-expression data in figure 5.8 is the stO_2 also drops after a MER. Maybe, similar as in sports, the glands and the muscle-like tissue around the alveoli need more oxygen.

Finally, in figure 5.9 and 5.10, the functional properties are correlated to the extracted milk volume. Notice that there are not much data points available. Water concentrations and b decrease more with increasing milk volume, see figure 5.9 and 5.10. Moreover, THb increases more with increasing milk volume for the pre-post-data, but decreases for the peri data. It is worth adding that a possible explanation for the rise in THb concentration lies in the fact that glands will come into the place where milk was, and milk does not contain blood, for the pre- and post-expression of the grid measurement. Still, this does not explain the decrease of THb in pre- and post-expression of the spot measurement. However, note that the peri-measurement measures 2 minutes directly after the breastfeeding and the post grid measurement is after that measurement. Thus, it could be that the different time frame is connected to this difference.

SHORTCOMINGS AND LIMITATIONS

Overall, all the findings need to be supported by more data. In order to do more quantitative statistical research. It was decided not to do several statistical analyses for example a Principal Component Analysis or multiple linear regression to distinguish the lactating or non-lactating breast, since it is important to know the distribution of the data. Since the biological breast can vary a lot between subjects, and especially the distribution of functional properties of the lactating breast is not well investigated, we decided to wait to do such statistical analysis, considering that only four (already very different) lactating breasts and five non-lactating breasts were measured.

For the absorption coefficient, there are two aspects that might be influenced by crosstalk. Sometimes the peak at 930 nm, mostly caused by lipid, disappeared, due to the dominant presence of water. The lactating breast could be more sensitive for this than the non-lactating breast, due to the higher water concentrations as stated earlier. To check if this is the case, it is necessary to examine the way the fit of the chromophores is made. The other aspect that could cause unwanted crosstalk is the melatonin in the skin with the lower wavelengths. However, since this is not a specific problem for the lactating breast, this should be accounted for in previous research with the normal breast. Moreover, all subjects participating were Caucasian. To see if melatonin has an effect, other skin types should also be included in the study. It is important to remember this aspect when analyzing the functional properties, in case of unrealistic values for lipid and (deoxy)hemoglobin.

Expected was that the sample time of the PERI-measurement was approximately 3 seconds. However, for the lactating subjects was this was approximately 8.9 seconds and for non-lactating subjects 6.3 seconds, which varied between subjects. For example, L5 had a mean sample time of 5.0 seconds and L1 had a mean sample time of 13 seconds, see table 5.3. This could be due to the breasts of this research's subject group contains more dense tissue than other subject groups that participates to previous DOSI research, where the mean age of the participants is normally higher. A higher sample frequency for the PERI-measurement would add to this research to differentiate between events better, such as MER's or breathing. This could help to create a better understanding for the physiology of breastfeeding and lactation.

CONCLUSION

Although not many participants contributed to this research yet, these first results already look promising. To elaborate, there can already a trend been seen in difference between the lactating breast for the optical and the functional properties. Especially approximately THb concentrations seems to be twice as high for the lactating breast. Also, the difference between lower lipid concentrations and higher water concentrations of the lactating breast indicates that the lactating breast contains more glandular tissue than adipose tissue. Thereby, the areola area carefully shows some differences to the non-areola area: THb concentrations, water concentrations, a and b are (slightly) higher and lipid concentrations are (slightly) lower. Unfortunately, not much can be said about the difference between pre- and post-expression. Nevertheless, the functional properties of the peri-data have some similarities to the milk flow rate, especially for THb and stO_2 a drop is observed during a MER. The experiments will be used to validate the model.

6. Validation and Prediction

Introduction

In this chapter, we validate the model to the experiments and evaluate the possibility to predict milk transfer from the DOSI experimental data. The objective of this chapter is to answer the following research questions:

Validation

6. How do the model outcomes compare to optical and functional properties obtained by the DOSI experiments?

Prediction

7. To what extent is it possible to predict milk transfer from DOSI experiments?
8. To what extent is the prediction influenced by biological variation between and within the breast?
9. What is the accuracy and precision with which the model can predict the ejected milk volume during a breastfeed, when comparing DOSI experiments to the weighted milk volume?

Evaluation prediction

10. How can the DOSI system be further optimized to measure milk supply in the lactating breast?

Methods

The validation of the model is carried out in two methods: The average model of the breast is compared to the median of the overall experiments and the model is fit to the μ_a spectrum of every subject using the possible variations. The following challenge is to predict milk transfer. First, a "water concentration" method is carried out. By only using the change in water measured by the experiment and the change of water of the model before and after expression, milk transfer can be predicted. Lastly, the model is again fitted to the μ_a every experiment per subject, but with a focus on fixed values of milk transfer. Below, a more elaborate explanation is given for every method.

In the model, the expressed milk is described in volume and in the experiments the expressed milk is weighted. The density of human milk is approximately 1.03 g/ml [73]. Therefore, in this research, 1 ml milk is assumed to be equal to 1 g milk.

Validation

For the first aforementioned validation: The optical and functional properties of the model and the experiments are combined. Thereby, in the previous chapter a linear regression model is plotted through the experiments. If the model adequately describes the average lactating breast and the pilot experimental data are representative for a large population, both the modeled data and the experimental data should be in the same range.

The second method, the fit of the model to the experiments of every subject, is slightly more complex.

Assumptions and simplifications

The model will not fit the μ_s' to the μ_s' of the experiments. For the reasons given in de discussion of the model, taking the μ_s' of the model into account will probably lead to a higher error between the model and the experiments, and more complexity. Although, the μ_s' spectrum and the functional properties will not be fitted to the experiment (directly), the model will still give an outcome of these properties when only fitting μ_a.

Some input variables are fixed, to make the model less complex and decrease the computational power. One of the fixed variables is the fat percentage in milk, since this does not change μ_a very much (approximately 0.001 mm^{-1}, see Appendix - Variations of the breast). Secondly, the volume of the lactating breast is fixed. An educated guess of the volume of the lactating breast is made, based on cup size. Finally, the light distribution has the same μ_s' and μ_a input values for the lactating and the non-lactating breast. The source-detector distance will

correspond to the used source-detector distance in the experiments. This results in 11 changeable variables: the thickness of the skin and subcutaneous fat layer of the areola and non-areola area, the ratio adipose to glandular tissue of the areola and non-areola area, the hematocrit of the blood, the correction for stO_2, the concentration of blood in the tissue, and, for the lactating subjects, the storage capacity of milk in the glands and milk extracted. Mostly, the approximate input variables of the average breast model are used as the initial set of input variables. The concentration of blood in the tissue is range to 0 to 1, where the concentration of blood is scaled to the minimum to the maximum concentration of blood reported in table 4.9 of every layer.

Another simplification is carried out; not every possible combination of the input variables is used to fit all μ_a spectra of every subject. This would cost too much computational power, since this will result in approximately 10^{12} possible models to be tested, when there are approximately 12 input variables and if 10 values of every input variable are tested. Therefore, a root finding algorithm is used. These algorithms search for zeros close to their input value (local optima). This research utilized the root finding algorithm "Newton-Raphson Method".

NEWTON-RAPHSON METHOD

Once the initial conditions are set, the following step is to fit the model to the datasets of every subject. The Newton-Raphson method is used to search for a solution:

$$X_{new} = X - \frac{f(X)}{f'(X)} \tag{6.1}$$

In this formula is $f(X) = model - experiment\ dataset\ of\ one\ subject$ and X are the input variables. $f'(X)$ is calculated with the finite difference approximation. The initial input variables X have the values of the average (non-)lactating breast. The input variables are fixed except for one changeable input variable. The variable that is not fixed, alternates in a loop including all changeable input variables. The new input variables, X_{new}, are checked if they exceed the boundary conditions (see the possible range of the variations of the breast in table 4.8 and table 4.9), if this happened the value is changed to the boundary condition. The script will run this multiple times. The script will stop running if:

- The error is zero.
- The maximum iteration is reached, which corresponds to 30 iterations. Specifically, one iteration is when all input variables have changed.
- A local maximum or minimum is reached.
- When the model does not converge to a solution. In this case the values of the input variables and model will become "not a number" (NaN) and the error will be relatively large.

A solution is found when the error is not too high ($|\ \mu_{a,model} - \mu_{a,experiment}| \leq 0.01\ mm^{-1}$ at every wavelength) and there are no values equal to NaN. In case no suitable solution is found, the initial values of X are tweaked to other realistic values of X. If this is the case, this is denoted in the results in the Appendix – Newton-Raphson fits what these changes are.

PREDICTION

Then, we try to see to what extent it is possible to predict milk transfer. For the water concentration method, there is an emphasis on the water percentage change between before and after a breastfeeding session, due to the fact that the majority of human milk consists of water and it has a high correlation (R-squared) in comparison to the other functional properties to the total expressed milk weight in the experiments, see figure 5.9 with corresponding table 5.5 and figure 5.10 with corresponding table 5.6. As stated in the physiological variability of the model, between before and during a breastfeed, some variables can change: The milk transfer (for lactating subjects), the blood dynamics and there could be an error in the placement of DOSI device or a transformation of the breast. Both blood dynamics and milk transfer are dependent on water. The water percentage is corrected

for the concentration of blood according to the same method as the model, see chapter 4. The model equation 4.1. The water percentage is corrected for the concentration of blood that undergoes changes:

$$water_{milk}[\%] = water_{total}[\%] - water_{blood}[\%] \tag{6.2}$$

The $water_{milk}$ should now only consist of the change of water due to milk transfer (for the lactating subjects). Thereby, there could still be an error due to the repeatability of the measurement. It is now possible to calculate the decrease in water concentration due to a breastfeed with the model of the average breast.

Furthermore, once again the Newton-Raphson method is used to investigate to what extent DOSI can predict milk transfer. For this, the input variable of the extracted milk volume is fixed. If the error is similar (tolerance= original error + 5%*original error) or even lower than the error of the original fit, this is accepted as a solution as well. This will give an accuracy for when the model fits.

RESULTS

VALIDATION

The average breast model is combined with the experimental data.

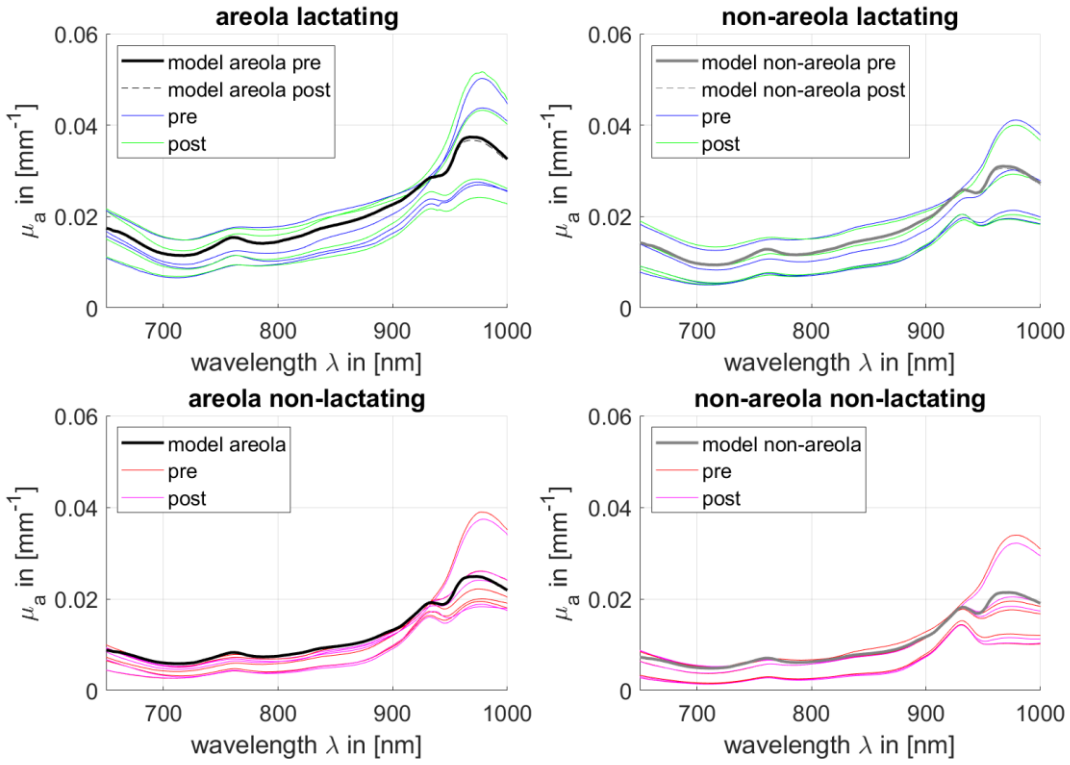

FIGURE 6.11: THE MEDIAN ABSORPTION COEFFICIENT PER SUBJECT OF THE GRID MEASUREMENT IN COMBINATION WITH THE AVERAGE BREAST MODEL. THIS FIGURE IS A COMBINATION OF FIGURE 4.10 AND FIGURE 5.4. THERE ARE MULTIPLE LINES OF THE PRE- AND POST-EXPERIMENTS. THESE LINES INDICATE THE MEDIAN OF THE MULTIPLE SUBJECTS. THE BLACK AND GRAY LINES ARE THE MODEL, WHERE THE SOLID LINE IS PRE-EXPRESSION, AND THE DOTTED LINE IS POST-EXPRESSION. FOR BOTH THE MODEL AS FOR THE EXPERIMENTS, IT CAN BE THAT PRE- AND POST-EXPRESSIONS LINES OVERLAP.

In figure 6.1, it is observed that the model average breast of μ_a is in between the experimental values of μ_a for the lactating breast. The model is slightly higher than the median of the experiments for the non-lactating breast for wavelengths below 900 nm (maximum differences between model and the median of the experiments $\mu_a \approx 0.001\ mm^{-1}$). However, for the wavelengths greater than 900 nm, the model is in range of the medians of the experiments.

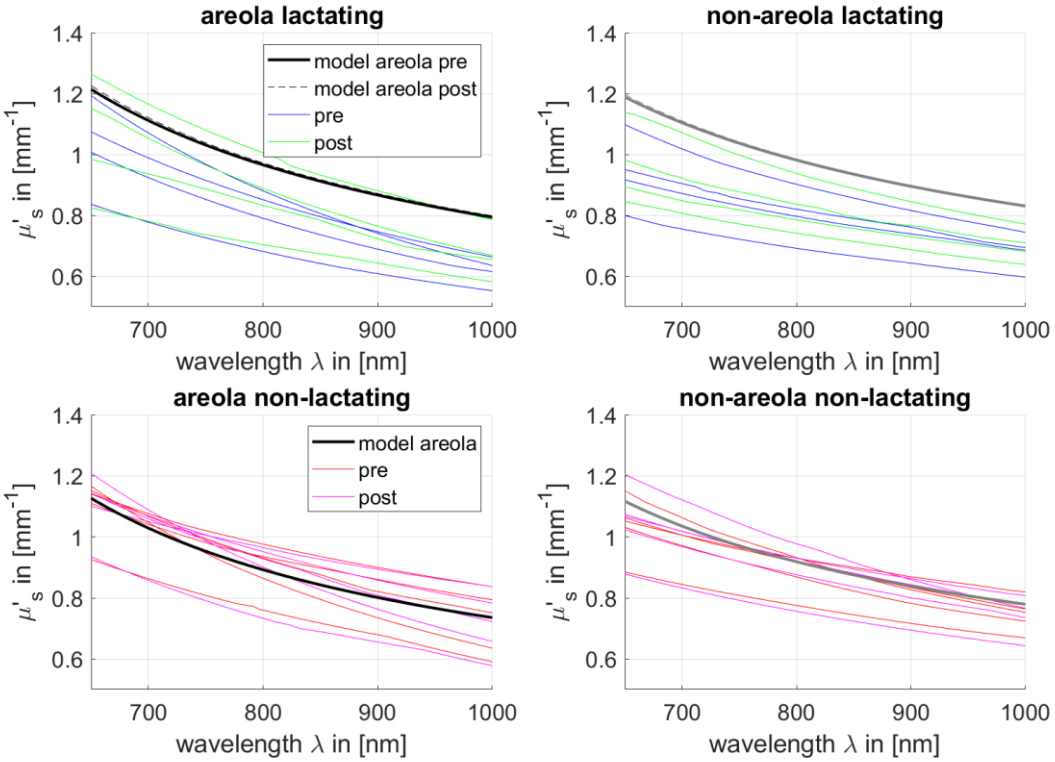

FIGURE 6.2: THE MEDIAN OF THE REDUCED SCATTERING COEFFICIENT PER SUBJECT AND THE MODEL OF THE AVERAGE BREAST. THIS FIGURE IS A COMBINATION OF FIGURE 4.10 AND FIGURE 5.5. THERE ARE MULTIPLE LINES OF THE PRE- AND POST-EXPERIMENTS. THESE LINES INDICATE THE MEDIAN OF THE MULTIPLE SUBJECTS. THE BLACK AND GRAY LINES ARE THE MODEL, WHERE THE SOLID LINE IS PRE-EXPRESSION, AND THE DOTTED LINE IS POST-EXPRESSION. FOR BOTH THE MODEL AS FOR THE EXPERIMENTS, IT CAN BE THAT PRE- AND POST-EXPRESSIONS LINES OVERLAP.

In this figure 6.2 it can be observed that the modelled μ_s' is in the range of the experimental μ_s' values for the non-lactating subjects. However, for the lactating subjects, especially in the non-areola area, the model is, in general, higher than the experiments (maximum difference between the model and the experimental median is approximately $\mu_s' \approx 0.06\ mm^{-1}$).

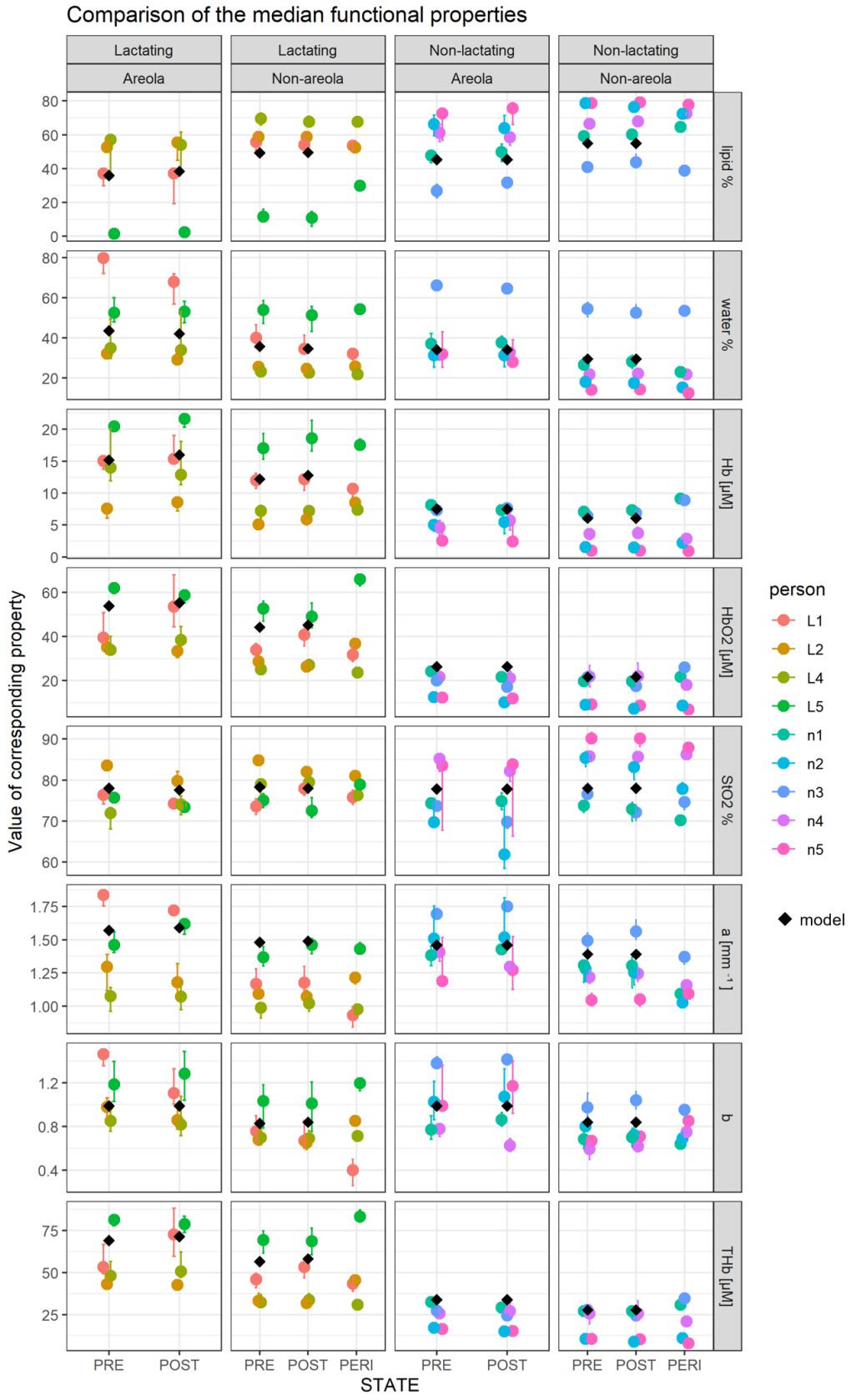

FIGURE 6.3: THE MEDIAN FUNCTIONAL PROPERTIES OF THE EXPERIMENT PER SUBJECT (COLORED DOTS) WITH THE MEDIAN FUNCTIONAL PROPERTIES OF THE AVERAGE BREAST MODEL (BLACK DIAMONDS). THIS IS A COMBINATION OF FIGURE 5.8 AND TABLE 4.10.

Above, in figure 6.3, the medians of the functional properties are shown of the experiments and the model. In general, the functional properties of the model are in the range of the experimental values. However, the THb concentration of the average non-lactating breast, and therefore the HbO_2 concentration as well, is 1 µM higher in the model than the highest median of THb concentration of the experiments (subject n1). Although mostly in the range of the experimental data, the values of the a of the model are relatively high, especially for the non-areola area on the lactating breast.

The Newton-Raphson method fits are too extensive to be displayed in this section, but they can be found in the Appendix – Newton-Raphson fits per subjects. First, the optical fits are discussed with their corresponding error plot. Overall, the errors of the absorption coefficient are small (below $\mu_a = 4 * 10^{-3}\ mm^{-1}$). The error is higher at the water peak (between 950 nm and 1000 nm) and slightly higher at 650 nm, compared to the rest of the spectrum. The water fit seems to be shifted slightly to the right-hand side (lower wavelength) of the experimental peak of each measurement. The μ_s' does not seem to converge to the experimental data.

The fits of the functional properties are shown in Appendix – Newton-Raphson fits and Appendix – Fit error functional properties. In this section the difference of the functional properties as outcome of the model fitted to the experiments using the Newton-Raphson method are compared to the functional properties fitted directly to the experiments. Again, the following observations are carried out. During these observations, the functional properties as outcome of the model by using the Newton-Raphson method is referred to as "the model's functional properties" and the functional properties fitted directly to the experiments are referred to as "the experiment's functional properties".

The **lipid concentrations** of the lactating breast differ more than 10% between the model and the experiments for L1 and L5 at the areola area. It is noticeable that both these subjects have a high absorption spectrum for water. For the non-areola area, the lipid concentrations do not differ more than 10%. For all the non-lactating subjects the model has a lower estimation for lipid concentration than the experiment median lipid concentration. For the non-areola area, the differences of the fits are below 10%, except for subject n3 and n5.

The difference between the model and the experiment for **water** and **Hb concentration** are below 10% and 3 µM, respectively.

The **HbO_2** and **THb concentrations** behave similarly: for the lactating subjects, the fits differences are around 0 (between -3 and 5 µM). For the non-lactating subject, the values of the fit by the model are higher than those of the experiments (between -1 and 17 µM).

The **stO_2** for the lactating subjects are similar: between -5 and 5%. The difference for the non-lactating subject is larger, namely between -10 to 15%.

The $\boldsymbol{a}$ and $\boldsymbol{b}$ indicate a large difference between model and experimental values, when compared to the average value of a and b, around $1.0\ mm^{-1}$ and 0.9, respectively. The difference for a is between -0.5 to $0.5\ mm^{-1}$ and for b is between -0.4 to 0.4.

PREDICTION

This section presents the outcome of the "water concentration" method. For every subject, the differences between the water concentration of the experiment before and after a breastfeed is used. First, a correction is done for the change in water concentration due to blood. This is followed by using the average lactating breast model to calculate how much milk volume is equal to the experimental water concentration. In the model of the average breast is 70 ml of ejected milk volume equal to 1.0% for the non-areola area and 1.5% of water for the non-areola area water concentration differences between pre- and post-expression. The relative value for the non-areola area is 2.8% and for the areola area is 3.5%. This results in table 6.3 and table 6.4.

TABLE 6.3: MILK TRANSFER CALCULATED FROM THE ABSOLUTE DIFFERENCES IN WATER CONCENTRATION BETWEEN BEFORE AND AFTER EXPRESSION WITH THE MODEL.

	Measured milk transfer (g)	Predicted milk transfer, from PRE and POST data (ml)		Predicted milk transfer, from PERI data (ml)
		Areola	Non-areola	Non-areola
L1	153.3	740	277	671
L2	45.3	143	63	185
L4	89.7	9	-22	231
L5	86.5	75	122	74
N1	0	-40	-52	-21
N2	0	-70	36	-51
N3	0	110	46	-103
N4	0	-59	-41	-70
N5	0	143	-16	13

TABLE 6.4: MILK TRANSFER CALCULATED FROM THE RELATIVE DIFFERENCES IN WATER CONCENTRATION BETWEEN BEFORE AND AFTER EXPRESSION.

	Measured milk transfer (g)	Predicted milk transfer, from PRE and POST data (ml)		Predicted milk transfer, from PERI data (ml)
		Areola	Non-areola	Non-areola
L1	153.3	440	281	765
L2	45.3	175	85	241
L4	89.7	8	-35	339
L5	86.5	52	87	48
N1	0	-51	-66	-36
N2	0	-84	64	-100
N3	0	65	25	-67
N4	0	-81	-74	-117
N5	0	96	-44	47

The outcome of the milk transfer by the Newton-Raphson method can be found in Appendix – Newton-Raphson fits. Thereby, the non-lactating subjects are also used as input of the lactating breast model. The fit stays at 0 ml milk extraction. The fit for the lactating subject using the Newton-Raphson method is summarized to table 6.5 and figure 6.4.

TABLE 6.5: MILK TRANSFER PREDICTION USING THE NEWTON-RAPHSON METHOD

	Measured milk transfer (g)	Fit (ml)	Range fit (ml)
L1	153.3	149	115-200
L2	45.3	180	0-200
L4	89.7	51	0-200
L5	86.5	47	0-100

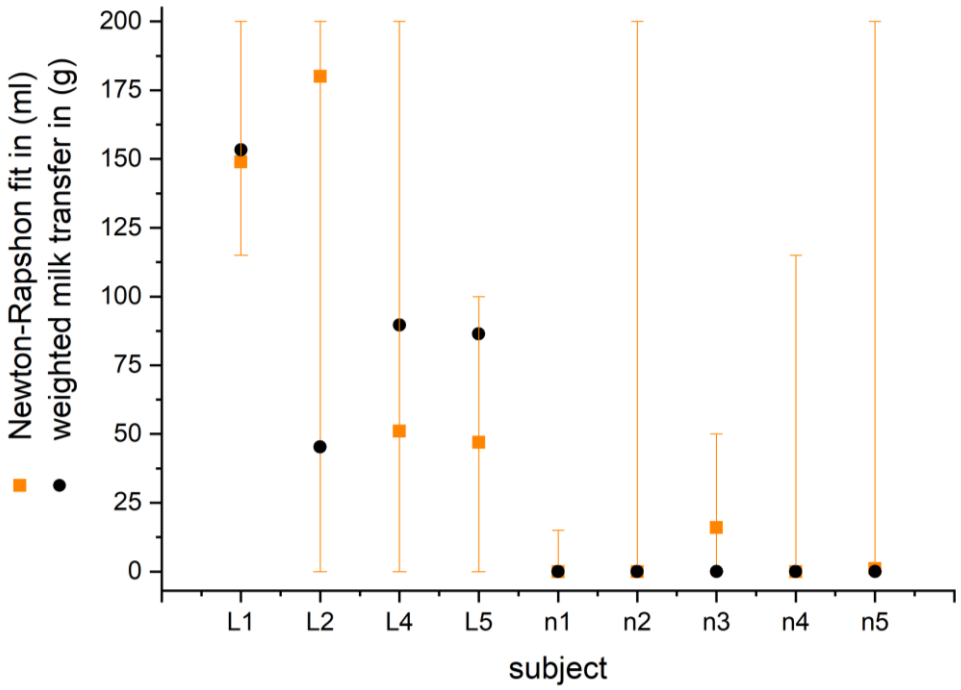

FIGURE 6.4 THE NEWTON-RAPHSON FITS PLOTTED. THE ERROR BARS REFLECT THE RANGE FOR WHICH THE ERROR WITHIN 5% OF THE ERROR OF THE FIT OF THE ORANGE SQUARE. THE INFORMATION OF TABLE 6.5 IS VISUALIZED FOR THE LACTATING SUBJECTS. THE NON-LACTATING SUBJECTS ARE THE CONTROL GROUP. WHEN ASSUMED IS THAT THEY ARE LACTATING SUBJECTS WILL GIVE THE RESULTS SHOWN.

The measured milk transfer by the scale is in the range of the fitted milk supply. The smallest range is of subject L1, with 85 ml bandwidth. The largest range is L2 and L4, it ranges from the lowest boundary of 0 ml to the highest boundary of 200 ml. It is important to stress that the error for the values of the boundaries of milk transfer is approximately the same or smaller than the fit with an unfixed value of milk extraction. Nevertheless, it is interesting to note that the fit for the unfixed milk extraction is the same for L1 and for the non-lactating subjects, except for n3.

DISCUSSION

VALIDATIONS

First, the validation is discussed. The average model seems to fit in the range of the medians of the experiments. Thereby, the μ_a is slightly higher for the lower wavelengths below 900 nm, the maximum difference of the medians is $\mu_a \approx 0.001\, mm^{-1}$. This is possibly due to the fact that the values of deoxyhemoglobin and oxyhemoglobin are lower in reality than in the present average model. However, this can be easily changed with certain variations of the model, such as concentration of blood, see Appendix – Variations of the breast. Furthermore, μ_s' spectrum of the model of the lactating breast is slightly too high in comparison to the experiments, the maximum difference of the medians is $\mu_s' \approx 0.06\, mm^{-1}$. This is also reflected in het functional property the scattering prefactor, a. Probably the model is not reliable for μ_s', as explained in the discussion of the model. Another reason can be that there are not enough experiments.

The fits obtained using the Newton-Raphson method match well with the μ_a-spectrum, see Appendix: The error is overall not higher than $\mu_a = 4 * 10^{-3}\, mm^{-1}$. For all subjects, the errors peaks at the 650 nm and around the water peak (970 nm). This could be due to the fact that melanin still plays a (limited) role. The absorption coefficient of water is slightly blue-shifted in the experiments compare to the chromophore sheet in figure 2.2 (hence, the model). This can be due to the fact that water is present in the tissue [84]. The μ_s' does not always converge to the experimental value, but then again, μ_s' is not taken into account when fitting the model to the spectra.

Overall, the functional properties are close to the model and the experiments, see Appendix – Fit error functional properties. However, there are some exceptions. The lipid concentration can have a considerable difference between the model and the experiments. This mostly occurs with a high water concentration relative to the other subjects. A possible explanation for this might be the absorption peak of water that overshadows the peak in the absorption spectrum of lipid. Again, the functional properties of scattering are very different, which can be expected since the reduction scattering coefficient is not included in minimizing the error of the fit.

In conclusion of this validation, the model seems to work well to match μ_a, but not to match μ_s'. This supports the anatomical and physiological theory on which the model of the μ_a spectra are based.

PREDICTION

The "water concentration" method is shown in, see table 6.3 and 6.4. As expected, the "water concentration" method does not work well. It Is necessary to consider that the range of milk transfer of the lactating breast lies between 0 and 200 ml, see table 3.2 and table 4.9. There are several values exceeding this boundary. The non-lactating subject should predict 0 ml milk extraction. However, the values differ between -117 ml and 143 ml. This can be potentially improved with more datasets, although it is debatable if there is a linear correlation between one of the functional properties and milk transfer at all.

The Newton-Raphson method gives a range of where the milk transfer should be for a low error fit of μ_a. The minimum range found was 85 ml. This value, compared to the average 70 ml milk extracted during a normal breastfeeding session, is already large. However, the weight of milk extracted was within this range. The range is probably true to reality since there are so many unknown input variables, such as the layer thickness of the skin or the amount of glandular tissue, a relatively large range can be expected. Thereby, DOSI is relatively more sensitive for the skin and subcutaneous fat layer than for the mammary tissue layer since this reaches mostly 1 cm below the surface of the breast. Also, the model extrapolates over the whole breast, which grants higher accuracy of the total amount of milk extracted from the breast.

Based on the results of this chapter, we can conclude that DOSI in combination with this model is not a suitable method to predict milk transfer. Although this prediction using the "Newton-Raphson" method has a nice accuracy for the 4 subjects, the prediction is imprecise. Suggest is to improve the μ_s' of the model. The use of the "water concentration" method is neither accuracy nor precise. However, perhaps this can be improved with more experimental data.

7. CONCLUSION AND OUTLOOK

CONCLUSION

In this report, a model of DOSI on the (lactating breast) is made and DOSI experiments are carried out. Thereby the experiments are used to validate the model and the model is used to predict ejected milk volume of the breast. To answer the research question: The fitted model to the DOSI measurement on the lactating breast is able to predict milk transfer. Unfortunately, the prediction is imprecise: the smallest range was 85 ml, and two lactating subjects where in the maximum range of 0-200 ml. This model can be improved, although the exact anatomical and physiological composition of the breast per subject remains uncertain, because the great variability of the (lactating) breast. This could be the cause that the possible extracted milk volumes can have a wide range.

This research also investigates the properties of the lactating breast. The important differences between the lactating breast and the non-lactating breast, which will influence DOSI in literature is that the lactating breast contains approximately twice as much blood and the lactating breast contains a lower ratio of adipose tissue to glandular tissue than the non-lactating breast, are implemented in the model and can be carefully confirmed by the experiments. Thereby, during the PERI-measurement a drop can be noticed for THb, and sometimes stO_2, during a MER. This could be interesting for the physiology of the mammary glands. Moreover, there is, with only four subjects, already a high inter- and intra-variability of the optical and functional properties of the lactating breast compare the non-lactating breast.

THE RECOMMENDATIONS

The shortcomings of the model and the experiments are already given through the report. The recommendations to overcome these shortcomings are explained below.

To indicate if the diffusion equation with all the assumptions made was sufficient enough its is usefully to develop models based on simulations with less assumptions, such as the Monte Carlo Simulations. Nienke Bosschaart attended me on the NIRSFast software [85] which also is promising for this purpose. To overcome problems such as the deformation of the breast due to milk transfer and the overall lack of literature and knowledge about (the layers of) the lactating breast it would help to investigate the lactating breast with other imaging modalities, such as MRI and ultrasound. For example, in case of researching the deformation of the breast, it would be interesting to see if after expression the milk ducts and alveoli are open or squeezed closed by the surrounding tissue. These improvements also may help to improve μ_s', which maybe can eventually help give a better accuracy for the prediction of milk transfer. The most important next step for the experiments to obtain a bigger data set. This will enable us to do statistical analysis since then the distribution of the data is known and then can be said if the differences observed are indeed significant. An interesting analysis can be to see which functional properties has the highest correlation to milk transfer. Another example can be to search for the wavelengths that are the most important for measuring on the lactating breast, because this can be interesting to use these wavelengths for the FDPM of the DOSI. Another recommendation for the experiments is measure on different skin types. At this moment, all the subjects are Caucasian, to be certain that melanin does not influence the measurement other skin types are preferred. Other wavelengths could be interesting to overcome overlay problem between water and lipid, because lipid has a peak at 1200 nm. A higher sample time is desirable to see more differences during a breastfeed. This can help to not focus on the milk, but indirect parameters to measure milk transfer such as stO2. Finally, eventually it would be helpful to also measure on mothers with breastfeeding problems like the perception of insufficient milk supply.

It is possible to improve the prediction of milk transfer with DOSI. This mainly entails minimizing the error of the fitted model to the experimental obtained spectra of the optical properties. This can be done by improving or changing the model or improving the DOSI device. Furthermore, the root finding model can be improved, by using a find all roots method, however this will take up a lot of computational power. Still, the “best” solution

can be found. Another option is not to use this model at all, but to make a new model using machine learning. However, for this, a big data training set is needed of the lactating breast with the ejected milk volume. To improve, for instance, the fit on lipid, it is perhaps useful to measure beyond 1000 nm to the 1200 nm peak of lipid, which will help with correction for the overlapping effect of the water peak over the lipid peak. However, it is debatable whether any of these methods will considerably change the accuracy of the milk transfer prediction, because the uncertainty over the specific anatomical and physiological composition of the breast will not be resolved.

OUTLOOK TO OTHER FIELDS

Except for DOSI on the lactating breast with purpose to do research to lactating, other directions could also be interesting in the future. There is already a lot of DOSI research about breast cancer. It is important to note that the optical and anatomical properties used to differentiate between a breast tumor and a normal breast are similar to the optical and anatomical properties of a normal breast and the lactating breast. One of the most common ways to distinguish between healthy and diseased tissue is the amount of blood in the tissue. Since the lactating breast is very dense and has a high blood concentration it would be harder to detect cancer in lactating breast, based on properties as blood supply and glandular tissue. This might further complicate the ability to distinguish between these two with imaging. This area might be worth investigating. Another outlook could be to do a study of the change of the breast during pregnancy. There is a case study available about involution [15], it could be interesting to investigate to opposite process: how the breast changes from non-lactating breast to a lactating breast during pregnancy. This could for example be interesting to see if changes are similar for example for women with breastfeeding problems as for mothers without breastfeeding issue.

Despite that the model is inconclusive until thus far, the results are promising to do further research on the lactating breast with DOSI.

REFERENCES

[1] S. Robinson and C. Fall, "Infant nutrition and later health: A review of current evidence," *Nutrients*, vol. 4, no. 8. MDPI AG, pp. 859–874, 2012, doi: 10.3390/nu4080859.

[2] C. R. Martin, P. R. Ling, and G. L. Blackburn, "Review of infant feeding: Key features of breast milk and infant formula," *Nutrients*, vol. 8, no. 5. MDPI AG, May 11, 2016, doi: 10.3390/nu8050279.

[3] WHO UNICEF, "Increasing Commitment To Breastfeeding Through Funding and Improved Policies and Programmes," *Glob. Breastfeed. Collect.*, no. 3, p. 4, 2019, [Online]. Available: https://www.who.int/nutrition/publications/infantfeeding/global-bf-scorecard-2019/en/.

[4] D. Peters, C. Lanting, and J. van Wouwe, "Peiling melkvoeding van zuigelingen," Leiden, 2015.

[5] L. Gatti, "Maternal perceptions of insufficient milk supply in breastfeeding," *J. Nurs. Scholarsh.*, vol. 40, no. 4, pp. 355–363, Dec. 2008, doi: 10.1111/j.1547-5069.2008.00234.x.

[6] J. C. Kent, A. R. Hepworth, D. B. Langton, and P. E. Hartmann, "Impact of Measuring Milk Production by Test Weighing on Breastfeeding Confidence in Mothers of Term Infants," *Breastfeed. Med.*, vol. 10, no. 6, pp. 318–325, Jul. 2015, doi: 10.1089/bfm.2015.0025.

[7] M. Thoresen and J. Wesche, "[ABSTRACT] Doppler measurements of changes in human mammary and uterine blood flow during pregnancy and lactation.," *Acta Obstet. Gynecol. Scand.*, vol. 67, no. 8, pp. 741–745, 1988, doi: 10.3109/00016349809004301.

[8] D. T. Geddes *et al.*, "Blood flow characteristics of the human lactating breast," *J. Hum. Lact.*, vol. 28, no. 2, pp. 145–152, May 2012, doi: 10.1177/0890334411435414.

[9] R. L. Kruger and B. A. Schueler, "A survey of clinical factors and patient dose in mammography," *Med. Phys.*, vol. 28, no. 7, pp. 1449–1454, 2001, doi: 10.1118/1.1382606.

[10] R. A. Geise and A. Palchevsky, "Composition of mammographic phantom materials.," *Radiology*, vol. 198, no. 2, pp. 347–350, Feb. 1996, doi: 10.1148/radiology.198.2.8596830.

[11] D. T. Ramsay, J. C. Kent, R. A. Hartmann, and P. E. Hartmann, "Anatomy of the lactating human breast redefined with ultrasound imaging," 2005.

[12] R. Chowdhury *et al.*, "Breastfeeding and maternal health outcomes: A systematic review and meta-analysis," *Acta Paediatrica, International Journal of Paediatrics*, vol. 104. Blackwell Publishing Ltd, pp. 96–113, Dec. 01, 2015, doi: 10.1111/apa.13102.

[13] O. E. M. Savenije and P. L. P. Brand, "Accuracy and precision of test weighing to assess milk intake in newborn infants," *Arch. Dis. Child. Fetal Neonatal Ed.*, vol. 91, no. 5, pp. 330–332, 2006, doi: 10.1136/adc.2005.091876.

[14] K. Hinde, "What we don't know about mother's milk," 2016. https://www.ted.com/talks/katie_hinde_what_we_don_t_know_about_mother_s_milk/up-next (accessed Apr. 07, 2020).

[15] N. Bosschaart *et al.*, "Diffuse optical spectroscopic imaging for the investigation of human lactation physiology: a case study on mammary involution," *J. Biomed. Opt.*, vol. 24, no. 05, p. 1, May 2019, doi: 10.1117/1.jbo.24.5.056006.

[16] M. Dantuma, R. van Dommelen, and S. Manohar, "Semi-anthropomorphic photoacoustic breast phantom.," *Biomed. Opt. Express*, vol. 10, no. 11, pp. 5921–5939, Nov. 2019, doi: 10.1364/BOE.10.005921.

[17] C. Boudoux, "Light transport in tissue," in *Fundamentals of Biomedical Optics*, Montréal: Pollux Editions, 2017, pp. 237–255.

[18] I. Vellekoop, “Radiative transfer - Lecture 6 and Diffusion - Lecture 7,” in *Biomedical Optics*, Enschede: University of Twente, 2019.

[19] B. Brooksby *et al.*, “Combining near-infrared tomography and magnetic resonance imaging to study in vivo breast tissue: implementation of a Laplacian-type regularization to incorporate magnetic resonance structure,” *J. Biomed. Opt.*, vol. 10, no. 5, p. 051504, 2005, doi: 10.1117/1.2098627.

[20] T. D. O’Sullivan, A. E. Cerussi, D. J. Cuccia, and B. J. Tromberg, “Diffuse optical imaging using spatially and temporally modulated light,” *J. Biomed. Opt.*, vol. 17, no. 7, p. 0713111, 2012, doi: 10.1117/1.jbo.17.7.071311.

[21] D. Grosenick, H. Rinneberg, R. Cubeddu, and P. Taroni, “Review of optical breast imaging and spectroscopy,” *J. Biomed. Opt.*, vol. 21, no. 9, p. 091311, 2016, doi: 10.1117/1.jbo.21.9.091311.

[22] J. Wang *et al.*, “In vivo quantitative imaging of normal and cancerous breast tissue using broadband diffuse optical tomography,” *Med. Phys.*, vol. 37, no. 7, pp. 3715–3724, 2010, doi: 10.1118/1.3455702.

[23] F. Dé Ric Bevilacqua, A. J. Berger, A. E. Cerussi, D. Jakubowski, and B. J. Tromberg, “Broadband absorption spectroscopy in turbidmedia by combined frequency-domain andsteady-state methods,” 2000.

[24] A. Cerussi, “Diffuse Optical Spectroscopic Imaging (DOSI),” *Beckman Laser Institute University of California Irvine*. https://sites.google.com/site/dosiatbli/home.

[25] F. Scholkmann *et al.*, “A review on continuous wave functional near-infrared spectroscopy and imaging instrumentation and methodology,” *NeuroImage*, vol. 85. pp. 6–27, Jan. 15, 2014, doi: 10.1016/j.neuroimage.2013.05.004.

[26] Z. Hussain, N. Roberts, G. H. Whitehouse, M. García-Fiñana, and D. Percy, “[ABSTRACT] Estimation of breast volume and its variation during the menstrual cycle using MRI and stereology.,” *Br. J. Radiol.*, vol. 72, no. 855, pp. 236–245, 1999, doi: 10.1259/bjr.72.855.10396212.

[27] A. Ringberg, E. Bågeman, C. Rose, C. Ingvar, and H. Jernström, “Of cup and bra size: Reply to a prospective study of breast size and premenopausal breast cancer incidence,” *Int. J. Cancer*, vol. 119, no. 9, pp. 2242–2243, 2006, doi: https://doi.org/10.1002/ijc.22104.

[28] N.-M. King, V. Lovric, W. C. H. Parr, W. R. Walsh, and P. Moradi, “What Is the Standard Volume to Increase a Cup Size for Breast Augmentation Surgery? A Novel Three-Dimensional Computed Tomographic Approach.,” *Plast. Reconstr. Surg.*, vol. 139, no. 5, pp. 1084–1089, May 2017, doi: 10.1097/PRS.0000000000003247.

[29] D. E. McGhee, L. G. Ramsay, C. E. Coltman, S. A. Gho, and J. R. Steele, “Bra band size measurements derived from three-dimensional scans are not accurate in women with large, ptotic breasts.,” *Ergonomics*, vol. 61, no. 3, pp. 464–472, Mar. 2018, doi: 10.1080/00140139.2017.1349936.

[30] D. Lieu, “Breast imaging for interventional pathologists,” *Archives of Pathology and Laboratory Medicine*, vol. 137, no. 1. pp. 100–119, Jan. 2013, doi: 10.5858/arpa.2012-0081-RA.

[31] E. N. Marieb and K. Hoehn, “Chapter 17 Blood, Chapter 27 The reproductive System and Chapter 28 Pregnancy and Human development,” in *Human Anatomy & Physiology, tenth edition*, 10th ed., Harlow: Pearson Education Limited, 2016, pp. 656–659 and 1046–1125.

[32] R. A. Jesinger, “Breast anatomy for the interventionalist,” *Techniques in Vascular and Interventional Radiology*, vol. 17, no. 1. pp. 3–9, Mar. 2014, doi: 10.1053/j.tvir.2013.12.002.

[33] World Health Organization, “SESSION 2: The physiological basis of breastfeeding,” in *Infant and Yong Child Feeding: Model Chapter for Textbooks for Medical Students and Allied Health Professionals*, Geneva, 2009.

[34] P. M. Prendergast, “Anatomy of the Breast,” in *Cosmetic Surgery Art and Techniques*, M. A. Shiffman

and A. Di Giuseppe, Eds. Springer Berlin Heidelberg, 2013, pp. 47–55.

[35] V. Kammath, “The breast,” *Teach Me Anatomy*, 2019. https://teachmeanatomy.info/thorax/organs/breasts/ (accessed Apr. 08, 2020).

[36] P. M. Prendergast, “Fascia, Nerve Supply, and Lymphatics of the Breast,” in *Aesthetic Surgery of the Breast*, M. A. Mugea Toma T.and Shiffman, Ed. Berlin, Heidelberg: Springer Berlin Heidelberg, 2015, pp. 39–42.

[37] D. T. Geddes, “Inside the Lactating Breast: The Latest Anatomy Research,” *J. Midwifery Women’s Heal.*, vol. 52, no. 6, pp. 556–563, Nov. 2007, doi: 10.1016/j.jmwh.2007.05.004.

[38] S. Chan *et al.*, “Menstrual cycle-related fluctuations in breast density measured by using three-dimensional MR imaging,” *Radiology*, vol. 261, no. 3, pp. 744–751, Dec. 2011, doi: 10.1148/radiol.11110506.

[39] D. R. Leff *et al.*, “Diffuse optical imaging of the healthy and diseased breast: A systematic review,” *Breast Cancer Res. Treat.*, vol. 108, no. 1, pp. 9–22, 2008, doi: 10.1007/s10549-007-9582-z.

[40] C. J. Wilde, A. Prentice, and M. Peaker, “Breast-feeding: matching supply with demand in human lactation,” *Proc. Nutr. Soc.*, vol. 54, no. 2, pp. 401–406, 1995, doi: 10.1079/pns19950009.

[41] S. R. Weaver and L. L. Hernandez, “Autocrine-paracrine regulation of the mammary gland,” *J. Dairy Sci.*, vol. 99, no. 1, pp. 842–853, 2016, doi: 10.3168/jds.2015-9828.

[42] S. Daly, A. Di Rosso, R. Owens, and P. Hartmann, “Degree of breast emptying explains changes in the fat content, but not fatty acid composition, of human milk,” *Exp. Physiol.*, vol. 78, no. 6, pp. 741–755, 1993, doi: 10.1113/expphysiol.1993.sp003722.

[43] J. C. Kent, D. T. Ramsay, D. Doherty, M. Larsson, and P. E. Hartmann, “Response of breasts to different stimulation patterns of an electric breast pump,” *J. Hum. Lact.*, vol. 19, no. 2, pp. 179–186, 2003, doi: 10.1177/0890334403252473.

[44] D. K. Prime, D. T. Geddes, D. L. Spatz, M. Robert, N. J. Trengove, and P. E. Hartmann, “Using milk flow rate to investigate milk ejection in the left and right breasts during simultaneous breast expression in women,” *Int. Breastfeed. J.*, vol. 4, Oct. 2009, doi: 10.1186/1746-4358-4-10.

[45] K. Tanimoto *et al.*, “Hemodynamic changes in the breast and frontal cortex of mothers during breastfeeding,” *Pediatr. Res.*, vol. 70, no. 4, pp. 400–405, 2011, doi: 10.1203/PDR.0b013e31822a363a.

[46] M. Van Der Hoek, L. Den Haan, A. Kaspers, W. Steenbergen, and N. Bosschaart, “Cutaneous perfusion of the human lactating breast: A pilot study with laser Doppler perfusion monitoring,” *Physiol. Meas.*, vol. 40, no. 5, pp. 1–10, 2019, doi: 10.1088/1361-6579/ab1ad7.

[47] M. Eriksson, T. Lundeberg, and K. Uvnäs-Moberg, “Studies on cutaneous blood flow in the mammary gland of lactating rats,” *Acta Physiol. Scand.*, vol. 158, no. 1, pp. 1–6, 1996, doi: 10.1046/j.1365-201X.1996.487226000.x.

[48] K. Ogawa, T. Kusaka, K. Tanimoto, T. Nishida, K. Isobe, and S. Itoh, “Changes in breast hemodynamics in breastfeeding mothers,” *J. Hum. Lact.*, vol. 24, no. 4, pp. 415–421, 2008, doi: 10.1177/0890334408323546.

[49] Y. Wang, Z. Yang, D. Hao, S. Zhang, Y. Yang, and Y. Zeng, “Measurement of subcutaneous adipose tissue thickness by near-infrared.,” *Australas. Phys. Eng. Sci. Med.*, vol. 36, no. 2, pp. 201–208, Jun. 2013, doi: 10.1007/s13246-013-0196-y.

[50] N. Bosschaart, G. J. Edelman, M. C. G. Aalders, T. G. van Leeuwen, and D. J. Faber, “A literature review and novel theoretical approach on the optical properties of whole blood.,” *Lasers Med. Sci.*, vol. 29, no. 2, pp. 453–479, Mar. 2014, doi: 10.1007/s10103-013-1446-7.

[51] R. Nachabé *et al.*, "Diagnosis of breast cancer using diffuse optical spectroscopy from 500 to 1600 nm: comparison of classification methods," *J. Biomed. Opt.*, vol. 16, no. 8, p. 087010, 2011, doi: 10.1117/1.3611010.

[52] Nederlandse Vereniging voor Klinische Chemie en Laboratoriumgeneeskunde, "zoek-een-test," 2011. https://www.nvkc.nl/zoek-een-test?id=223 (accessed Nov. 11, 2020).

[53] H. H Mitchell, T. S. Hamilton, R. Steggerda, and H. W. Bean, "THE CHEMICAL COMPOSITION OF THE ADULT HUMAN BODY AND ITS BEARING ON THE BIOCHEMISTRY OF GROWTH," Urbana, 1945. [Online]. Available: http://www.jbc.org/content/158/3/625.citation.

[54] T. L. Pope, M. E. Read, T. Medsker, A. J. Buschi, and A. N. Brenbridge, "Breast skin thickness: normal range and causes of thickening shown on film-screen mammography," *J. Can. Assoc. Radiol.*, vol. 35, no. 4, p. 365—368, Dec. 1984, [Online]. Available: http://europepmc.org/abstract/MED/6526847.

[55] S. Y. Huang, J. M. Boone, K. Yang, A. L. C. Kwan, and N. J. Packard, "The effect of skin thickness determined using breast CT on mammographic dosimetry," *Med. Phys.*, vol. 35, no. 4, pp. 1199–1206, 2008, doi: 10.1118/1.2841938.

[56] H. Gardner, C. T. Lai, L. C. Ward, and D. T. Geddes, "Thermal physiology of the lactating nipple influences the removal of human milk," *Sci. Rep.*, vol. 9, no. 1, Dec. 2019, doi: 10.1038/s41598-019-48358-z.

[57] I. V. Meglinski and S. J. Matcher, "Quantitative assessment of skin layers absorption and skin reflectance spectra simulation in the visible and near-infrared spectral regions," *Physiol. Meas.*, vol. 23, no. 4, pp. 741–753, Nov. 2002, doi: 10.1088/0967-3334/23/4/312.

[58] Y. Shimojo, T. Nishimura, H. Hazama, T. Ozawa, and K. Awazu, "Measurement of absorption and reduced scattering coefficients in Asian human epidermis, dermis, and subcutaneous fat tissues in the 400- to 1100-nm wavelength range for optical penetration depth and energy deposition analysis," *J. Biomed. Opt.*, vol. 25, no. 4, pp. 1 – 14, 2020, doi: 10.1117/1.JBO.25.4.045002.

[59] S.-H. Tseng, A. Grant, and A. J. Durkin, "In vivo determination of skin near-infrared optical properties using diffuse optical spectroscopy," *J. Biomed. Opt.*, vol. 13, no. 1, p. 14016, 2008, doi: 10.1117/1.2829772.

[60] H. Jonasson, I. Fredriksson, S. Bergstrand, C. J. Östgren, M. Larsson, and T. Strömberg, "In vivo characterization of light scattering properties of human skin in the 475- to 850-nm wavelength range in a Swedish cohort.," *J. Biomed. Opt.*, vol. 23, no. 12, pp. 1–6, Sep. 2018, doi: 10.1117/1.JBO.23.12.121608.

[61] C. Mignon, D. J. Tobin, M. Zeitouny, and N. E. Uzunbajakava, "Shedding light on the variability of optical skin properties: finding a path towards more accurate prediction of light propagation in human cutaneous compartments," *Biomed. Opt. Express*, vol. 9, no. 2, pp. 852–872, Feb. 2018, doi: 10.1364/BOE.9.000852.

[62] D. Geraskin, H. Boeth, and M. Kohl-Bareis, "Optical measurement of adipose tissue thickness and comparison with ultrasound, magnetic resonance imging, and callipers," *J. Biomed. Opt.*, vol. 14, no. 4, pp. 1–12, 2009, doi: 10.1117/1.3184425.

[63] P. Störchle, W. Müller, M. Sengeis, S. Lackner, S. Holasek, and A. Fürhapter-Rieger, "Measurement of mean subcutaneous fat thickness: eight standardised ultrasound sites compared to 216 randomly selected sites," *Sci. Rep.*, vol. 8, no. 1, p. 16268, 2018, doi: 10.1038/s41598-018-34213-0.

[64] S. Homma, T. Fukunaga, and A. Kagaya, "Influence of Adipose Tissue Thickness on Near Infrared Spectroscopic Signals in the Measurement of Human Muscle," *J. Biomed. Opt.*, vol. 1, no. 4, pp. 418–424, 1996.

[65] B. Ludescher, M. Rommel, T. Willmer, A. Fritsche, F. Schick, and J. Machann, "Subcutaneous adipose

tissue thickness in adults – correlation with BMI and recommendations for pen needle lengths for subcutaneous self-injection," *Clin. Endocrinol. (Oxf).*, vol. 75, no. 6, pp. 786–790, 2011, doi: https://doi.org/10.1111/j.1365-2265.2011.04132.x.

[66] L. W. Thomas, "the Chemical Composition of Adipose Tissue of Man and Mice," *Q. J. Exp. Physiol. Cogn. Med. Sci.*, vol. 47, no. 2, pp. 179–188, 1962, doi: 10.1113/expphysiol.1962.sp001589.

[67] M. Kuroiwa *et al.*, "Relationship of Total Hemoglobin in Subcutaneous Adipose Tissue with Whole-Body and Visceral Adiposity in Humans," *Appl. Sci.*, vol. 9, no. 12, 2019, doi: 10.3390/app9122442.

[68] I. G. Lempesis, R. L. J. van Meijel, K. N. Manolopoulos, and G. H. Goossens, "Oxygenation of adipose tissue: A human perspective.," *Acta Physiol. (Oxf).*, vol. 228, no. 1, p. e13298, Jan. 2020, doi: 10.1111/apha.13298.

[69] V. G. Peters, D. R. Wyman, M. S. Patterson, and G. L. Frank, "Optical properties of normal and diseased human breast tissues in the visible and near infrared," *Phys. Med. Biol.*, vol. 35, no. 9, pp. 1317–1334, 1990, doi: 10.1088/0031-9155/35/9/010.

[70] A. Tagliafico *et al.*, "Breast density assessment using a 3T MRI system: Comparison among different sequences," *PLoS One*, vol. 9, no. 6, Jun. 2014, doi: 10.1371/journal.pone.0099027.

[71] M. J. Yaffe *et al.*, "The myth of the 50-50 breast.," *Med. Phys.*, vol. 36, no. 12, pp. 5437–5443, Dec. 2009, doi: 10.1118/1.3250863.

[72] O. Ballard and A. L. Morrow, "Human Milk Composition. Nutrients and Bioactive Factors," *Pediatr. Clin. North Am.*, vol. 60, no. 1, pp. 49–74, 2013, doi: 10.1016/j.pcl.2012.10.002.

[73] Institute of Medicine (US) Committee on Nutritional Status During Pregnancy and Lactation, "Nutrition During Lactating," in *Nutrition During Lactation*, National Academies Press (US), 1991.

[74] T. Hennet, A. Weiss, and L. Borsig, "Decoding breast milk oligosaccharides," *Swiss Med. Wkly.*, vol. 144, no. February, pp. 1–9, 2014, doi: 10.4414/smw.2014.13927.

[75] T. Saarela, J. Kokkonen, and M. Koivisto, "Macronutrient and energy contents of human milk fractions during the first six months of lactation," *Acta Paediatr. Int. J. Paediatr.*, vol. 94, no. 9, pp. 1176–1181, 2005, doi: 10.1080/08035250510036499.

[76] C. Veenstra, A. Lenferink, W. Petersen, W. Steenbergen, and N. Bosschaart, "Optical properties of human milk," *Biomed. Opt. Express*, vol. 10, no. 8, p. 4059, Aug. 2019, doi: 10.1364/boe.10.004059.

[77] B. Aernouts, R. Van Beers, R. Watté, T. Huybrechts, J. Lammertyn, and W. Saeys, "Visible and near-infrared bulk optical properties of raw milk," *J. Dairy Sci.*, vol. 98, no. 10, pp. 6727–6738, Oct. 2015, doi: 10.3168/jds.2015-9630.

[78] S. Stocker *et al.*, "Broadband Optical Properties of Milk," *Appl. Spectrosc.*, vol. 71, no. 5, pp. 951–962, May 2017, doi: 10.1177/0003702816666289.

[79] C. Veenstra, D. E. Every, W. Petersen, J. B. van Goudoever, W. Steenbergen, and N. Bosschaart, "Dependency of the optical scattering properties of human milk on casein content and common sample preparation methods," *J. Biomed. Opt.*, vol. 25, no. 04, p. 1, Apr. 2020, doi: 10.1117/1.jbo.25.4.045001.

[80] T. A. Krouskop, T. M. Wheeler, F. Kallel, B. S. Garra, and T. Hall, "Elastic moduli of breast and prostate tissues under compression.," *Ultrason. Imaging*, vol. 20, no. 4, pp. 260–274, Oct. 1998, doi: 10.1177/016173469802000403.

[81] T. Umemoto *et al.*, "Ex Vivo and In Vivo Assessment of the Non-linearity of Elasticity Properties of Breast Tissues for Quantitative Strain Elastography," *Ultrasound Med. Biol.*, vol. 40, no. 8, pp. 1755–1768, 2014, doi: https://doi.org/10.1016/j.ultrasmedbio.2014.02.005.

[82] M. Friebel, J. Helfmann, U. Netz, and M. Meinke, "Influence of oxygen saturation on the optical

scattering properties of human red blood cells in the spectral range 250 to 2000 nm," *J. Biomed. Opt.*, vol. 14, no. 3, p. 034001, 2009, doi: 10.1117/1.3127200.

[83] T. D. O'Sullivan, "IRBForm - Diffuse Optical Imaging Device Pictures." pp. 98–99, 2019.

[84] S. H. Chung, A. E. Cerussi, S. I. Merritt, J. Ruth, and B. J. Tromberg, "Non-invasive tissue temperature measurements based on quantitative diffuse optical spectroscopy (DOS) of water.," *Phys. Med. Biol.*, vol. 55, no. 13, pp. 3753–3765, Jul. 2010, doi: 10.1088/0031-9155/55/13/012.

[85] Thayer school of Engineering at Darthmouth *et al.*, "NIRFAST." https://www.dartmouth.edu/~nir/nirfast/index.php (accessed May 01, 2021).

APPENDIX – MATHEMATICS DOSI

FROM RTE TO DE

radiative transfer equation (RTE) [18]:

$$\frac{\partial I(\boldsymbol{r},\boldsymbol{s},t)}{c\,\partial t} = -\boldsymbol{s}\cdot\nabla I(\boldsymbol{r},\boldsymbol{s},t) - (\mu_a+\mu_s)I(\boldsymbol{r},\boldsymbol{s},t) + \epsilon(\boldsymbol{r},\boldsymbol{s},t) + \mu_s\iint_{4\pi}^{0} p(\boldsymbol{s},\boldsymbol{s}')I(\boldsymbol{r},\boldsymbol{s}',t)\,d\Omega$$

The RTE is a balance of radiance. $I(\boldsymbol{r},\boldsymbol{s},t)$ is the radiance, the light intensity in a specific direction. Therefore, $I(\boldsymbol{r},\boldsymbol{s},t)$ is sometimes referred to as specific intensity. The unit of radiance is [W m^{-2} sr^{-1}].

The RTE will be explained per term.

$$\frac{\partial I(\boldsymbol{r},\boldsymbol{s},t)}{c\,\partial t}$$

Is the energy that is currently present in the medium.

$$-\boldsymbol{s}\cdot\nabla I(\boldsymbol{r},\boldsymbol{s},t)$$

Is the incoming and outgoing radiation of the source in a specific direction.

$$-(\mu_a+\mu_s)I(\boldsymbol{r},\boldsymbol{s},t)$$

Resembles the intensity loss by absorption and scattering.

$$+\epsilon(\boldsymbol{r},\boldsymbol{s},t)$$

Is an extra source in the medium. This can be for example processes like fluorescence.

$$\mu_s\iint_{4\pi}^{0} p(\boldsymbol{s},\boldsymbol{s}')I(\boldsymbol{r},\boldsymbol{s}',t)\,d\Omega$$

This term represents the intensity that can be gained by scattering. Here, p is the phase function.

Again, please note that the RTE neglect the wave character of light. It does not consider behaviours like interference, diffraction, or polarization.

Using Fick's laws, it is possible to simplify the radiative transfer equation to the diffusion equation.

Fick's law 1:

$$\boldsymbol{F} = -D\nabla u$$

This law describes that a high concentration tends to flow to a lower concentration area. Hereby, $\boldsymbol{F}$ is flux in [J m^{-2} s^{-1}], D the diffusion constant in [m^2 s^{-1}] and u the optical density in [J m^{-3}].

Fick's law 2:

$$\frac{\partial u}{\partial t} = S + -\nabla\mathbf{F} - Q$$

The second law describes the energy balance and how the concentration can change over time. Here S is a source in [J m^{-3} s^{-1}] and Q is energy loss (absorption) in [J m^{-3} s^{-1}]

For light, the diffusion equation (DE) becomes:

$$\frac{\partial u}{\partial t} = D\nabla^2 u - c\mu_a u + S$$

The assumption is made that the source is isotropic. Since most biological tissue is highly anisotropic, the diffusion equation should be used when encounters dominant scattering tissue (rule of thumb: $10\ \mu_a \leq\ \mu_s'$) and the light pathway should be long enough in comparison to the mean free path $l_{tr} = \frac{1}{\mu_s'}$, for tissue it is typical that light is completely diffuse after 1 mm. The diffusion constant can be found by combining the RTE and Fick's first law. The source term will become isotropic, the extra source in the medium is not present and the scattering gain will be described by the scattering coefficient in combination with the anisotropy factor, g. The derivation of the diffusion constant is shown here:

$$\frac{\partial \boldsymbol{F}}{c\ \partial t} = -\frac{1}{3}\nabla U - (\mu_a + \mu_s -\ \mu_s g)\boldsymbol{F}$$

$$\frac{\partial \boldsymbol{F}}{c\ \partial t} = -\frac{1}{3}\nabla U - (\mu_a + \mu_s(1-g))\boldsymbol{F}$$

The change over time is zero:

$$\frac{\cancel{\partial \boldsymbol{F}}}{c\ \cancel{\partial t}} = -\frac{1}{3}\nabla U - (\mu_a + \mu_s')\boldsymbol{F}$$

$$\boldsymbol{F}\ = -\frac{1}{3(\mu_a + \mu_s')}\nabla U$$

Fick's first law was:

$$\boldsymbol{F} = -D\nabla u$$

Resulting into:

$$D = \frac{1}{3(\mu_a + \mu_s')}$$

The diffusion constant is often described with or without the speed of light, c. In this report we choose to include the speed of light, c, into the diffusion constant.

$$D = \frac{c}{3(\mu_a + \mu_s')}$$

Here an overview is shown that repeat the symbols and there meaning used.

Symbol	Meaning	SI-unit
u	Optical density	[J m^{-3}]
D	Diffusion constant	[m^2 s^{-1}]
S	source	[W m^{-3}]
Q	Absorption	[W m^{-3}]
t	Time	[s]
c	Speed of light	[m s^{-1}]
μ_a	Absorption coefficient	[m^{-1}]
μ_s'	Reduced scattering coefficient	[m^{-1}]
μ_s	Scattering coefficient	[m^{-1}]
g	anisotropy factor	Unitless

$\boldsymbol{F}$	Flux	[W m^{-2}]
$I(\boldsymbol{r}, \boldsymbol{s}, t)$	Radiance	[W m^{-2} sr^{-1}]
U	Fluence rate	[W m^{-2}]

DERIVATION STEADY STATE

Assuming that S is constant over time and a point source at the origin than $\frac{\partial u}{\partial t}$ is constant over time. $S = S_0\delta(\vec{r})$.
Resulting in a diffusion equation:

$$0 = D\nabla^2 u - c\mu_a u + S_0\delta(\vec{r})$$

On point $\vec{r} = \begin{matrix}0\\0\\0\end{matrix}$ $u = S_0$, where S_0 is the energy density of the source. Everywhere else the source is equal to zero.
The diffusion equation is:

$$0 = D\nabla^2 u - c\mu_a u + 0$$

Rewritten, will give the differential equation:

$$\nabla^2 u - \frac{c\mu_a}{D}u = 0$$

A possible solution for this equation:

$$u = Ae^{-b\vec{r}}$$

Where:

$$\nabla u = -bAe^{-b\vec{r}}$$

And:

$$\nabla^2 u = b^2 Ae^{-b\vec{r}}$$

It should satisfy $\vec{r} = \begin{matrix}0\\0\\0\end{matrix}$ $u = S_0$, therefore $u\begin{pmatrix}0\\0\\0\end{pmatrix} = Ae^{-b\begin{pmatrix}0\\0\\0\end{pmatrix}} = S_0$. Resulting into $A = S_0$.

Substituting into the diffusion equation will give:

$$b^2 u_0 e^{-b\vec{r}} - \frac{c\mu_a}{D}u_0 e^{-b\vec{r}} = 0$$

$$b^2 u_0 e^{-b\vec{r}} = \frac{c\mu_a}{D}u_0 e^{-b\vec{r}}$$

$$b^2 = \frac{c\mu_a}{D}$$

$$b = \pm\sqrt{\frac{c\mu_a}{D}}$$

Resulting into:

$$u = S_0 e^{\pm\sqrt{\frac{c\mu_a}{D}}\vec{r}}$$

Since you can assume a homogeneous source and that light will travel (approximately) isotropic through the tissue. It is possible that only the radius to the source (r) is important and not the coordinate $\vec{r}$. Therefore, this can be further simplified as:

$$u = \frac{cS_0}{4\pi Dr} e^{-\sqrt{\frac{c\mu_a}{D}}r}$$

DERIVATION AMPLITUDE MODULATION

Now the source S is no longer constant over time, but has a constant amplitude, driven by direct current (DC), and a fluctuating part, driven by an alternating current (AC): $S = \delta(\vec{r})(S_{DC} + S_{AC}(\omega)e^{(-i\omega t)})$, where ω is the frequency of the amplitude modulation. Note that $e^{-i\omega t}$ is often used for describing fluctuation over time in electromagnetics. When assuming linear behavior, the photon density can be described by: $u\,(\vec{r},\omega) = u(\vec{r},\omega = = 0) + u(\vec{r},\omega)\; e^{(-i\omega t)}$. In the previous paragraph we already derived the steady state. This is equal to the DC part of this equation.

Resulting into a DE for only the AC part:

$$\frac{\partial u}{\partial t} = D\nabla^2 u - c\mu_a u + S$$

$$-i\omega\, u = D\nabla^2 u - c\mu_a u + \left(S_{AC}(\omega)e^{(-i\omega t)}\right)\delta(\vec{r})$$

Rewritten as:

$$\frac{-i\omega + c\mu_a}{D} u - \nabla^2 u = \left(S_{AC}(\omega)e^{(-i\omega t)}\right)\delta(\vec{r})$$

Again on $\vec{r} = \begin{matrix}0\\0\\0\end{matrix}$ $u = \left(S_{AC}(\omega)e^{(-i\omega t)}\right)$. Everywhere else the source is equal to zero since this is a point source. The diffusion equation is:

$$\frac{-i\omega + c\mu_a}{D} u - \nabla^2 u = 0$$

$$\frac{i\omega - c\mu_a}{D} u + \nabla^2 u = 0$$

Often propagation constant 'κ^2' is used to describe this pre factor before u , resulting into:

$$\nabla^2 u + \kappa^2 u = 0$$

This form of equation is in the optical field known as the Helmholtz equation. The solution of this equation can be:

$$u = c_1 e^{b_1 \vec{r}} + c_2 e^{b_2 \vec{r}}$$

Then:

$$\nabla u = c_1 b_1 e^{b_1 \vec{r}} + c_2 b_2 e^{b_2 \vec{r}}$$

And:

$$\nabla^2 u = {b_1}^2 c_1 e^{b_1 \vec{r}} + {b_2}^2 c_2 e^{b_2 \vec{r}}$$

Substituting this in the diffusion equation:

$${b_1}^2 c_1 e^{b_1 \vec{r}} + {b_2}^2 c_2 e^{b_2 \vec{r}} + \kappa^2 \left(c_1 e^{b_1 \vec{r}} + c_2 e^{b_2 \vec{r}}\right) = 0$$

$$\left(\kappa^2 + {b_1}^2\right) c_1 e^{b_1 \vec{r}} + \left(\kappa^2 + {b_2}^2\right) c_2 e^{b_2 \vec{r}} = 0$$

$$\kappa^2 + {b_1}^2 = \kappa^2 + {b_2}^2 = 0$$

$$b_1 = -\sqrt{-\kappa^2} = -i\kappa = -i\sqrt{\frac{i\omega - c\mu_a}{D}}$$

$$b_2 = \sqrt{-\kappa^2} = i\kappa = i\sqrt{\frac{i\omega - c\mu_a}{D}}$$

Resulting in:

$$u = c_1 e^{\pm i\kappa \vec{r}}$$

c_1 is again on $\vec{r} = \begin{matrix} 0 \\ 0 \\ 0 \end{matrix}$ $u = \left(S_{AC}(\omega) e^{(-i\omega t)}\right)$. , thus $c_1 = \left(S_{AC}(\omega) e^{(-i\omega t)}\right)$. Therefore:

$$u = S_{AC}(\omega) e^{-i\omega t} e^{\pm i\kappa \vec{r}}$$

Again, changing the coordinates $\vec{r}$ to only the radiance r will simplify this equation:

$$u = \frac{c S_{AC}(\omega)}{4\pi D r} e^{-i\omega t} e^{i\kappa r}$$

$$u = \frac{c S_{AC}(\omega)}{4\pi D r} e^{i\kappa r - i\omega t}$$

If there is assumed that this process is linear, the superposition principle can be used. Thus, the DC solution (steady state) can be added to the AC solution just found:

$$u = \frac{c S_{DC}}{4\pi D r} e^{-\sqrt{\frac{c\mu_a}{D}} r} + \frac{c S_{AC}(\omega)}{4\pi D r} e^{i\kappa r - i\omega t}$$

APPENDIX – DOSI ON THE BREAST

Table A1 gives an overview of the values of the functional properties found in literature by using DOSI or other similar optical techniques on the breast. For 1 article the optical properties are provided as well. Note that the optical properties are dependent on wavelength and are hardly to capture in one value. This is easier accomplished for μ_s' than for μ_a, since there is an exponential relation between wavelength and μ_s', see equation 2.4. However, μ_a relation to wavelength is more complex. Therefore, mostly the chromophores are used to build μ_a in the model.

TABLE A1 OVERVIEW OF REDUCED SCATTERING COEFFICIENT AND FUNCTIONAL PROPERTIES FOUND IN LITERATURE REGARDING DOSI ON THE BREAST. THE SCATTERING POWER B AND A ARE VALUES FOR EQUATION 2.4, EVEN AS VALUES FOR λ_0. FOR THE PAPER OF WANG ET AL. VALUES ARE DENOTED AS MEAN (STANDARD ERROR) AND THE VALUES OF OTHER PAPERS ARE DENOTED AS MEAN ± STANDARD DEVIATION. THE COLUMN "IS LAC?" MEANS ARE THE SUBJECTS OF THIS RESEARCH LACTATING? Y=YES AND N=NO.

Article		Value	Is lac?
Reduced scattering coefficient μ_s'			
Leff et al. [39] **(review)**	Healthy pre-menopausal, Shah et al. (16), λ = 600-700 nm	$1.0 \pm 1.0\ mm^{-1}$	N
	Average healthy breast tissue, λ = 600-700 nm	$1.0 \pm 0.5\ mm^{-1}$	N
	Average healthy breast tissue, λ = 700-800 nm	$0.8 \pm 0.4\ mm^{-1}$	N
	Average healthy breast tissue, λ = 800-900 nm	$0.8 \pm 0.4\ mm^{-1}$	N
Absorption coefficient μ_a			
Leff et al. [39] **(review)**	Average healthy breast tissue, λ = 600-700 nm	$0.0004 \pm 0.0002\ mm^{-1}$	N
	Average healthy breast tissue, λ = 700-800 nm	$0.0004 \pm 0.0002\ mm^{-1}$	N
	Average healthy breast tissue, λ = 800-900 nm	$0.0005 \pm 0.0002\ mm^{-1}$	N
Scattering power b & scattering prefactor a			
Bosschaart et al. [15]	Day 0, Areola:	$a = 1.35\ mm^{-1}$ $b = 1.3$ $\lambda_0 = 500\ nm$	Y
	Day 0, Non-areola:	$a = 1.35\ mm^{-1}$ $b = 0.8$ $\lambda_0 = 500\ nm$	Y
	Day 237, Areola:	$a = 1.7\ mm^{-1}$ $b = 1.4$ $\lambda_0 = 500\ nm$	N
	Day 237, Non-areola:	$a = 1.2\ mm^{-1}$ $b = 0.7$ $\lambda_0 = 500\ nm$	N
Wang et al. [22]	Scatter/fatty tissue:	$a = 0.9\ (0.1)$ (no unit?) $b = 0.8\ (0.2)$ $\lambda_0 = unknown$	N
	Extremely dense/heterogeneously dense tissue:	$a = 0.8\ (0.1)$ (no unit?) $b = 1.6\ (0.2)$ $\lambda_0 = unknown$	N
Grosenick et al. [21] **(review)**	Healthy breast, Grosenick et al. (134)	$b = 0.99 \pm 0.35$	N
	Healthy breast, Spinelli et al. (135)	$b = 0.88 \pm 0.39$ $b = 0.82 \pm 0.60$ $b = 0.93 \pm 0.60$	N
	Healthy breast, Cerussi et al. (72)	$b = 0.58 \pm 0.23$	N
	Healthy breast, Fang et al. (88)	$b = 0.91 \pm 0.01$	N

	Pre-menopausal, Blackmore et al. (117)	$a = 1.46 \pm 0.34\ mm^{-1}$ $b = 0.35 \pm 0.31$ $\lambda_0 = unknown$	N
	Pre-menopausal, Taroni et al. (204)	$a = 1.49 \pm 0.29\ mm^{-1}$ $b = 0.70 \pm 0.27$ $\lambda_0 = 600\ nm$	N
THb in [µM]			
Bosschaart et al. [15]	Day 0, Areola:	58	Y
	Day 0, Non-areola:	48	Y
	Day 237, Areola:	35	N
	Day 237, Non-areola:	25	N
Leff et al. [39] **(review)**	Average:	34 ± 9	N
Ogawa et al. [48]	Group A:	70.1±37.9	Y
	Group B:	67.5±23.8	Y
Grosenick et al. [21] **(review)**	Healthy breast, Grosenick et al. (134)	17.3±6.2	N
	Healthy breast, Spinelli et al. (135)	12.6±5.9	N
	Healthy breast, Cerussi et al. (72)	17.5±7.5	N
	Healthy breast, Fang et al. (88)	19.2±6.5	N
	Premenopausal, Blackmore et al. (117)	15.7±4.8	N
	Premenopausal, Taroni et al. (204)	13.6±4.1	N
Wang et al. [22]	Scatter/fatty tissue	13.1 (1.5)	N
	Extremely dense/heterogeneously dense tissue	21.4 (1.9)	N
stO_2 [%]			
Bosschaart et al. [15]	Day 0, Areola:	52	Y
	Day 0, Non-areola:	65	Y
	Day 237, Areola:	65	N
	Day 237, Non-areola:	73	N
Leff et al. [39] **(review)**	Average:	75±2	N
Ogawa et al. [48]	Group A:	77.5±3.8	Y
	Group B:	76.6±2.4	Y
Grosenick et al. [21] **(review)**	Healthy breast, Grosenick et al. (134)	74 ± 7	N
	Healthy breast, Spinelli et al. (135)	71.3±17.6	N
	Healthy breast, Cerussi et al. (72)	67.7±9.3	N
	Healthy breast, Fang et al. (88)	73±6	N
	Premenopausal, Blackmore et al. (117)	70.5±7.6	N
	Premenopausal, Taroni et al. (204)	86.8±9.6	N
Wang et al. [22]	Scatter/fatty tissue:	59.2 (2.7)	N
	Extremely dense/heterogeneously dense tissue:	62.4 (3.5)	N
Water [%]			
Bosschaart et al. [15]	Day 0, Areola:	85	Y
	Day 0, Non-areola:	67	Y
	Day 237, Areola:	60	N
	Day 237, Non-areola:	25	N
Grosenick et al. [21] **(review)**	Healthy breast, Cerussi et al. (72)	18.7±10.3	N
	Premenopausal, Blackmore et al. (117)	21.3±7.2	N
	Scatter/fatty tissue:	26.9 (5.4)	N

Wang et al. [22]	Extremely dense/heterogeneously dense tissue:	52.6 (6.9)	N
Lipid [%]			
Bosschaart et al. [15]	Day 0, Areola:	10	Y
	Day 0, Non-areola:	40	Y
	Day 237, Areola:	35	N
	Day 237, Non-areola:	60	N
Grosenick et al. [21] **(review)**	Healthy breast, Cerussi et al. (72)	66.1±10.3	N
	Premenopausal, Blackmore et al. (117)	61.5±10.2	N
Wang et al. [22]	Scatter/fatty tissue:	76.2 (4.3)	N
	Extremely dense/heterogeneously dense tissue:	61.4 (5.5)	N

A short introduction of the used articles is given, to sketch how the values for the functional properties are obtained.

Firstly, the case study mentioned earlier in the introduction paragraph by Bosschaart and O'Sullivan et al. [15]. Again, this study also uses DOSI and studied the involution process, from day 0, when this mother ceased breastfeeding, to day 237, when the study stopped. A sidenote is that at the end of the experiment the participant was pregnant again. At day 0, the participant is subdivided as lactating subject and at the 237 days mark this subject is subdivided as non-lactating subject. The values are obtained by interpreting Figure 4 of this paper.

Furthermore, two research papers are consulted, one by Leff et al. [39] comparing healthy and diseased breast with diffuse optical imaging, and one by Grosenick et al. [21], reviewing the optical techniques available for breast imaging. Only the values for the group of healthy and premenopausal breast are included in the overview table A1 from both these review papers. Since these are review papers, the secondary references used for the overview table A1 can be found in table A2. Note that in the overview table A1, if the value is directly cited from another article, this article is noted separately. If the value is a conclusion of multiple articles in the review paper, then only the review paper is cited.

TABEL A2 THE USED SECONDARY REFERENCES OF THE REVIEW PAPERS WITH THE NUMBER OF PARTICIPANTS.

Review paper	Secondary references with number of subjects
Grosenick et al. [21]	Blackmore et al. (117) n=95 Taroni et al. (204) n=93 Grosenick et al. (134) n=87 Spinelli et al. (135) n=32 Cerussi et al. (72) n=58 Fang et al. (88) n=26
Leff et al. [39]	Shah (16) n=14 Shah (17) n=31 Grosenick (31) n=35 Intes (27) n=49 Taroni (39) n=101 Suzuki (25) n=30 Grosenick (34) n=87 Durduran (21) n=52 Spinelli (15) n=150 Pogue (18) n=46 Poplack (45) n=23

Ogawa et al. [48] used near-infrared time-resolved spectroscopy (TRS) to measure the concentrations of oxy- and deoxyhemoglobin in the detected volume. 40 breastfeeding lactating mothers participated in this study. The measurements were performed on the edge of the areola. They were divided randomly into the following groups: participants of group A were measured contralateral (n=18), and participants of group B were measured ipsilateral (n=22). For further clarification, in group B the measurements were carried out on the right breast, while the baby was suckling from the right breast. In group A, the measurements were carried out on the right breast while the baby was suckling from the left breast. The probe, which had a source-detector distance of 30 mm, was placed on the right breast directly above the areola.

The article by Wang et al. [22] studies the normal and cancerous breast using DOSI. The values presented in the overview are from nine participants who are healthy women with an age of around 50.

APPENDIX – A SMALL RESEARCH TO THE BEHAVIOR OF THE LIGHT PROPAGATION DISTRIBUTION.

The light propagation distribution is influenced by μ_a and μ_s', since they are wavelength dependent as well as the light propagation distribution. However, to calculate a light propagation distribution for every μ_a and μ_s' per wavelength takes a lot of computational work. Thereby, the μ_a and μ_s' spectra are unknown for the overall breast since these are also the results of our model. However, the μ_a and μ_s' per layer are obtained. To see if it is possible to simplify this problem, it is important to do a quick sidestep to investigate the behavior of the light distribution. The research question is:

To what extent does the light propagation distribution influence the outcome of the model (of the average breast)?

First, the extreme values of μ_a and μ_s' of the layers are used to see if there is a big difference between the minimum attenuation and the maximum attenuation, to see if that changes the sensitivity of the layers at all. Note, when looking at the spectra of figure A1, that for μ_s', the maximum is at the lower wavelengths and the minimum at higher wavelengths. This is logical, because of the exponential relation. μ_a is a summation of the extinction coefficient spectra of the chromophores. By studying these spectra, this seems to behave in the opposite way in comparison to μ_s'. Thus, μ_a is low for smaller wavelengths and high for bigger wavelengths. The minimum value of μ_s' at the corresponding wavelength is used to search the minimum value for μ_a. The same is done for μ_a as for μ_s' and for both the maximum values. These results can be found in table A3-A5 & figures A1 and A2. The maximum of μ_a and the minimum of μ_s' are approximately at 980 nm and the minimum of μ_a and the maximum of μ_s' are approximately at 650. The sensitivity for the layers of the average breast is calculated.

RESULTS

TABLE A3: MAXIMUM AND MINIMUM VALUES FOR μ_a AND μ_s' FOR 650 NM

650 nm	μ_s' [mm^-1]	source	μ_a [mm^-1]	source
Max	2	Skin	0.04	Skin
Min	0.5	Mammary (adi)	0.005	Sub. Fat

TABLE A4: MAXIMUM AND MINIMUM VALUES FOR μ_a AND μ_s' FOR 980 NM

980 nm	μ_s' [mm^-1]	source	μ_a [mm^-1]	source
Max	1	Subcutaneous fat	0.07	Skin
Min	0.3	Mammary (adi)	0.01	Sub. Fat

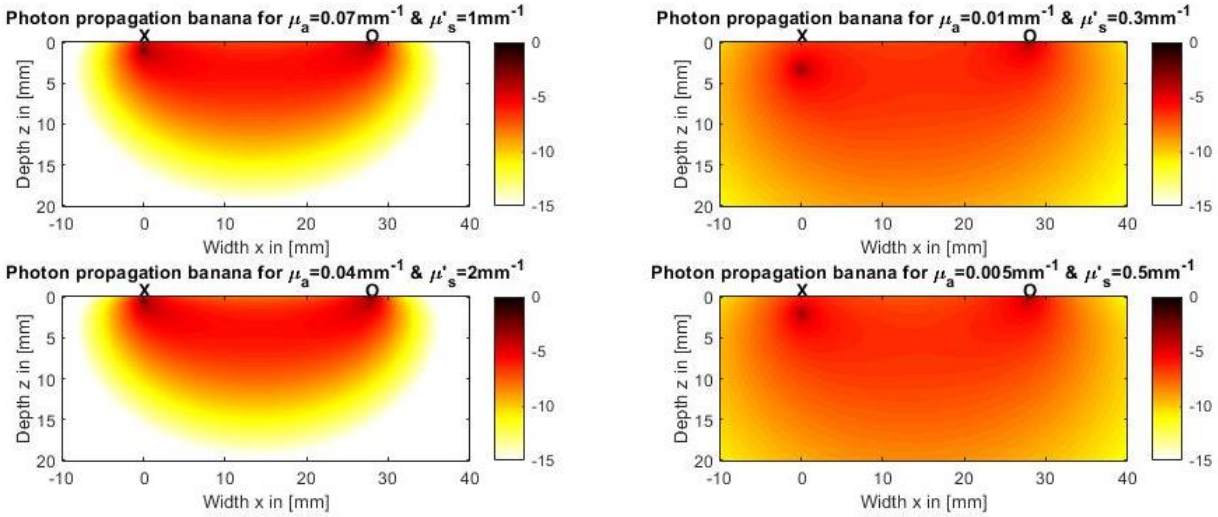

FIGURE A1 THE EXPONENTIAL LOG OF THE NORMALIZED SENSITIVITY PLOT OF THE LIGHT PROPAGATION DISTRIBUTION OF THE EXTREME VALUES IN ARBITRARY UNITS. THE FIGURES ARE SCALED THE SAME WAY, TO MAKE COMPARISON EASY. TOP RIGHT: THE MAXIMUM VALUE FOR μ_a WITH CORRESPONDING MAXIMUM VALUE OF μ'_s (ON THE SAME WAVELENGTH=980 NM). BOTTOM RIGHT: MAXIMUM VALUE FOR μ'_s WITH CORRESPONDING VALUE FOR μ_a (ON THE SAME WAVELENGTH=650 NM). TOP LEFT: MINIMUM VALUE FOR μ'_s WITH CORRESPONDING VALUE FOR μ_a (ON 650 NM). BOTTOM LEFT: MINIMUM VALUE FOR μ_a WITH CORRESPONDING VALUE μ'_s.

This figure A1 shows the light propagation distributions for the extreme values. Note that the two small light distributions and the two big light distributions are almost equal. In figure A2, only the sensitivity over depth is plotted and shows sensitivity versus depth for the maximum (at 650 nm) and minimum (at 980 nm) light distribution, for the average breast. In table A5, the corresponding values for the sensitivity per layer can be found.

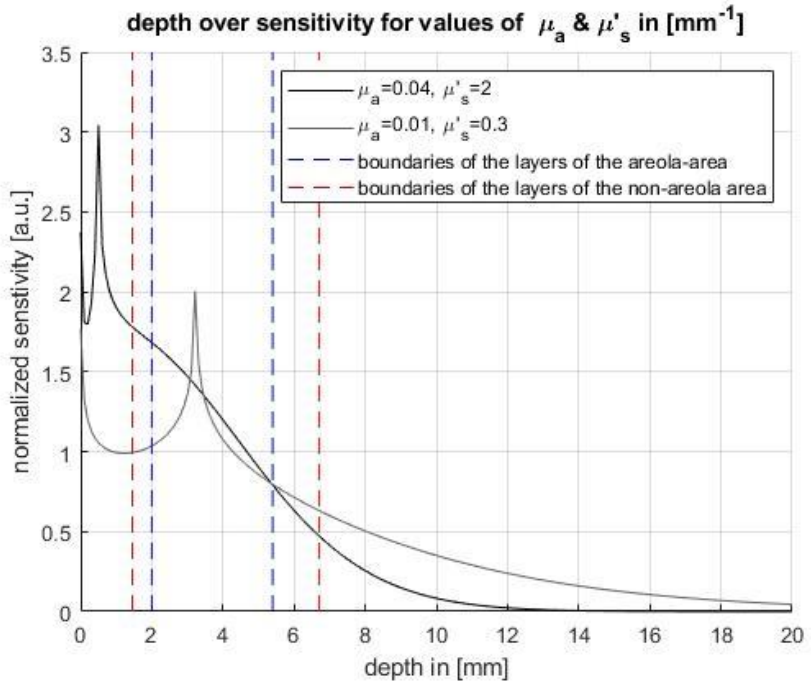

FIGURE A2 THE SENSITIVITY OVER DEPTH FOR CORRESPONDING M_A & M_S^', THE BOUNDARIES OF THE LAYERS OF THE AVERAGE BREAST ARE SHOWN. THE RIGHT BOUNDARY IS FROM THE SKIN TO THE SUBCUTANEOUS FAT LAYER. THE LEFT BOUNDARY IS THE BOUNDARY FROM SUBCUTANEOUS FAT TO THE MAMMARY TISSUE.

TABLE A56 THE SENSITIVITY OF EVERY LAYERS FOR THE SMALLEST AND LARGEST LIGHT PROPAGATION DISTRIBUTION.

	layer	Sensitivity in (%) areola	Non-areola (%)
Maximum at 650 nm	Skin	39.4	30.7
	Subcutaneous fat	43.4	60.2
	Mammary tissue	17.2	9.02
Minimum at 950 nm	Skin	21.6	16.6
	Subcutaneous fat	38.1	52.4
	Mammary tissue	40.3	31.1

DISCUSSION

Overall, it seems that the light distribution could affect the outcome of the model. For example, the sensitivity for mammary tissue is important to measure milk supply and this can vary between 31.1% and 9.02% for the non-areola area and between 17.2% and 40.3% for the areola area for the maximum and the minimum light distributions, see table A5. The two maximum light distributions are compared to each other and the two minimal light distributions as well. There is almost no difference in maximum value and minimum value of the two light distributions. Therefore, the influence of wavelength is assumed to be neglectable.

Note that the minimum and maximum light distributions are based on the approximate maximum and minimum value for μ_a and μ_s'. This is not necessarily the case; it can be that the minimum or maximum light distribution is on a different wavelength. Thereby, this is done based on the values for the average breast, considering that the values for different breast can be different in reality. Moreover, note that when $\mu_s' = 0.3\ mm^{-1}$, $l_{tr} \approx 3.3\ mm$, this is deeper than the calculated thickness of the skin. Therefore, the sensitivity calculated here is not suitable for these layers. However, this side study is only done to give an idea of within what range the light propagation distribution can change, in order to be able to give an educated guess regarding the outcomes of DOSI on an average breast.

APPENDIX – LAYERS TOTAL HEMOGLOBIN

In the figure … the four chromophores can be found. Total hemoglobin (THb) is the sum of oxyhemoglobin and deoxyhemoglobin. The values of Meglinski and Matcher [57] from table 3.4 are used to obtain the thickness of the layers in the skin and the corresponding concentration. This concentration is the volume fraction of blood in this layer of the skin. This layer is also used for the subcutaneous fat. We chose to use the values of Brooksky et al. [19] for adipose and glandular tissue. The reason to not use the values given by Nachabé et al. [51] is that Nachabé et al. does not measure in vivo, which in the case of blood could be relevant, since blood is pushed through the tissue. Since the ratio of glandular tissue and adipose tissue is known, the blood concentration can be calculated for the mammary tissue layer. In pure blood of women there is approximately 2.19 mM THb [52]. The values of the concentration of blood in the tissue layer are multiplied with that of THb. This will give the values of THb shown in table A6 and figure A3.

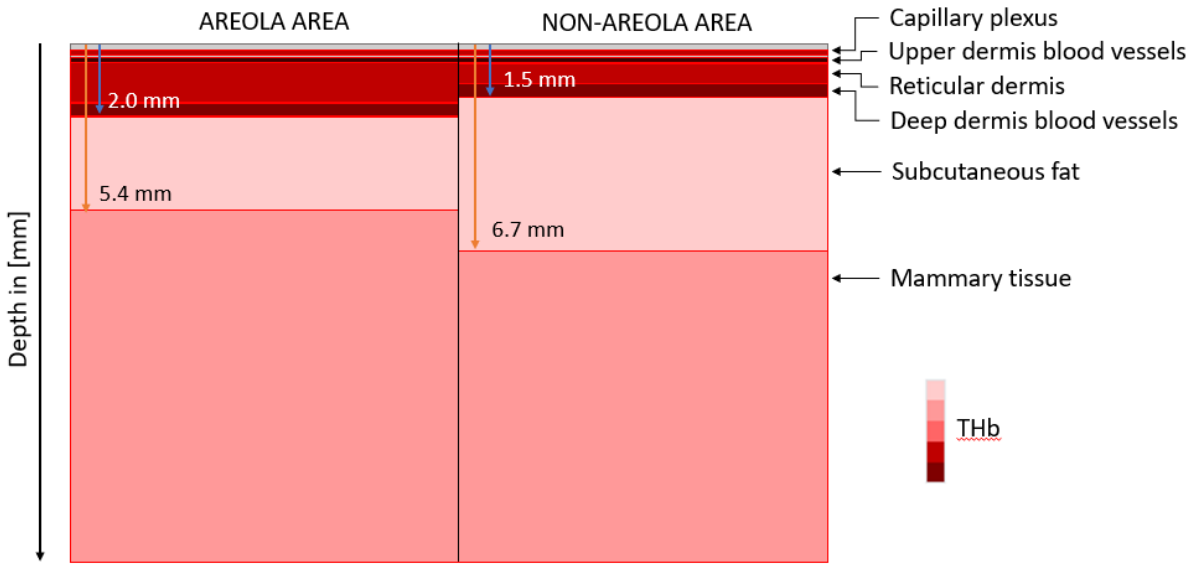

FIGURE A3: THE MODEL FOR THE TOTAL HEMOGLOBIN CONCENTRATION OF THE AVERAGE BREAST IN DETAILED LAYERS.

TABLE A6: THE MODEL PARAMETERS FOR AN AVERAGE BREAST: TOTAL HEMOGLOBIN CONCENTRATIONS

THb	Lactating breast [µM]	Non-lactating breast [µM]
Capillary plexus	184.6	92.3
Upper dermis	1384.8	692.4
Reticular dermis	184.6	92.3
Deep dermis	461.6	230.8
Subcutaneous fat	230.8	115.4
Adipose tissue	34.6	17.3
Glandular tissue	57.6	28.8

APPENDIX – VARIATIONS OF THE BREAST

First the optical properties are shown. The blue lines reflect the minimal value, and red lines reflect the maximum value of the range of the corresponding parameter discussed in table 4.8 and table 4.9. Then the functional properties are shown. Note that HbO_2 is oxyhemoglobin, Hb is deoxyhemoglobin, non-ar is non areola area, ar is areola area, non-lac is the non-lactating breast, lac pre is the lactating breast before breastfeeding and lac post is the lactating breast after breastfeeding. Furthermore, the values in red reflect how much lower these values are in comparison to the average breast due to the mutation of this parameter. Green values indicate the ones that increase in comparison to the average breast due to the changes of the corresponding parameter.

BIOLOGICAL VARIATIONS

THICKNESS SKIN

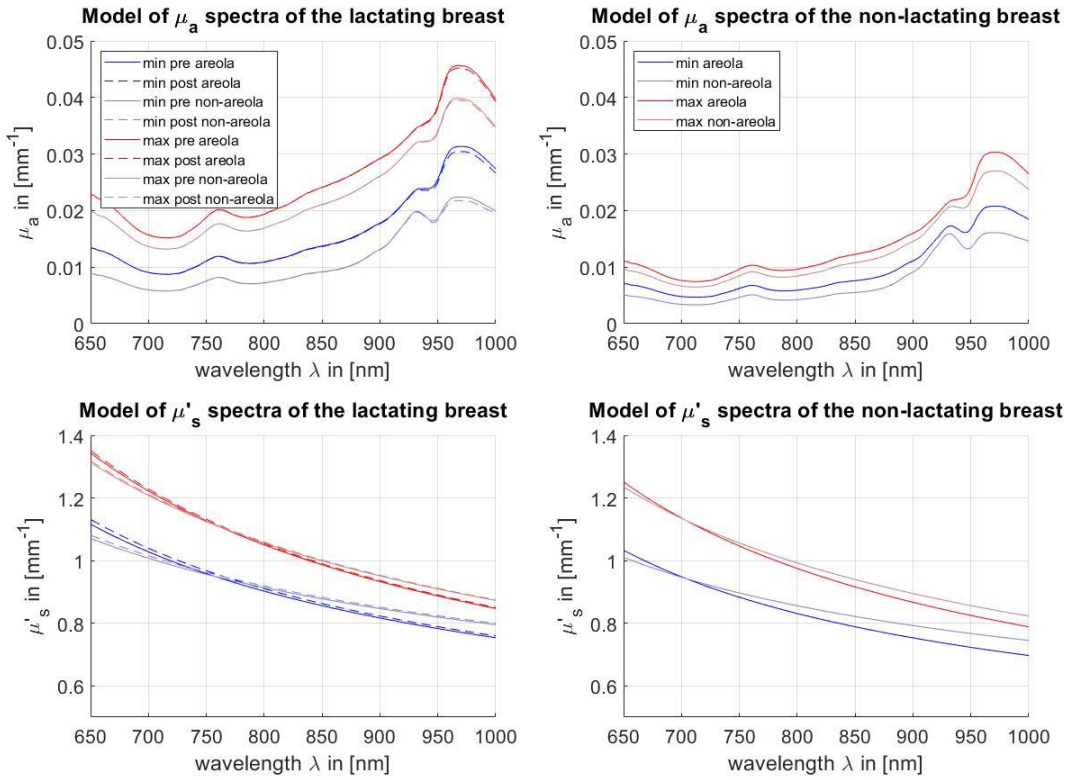

Thin skin

	HbO₂ [µM]	Hb [µM]	THb [µM]	StO₂ %	Lipid %	Water %	$a\ mm^{-1}$	b
non-ar non-lac	-8.1	-1.9	-10.0	-1.8	9.3	-6.5	-0.17	-0.13
non-ar lac pre	-19.4	-4.5	-23.9	-2.0	9.6	-6.5	-0.20	-0.14
non-ar lac post	-19.1	-4.4	-23.5	-2.3	9.7	-6.8	-0.19	-0.14
ar non-lac	-6.4	-1.4	-7.8	-1.2	6.6	-4.9	-0.15	-0.08
ar lac pre	-14.9	-3.3	-18.2	-1.4	5.3	-3.8	-0.15	-0.07
ar lac post	-14.6	-3.1	-17.7	-1.6	5.4	-4.2	-0.15	-0.07

Thick skin

	HbO₂ [µM]	Hb [µM]	THb [µM]	StO₂ %	Lipid %	Water %	$a\ mm^{-1}$	b
non-ar non-lac	8.6	2.0	10.6	1.0	-9.4	6.8	0.19	0.11
non-ar lac pre	20.4	4.7	25.1	0.9	-9.4	6.4	0.21	0.12
non-ar lac post	20.0	4.5	24.6	1.1	-9.4	6.8	0.20	0.11
ar non-lac	8.5	1.9	10.4	1.0	-8.6	6.5	0.20	0.08
ar lac pre	20.3	4.5	24.8	1.0	-7.5	5.3	0.21	0.09
ar lac post	19.8	4.3	24.0	1.2	-7.6	5.8	0.20	0.08

THICKNESS SUBCUTANEOUS FAT

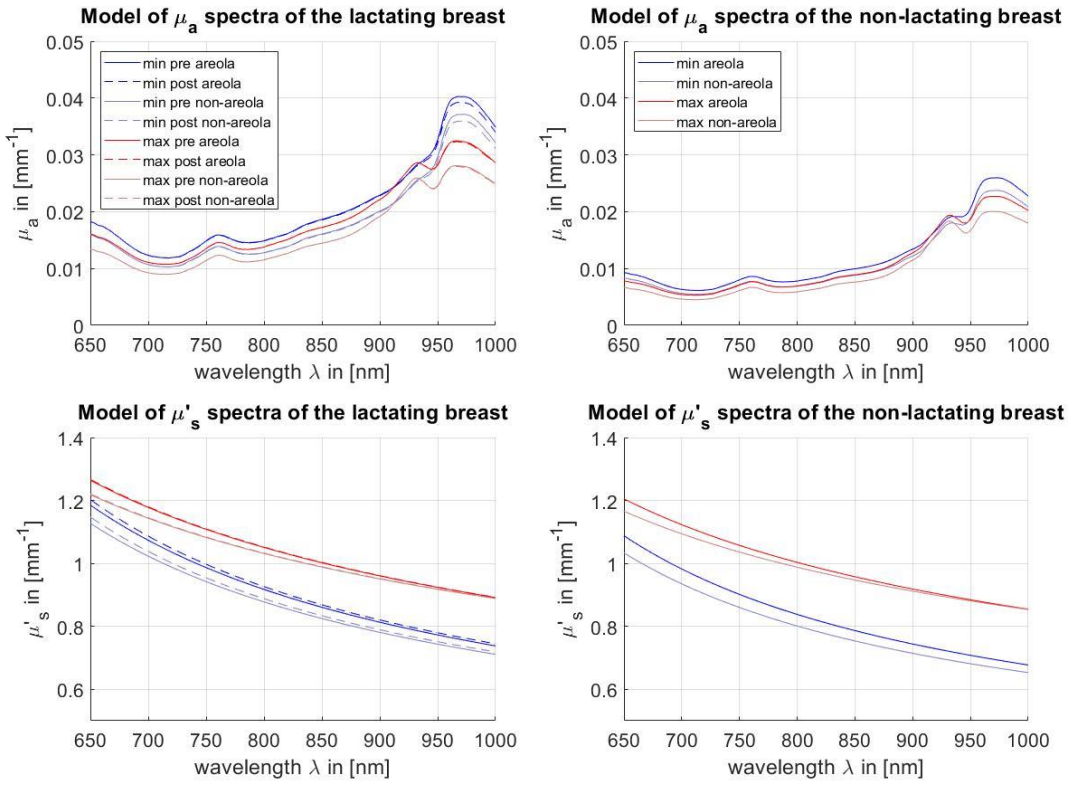

Thin sf

	HbO₂ [µM]	Hb [µM]	THb [µM]	StO₂ %	Lipid %	Water %	$a\ mm^{-1}$	b
non-ar non-lac	1.8	1.2	3.0	-1.6	-11.6	3.9	-0.02	0.23
non-ar lac pre	1.3	2.0	3.4	-2.2	-20.7	12.3	0.01	0.24
non-ar lac post	2.8	2.8	5.6	-2.4	-20.4	10.8	0.03	0.25
ar non-lac	0.8	0.5	1.4	-0.6	-5.4	1.8	-0.01	0.11
ar lac pre	0.6	1.0	1.6	-0.9	-9.8	5.8	0.01	0.12
ar lac post	1.3	1.3	2.6	-1.0	-9.6	5.1	0.02	0.12

Thick sf

	HbO₂ [µM]	Hb [µM]	THb [µM]	StO₂ %	Lipid %	Water %	$a\ mm^{-1}$	b
non-ar non-lac	-1.1	-0.7	-1.8	1.1	6.8	-2.3	0.02	-0.11
non-ar lac pre	-0.6	-1.0	-1.6	1.1	9.8	-5.8	0.00	-0.10
non-ar lac post	-1.3	-1.3	-2.6	1.3	9.7	-5.1	-0.01	-0.10
ar non-lac	-1.7	-1.1	-2.8	1.5	10.9	-3.7	0.03	-0.19
ar lac pre	-1.1	-1.6	-2.7	1.6	16.8	-9.9	-0.01	-0.17
ar lac post	-2.3	-2.2	-4.5	1.8	16.5	-8.7	-0.02	-0.18

RATIO ADIPOSE TISSUE TO GLANDULAR TISSUE

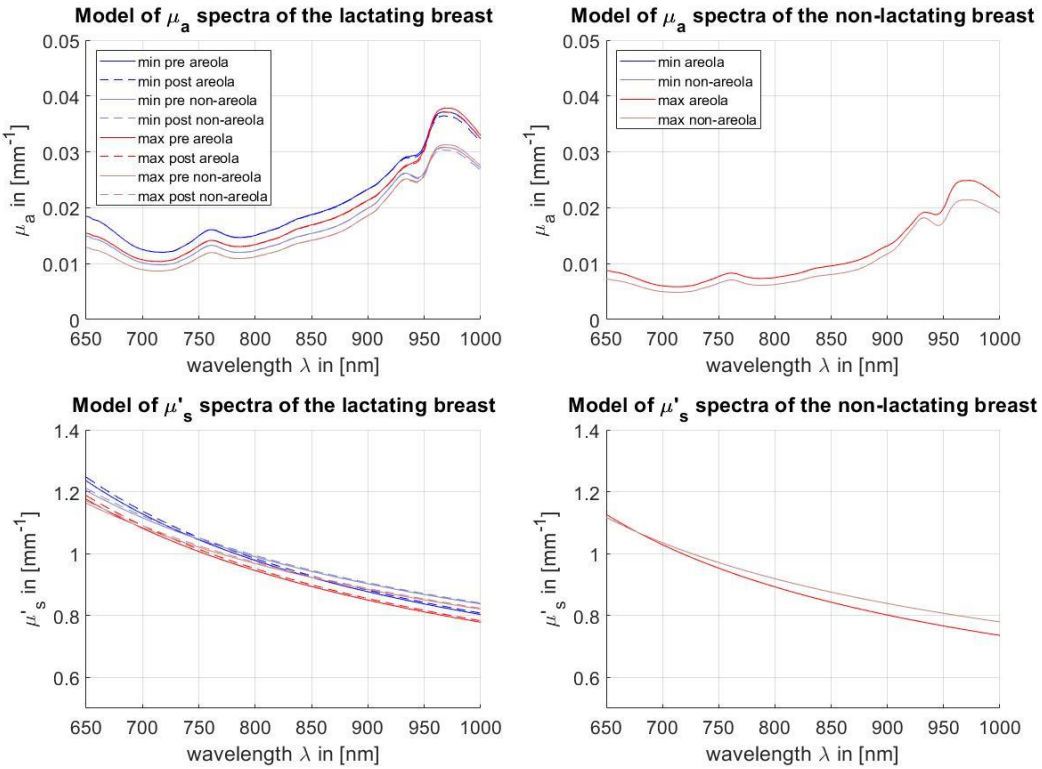

No intraglandular fat

	HbO₂ [µM]	Hb [µM]	THb [µM]	StO₂ %	Lipid %	Water %	$a\ mm^{-1}$	b
non-ar non-lac	0.6	0.9	1.5	-1.8	-10.3	5.8	0.11	0.06
non-ar lac pre	0.1	0.2	0.3	-0.2	-1.5	1.1	0.01	0.01
non-ar lac post	0.1	0.2	0.3	-0.2	-1.7	1.1	0.02	0.01
ar non-lac	0.9	1.2	2.0	-2.0	-13.9	7.9	0.15	0.07
ar lac pre	0.2	0.2	0.4	-0.2	-2.2	1.6	0.02	0.01
ar lac post	0.2	0.3	0.5	-0.2	-2.5	1.6	0.02	0.01

Lactating breast: 0.5 ratio adipose tissue to glandular tissue.
Non-lactating breast: 1 ratio adipose tissue to glandular tissue.

	HbO₂ [µM]	Hb [µM]	THb [µM]	StO₂ %	Lipid %	Water %	$a\ mm^{-1}$	b
non-ar non-lac	-0.6	-0.9	-1.5	2.0	10.3	-5.8	-0.11	-0.07
non-ar lac pre	-0.5	-0.6	-1.1	0.7	5.9	-4.4	-0.05	-0.03
non-ar lac post	-0.6	-0.8	-1.4	0.9	6.3	-4.2	-0.06	-0.03
ar non-lac	-0.9	-1.2	-2.0	2.2	13.9	-7.9	-0.15	-0.08
ar lac pre	-0.7	-0.9	-1.6	0.9	8.8	-6.5	-0.07	-0.03
ar lac post	-0.9	-1.2	-2.0	1.0	9.3	-6.2	-0.09	-0.04

THb

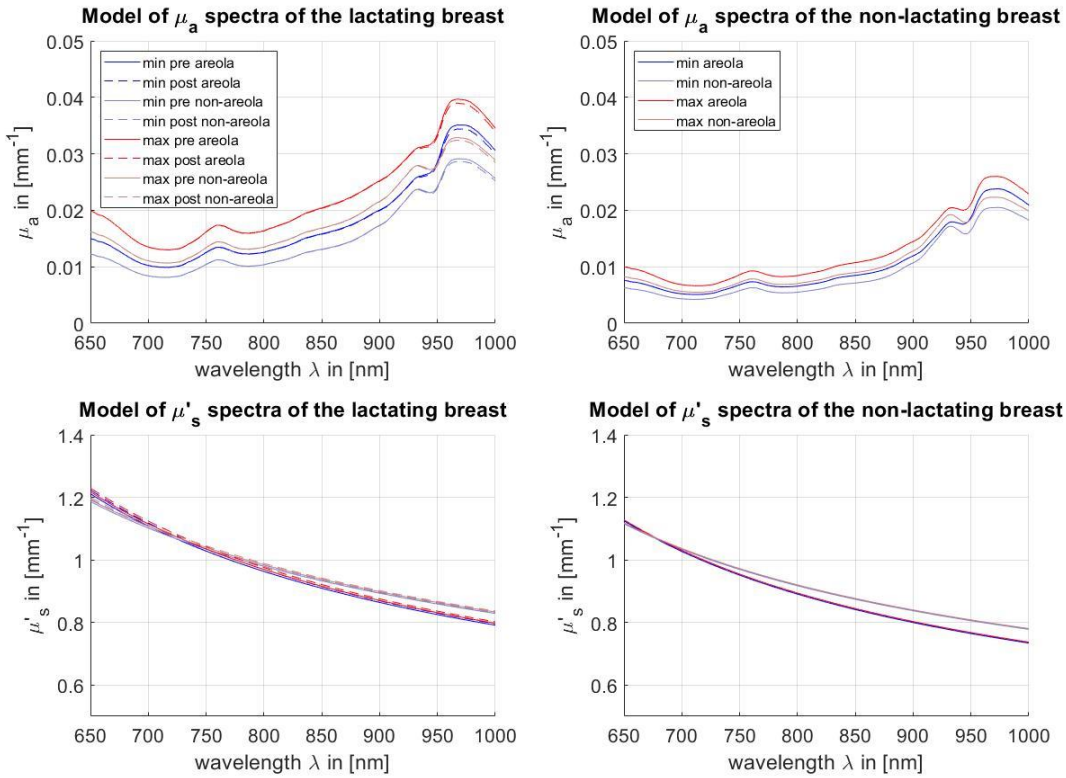

Low hemoglobin level

	HbO_2 [µM]	Hb [µM]	THb [µM]	StO_2 %	Lipid %	Water %	$a\ mm^{-1}$	b
non-ar non-lac	-3.1	-0.9	-4.0	0.0	0.0	0.0	0.00	0.00
non-ar lac pre	-6.3	-1.7	-8.1	0.0	0.0	0.0	0.00	0.00
non-ar lac post	-6.5	-1.8	-8.3	0.0	0.0	0.0	0.00	0.00
ar non-lac	-3.8	-1.1	-4.8	0.0	0.0	0.0	0.00	0.00
ar lac pre	-7.7	-2.2	-9.9	0.0	0.0	0.0	0.00	0.00
ar lac post	-7.9	-2.3	-10.2	0.0	0.0	0.0	0.00	0.00

High hemoglobin level

	HbO_2 [µM]	Hb [µM]	THb [µM]	StO_2 %	Lipid %	Water %	$a\ mm^{-1}$	b
non-ar non-lac	3.1	0.9	4.0	0.0	0.0	0.0	0.00	0.00
non-ar lac pre	6.3	1.7	8.1	0.0	0.0	0.0	0.00	0.00
non-ar lac post	6.5	1.8	8.3	0.0	0.0	0.0	0.00	0.00
ar non-lac	3.8	1.1	4.8	0.0	0.0	0.0	0.00	0.00
ar lac pre	7.7	2.2	9.9	0.0	0.0	0.0	0.00	0.00
ar lac post	7.9	2.3	10.2	0.0	0.0	0.0	0.00	0.00

ONLY FOR THE LACTATING BREAST

FAT IN MILK.

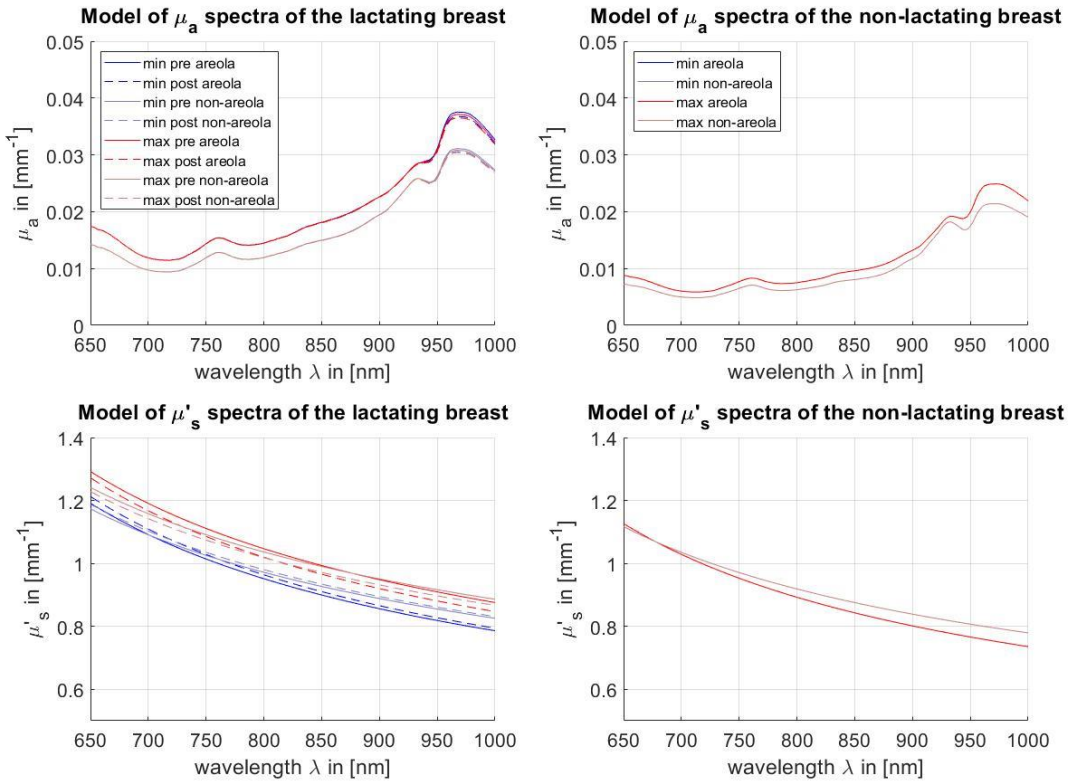

Low level fat (foremilk scattering)

	HbO_2 [µM]	Hb [µM]	THb [µM]	StO_2 %	Lipid %	Water %	$a\ mm^{-1}$	b
non-ar non-lac	0.0	0.0	0.0	0.0	0.0	0.0	0.00	0.00
non-ar lac pre	0.0	0.0	0.0	0.0	-0.2	0.2	-0.03	-0.02
non-ar lac post	0.0	0.0	0.0	0.0	-0.1	0.1	-0.02	-0.01
ar non-lac	0.0	0.0	0.0	0.0	0.0	0.0	0.00	0.00
ar lac pre	0.0	0.0	0.0	0.0	-0.3	0.3	-0.04	-0.02
ar lac post	0.0	0.0	0.0	0.0	-0.2	0.2	-0.02	-0.01

High level fat (hindmilk scattering)

	HbO_2 [µM]	Hb [µM]	THb [µM]	StO_2 %	Lipid %	Water %	$a\ mm^{-1}$	b
non-ar non-lac	0.0	0.0	0.0	0.0	0.0	0.0	0.00	0.00
non-ar lac pre	0.0	0.0	0.0	0.0	0.4	-0.4	0.05	-0.05
non-ar lac post	0.0	0.0	0.0	0.0	0.2	-0.2	0.03	-0.03
ar non-lac	0.0	0.0	0.0	0.0	0.0	0.0	0.00	0.00
ar lac pre	0.0	0.0	0.0	0.0	0.6	-0.6	0.06	-0.08
ar lac post	0.0	0.0	0.0	0.0	0.3	-0.3	0.04	-0.05

MILK STORAGE CAPACITY.

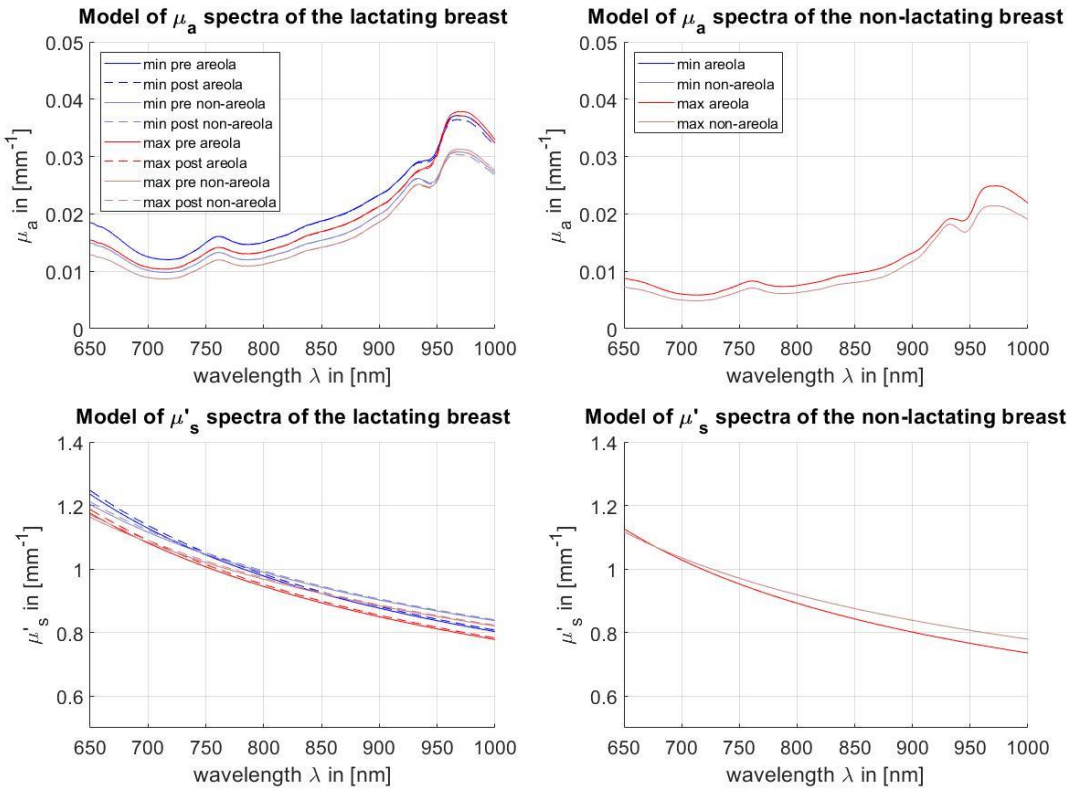

Low storage capacity (70 ml)

	HbO_2 [µM]	Hb [µM]	THb [µM]	StO_2 %	Lipid %	Water %	$a\ mm^{-1}$	b
non-ar non-lac	0.0	0.0	0.0	0.0	0.0	0.0	0.00	0.00
non-ar lac pre	1.4	0.7	2.2	-0.5	0.0	-1.3	0.02	0.01
non-ar lac post	1.4	0.7	2.2	-0.4	0.0	-1.3	0.02	0.01
ar non-lac	0.0	0.0	0.0	0.0	0.0	0.0	0.00	0.00
ar lac pre	2.1	1.1	3.2	-0.5	0.1	-1.9	0.03	0.01
ar lac post	2.1	1.1	3.2	-0.5	0.1	-1.9	0.03	0.01

High storage capacity (355 ml)

	HbO_2 [µM]	Hb [µM]	THb [µM]	StO_2 %	Lipid %	Water %	$a\ mm^{-1}$	b
non-ar non-lac	0.0	0.0	0.0	0.0	0.0	0.0	0.00	0.00
non-ar lac pre	-2.7	-1.4	-4.0	0.9	-0.1	2.4	-0.04	-0.02
non-ar lac post	-2.7	-1.4	-4.0	0.9	-0.1	2.4	-0.04	-0.02
ar non-lac	0.0	0.0	0.0	0.0	0.0	0.0	0.00	0.00
ar lac pre	-3.9	-2.0	-6.0	1.1	-0.1	3.6	-0.06	-0.03
ar lac post	-3.9	-2.0	-6.0	1.1	-0.1	3.6	-0.06	-0.03

volume breast

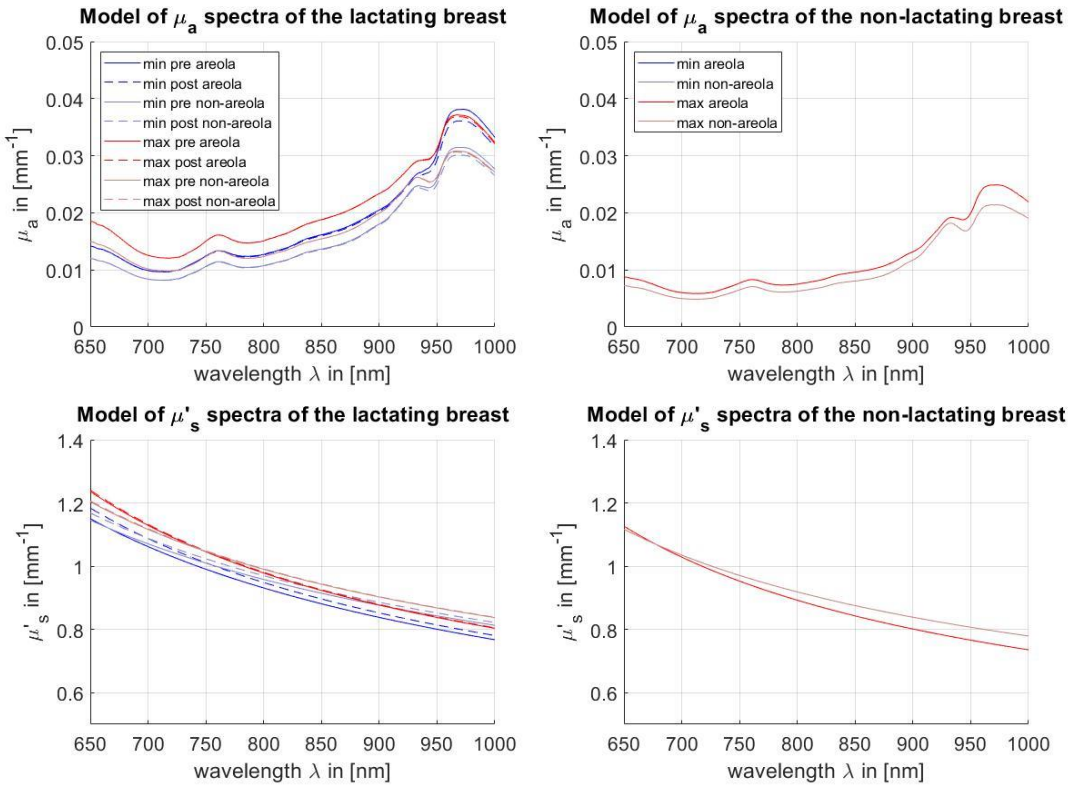

Small volume of the lactating breast (270 ml)

	HbO_2 [µM]	Hb [µM]	THb [µM]	StO_2 %	Lipid %	Water %	$a\ mm^{-1}$	b
non-ar non-lac	0.0	0.0	0.0	0.0	0.0	0.0	0.00	0.00
non-ar lac pre	-4.4	-2.3	-6.6	1.6	-0.1	4.0	-0.07	-0.04
non-ar lac post	-2.6	-1.3	-3.9	0.9	0.3	2.1	-0.04	-0.02
ar non-lac	0.0	0.0	0.0	0.0	0.0	0.0	0.00	0.00
ar lac pre	-6.5	-3.3	-9.8	2.0	-0.2	5.9	-0.10	-0.05
ar lac post	-3.8	-2.0	-5.8	1.0	0.4	3.2	-0.07	-0.03

High volume of the lactating breast (2000 ml)

	HbO_2 [µM]	Hb [µM]	THb [µM]	StO_2 %	Lipid %	Water %	$a\ mm^{-1}$	b
non-ar non-lac	0.0	0.0	0.0	0.0	0.0	0.0	0.00	0.00
non-ar lac pre	1.5	0.8	2.3	-0.5	0.0	-1.4	0.02	0.01
non-ar lac post	0.9	0.5	1.4	-0.3	-0.1	-0.7	0.02	0.01
ar non-lac	0.0	0.0	0.0	0.0	0.0	0.0	0.00	0.00
ar lac pre	2.2	1.2	3.4	-0.6	0.1	-2.0	0.03	0.01
ar lac post	1.3	0.7	2.0	-0.3	-0.1	-1.1	0.02	0.01

PHYSIOLOGICAL CHANGES

BLOOD CONCENTRATION

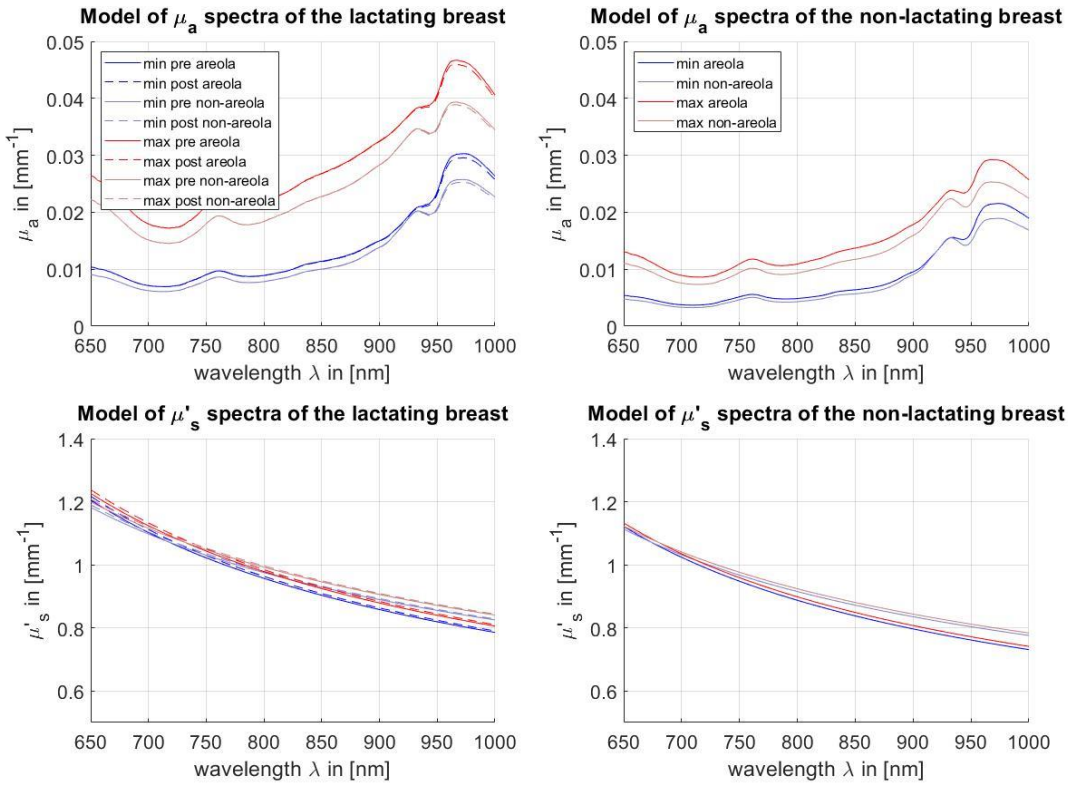

Low blood concentration

	HbO_2 [µM]	Hb [µM]	THb [µM]	StO_2 %	Lipid %	Water %	$a\ mm^{-1}$	b
non-ar non-lac	-7.9	-2.2	-10.1	-0.1	0.0	-0.4	0.00	0.00
non-ar lac pre	-16.6	-4.5	-21.2	-0.1	0.0	-0.8	-0.01	0.00
non-ar lac post	-16.9	-4.7	-21.7	-0.1	0.0	-0.8	-0.01	0.00
ar non-lac	-10.7	-3.0	-13.7	-0.3	0.0	-0.5	0.00	0.00
ar lac pre	-22.5	-6.2	-28.8	-0.3	0.0	-1.0	-0.01	0.01
ar lac post	-23.0	-6.5	-29.5	-0.3	0.0	-1.1	-0.01	0.01

High blood concentration

	HbO_2 [µM]	Hb [µM]	THb [µM]	StO_2 %	Lipid %	Water %	$a\ mm^{-1}$	b
non-ar non-lac	12.4	3.3	15.7	0.3	0.0	0.6	0.01	0.00
non-ar lac pre	26.3	7.0	33.2	0.3	0.0	1.2	0.01	-0.01
non-ar lac post	26.6	7.1	33.7	0.3	0.0	1.2	0.01	-0.01
ar non-lac	13.8	3.8	17.5	0.3	0.0	0.6	0.01	-0.01
ar lac pre	29.2	7.9	37.1	0.3	0.0	1.3	0.01	-0.01
ar lac post	29.7	8.1	37.9	0.3	0.0	1.4	0.01	-0.01

STO₂ CORRECTION

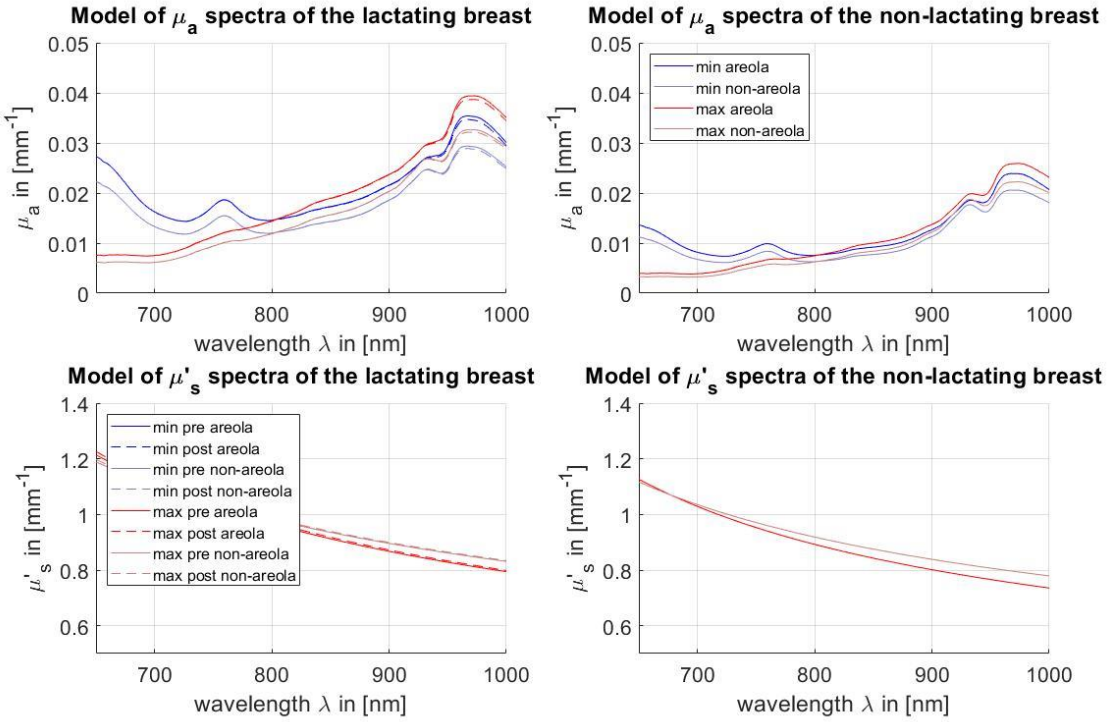

Low oxygen saturation

	HbO₂ [µM]	Hb [µM]	THb [µM]	StO₂ %	Lipid %	Water %	$a\ mm^{-1}$	b
non-ar non-lac	-5.6	5.6	0.0	-20.0	0.0	0.0	0.00	0.00
non-ar lac pre	-11.3	11.3	0.0	-20.0	0.0	0.0	0.00	0.00
non-ar lac post	-11.6	11.6	0.0	-20.0	0.0	0.0	0.00	0.00
ar non-lac	-6.8	6.8	0.0	-20.0	0.0	0.0	0.00	0.00
ar lac pre	-13.8	13.8	0.0	-20.0	0.0	0.0	0.00	0.00
ar lac post	-14.3	14.3	0.0	-20.0	0.0	0.0	0.00	0.00

High oxygen saturation

	HbO₂ [µM]	Hb [µM]	THb [µM]	StO₂ %	Lipid %	Water %	$a\ mm^{-1}$	b
non-ar non-lac	5.6	-5.6	0.0	20.0	0.0	0.0	0.00	0.00
non-ar lac pre	11.3	-11.3	0.0	20.0	0.0	0.0	0.00	0.00
non-ar lac post	11.6	-11.6	0.0	20.0	0.0	0.0	0.00	0.00
ar non-lac	6.8	-6.8	0.0	20.0	0.0	0.0	0.00	0.00
ar lac pre	13.8	-13.8	0.0	20.0	0.0	0.0	0.00	0.00
ar lac post	14.3	-14.3	0.0	20.0	0.0	0.0	0.00	0.00

ONLY FOR THE LACTATING BREAST

MILK EXTRACTION DURING BREASTFEED

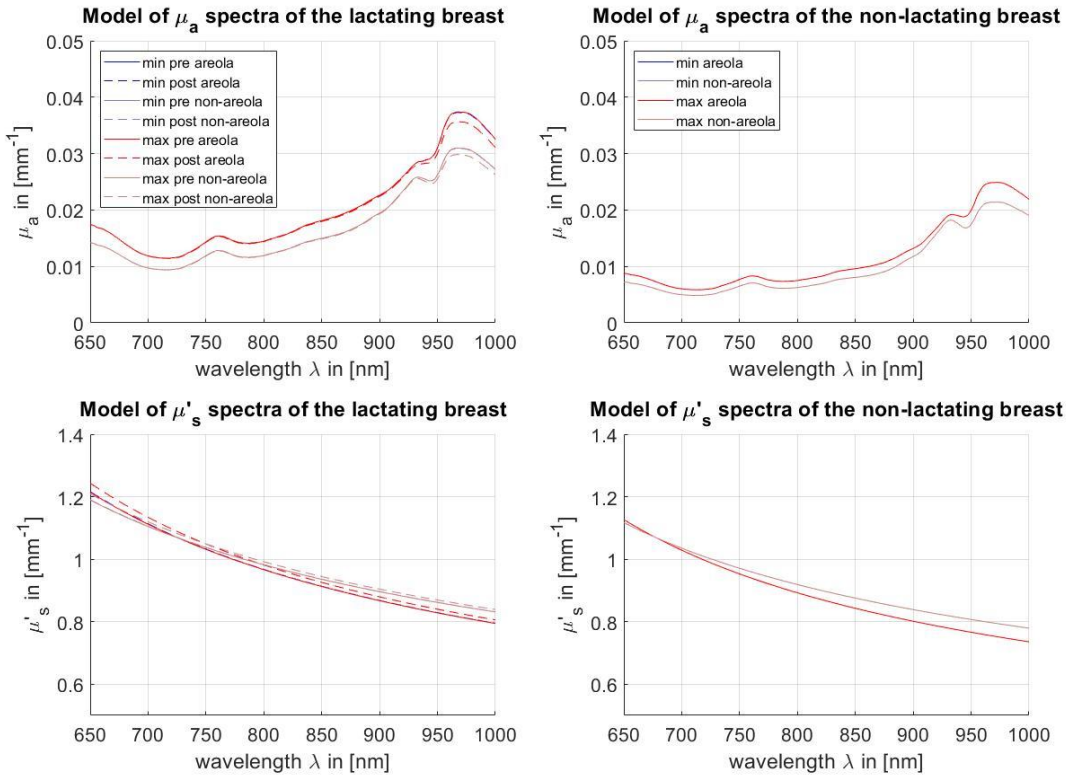

Little milk extraction (10 ml)

	HbO_2 [µM]	Hb [µM]	THb [µM]	StO_2 %	Lipid %	Water %	$a\ mm^{-1}$	b
non-ar non-lac	0.0	0.0	0.0	0.0	0.0	0.0	0.00	0.00
non-ar lac pre	0.0	0.0	0.0	0.0	0.0	0.0	0.00	0.00
non-ar lac post	-0.9	-0.4	-1.3	0.3	-0.2	0.9	-0.01	-0.01
ar non-lac	0.0	0.0	0.0	0.0	0.0	0.0	0.00	0.00
ar lac pre	0.0	0.0	0.0	0.0	0.0	0.0	0.00	0.00
ar lac post	-1.3	-0.7	-1.9	0.3	-0.3	1.3	-0.02	-0.01

A lot of milk extraction (170 ml)

	HbO_2 [µM]	Hb [µM]	THb [µM]	StO_2 %	Lipid %	Water %	$a\ mm^{-1}$	b
non-ar non-lac	0.0	0.0	0.0	0.0	0.0	0.0	0.00	0.00
non-ar lac pre	0.0	0.0	0.0	0.0	0.0	0.0	0.00	0.00
non-ar lac post	1.4	0.7	2.2	-0.4	0.3	-1.5	0.02	0.01
ar non-lac	0.0	0.0	0.0	0.0	0.0	0.0	0.00	0.00
ar lac pre	0.0	0.0	0.0	0.0	0.0	0.0	0.00	0.00
ar lac post	2.1	1.1	3.2	-0.5	0.5	-2.2	0.03	0.01

DEFORMATION DUE TO 70ML MILK EXTRACTION DURING BREASTFEED.

Glandular tissue and adipose tissue will replace the empty space.

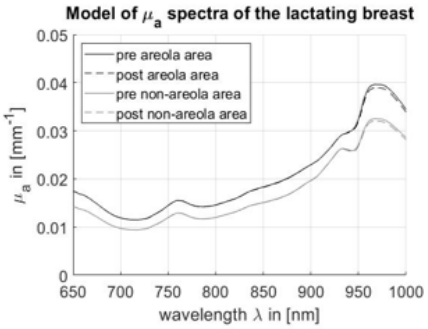

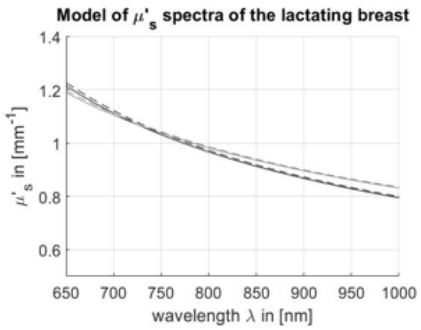

Nothing replaces the ejected milk volume.

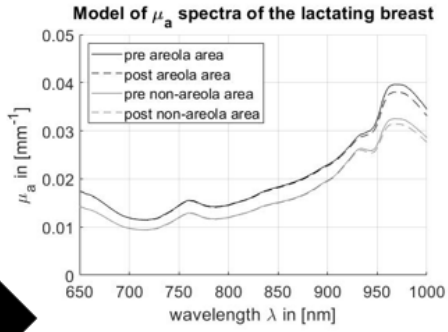

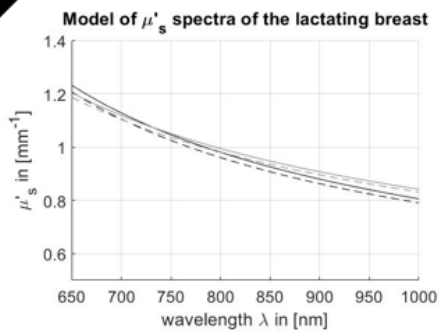

Differences between average model and when nothing replaces the milk volume ejected.

	HbO₂ [µM]	Hb [µM]	THb [µM]	StO₂ %	Lipid %	Water %	$a\ mm^{-1}$	b
non-ar non-lac	0.0	0.0	0.0	0.0	0.0	0.0	0.00	0.00
non-ar lac pre	0.0	0.0	0.0	0.0	0.0	0.0	0.00	0.00
non-ar lac post	-1.0	-0.5	-1.5	0.3	-0.3	-1.2	-0.04	-0.01
ar non-lac	0.0	0.0	0.0	0.0	0.0	0.0	0.00	0.00
ar lac pre	0.0	0.0	0.0	0.0	0.0	0.0	0.00	0.00
ar lac post	-1.5	-0.8	-2.3	0.4	-0.5	-1.9	-0.05	-0.01

APPENDIX – QUALITATIVE ANALYSIS PER SUBJECT

In this appendix, an extra analysis is carried out per lactating subject. The reason for this is that there were not much lactating subject participating and since there is not much know about the lactating breast an in-depth analysis can contribute to the overall knowledge of the lactating breast. Moreover, this can also illustrate how much variances there is between the subjects.

Per subject, two figures are shown. In the first figure, the grid measurement per functional property is shown. The purpose of this figure is to see local differences in functional properties, as well as how these local differences change between pre- and post-expression. In the second figure, the chromophores over time and the milk flow rate are shown. Here it is possible to see the effect of the events as pumping or a MER on the chromophores. The grid figures are made using MATLAB and the during breastfeed are made in Origin. The functional properties oxyhemoglobin and deoxyhemoglobin, for both figures, and a and b for the second figure, are not implemented in this figure purposely to maintain readability of the figures. Oxyhemoglobin and deoxyhemoglobin are disregarded since they will give similar information as THb and stO_2.

SUBJECT L1

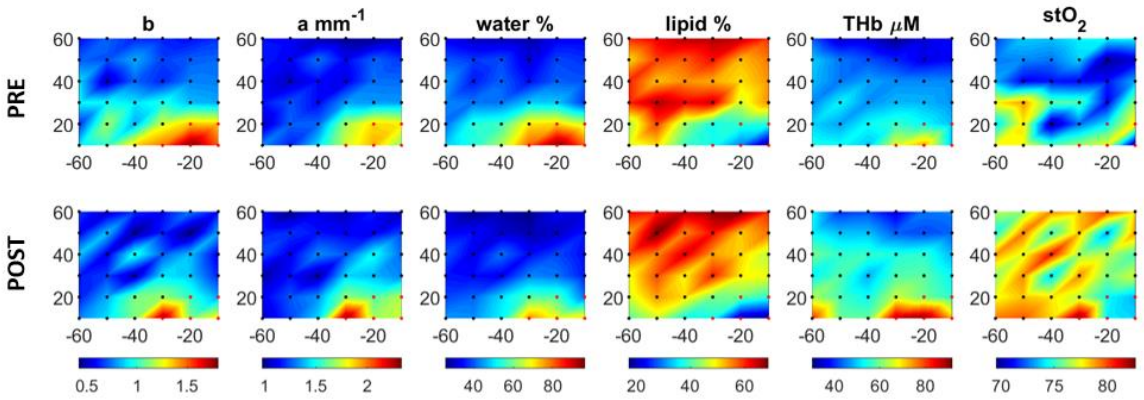

FIGURE 2 GRID MEASUREMENTS OF L1 PER FUNCTIONAL PROPERTY. DOTS INDICATED MEASURING POINTS, IN BETWEEN THERE IS INTERPOLATED. THE RED DOTS RESEMBLE THE AREOLA AREA AND THE BLACK DOTS THE NON-AREOLA AREA. THE X-AXIS, Y-AXIS REPRESENT THE X COORDINATES AND Y COORDINATES IN MM WITH RESPECT TO THE NIPPLE, RESPECTIVELY.

Around $x = -50\ mm$ and $y = 20\ mm$, there is an interesting spot. Here the slope, water concentration and oxygen saturation are higher for the pre-expression measurements than for the other non-areola aera grid points. Moreover, it is remarkable that post-expression these values seems to differ not that much from other non-areola area grid points. This could indicate a gland. Also breastfeeding seems to have effect on the values of the areola area more, since these changes a lot before and after breastfeeding.

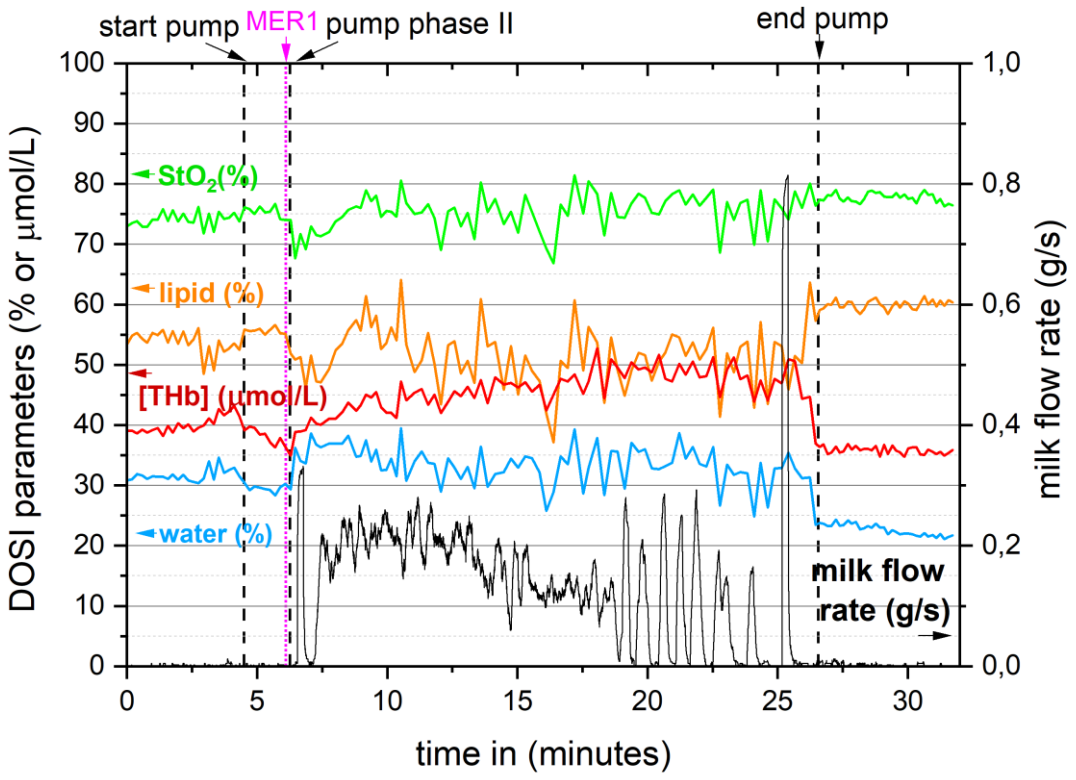

FIGURE 3 CHROMOPHORES AND MILK FLOW RATE OF SUBJECT L1

For this subject, there is reported that sometimes the milk will accumulate in the breast shield, causing that the sometimes the milk flow down into the bottle all at ones. It is notices that all chromophores react on turning the pump on and off. The signal when the pump is turned on has a very noisy appearance. Therefore, it is hard to corelate events like MERs or other milk flow behaviour to the chromophores. This noisy appearance could be due to the low sampling rate. However, after the first MER, there is a temporary decrease for stO_2 and lipid concentrations and water and THb concentrations seems to increase.

SUBJECT L2

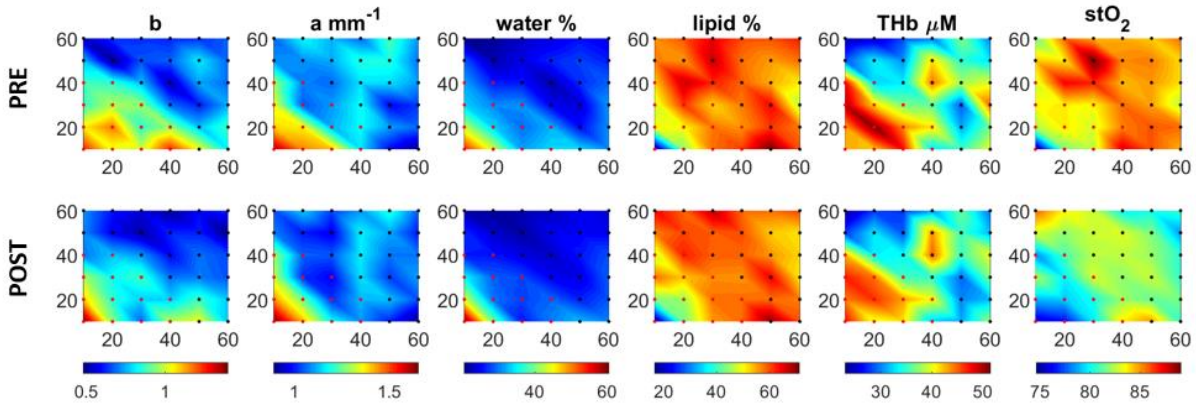

FIGURE 4 GRID MEASUREMENTS OF L2 PER FUNCTIONAL PROPERTY. DOTS INDICATED MEASURING POINTS, IN BETWEEN THERE IS INTERPOLATED. THE RED DOTS RESEMBLE THE AREOLA AREA AND THE BLACK DOTS THE NON-AREOLA AREA. THE X-AXIS, Y-AXIS REPRESENT THE X COORDINATES AND Y COORDINATES IN MM WITH RESPECT TO THE NIPPLE, RESPECTIVELY.

StO_2 levels are lower after breastfeeding over almost the whole grid. Also, the decrease in the areola area of the slope is remarkable. Around $x = 40\ mm$ and $y = 40\ mm$ is a spot wherein THb concentration is higher. Maybe this is a superficial blood vessel.

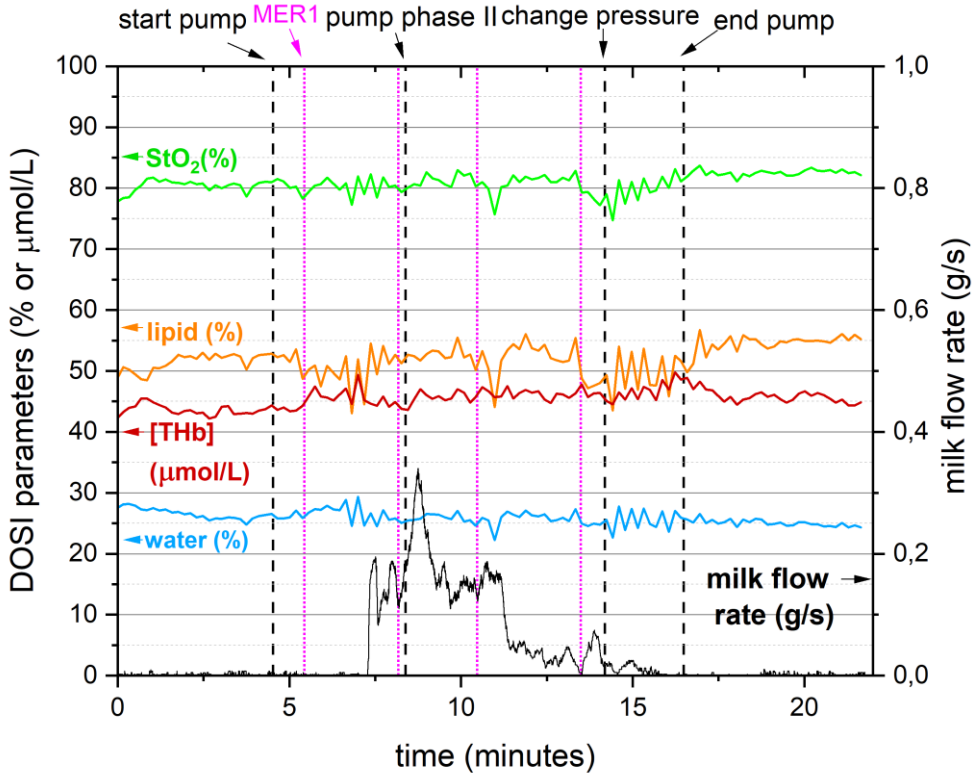

FIGURE 5 CHROMOPHORES AND MILK FLOW RATE OF SUBJECT L2

Noticeable is that at the third MER the water concentration, lipid concentration and stO2 decrease. Before last noted MER, the water concentration, lipid concentration and stO2 increase.

SUBJECT L4

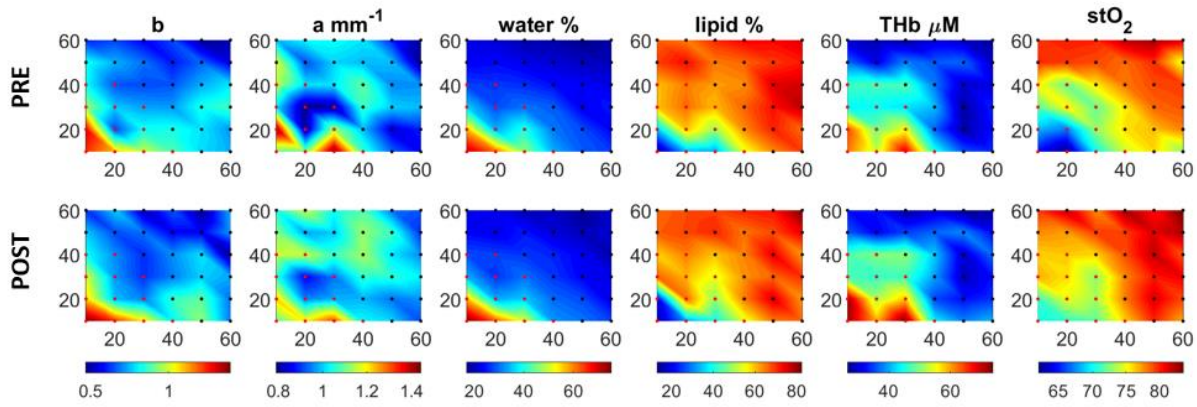

FIGURE 6 GRID MEASUREMENTS OF L4 PER FUNCTIONAL PROPERTY. DOTS INDICATED MEASURING POINTS, IN BETWEEN THERE IS INTERPOLATED. THE RED DOTS RESEMBLE THE AREOLA AREA AND THE BLACK DOTS THE NON-AREOLA AREA. THE X-AXIS, Y-AXIS REPRESENT THE X COORDINATES AND Y COORDINATES IN MM WITH RESPECT TO THE NIPPLE, RESPECTIVELY.

Saturation for the areola is higher post-expression, but lower for the non-areola area post-expression. Not much water in the breast, lot of lipid.

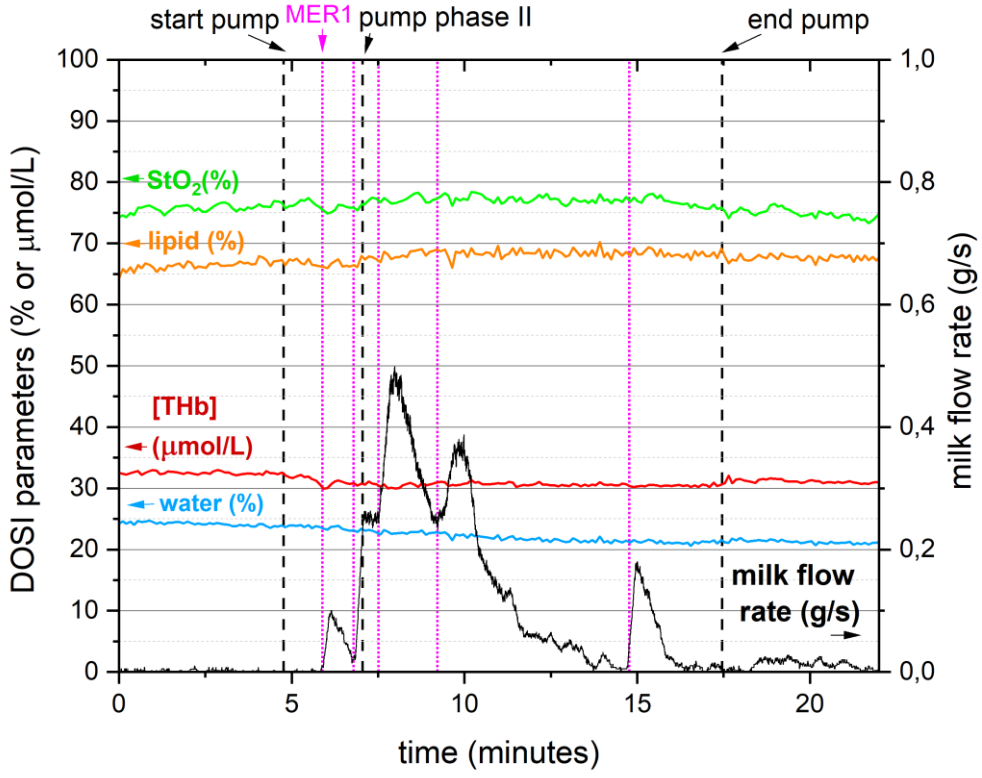

FIGURE 7 CHROMOPHORES AND MILK FLOW RATE OF SUBJECT L4

Although very clear MERs can be observed, there is almost no response of the chromophores. In the grid figure higher concentrations of lipid can be found 6 cm above the areola. It could be that the DOSI device was not able to measure deeper than the subcutaneous fat or measured a lot of intraglandular fat.

SUBJECT L5

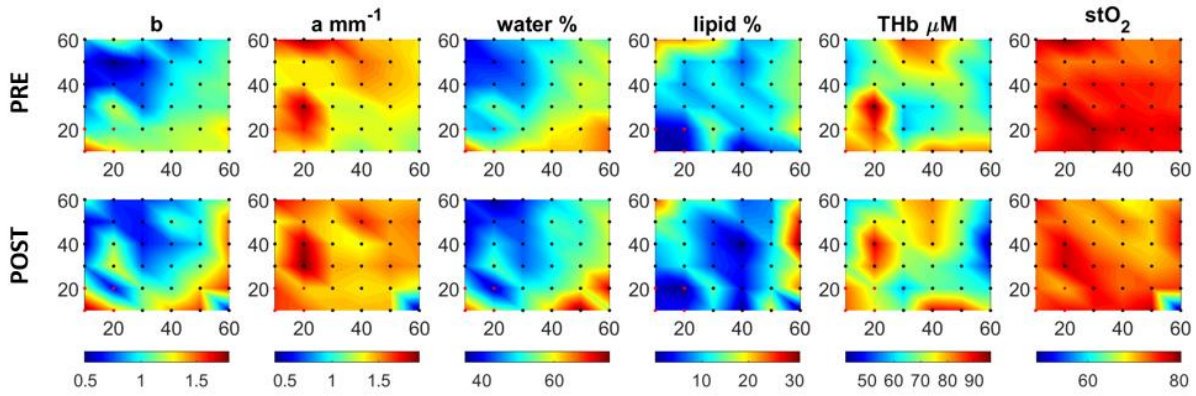

FIGURE 8 GRID MEASUREMENTS OF L5 PER FUNCTIONAL PROPERTY. DOTS INDICATED MEASURING POINTS, IN BETWEEN THERE IS INTERPOLATED. THE RED DOTS RESEMBLE THE AREOLA AREA AND THE BLACK DOTS THE NON-AREOLA AREA. THE X-AXIS, Y-AXIS REPRESENT THE X COORDINATES AND Y COORDINATES IN MM WITH RESPECT TO THE NIPPLE, RESPECTIVELY. NOTE THAT, FOR SUBJECT L5, THE SOURCE DETECTOR-DISTANCE WAS 22 MM FOR THE GRID MEASUREMENT.

There is a low concentration lipid concentration in the breast. At $x = 40\ mm$, the concentration lipid and water decrease comparing the post-expression grid with the pre-expression grid. This maybe could indicate a gland. Since the breast for L5 attenuated too much, probably due to the high THb, there is chosen for a smaller source-detector distance of 22 mm.

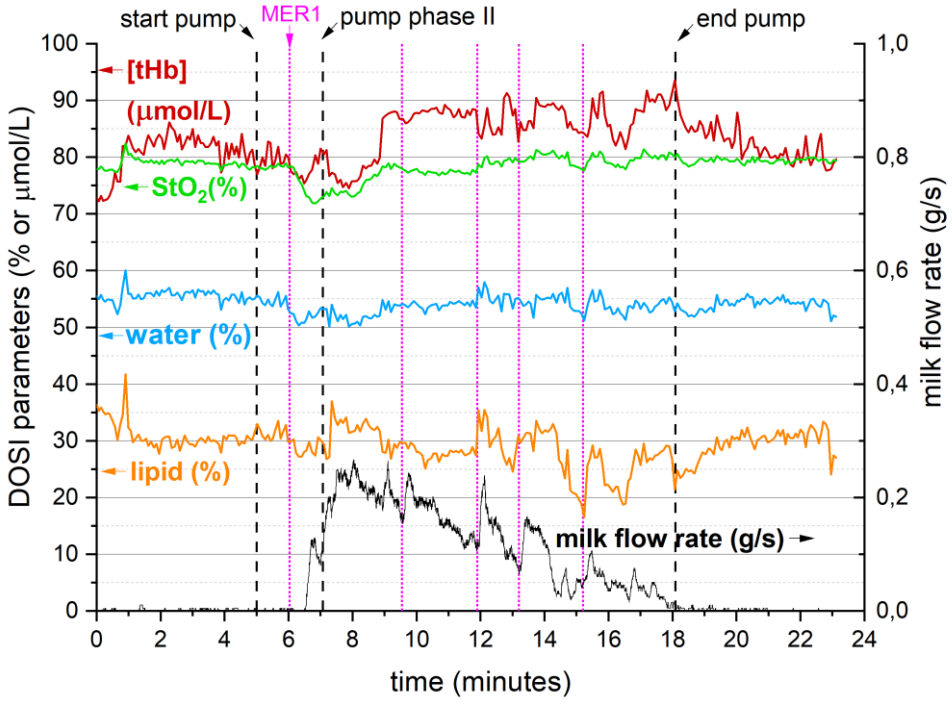

FIGURE 9 CHROMOPHORES AND MILK FLOW RATE OF SUBJECT L5.

For this subject, multiple MERs are observed. The first MER is felt, the rest of the MERs are determined from the begin of the increase of the milk flow rate. Thereby, there could be a dispersion between the milk flow rate (in the bottle) and between the chromophores that are directly measured on the breast. Therefore, the timing of

the MERs in the chromophores are expected slightly earlier than in milk flow rate, except for the first MER. Overall, the chromophores seem to react on the MERs. Although, the effect on the chromophores seems to differ.

At the first MER, the value of every chromophores decreases. At the second MER, there is not a clear effect on the chromophores. At the third MER, the water and lipid concentrations increase while the THb concentration decreases. At the fourth MER, lipid and THb decrease before, and increase after the MER is marked. At the last MER, all values of every chromophore decrease before the increase of milk flow rate and increase after the indication of the MER.

To conclude, there is not really a consensus in the way the milk flow rate and MER's effect the chromophores. This could be due to different events that can occur.

NON-LACTATING SUBJECT GRIDS.

The grids of the non-lactating subject are also presented to compare the changes of the lactating breast with the non-lactating breast. Notice that less changes occur. The peri-data is not added, because not much happens, see also figure 5.8, there is also not much differences between pre and post.

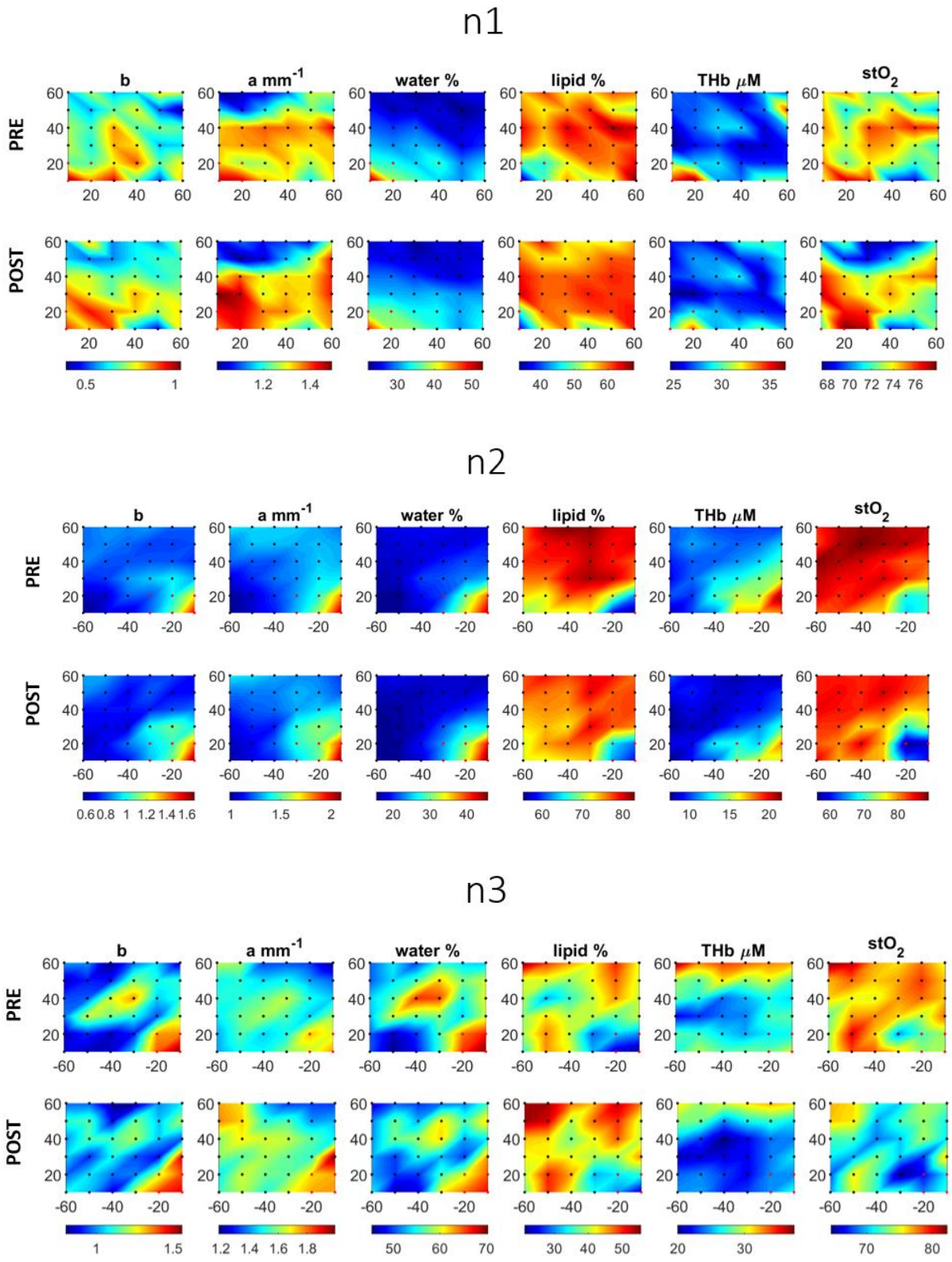

n4

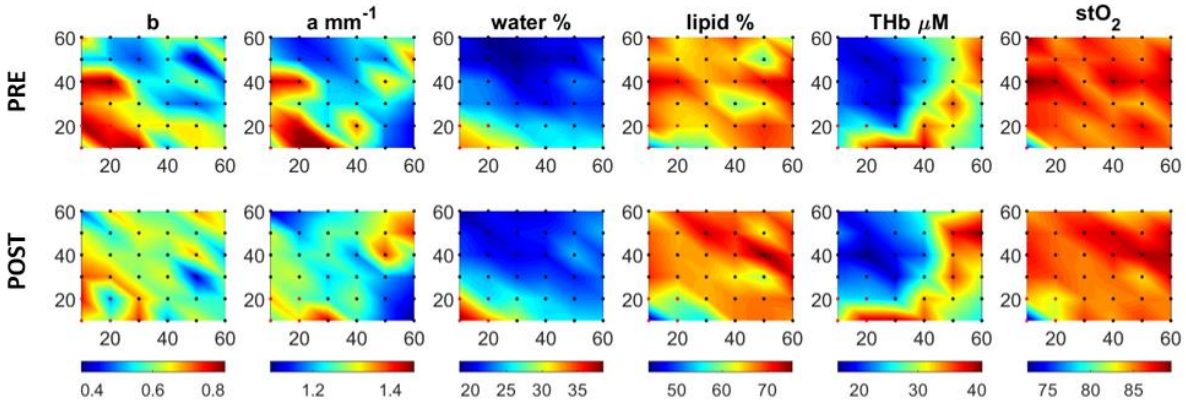
b
a mm-1
water %
lipid %
THb μM
stO2
PRE
POST

n5

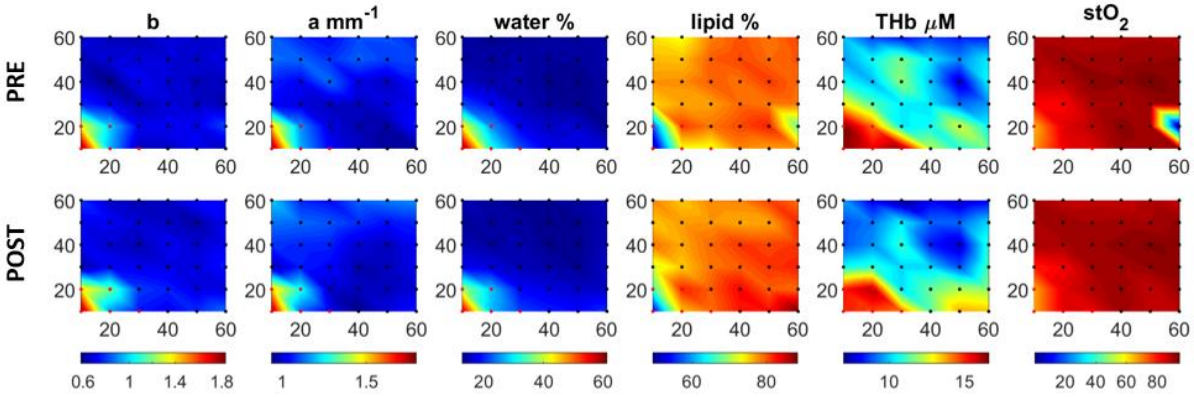
b
a mm-1
water %
lipid %
THb μM
stO2
PRE
POST

APPENDIX – NEWTON-RAPHSON FITS

In this appendix the results of the Newton-Raphson method are shown for every participant. The variable that undergoes Newton-Raphson varies every loop in the following sequence:

- the skin depth of the non-areola
- the skin depth of the areola
- the ratio adipose to glandular tissue of the areola
- the ratio adipose to glandular tissue of the non-areola
- the depth of the subcutaneous fat of the non-areola
- the depth of subcutaneous fat of the areola
- the state of blood pre
- the state of blood post
- the milk storage
- the hematocrit
- the correction for stO_2 pre
- the correction for stO_2 post
- (milk transfer volume).

The input value of every lactating and every non-lactating subject is the average breast model. It is reported when this is not the case (for example when the error stays to high).

In the first figure, the solution of μ_a and μ_s' are shown. The gray line is the fit of the pre-expression measurement: That is the blue line for the lactating subjects and the red line for the non-lactating subjects. The dashed gray line should fit the post-expression measurement: That is the green line for the lactating subjects and the magenta line for non-lactating subjects. The next figure resembles the error plot of the μ_a. This is followed by a table of the input variables of the fit of the found model. For the lactating subjects, also the obtained input variables are given for the found boundary conditions of milk supply. Lastly, the functional properties of the fit are reflected in a table.

SUBJECT L1

For this subject, the input values of the Newton-Raphson method deviate from the average breast model. The input value for the concentration of blood is increase from 0.4 to 0.9.

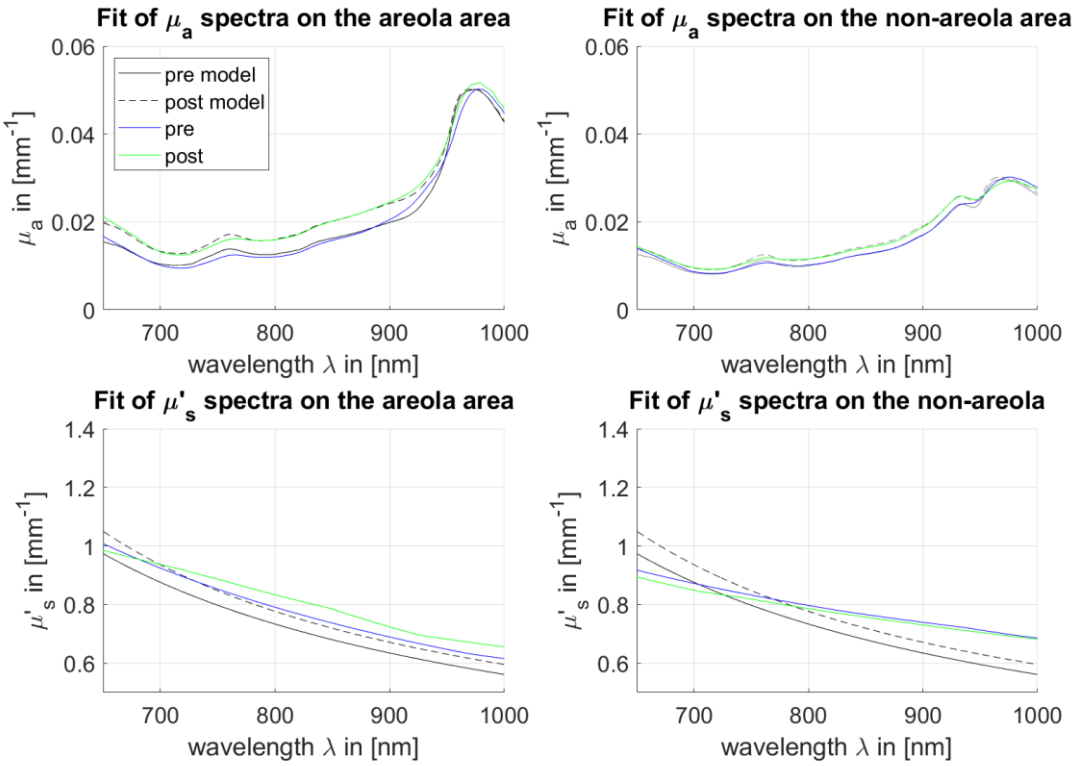

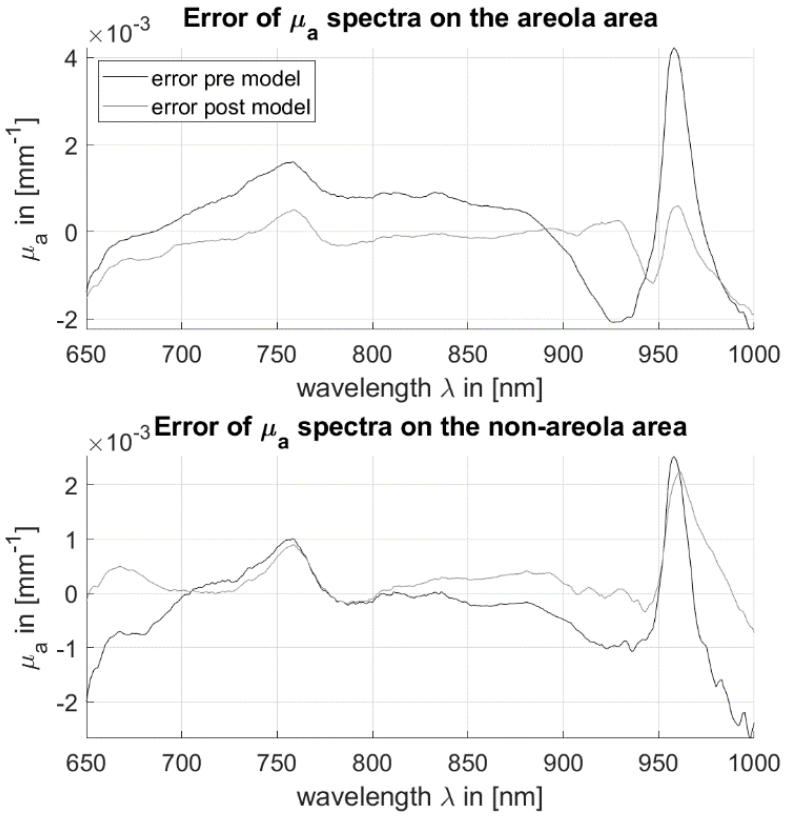

Input variables	Value	Value minimum milk transfer	Value maximum milk transfer
Fixed			
Source-detector distance	28 mm	28 mm	28 mm
μ_a	0.02 mm^{-1}	0.02 mm^{-1}	0.02 mm^{-1}
μ_s'	1 mm^{-1}	1 mm^{-1}	1 mm^{-1}
Volume of the lactating breast	590 ml	590 ml	590 ml
Fat in milk	3.8%	3.8%	3.8%
Change by fit			
Thickness of the skin of the areola	1.65 mm	1.74 mm	1.63 mm
Thickness of the skin of non-areola	0.84 mm	0.82 mm	0.89 mm
depth of the sub. fat of the areola	1.65 mm	1.74 mm	6.24 mm
depth of the sub. fat of non-areola	6.16 mm	6.31 mm	6.24 mm
Ratio adipose tissue to glandular tissue of areola area	0.04	0.07	0.02
Ratio adipose tissue to glandular tissue of non-areola area	0.04	0.01	0.00
THb in blood (hematocrit)	2.50 µM	2.50 µM	2.50 µM
Storage capacity of milk in the glands	449 ml	446 ml	456 ml
C_{blood} ratio pre	0.71	0.68	0.69
C_{blood} ratio post	0.75	0.76	0.70
stO_2 correction pre	-0.05	-0.05	-0.05
stO_2 correction post	-0.01	-0.03	0.00
Milk extracted	149 ml	115 ml	200 ml

	HbO_2 [µM]	Hb [µM]	THb [µM]	StO_2 %	Lipid %	Water %	$a\ mm^{-1}$	b
non-areola pre	35.03	11.23	46.26	75.72	55.16	38.12	1.26	0.67
non-areola post	42.09	12.15	54.24	77.60	55.51	35.14	1.30	0.70
Areola pre	42.28	14.08	56.36	75.02	5.07	77.36	1.36	1.28
Areola post	56.63	17.85	74.48	76.04	6.07	69.12	1.48	1.32

SUBJECT L2

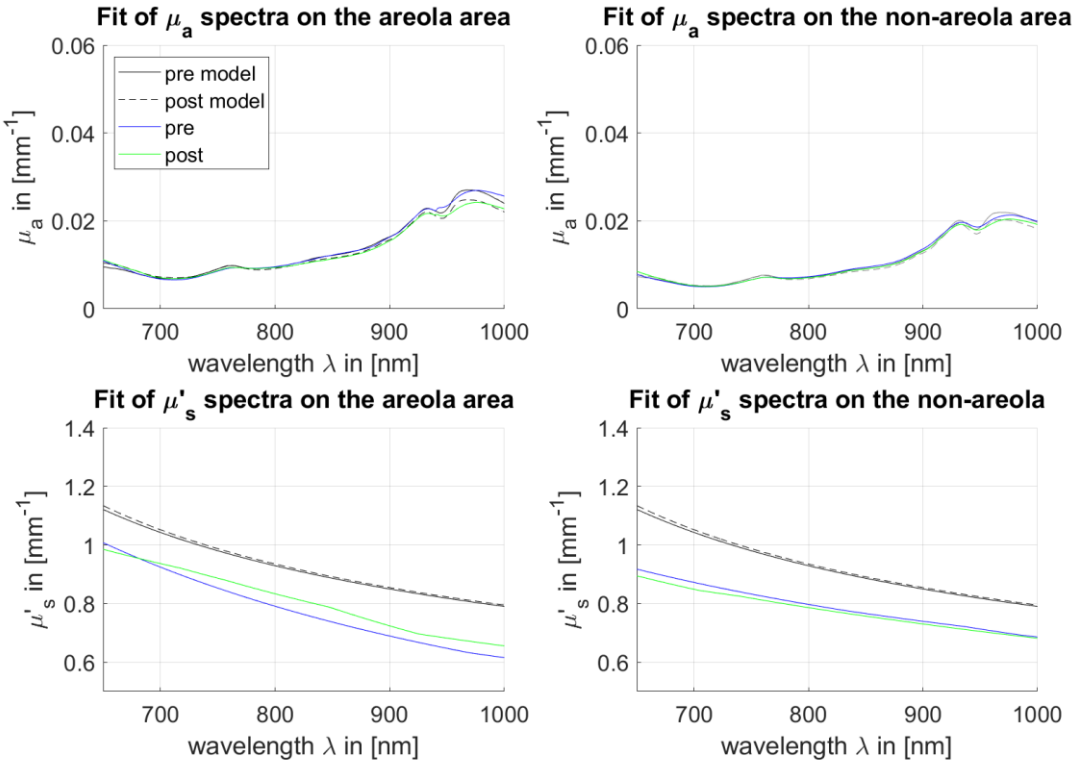
Fit of μ_a spectra on the areola area
pre model
post model
pre
post
μ_a in [mm^{-1}]
wavelength λ in [nm]
Fit of μ_a spectra on the non-areola area
Fit of μ'_s spectra on the areola area
μ'_s in [mm^{-1}]
Fit of μ'_s spectra on the non-areola

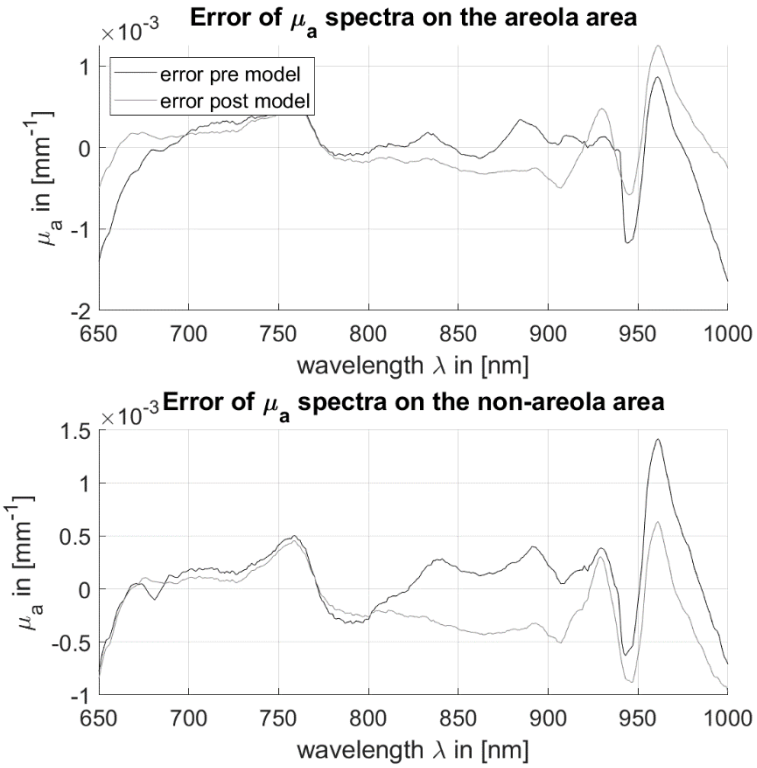
Error of μ_a spectra on the areola area
$\times 10^{-3}$
error pre model
error post model
μ_a in [mm^{-1}]
wavelength λ in [nm]
Error of μ_a spectra on the non-areola area

Input variables	Value	Value minimum milk transfer	Value maximum milk transfer
Fixed			
Source-detector distance	28 mm	28 mm	28 mm
μ_a	0.02 mm^{-1}	0.02 mm^{-1}	0.02 mm^{-1}
μ_s'	1 mm^{-1}	1 mm^{-1}	1 mm^{-1}
Volume of the lactating breast	850 ml	850 ml	850 ml
Fat in milk	3.8%	3.8%	3.8%
Change by fit			
Thickness of the skin of the areola	1.17 mm	1.15 mm	1.15 mm
Thickness of the skin of non-areola	0.60 mm	0.61 mm	0.62 mm
depth of the sub. fat of the areola	5.73 mm	6.01 mm	5.93 mm
depth of the sub. fat of non-areola	6.47 mm	6.70 mm	6.71 mm
Ratio adipose tissue to glandular tissue of areola area	0.29	0.29	0.27
Ratio adipose tissue to glandular tissue of non-areola area	0.05	0.22	0.17
THb in blood (hematocrit)	2.19 µM	2.18 µM	2.21 µM
Storage capacity of milk in the glands	180 ml	165 ml	237 ml
C_{blood} ratio pre	0.46	0.46	0.46
C_{blood} ratio post	0.37	0.40	0.37
stO_2 correction pre	0.05	0.06	0.05
stO_2 correction post	0.03	0.01	0.03
Milk extracted	180 ml	0 ml	200 ml

	HbO_2 [µM]	Hb [µM]	THb [µM]	StO_2 %	Lipid %	Water %	$a\ mm^{-1}$	b
non-areola pre	26.82	5.60	32.42	82.73	61.22	27.73	1.29	0.66
non-areola post	24.85	6.34	31.19	79.67	61.54	25.20	1.33	0.69
Areola pre	37.15	7.22	44.36	83.74	52.62	32.54	1.39	0.81
Areola post	34.15	8.71	42.86	79.67	54.18	29.13	1.41	0.82

SUBJECT L4

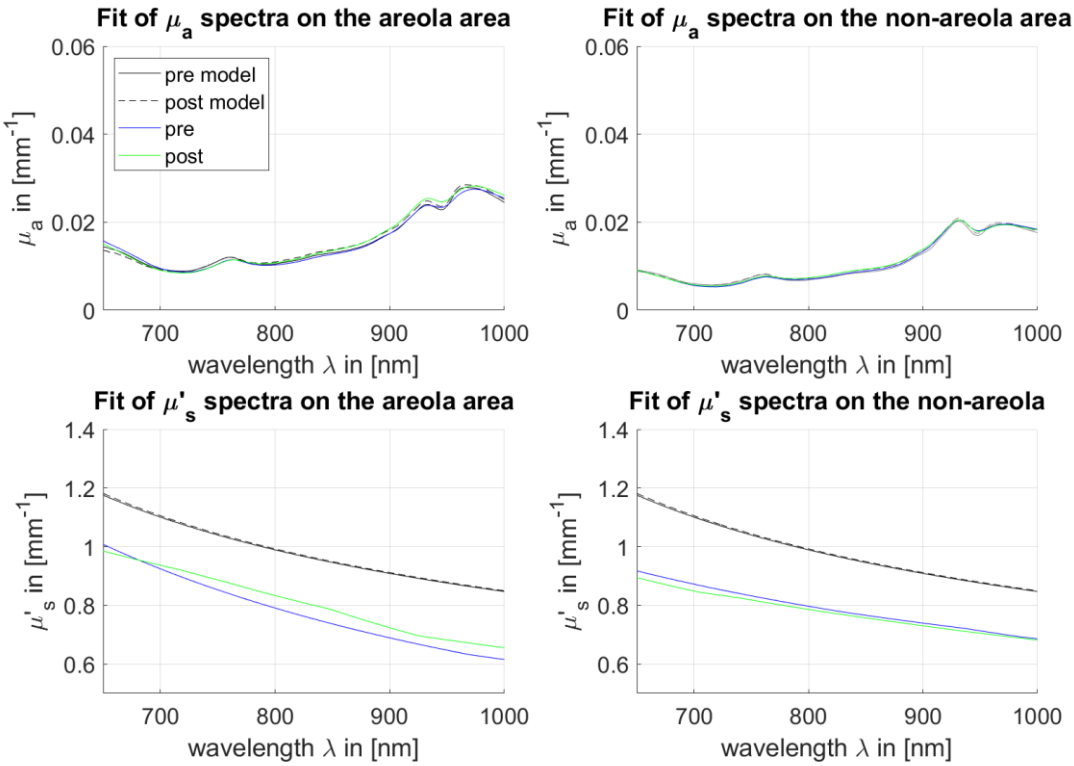
Fit of μ_a spectra on the areola area
pre model
post model
pre
post
μ_a in [mm^{-1}]
wavelength λ in [nm]
Fit of μ_a spectra on the non-areola area
μ_a in [mm^{-1}]
wavelength λ in [nm]
Fit of μ'_s spectra on the areola area
μ'_s in [mm^{-1}]
wavelength λ in [nm]
Fit of μ'_s spectra on the non-areola
μ'_s in [mm^{-1}]
wavelength λ in [nm]

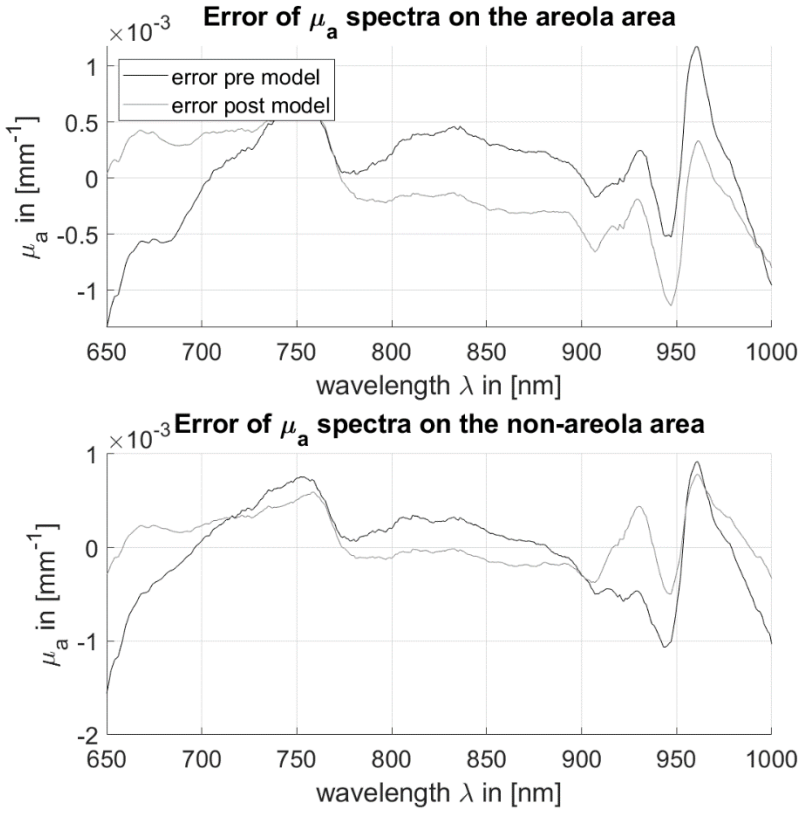
Error of μ_a spectra on the areola area
$\times 10^{-3}$
error pre model
error post model
μ_a in [mm^{-1}]
wavelength λ in [nm]
Error of μ_a spectra on the non-areola area
$\times 10^{-3}$
μ_a in [mm^{-1}]
wavelength λ in [nm]

Input variables	Value	Value minimum milk transfer	Value maximum milk transfer
Fixed			
Source-detector distance	28 mm	28 mm	28 mm
μ_a	0.02 mm^{-1}	0.02 mm^{-1}	0.02 mm^{-1}
μ_s'	1 mm^{-1}	1 mm^{-1}	1 mm^{-1}
Volume of the lactating breast	480 ml	480 ml	480 ml
Fat in milk	3.8%	3.8%	3.8%
Change by fit			
Thickness of the skin of the areola	1.38 mm	1.41 mm	1.42 mm
Thickness of the skin of non-areola	0.69 mm	0.69 mm	0.61 mm
depth of the sub. fat of the areola	7.82 mm	7.62 mm	7.81 mm
depth of the sub. fat of non-areola	8.56 mm	8.57 mm	0.17 mm
Ratio adipose tissue to glandular tissue of areola area	0.08	0.00	0.17
Ratio adipose tissue to glandular tissue of non-areola area	0.41	0.34	0.28
THb in blood (hematocrit)	2.23 µM	2.19 µM	2.25 µM
Storage capacity of milk in the glands	251 ml	189 ml	295 ml
C_{blood} ratio pre	0.48	0.47	0.46
C_{blood} ratio post	0.51	0.51	0.46
stO_2 correction pre	-0.07	-0.06	-0.08
stO_2 correction post	-0.03	-0.03	-0.01
Milk extracted	51 ml	0 ml	200 ml

	HbO_2 [µM]	Hb [µM]	THb [µM]	StO_2 %	Lipid %	Water %	$a\ mm^{-1}$	b
non-areola pre	22.97	8.27	31.24	73.52	70.78	23.90	1.25	0.57
non-areola post	25.87	7.58	33.45	77.34	71.28	23.13	1.26	0.57
Areola pre	35.76	13.45	49.21	72.67	54.77	33.53	1.44	0.76
Areola post	39.87	11.92	51.79	76.98	54.90	32.89	1.44	0.76

SUBJECT L5

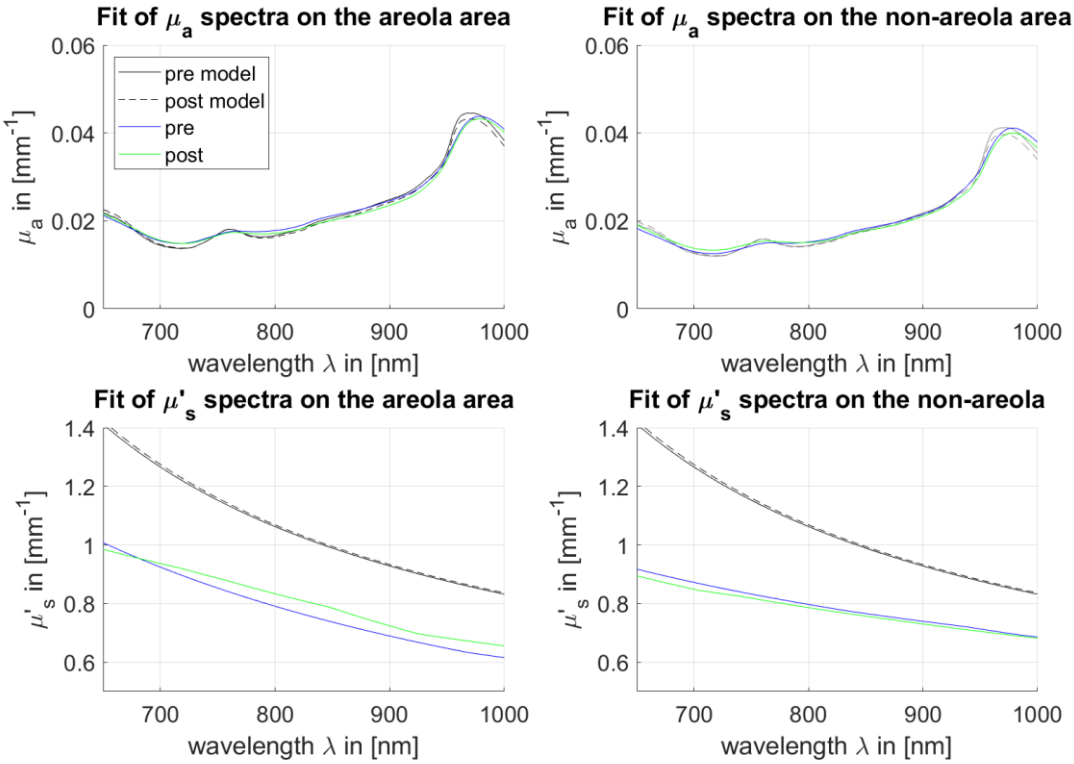
Fit of μ_a spectra on the areola area
pre model
post model
pre
post
μ_a in [mm^{-1}]
wavelength λ in [nm]
Fit of μ_a spectra on the non-areola area
Fit of μ'_s spectra on the areola area
μ'_s in [mm^{-1}]
Fit of μ'_s spectra on the non-areola

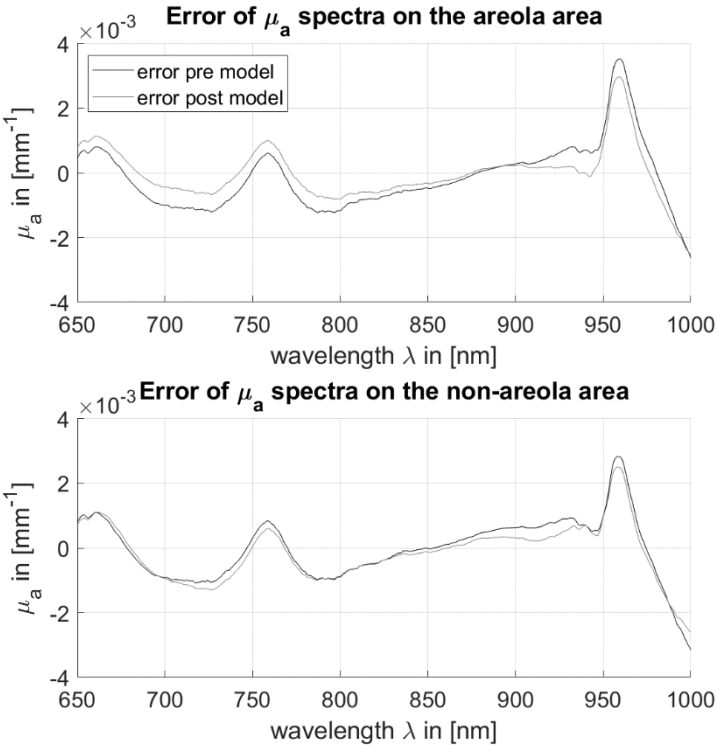
Error of μ_a spectra on the areola area
$\times 10^{-3}$
error pre model
error post model
μ_a in [mm^{-1}]
wavelength λ in [nm]
Error of μ_a spectra on the non-areola area

Input variables	Value	Value minimum milk transfer	Value maximum milk transfer
Fixed			
Source-detector distance	22 mm	22 mm	22 mm
μ_a	0.02 mm^{-1}	0.02 mm^{-1}	0.02 mm^{-1}
μ_s'	1 mm^{-1}	1 mm^{-1}	1 mm^{-1}
Volume of the lactating breast	390 ml	390 ml	390 ml
Fat in milk	3.8%	3.8%	3.8%
Change by fit			
Thickness of the skin of the areola	3.48 mm	3.41 mm	3.42 mm
Thickness of the skin of non-areola	2.52 mm	2.61 mm	2.56 mm
depth of the sub. fat of the areola	5.02 mm	5.12 mm	4.93 mm
depth of the sub. fat of non-areola	3.70 mm	4.30 mm	4.12 mm
Ratio adipose tissue to glandular tissue of areola area	0.00	0.00	0.00
Ratio adipose tissue to glandular tissue of non-areola area	0.06	0.00	0.00
THb in blood (hematocrit)	2.12 µM	2.13 µM	2.16 µM
Storage capacity of milk in the glands	47 ml	54 ml	100 ml
C_{blood} ratio pre	0.38	0.39	0.39
C_{blood} ratio post	0.35	0.37	0.35
stO_2 correction pre	-0.04	-0.04	-0.05
stO_2 correction post	-0.05	-0.06	-0.05
Milk extracted	47 ml	0 ml	100 ml

	HbO_2 [µM]	Hb [µM]	THb [µM]	StO_2 %	Lipid %	Water %	$a\ mm^{-1}$	b
non-areola pre	50.00	17.83	67.83	73.71	15.85	53.75	1.81	1.23
non-areola post	48.41	18.83	67.24	72.00	16.24	51.09	1.84	1.24
Areola pre	59.26	20.12	79.39	74.65	14.51	55.10	1.95	1.23
Areola post	56.36	21.38	77.74	72.50	14.56	53.61	1.97	1.23

SUBJECT N1

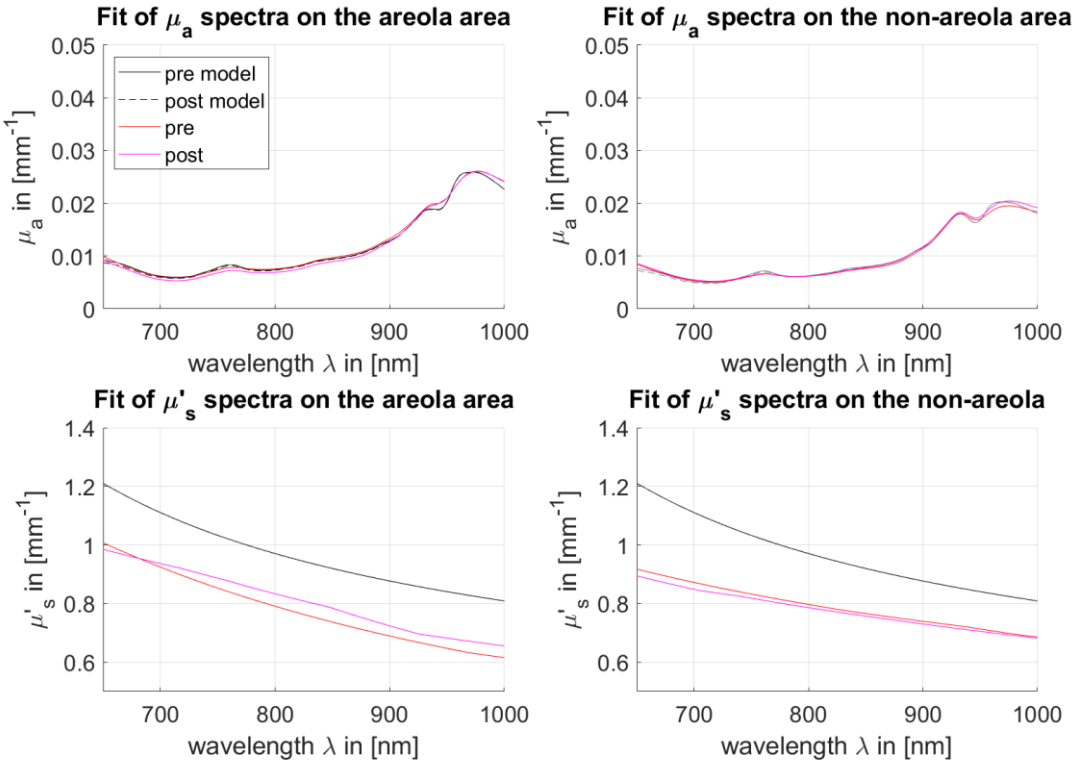
Fit of μ_a spectra on the areola area
pre model
post model
pre
post
μ_a in [mm^{-1}]
wavelength λ in [nm]
Fit of μ_a spectra on the non-areola area
Fit of μ'_s spectra on the areola area
μ'_s in [mm^{-1}]
Fit of μ'_s spectra on the non-areola

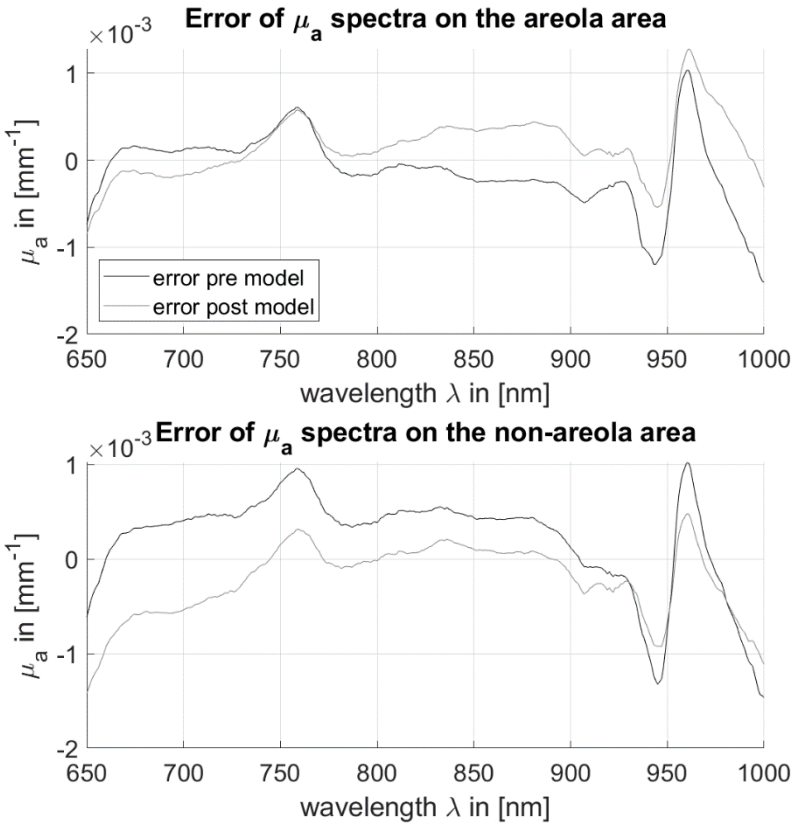
Error of μ_a spectra on the areola area
$\times 10^{-3}$
error pre model
error post model
μ_a in [mm^{-1}]
wavelength λ in [nm]
Error of μ_a spectra on the non-areola area

Input variables	Value
Fixed	
Source-detector distance	28 mm
μ_a	0.01 mm^{-1}
μ_s'	0.9 mm^{-1}
Change by fit	
Thickness of the skin of the areola	1.80 mm
Thickness of the skin of non-areola	1.33 mm
Depth of the sub. fat of the areola	6.74 mm
Depth of the sub. fat of non-areola	4.44 mm
Ratio adipose tissue to glandular tissue of areola area	0.00
Ratio adipose tissue to glandular tissue of non-areola area	0.72
THb in blood (hematocrit)	2.18 µM
C_{blood} ratio pre	0.17
C_{blood} ratio post	0.16
stO_2 correction pre	-0.02
stO_2 correction post	0.00

	HbO_2 [µM]	Hb [µM]	THb [µM]	StO_2 %	Lipid %	Water %	$a\ mm^{-1}$	b
non-areola pre	21.47	6.63	28.10	76.40	56.23	27.08	1.27	0.91
non-areola post	21.58	6.10	27.68	77.97	56.23	27.07	1.27	0.91
Areola pre	24.83	8.31	33.13	74.93	41.81	37.05	1.55	0.94
Areola post	24.96	7.67	32.63	76.49	41.81	37.03	1.55	0.94

SUBJECT N2

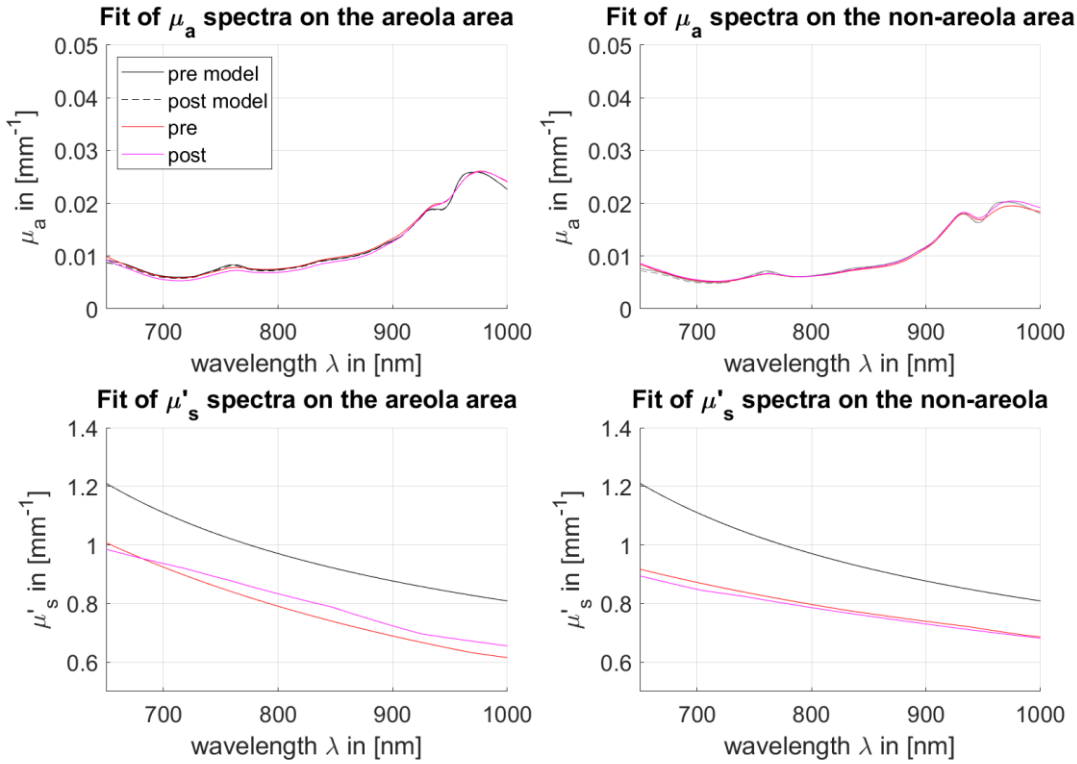
Fit of μ_a spectra on the areola area
pre model
post model
pre
post
μ_a in [mm^{-1}]
wavelength λ in [nm]
Fit of μ_a spectra on the non-areola area
Fit of μ'_s spectra on the areola area
μ'_s in [mm^{-1}]
Fit of μ'_s spectra on the non-areola

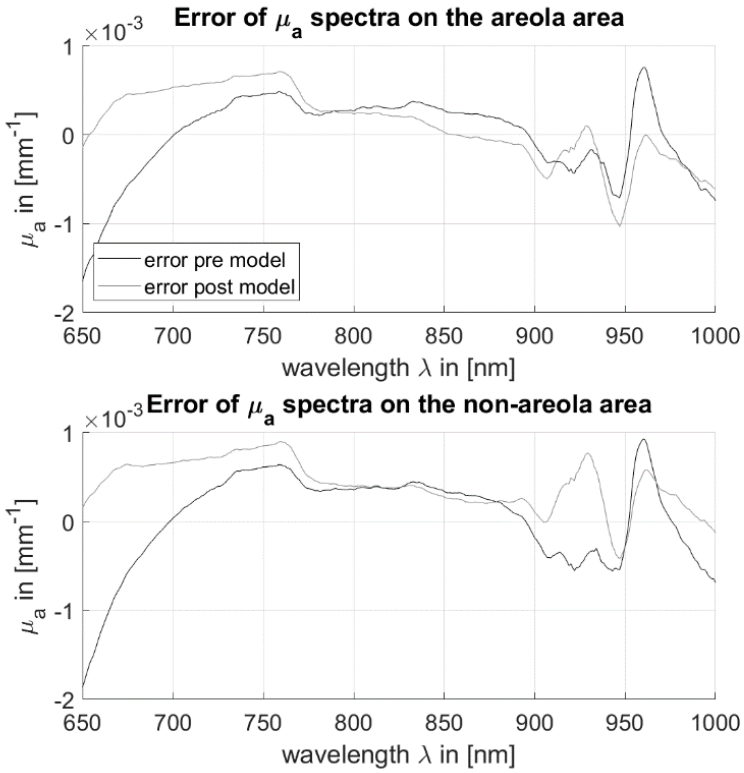
Error of μ_a spectra on the areola area
$\times 10^{-3}$
error pre model
error post model
μ_a in [mm^{-1}]
wavelength λ in [nm]
Error of μ_a spectra on the non-areola area

Input variables	Value
Fixed	
Source-detector distance	28 mm
μ_a	0.01 mm^{-1}
μ_s'	0.9 mm^{-1}
Change by fit	
Thickness of the skin of the areola	2.10 mm
Thickness of the skin of non-areola	0.60 mm
Depth of the sub. fat of the areola	14.06 mm
Depth of the sub. fat of non-areola	9.8 mm
Ratio adipose tissue to glandular tissue of areola area	0.50
Ratio adipose tissue to glandular tissue of non-areola area	1.00
THb in blood (hematocrit)	1.88 µM
C_{blood} ratio pre	0.02
C_{blood} ratio post	0.00
stO_2 correction pre	-0.02
stO_2 correction post	-0.05

	HbO_2 [µM]	Hb [µM]	THb [µM]	StO_2 %	Lipid %	Water %	$a\ mm^{-1}$	b
non-areola pre	8.82	2.43	11.25	78.37	77.81	17.38	1.20	0.53
non-areola post	7.81	2.61	10.42	74.96	77.81	17.35	1.20	0.53
Areola pre	14.28	3.99	18.27	78.16	58.67	29.58	1.51	0.76
Areola post	12.41	4.20	16.61	74.74	58.67	29.51	1.51	0.76

SUBJECT N3

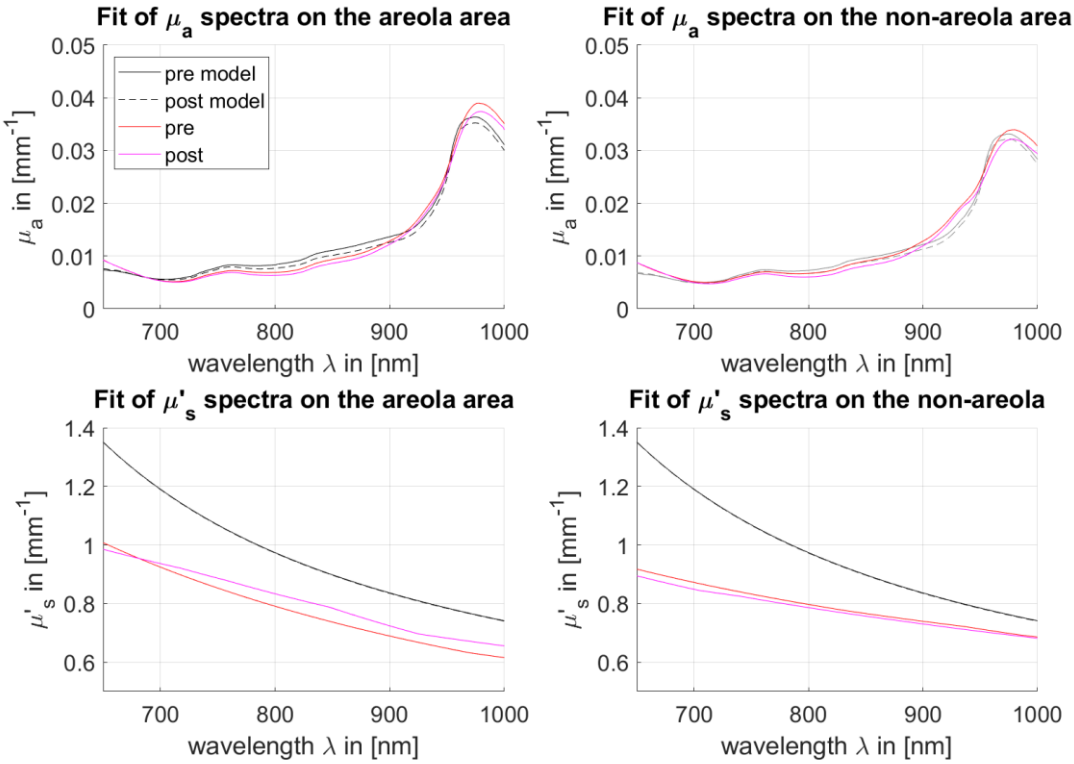
Fit of μ_a spectra on the areola area
pre model
post model
pre
post
μ_a in [mm^{-1}]
wavelength λ in [nm]
Fit of μ_a spectra on the non-areola area
Fit of μ'_s spectra on the areola area
μ'_s in [mm^{-1}]
Fit of μ'_s spectra on the non-areola

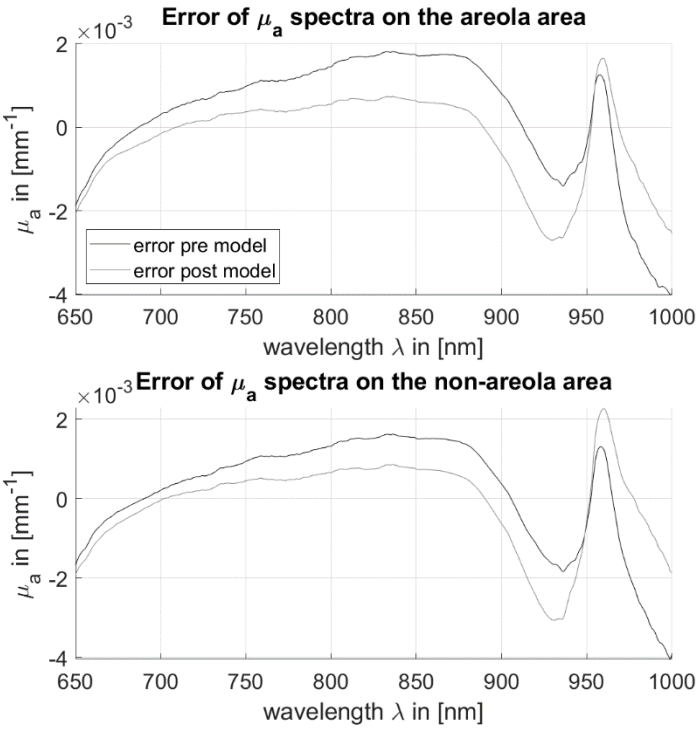
Error of μ_a spectra on the areola area
$\times 10^{-3}$
error pre model
error post model
μ_a in [mm^{-1}]
wavelength λ in [nm]
Error of μ_a spectra on the non-areola area

Input variables	Value
Fixed	
Source-detector distance	28 mm
μ_a	0.01 mm^{-1}
μ_s'	0.9 mm^{-1}
Change by fit	
Thickness of the skin of the areola	4.00 mm
Thickness of the skin of non-areola	2.70 mm
Depth of the sub. fat of the areola	4.14 mm
Depth of the sub. fat of non-areola	3.38 mm
Ratio adipose tissue to glandular tissue of areola area	0
Ratio adipose tissue to glandular tissue of non-areola area	0
THb in blood (hematocrit)	2.09 µM
C_{blood} ratio pre	0.07
C_{blood} ratio post	0.04
stO_2 correction pre	0.09
stO_2 correction post	0.06

	HbO_2 [µM]	Hb [µM]	THb [µM]	StO_2 %	Lipid %	Water %	$a\ mm^{-1}$	b
non-areola pre	26.23	5.09	31.32	83.74	9.31	52.84	1.80	1.34
non-areola post	22.66	5.71	28.37	79.86	9.31	52.73	1.80	1.34
Areola pre	31.21	5.41	36.62	85.24	4.04	56.91	1.95	1.39
Areola post	26.86	6.15	33.01	81.37	4.04	56.78	1.95	1.40

SUBJECT N4

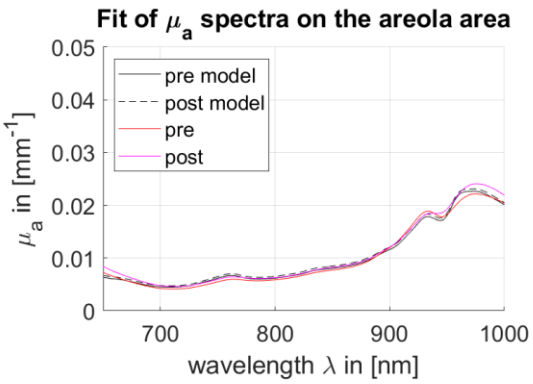
Fit of μ_a spectra on the areola area
pre model
post model
pre
post
μ_a in [mm^{-1}]
wavelength λ in [nm]

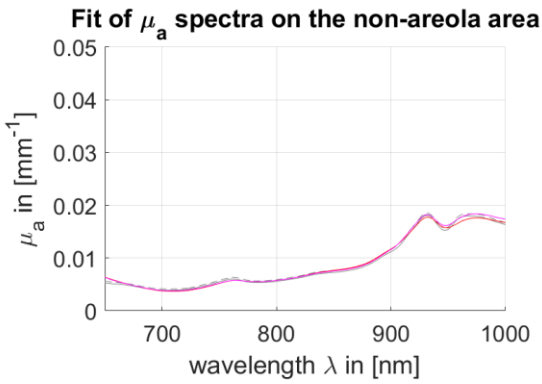
Fit of μ_a spectra on the non-areola area
μ_a in [mm^{-1}]
wavelength λ in [nm]

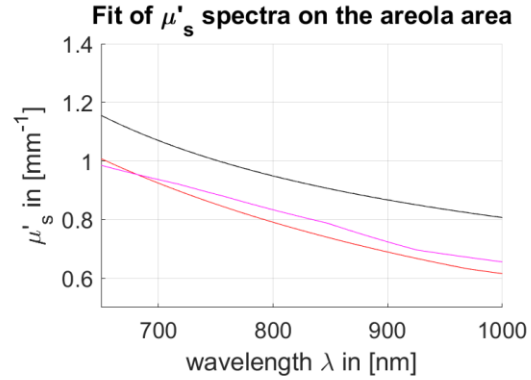
Fit of μ'_s spectra on the areola area
μ'_s in [mm^{-1}]
wavelength λ in [nm]

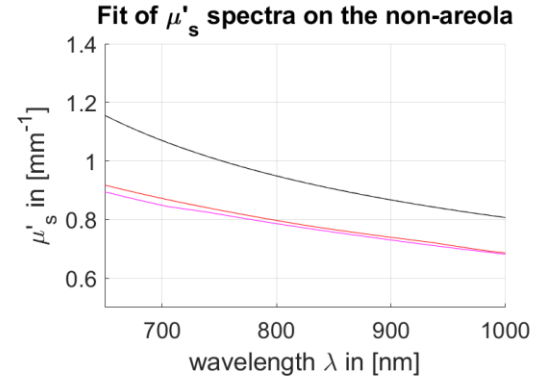
Fit of μ'_s spectra on the non-areola
μ'_s in [mm^{-1}]
wavelength λ in [nm]

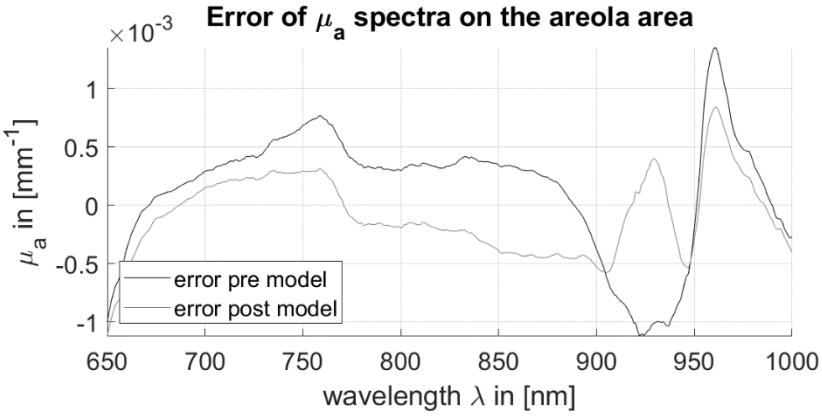
Error of μ_a spectra on the areola area
$\times 10^{-3}$
error pre model
error post model
μ_a in [mm^{-1}]
wavelength λ in [nm]

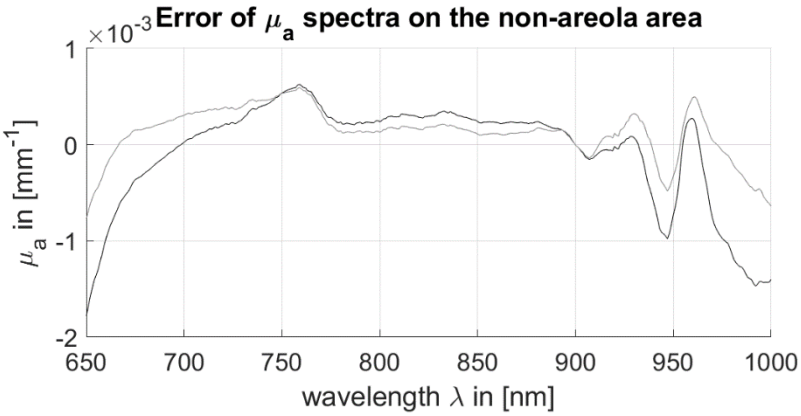
Error of μ_a spectra on the non-areola area
$\times 10^{-3}$
μ_a in [mm^{-1}]
wavelength λ in [nm]

Input variables	Value
Fixed	
Source-detector distance	28 mm
μ_a	0.01 mm^{-1}
μ_s'	0.9 mm^{-1}
Change by fit	
Thickness of the skin of the areola	1.19 mm
Thickness of the skin of non-areola	1.14 mm
Depth of the sub. fat of the areola	6.86 mm
Depth of the sub. fat of non-areola	5.86 mm
Ratio adipose tissue to glandular tissue of areola area	0.00
Ratio adipose tissue to glandular tissue of non-areola area	0.87
THb in blood (hematocrit)	2.18 µM
C_{blood} ratio pre	0.16
C_{blood} ratio post	0.19
stO_2 correction pre	0.06
stO_2 correction post	0.06

	HbO_2 [µM]	Hb [µM]	THb [µM]	StO_2 %	Lipid %	Water %	$a\ mm^{-1}$	b
non-areola pre	21.24	3.68	24.92	85.22	65.59	22.81	1.23	0.76
non-areola post	22.66	3.91	26.57	85.30	65.59	22.87	1.23	0.76
Areola pre	22.36	4.88	27.24	82.08	49.75	32.25	1.44	0.83
Areola post	23.85	5.17	29.02	82.18	49.75	32.31	1.44	0.83

SUBJECT N5

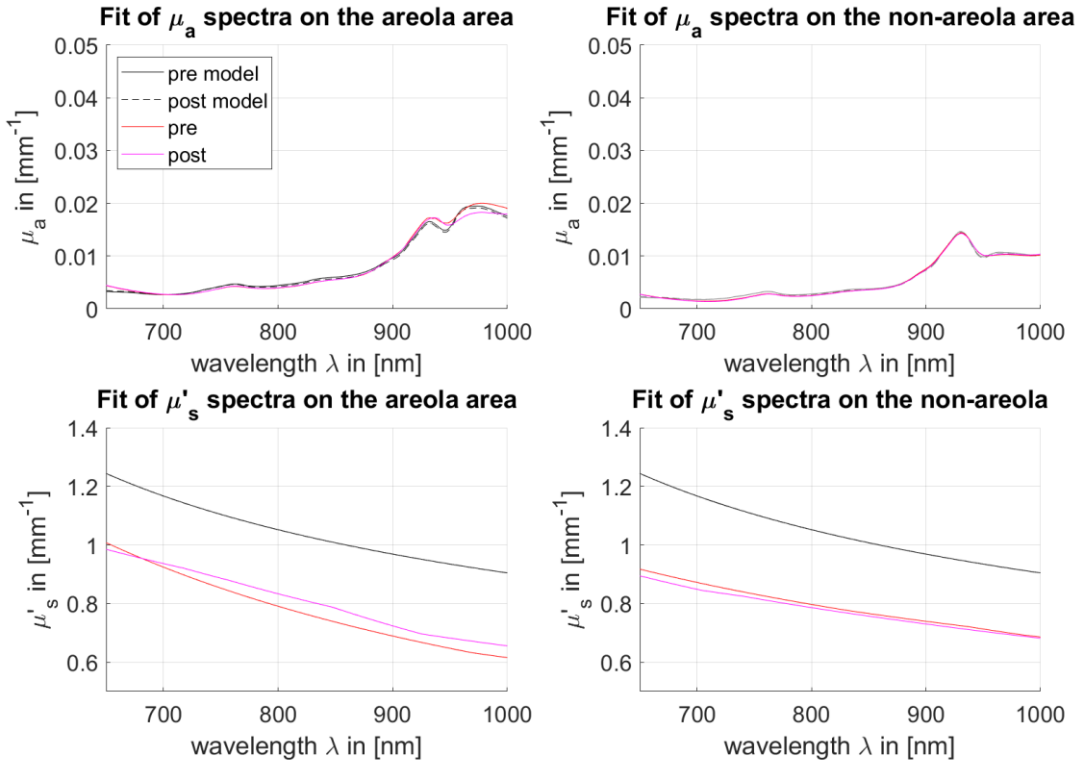
Fit of μ_a spectra on the areola area
pre model
post model
pre
post
μ_a in [mm^{-1}]
wavelength λ in [nm]
Fit of μ_a spectra on the non-areola area
μ_a in [mm^{-1}]
wavelength λ in [nm]
Fit of μ'_s spectra on the areola area
μ'_s in [mm^{-1}]
wavelength λ in [nm]
Fit of μ'_s spectra on the non-areola
μ'_s in [mm^{-1}]
wavelength λ in [nm]

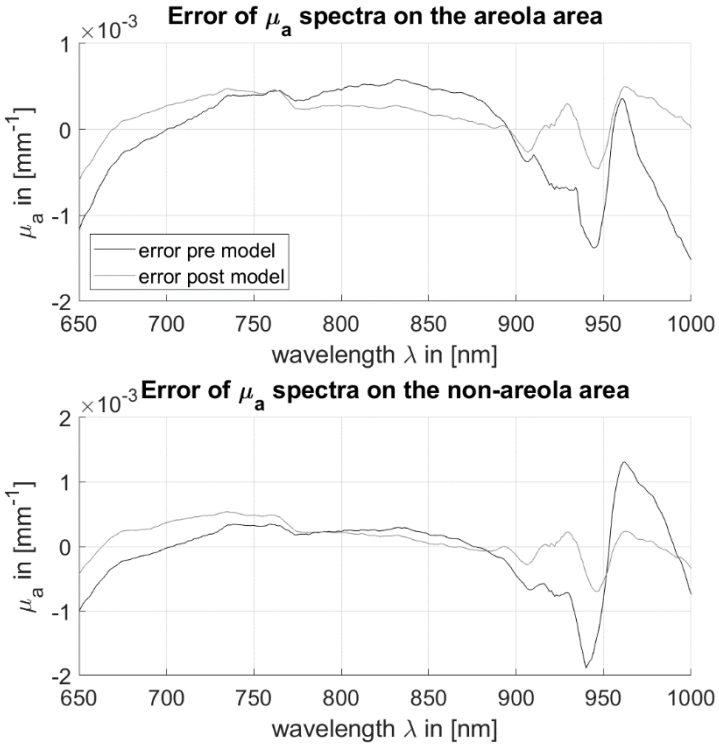
Error of μ_a spectra on the areola area
$\times 10^{-3}$
error pre model
error post model
μ_a in [mm^{-1}]
wavelength λ in [nm]
Error of μ_a spectra on the non-areola area
$\times 10^{-3}$
μ_a in [mm^{-1}]
wavelength λ in [nm]

Input variables	Value
Fixed	
Source-detector distance	28 mm
μ_a	0.01 mm^{-1}
μ_s'	0.9 mm^{-1}
Change by fit	
Thickness of the skin of the areola	2.08 mm
Thickness of the skin of non-areola	0.60 mm
Depth of the sub. fat of the areola	20.00 mm
Depth of the sub. fat of non-areola	2.82 mm
Ratio adipose tissue to glandular tissue of areola area	0.78
Ratio adipose tissue to glandular tissue of non-areola area	1.00
THb in blood (hematocrit)	1.88 µM
C_{blood} ratio pre	0.03
C_{blood} ratio post	0.01
stO_2 correction pre	0.11
stO_2 correction post	0.08

	HbO_2 [µM]	Hb [µM]	THb [µM]	StO_2 %	Lipid %	Water %	$a\ mm^{-1}$	b
non-areola pre	21.24	3.68	24.92	85.22	65.59	22.81	1.23	0.76
non-areola post	22.66	3.91	26.57	85.30	65.59	22.87	1.23	0.76
Areola pre	22.36	4.88	27.24	82.08	49.75	32.25	1.44	0.83
Areola post	23.85	5.17	29.02	82.18	49.75	32.31	1.44	0.83

APPENDIX – FIT ERROR FUNCTIONAL PROPERTIES

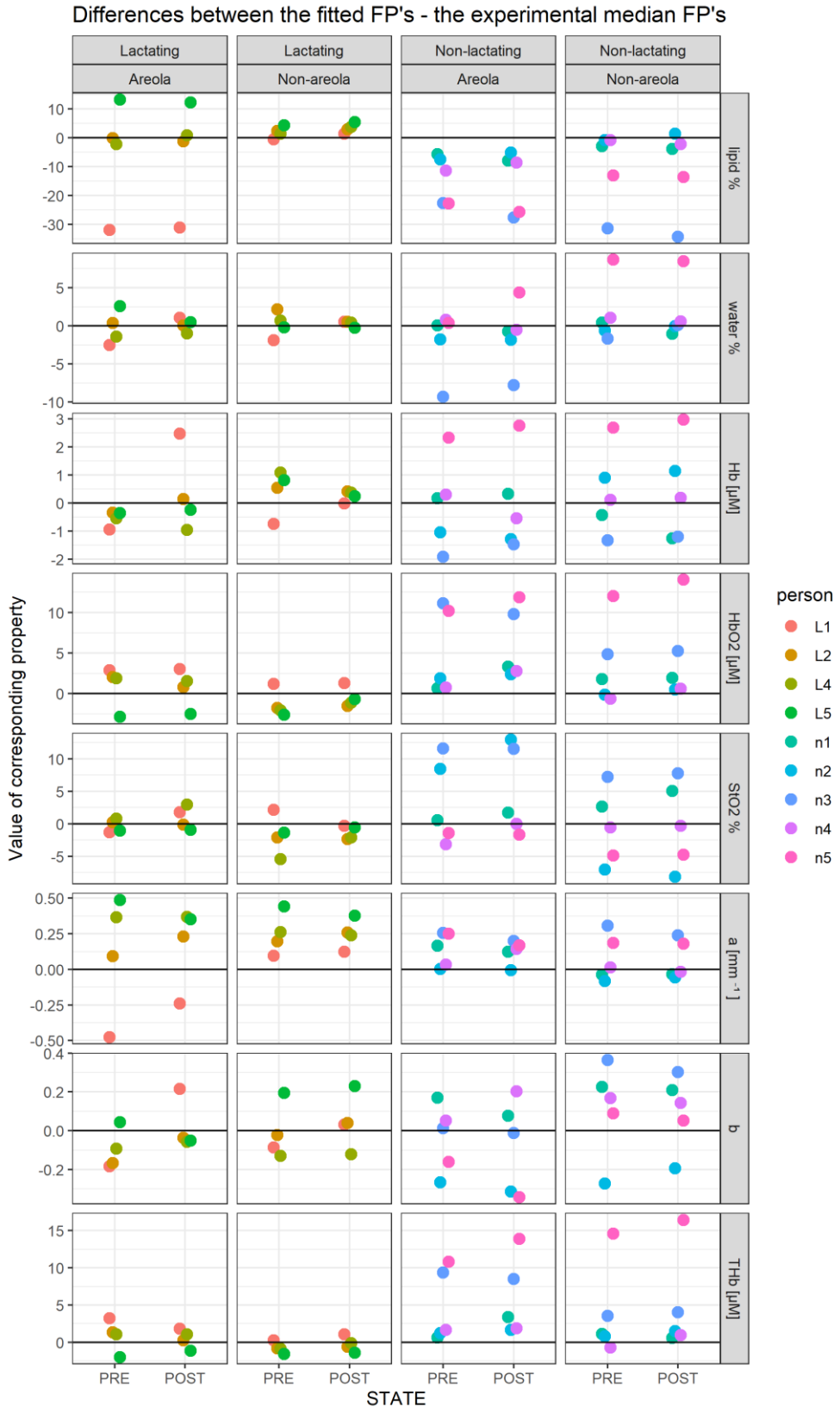

FIGURE 10 THE DIFFERENCES BETWEEN THE FUNCTIONAL PROPERTIES OBTAINED BY FITTING THE MODEL TO THE EXPERIMENTS USING THE NEWTON-RAPHSON METHOD AND THE FUNCTIONAL PROPERTIES OBTAINED BY FITTING THE FUNCTIONAL PROPERTIES TO THE EXPERIMENTAL OBTAINED OPTICAL PROPERTIES DIRECTLY.